



National Library
of Canada

Acquisitions and
Bibliographic Services Branch

395 Wellington Street
Ottawa, Ontario
K1A 0N4

Bibliothèque nationale
du Canada

Direction des acquisitions et
des services bibliographiques

395, rue Wellington
Ottawa (Ontario)
K1A 0N4

Your file Votre référence

Our file Notre référence

NOTICE

The quality of this microform is heavily dependent upon the quality of the original thesis submitted for microfilming. Every effort has been made to ensure the highest quality of reproduction possible.

If pages are missing, contact the university which granted the degree.

Some pages may have indistinct print especially if the original pages were typed with a poor typewriter ribbon or if the university sent us an inferior photocopy.

Reproduction in full or in part of this microform is governed by the Canadian Copyright Act, R.S.C. 1970, c. C-30, and subsequent amendments.

AVIS

La qualité de cette microforme dépend grandement de la qualité de la thèse soumise au microfilmage. Nous avons tout fait pour assurer une qualité supérieure de reproduction.

S'il manque des pages, veuillez communiquer avec l'université qui a conféré le grade.

La qualité d'impression de certaines pages peut laisser à désirer, surtout si les pages originales ont été dactylographiées à l'aide d'un ruban usé ou si l'université nous a fait parvenir une photocopie de qualité inférieure.

La reproduction, même partielle, de cette microforme est soumise à la Loi canadienne sur le droit d'auteur, SRC 1970, c. C-30, et ses amendements subséquents.

Canada

UNIVERSITY OF ALBERTA

THE MEASUREMENT AND APPLICATION OF ABSOLUTE INTENSITIES IN
THE IR SPECTRA OF LIQUIDS

BY

ZHIDA LAN



A thesis submitted to the Faculty of Graduate Studies and Research in partial
fulfillment of the requirements for the degree of DOCTOR OF PHILOSOPHY.

DEPARTMENT OF CHEMISTRY

Edmonton, Alberta

Spring 1996



National Library
of Canada

Acquisitions and
Bibliographic Services Branch

395 Wellington Street
Ottawa, Ontario
K1A 0N4

Bibliothèque nationale
du Canada

Direction des acquisitions et
des services bibliographiques

395, rue Wellington
Ottawa (Ontario)
K1A 0N4

Your file Votre référence

Our file Notre référence

The author has granted an irrevocable non-exclusive licence allowing the National Library of Canada to reproduce, loan, distribute or sell copies of his/her thesis by any means and in any form or format, making this thesis available to interested persons.

L'auteur a accordé une licence irrévocable et non exclusive permettant à la Bibliothèque nationale du Canada de reproduire, prêter, distribuer ou vendre des copies de sa thèse de quelque manière et sous quelque forme que ce soit pour mettre des exemplaires de cette thèse à la disposition des personnes intéressées.

The author retains ownership of the copyright in his/her thesis. Neither the thesis nor substantial extracts from it may be printed or otherwise reproduced without his/her permission.

L'auteur conserve la propriété du droit d'auteur qui protège sa thèse. Ni la thèse ni des extraits substantiels de celle-ci ne doivent être imprimés ou autrement reproduits sans son autorisation.

ISBN 0-612-10606-3

Canada

UNIVERSITY OF ALBERTA

RELEASE FORM

NAME OF AUTHOR: ZHIDA LAN

TITLE OF THESIS: THE MEASUREMENT AND APPLICATION OF ABSOLUTE
INTENSITIES IN THE IR SPECTRA OF LIQUIDS

DEGREE: PH.D.

YEAR THIS DEGREE GRANTED: 1996

Permission is hereby granted to the University of Alberta Library to reproduce single copies of this thesis and to lend or sell such copies for private, scholarly or scientific research purposes only.

The author reserves all other publication and other rights in association with the copyright in the thesis, and except as herein before provided neither the thesis nor any substantial portion thereof may be printed or otherwise reproduced in any material form whatever without the author's prior permission.

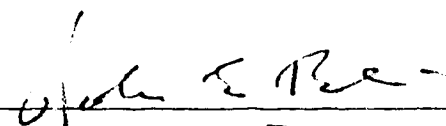


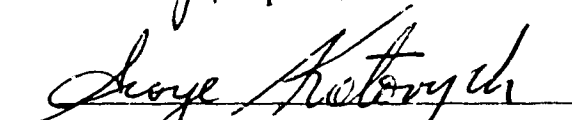
Zhida Lan
5023-13 Avenue
Edmonton, Alberta
T6L 1Z5

DATE: MARCH 19, 1996

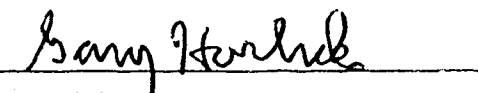
UNIVERSITY OF ALBERTA
FACULTY OF GRADUATE STUDIES AND RESEARCH

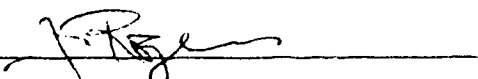
The undersigned certify that they have read, and recommend to the Faculty of Graduate Studies and Research for acceptance, a thesis entitled THE MEASUREMENT AND APPLICATION OF ABSOLUTE INTENSITIES IN THE IR SPECTRA OF LIQUIDS submitted by ZHIDA LAN in partial fulfillment of the requirements for the degree of DOCTOR OF PHILOSOPHY.

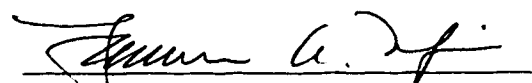

J. E. Bertie, Supervisor


G. Kotovych


G. R. Loppnow


G. Horlick


J. S. Rogers


L. A. Nafie, External Examiner

DATE: March 11, 1996

To Maojuan and Cecily

Abstract

This thesis presents the work done to measure absolute intensities in the IR spectra of liquid samples by transmission and attenuated total reflection (ATR) methods, and to apply the intensities to investigate the hydrogen bonding interaction in water solutions. The intensities are measured by the infrared optical constant, k and n , spectra, and the n spectrum is usually calculated from the k spectrum through the Kramers-Kronig (KK) transform. This work presents an approach for colorless liquids to obtain the contribution from electronic absorption to improve the n value calculated. Results for ten common liquids are presented.

Transmission method was used to measure liquid dichloromethane to obtain optical constant and molar absorption coefficient spectra between 6500 and 800 cm^{-1} . The estimated accuracy of the integrated intensities over 25 bands is $\pm 1.5\%$. Nine of the bands are accepted as the secondary standards for infrared absorption intensity of liquids by the International Union of Pure and Applied Chemistry (IUPAC).

ATR is another method to measure IR spectra. A modified KK transform from reflectance to the phase shift with non constant phase correction was developed to improve the non iterative procedure of refining ATR spectra. This transform gives errors less than 0.1% for the value of the k spectrum recovered from the simulated spectra. The ATR method was used to measure the spectra of water and water-acetonitrile mixtures. The reproducibility of the ATR spectra for water has been improved. The precision of the k spectrum is now 0.3% for the area in the region

4000-2660 cm^{-1} . The recommended k and n spectra between 15000 and 1 cm^{-1} for liquid water at 24.5 ± 1 °C are presented. The k and n spectra between 6500-700 cm^{-1} were determined for the water-acetonitrile mixtures over the full composition range at 24.5 ± 1 °C. Their intensities under the OH and CN stretching bands were examined as the function of the composition by using molar polarizability spectra,

$\bar{\alpha}_m(\tilde{\nu}) = \alpha'_m(\tilde{\nu}) + i\alpha''_m(\tilde{\nu})$. The hydrogen bonding interaction between the water and acetonitrile molecules in the mixtures are investigated. The results provide specific details of the structure of the mixture for the first time.

Acknowledgments

I would like to thank Dr. John E. Bertie for suggesting this project to me and for his guidance, patience and encouragement throughout the course of the project and preparation of the thesis.

I express my appreciation to the following persons for their discussion in my research; Y. Apelblat, D. Keef, L. Zhang and Dr. R. N. Jones. Also, the appreciation is extended to M. K. Jones for her proof reading of my water paper.

List of Tables

Table 2.1	The real refractive indices of ten liquids in the visible region and their temperature dependence at 25°C.....	29
Table 2.2	The contribution, $\Delta n_{IR}(\tilde{\nu}_a)$, of infrared absorption to the visible and near-infrared refractive indices of ten liquids at 25°C	31
Table 2.3	Contribution to the Visible Refractive Index From Different Infrared Regions.....	33
Table 2.4	Fits of Equations (2.2), (2.2a) and (2.3) to the Visible Real Refractive Indices of Ten Liquids	37
Table 2.5	The coefficients of the polynomial required to correct the published infrared refractive indices and the size of the correction at 8000, 4000 and 0 cm^{-1}	41
Table 2.6	Electronic Molar Polarizabilities Between 20,500 and 0 cm^{-1} of Ten Liquids at 25°C	42
Table 3.1	Linear absorption coefficients and imaginary refractive indices at anchor points for liquid dichloromethane at 25°C.....	52
Table 3.2	Pathlengths, high-wavenumber refractive index, and number of spectra from each spectroscopist, for the region processed.	53
Table 3.3	Spectroscopist average areas under the absorption index bands.	56
Table 3.4	Spectroscopist average absorption index peak heights, k_{max}	57
Table 3.5	Overall average areas under the absorption index bands.....	59
Table 3.6	Overall average peak heights in the absorption index spectra	60
Table 3.7	Absorption indices between 6500 and 800 cm^{-1} for liquid dichloromethane at 25 °C	62
Table 3.8	Real refractive index between 6500 and 800 cm^{-1} of liquid dichloromethane at 25 °C	65

Table 3.9	Molar absorption coefficients between 6500 and 800 cm^{-1} of liquid dichloromethane at 25 $^{\circ}\text{C}$	68
Table 3.10	Overall average areas under molar absorption coefficient bands of liquid dichloromethane at 25 $^{\circ}\text{C}$	70
Table 3.11	Overall average peak heights in the molar absorption coefficient spectrum of liquid dichloromethane at 25 $^{\circ}\text{C}$	71
Table 4.1	Different definitions of the reflection coefficient, \hat{r}_s , and dielectric constant, $\hat{\epsilon}$, the phase shift for s-polarised light, θ_s	82
Table 4.2	Classical Damped Harmonic Oscillator Parameters for Simulated Spectra of "Benzene" and "Methanol"	91
Table 5.1	Peak Height and Integrated Intensity of the OH Stretching $\tilde{\nu}$ and of H_2O (ℓ) at 25 $^{\circ}\text{C}$	131
Table 5.2	Imaginary refractive indices between 4154.88 and 1 cm^{-1} of liquid water at 25 $^{\circ}\text{C}$	147
Table 5.3	Real refractive indices between 15000 and 1 cm^{-1} of liquid water at 25 $^{\circ}\text{C}$	149
Table 5.4	Molar absorption coefficients between 15000 and 1 cm^{-1} of liquid water at 25 $^{\circ}\text{C}$	151
Table 6.1	The volumes used to make 50 grams of $\text{CH}_3\text{CN}+\text{H}_2\text{O}$ mixture solution	160
Table 6.2	Properties of $\text{H}_2\text{O}+\text{CH}_3\text{CN}$ mixtures ¹⁵	162
Table 6.3	Imaginary refractive indices between 8000.25 and 700 cm^{-1} of liquid mixture water-acetonitrile with $x_{\text{CH}_3\text{CN}}=0.20$ at 25 $^{\circ}\text{C}$	166
Table 6.4	Imaginary refractive indices between 8000.25 and 700.0 cm^{-1} of liquid water-acetonitrile with $x_{\text{CH}_3\text{CN}}=0.50$ at 25 $^{\circ}\text{C}$	167
Table 6.5	Imaginary refractive indices between 8000.25 and 700.0 cm^{-1} of liquid water-acetonitrile with $x_{\text{CH}_3\text{CN}}=0.70$ at 25 $^{\circ}\text{C}$	168
Table 6.6	Imaginary refractive indices between 8000.25 and 700.0 cm^{-1} of liquid acetonitrile at 25 $^{\circ}\text{C}$	169
Table 6.7	Real refractive indices between 8000.25 and 700 cm^{-1} of liquid mixture water -acetonitrile with $x_{\text{CH}_3\text{CN}}=0.20$ at 25 $^{\circ}\text{C}$	170

Table 6.8	Real refractive indices between 8000.25 and 700.0 cm^{-1} of liquid water-acetonitrile with $x_{\text{CH}_3\text{CN}}=0.50$ at 25 °C.....	171
Table 6.9	Real refractive indices between 8000.25 and 700.0 cm^{-1} of liquid water-acetonitrile with $x_{\text{CH}_3\text{CN}}=0.70$ at 25 °C.....	172
Table 6.10	Real refractive indices between 8000.25 and 700.0 cm^{-1} of liquid acetonitrile at 25 °C.....	173
Table 6.11	The areas under the OH and CN stretching bands and the fractions of H-bonded CN groups and of O-H...O bonded and non bonded OH groups.	184
Table 6.12	The integrated Intensities and Dipole Moment Derivatives of the O-H and $\text{C}\equiv\text{N}$ Stretching Vibrations in $\text{CH}_3\text{CN}+\text{H}_2\text{O}$ mixture at 25 °C.....	199

List of Figures

Figure 1.1	Refractive index spectra between 4000 and 700 cm^{-1} of liquid water at 25 °C	5
Figure 1.2	Three different spectra between 4000 and 700 cm^{-1} of liquid water at 25 °C. Top box: Molar absorption coefficient $\epsilon_m(\tilde{\nu})$, Middle box: Imaginary molar polarizability $\alpha''_m(\tilde{\nu})$; Bottom box: $\tilde{\nu}\alpha'_m(\tilde{\nu})$	8
Figure 1.3	Schematic of a transmission cell. I_o is the incident energy flux, I_r is the reflected energy flux and I_t the transmitted energy flux.	11
Figure 1.4	Two simulated spectra between 4000 and 700 cm^{-1} of liquid water at 25 °C. Top box: $EA(\tilde{\nu})$ with CaF_2 as window and $d=10\mu\text{m}$. Bottom box: pATR($\tilde{\nu}$) with ZnSe as rod and $\text{NRF}=3$	12
Figure 1.5	Schematic of an ATR CIRCLE cell.	15
Figure 2.1	A real refractive index spectrum of a colorless liquid, based approximately on that of benzene. The visible and near infrared region is expanded in the lower box.	24
Figure 2.2	The contribution Δn_{IR} to the visible refractive index from infrared absorption between 8000 and 500 cm^{-1} (C_6H_6), 2 cm^{-1} (CH_3OH) or 10 cm^{-1} (H_2O). The points \square , Δ , and O were calculated from the infrared imaginary refractive index spectra through the Kramers-Kronig transform, Eq. (2.5). The solid and dashed lines are the functions $-\frac{a_{-2}}{\tilde{\nu}^2}$ and $-\frac{a_{-2}}{\tilde{\nu}^2} - \frac{a_{-4}}{\tilde{\nu}^4}$, respectively, with the experimental values of the parameters a_{-2} and a_{-4} taken from Table 2.2.	35
Figure 3.1	Average areas under the absorption index spectra (dots) and their 95% confidence limits (vertical error bars) for the five spectroscopists in three spectral regions from Table 3.3. Also shown for each region above the label 'Average' is the unweighted average area from Table 3.5 (dot) and the maximum deviation from it.	55

Figure 3.2	Absorption index (imaginary refractive index), k , spectrum between 6500 and 800 cm^{-1} of dichloromethane at 25°C. The ordinate labels are for the lower spectrum in each box; they must be divided by 75 or 10, as shown, for the upper spectrum in the box.....	61
Figure 3.3	Real refractive index, n , spectrum between 6500 and 800 cm^{-1} of dichloromethane at 25°C.....	64
Figure 3.4	Molar absorption coefficient, E_m , spectrum between 6500 and 800 cm^{-1} of dichloromethane at 25°C. The ordinate labels are for the lower spectrum in each box; they must be divided by 75 or 10, as shown, for the upper spectrum in the box.	67
Figure. 4.1	The simulated refractive index spectra of liquid methanol, 7800 to 2 cm^{-1} . Lower box: k , Upper box: n	92
Figure 4.2	The simulated refractive index spectra of liquid benzene, 8000 to 2 cm^{-1} Lower box: k , Upper box: n	93
Figure 4.3	The simulated single-reflection pATR spectra of methanol calculated for the CIRCLE cell (Eq. 4.14.) with different sets of n_o values. Lower box: constant $n_o=2.38$, approximates ZnSe; Middle box: $n_o(\tilde{\nu})$ values of ZnSe; Upper box: $n_o(\tilde{\nu})$ values of Si. Note that the spectrum in the middle box stops at 700 cm^{-1}	96
Figure 4.4	The simulated single-reflection pATR spectrum of benzene calculated for the CIRCLE cell (Eq. 4.14) with Lower box constant $n_o=3.5$, approximates Si; Middle box: $n_o(\tilde{\nu})$ values of ZnSe; Upper box: $n_o(\tilde{\nu})$ values of Si. Note that the spectrum in the middle box stops at 700 cm^{-1}	97
Figure 4.5	The real refractive indices of Si ¹⁸⁻²⁰ and ZnSe ²¹ at room temperature 25°C.....	98
Figure 4.6	Results for the phase shift (top), imaginary refractive index (middle) and real refractive index (bottom) of "methanol" with constant $n_o = 2.38$ and recovered with constant phase correction. Curves a are Synthesized spectra; Curves b were recovered with Eqs. (4.3) and (4.19); Curves c were recovered with Eqs. (4.2) and (4.19); Curves d were recovered with Eqs. (4.17) and (4.19).	

	The curves a to d in the middle box, and a, c and d in the top and bottom boxes, overlap	103
Figure 4.7	Errors in the phase shifts and refractive indices of "methanol" with constant $n_o = 2.38$ and recovered with constant phase correction. Top box: Error in phase shift; <i>curve c</i> minus <i>curve a</i> of the top box of Fig. 4.6. Upper Middle box: Error in phase shift; <i>curve d</i> minus <i>curve a</i> of the top box of Fig. 4.6. Lower Middle box: % error in k from Eqs. (4.17) and (4.19); (<i>Curve d</i> minus <i>Curve a</i>) \div <i>Curve a</i> $\times 100\%$ from middle box of Fig. 4.6. Bottom box: % error in n from Eqs. (4.17) and (4.19); (<i>Curve d</i> minus <i>Curve a</i>) \div <i>Curve a</i> $\times 100\%$ from bottom box of Fig. 4.6.....	104
Figure 4.8.	Results for the phase shift (top), imaginary refractive index (middle) and real refractive index (bottom) of "methanol" with $n(\tilde{\nu})$ of Si, recovered with constant and with non-constant phase correction. In each box, C indicates the correct (synthesized) spectrum, R indicates recovery with Eqs. (4.17) and (4.19), and M indicates recovery with Eqs. (4.17) and (4.20).....	108
Figure 4.9	Results for the phase shift (top), imaginary refractive index (middle) and real refractive index (bottom) of "benzene" with $n(\tilde{\nu})$ of Si, recovered with constant and with non-constant phase correction. In each box, C indicates the correct (synthesized) spectrum, R indicates recovery with Eqs. (4.17) and (4.19), and M indicates recovery with Eqs. (4.17) and (4.20). All curves in the middle box, and curves C and M in the top and bottom boxes, overlap.....	109
Figure 4.10	Error in the phase shift (top) and percent errors in the imaginary refractive index (middle) and real refractive index (bottom) of "methanol" with $n(\tilde{\nu})$ of Si, recovered with non-constant phase correction, Eqs (4.17) and (4.20). Top Box: <i>Curve M</i> minus <i>Curve C</i> from the top box of Fig. 4.8. Middle box: % error in k from Eqs. (4.17) and (4.20); (<i>Curve M</i> minus <i>Curve C</i>) \div <i>Curve C</i> $\times 100\%$ from middle box of Fig. 4.8. Bottom box: % error in n from Eqs. (4.17) and (4.20); (<i>Curve M</i> minus <i>Curve C</i>) \div <i>Curve C</i> $\times 100\%$ from bottom box of Fig.4.8..	111

Figure 4.11	The effect of a truncated reflectance spectrum on the recovered phase shift (top), imaginary refractive index (middle) and real refractive index (bottom) spectrum of "methanol" on ZnSe. In each box, Curve M shows the errors or percent errors in the spectrum recovered with Eqs. (4.17) and (4.20), Curve PL shows smaller errors in the spectrum obtained from Curves M by refinement with the linear extension of the k spectrum, and Curve PC shows the very small errors in the spectrum obtained from Curves M by refinement with the exact extension of the k spectrum.	113
Figure 4.12	The integral contour on the complex frequency plane	118
Figure 5.1	Imaginary refractive index spectra of $H_2O(l)$ at $25 \pm 1^\circ C$ determined in this laboratory by calibrated multiple attenuated total reflection spectroscopy. Three spectra are shown. Two extend from 4000 to 1250 cm^{-1} and almost coincide. They were reported previously ^{1,8} from measurements with the long (6 cm) cell. The spectrum determined in this work with the short (3cm) cell extends from 4000 to 700 cm^{-1} and is the highest curve at the peak of the OH stretching band.	130
Figure 5.2	Imaginary refractive index spectra of $H_2O(l)$ between 15,000 and 3000 cm^{-1} determined by different workers. Top two boxes: Dashed line, Kou et al ¹¹ ($22^\circ C$); dotted line, Palmer and Williams ¹² ($27^\circ C$); crosses x, Hale and Query ¹³ ($25^\circ C$); plus sign +, Zolotarev and Demin ³ ($25^\circ C$). Bottom box, as in the other boxes except without Kou et al's spectrum and with: dotted line, Downing and Williams ⁶ ($27^\circ C$) instead of Palmer and Williams; dash-dotted line, this work by ATR ($25^\circ C$).	134
Figure 5.3	Imaginary refractive index spectra of $H_2O(l)$ between 3000 and 0 cm^{-1} determined by different workers. Top box: Dotted line, Downing and Williams ⁶ ($27^\circ C$); Crosses x, Hale and Query ¹³ ($25^\circ C$); Plus sign +, Zolotarev and Demin ³ ($25^\circ C$); Dash-dotted line, this work by ATR ($25^\circ C$); upper dashed line, This work by transmission ($25^\circ C$); Lower dashed line, Marley, Gaffney and Cunningham ¹⁵ (no temperature given). Middle box:	

	As top box except without this work by transmission. Bottom box: As in middle box except without Marley, Gaffney and Cunningham and with: dashed line, Zelsmann ¹⁶ (25°C); Open circle o, Afsar and Hasted ¹⁹ (19 °C); Solid line, Afsar and Hasted ²⁷ (25 °C).....	140
Figure 5.4	The recommended imaginary refractive index spectrum of H ₂ O(<i>l</i>) between 15000 and 1 cm ⁻¹ . For the upper two curves in the top box the ordinate labels must be divided by 100 or 3000 as shown.	146
Figure 5.5	The recommended real refractive index spectrum of H ₂ O(<i>l</i>) between 15000 and 1 cm ⁻¹	148
Figure 5.6	The recommended molar absorption coefficient spectrum of H ₂ O(<i>l</i>) between 15000 and 1 cm ⁻¹ . For the upper two curves in the top box the ordinate labels must be divided by 100 or 3000 as shown.	150
Figure 6.1	Imaginary refractive index spectra of five CH ₃ CN+H ₂ O mixtures at 25 °C: a x _{CH₃CN} =0.0; b x _{CH₃CN} =0.20; c x _{CH₃CN} =0.50; d x _{CH₃CN} =0.70; e x _{CH₃CN} =1.00.....	164
Figure 6.2	Real refractive index spectra of five CH ₃ CN+H ₂ O mixtures at 25 °C: a x _{CH₃CN} =0.0; b x _{CH₃CN} =0.20; c x _{CH₃CN} =0.50; d x _{CH₃CN} =0.70; e x _{CH₃CN} =1.00.....	165
Figure 6.3	$\tilde{\nu}\alpha''_m(\tilde{\nu})$ spectra of five CH ₃ CN+H ₂ O mixtures at 25 °C: a x _{CH₃CN} =0.0; b x _{CH₃CN} =0.20; c x _{CH₃CN} =0.50; d x _{CH₃CN} =0.70; e x _{CH₃CN} =1.00.....	176
Figure 6.4	The areas under the $\tilde{\nu}\alpha''_m(\tilde{\nu})$ spectra in the CH ₃ deformation (top box) and CH ₃ rocking (bottom box) regions for thirteen CH ₃ CN+H ₂ O mixtures at 25 °C. The baseline was a straight line through the curve at the integration limits. The integration limits are shown and the error bars show the maximum deviations. The straight lines show the behaviour expected for an ideal solution	179
Figure 6.5	The areas under the $\tilde{\nu}\alpha''_m(\tilde{\nu})$ spectra of thirteen CH ₃ CN+H ₂ O mixtures at 25 °C in the O-H stretching region between 4000 and 2660 cm ⁻¹ . The C-H stretching contribution has been removed as described in the text. The error bars are the 95% confidence limits.	

	The straight line shows the behaviour expected for an ideal solution.....	182
Figure 6.6	The areas under the $\tilde{\nu}\alpha''_m(\tilde{\nu})$ spectra of thirteen CH ₃ CN+H ₂ O mixtures at 25 °C in the C≡N stretching region 2275-2210 cm ⁻¹ : (Δ) indicates the total area, (x) indicates the area corrected for the water contribution by the first method described in the text, (o) indicates the area corrected for the water contribution by the second method described in the text, (●) the final areas used. The error bars are the 95% confidence limits. The straight line shows the behaviour expected for an ideal solution..	183
Figure 6.7	The percentages of acetonitrile molecules in water-acetonitrile mixtures that are free (o) and H-bonded (●).....	188
Figure 6.8	The percentage of free (o), water bonded (▲), acetonitrile bonded (Δ), and total hydrogen bonded O-H groups (●) as functions of composition.	192

List of Symbols

General

λ	Vacuum wavelength.
$\tilde{\nu}$	Vacuum wavenumber; usual unit cm^{-1} . $\tilde{\nu} = 1/\lambda$
c	Velocity of light in vacuum.
C	Molar concentration; usual unit mole L^{-1} .
V_m	Molar volume; usual unit $\text{cm}^3 \text{mole}^{-1}$.
\wedge	used to indicate a complex quantity.
i	$\sqrt{-1}$

Wavenumber dependent Quantities

$\hat{n}(\tilde{\nu})$	Complex refractive index, $\hat{n}(\tilde{\nu}) = n(\tilde{\nu}) + i k(\tilde{\nu})$.
$n(\tilde{\nu})$	Real refractive index.
$k(\tilde{\nu})$	Imaginary refractive index, also called the absorption index.
$\hat{\epsilon}(\tilde{\nu})$	Complex dielectric constant, $\hat{\epsilon}(\tilde{\nu}) = \epsilon'(\tilde{\nu}) + i \epsilon''(\tilde{\nu})$.
$\epsilon'(\tilde{\nu})$	Real dielectric constant.
$\epsilon''(\tilde{\nu})$	Imaginary dielectric constant.
$\hat{\alpha}_m(\tilde{\nu})$	Complex molar polarizability, $\hat{\alpha}_m(\tilde{\nu}) = \alpha'_m(\tilde{\nu}) + i \alpha''_m(\tilde{\nu})$
$\alpha'_m(\tilde{\nu})$	Real molar polarizability.
$\alpha''_m(\tilde{\nu})$	Imaginary molar polarizability
$E_m(\tilde{\nu})$	(Decadic) molar absorption coefficient; usual unit $\text{cm}^2 \text{mole}^{-1}$.
$K(\tilde{\nu})$	(Decadic) linear absorption coefficient; usual unit cm^{-1} .

Integrated Intensity Quantities

A_j	Area under band j in 2.303 E_m spectrum; usual unit km mole^{-1} .
C_j	Area under band j in $\tilde{\nu} \alpha''_m(\tilde{\nu})$ spectrum; usual unit km mole^{-1} .

Molecular Properties

μ_j Magnitude of dipole moment derivative with respect to normal coordinate j ; usual unit Debye Å⁻¹ amu^{-1/2}.

Table of Contents

Chapter 1 Introduction	1
1.1 The Absolute Intensities of the IR Spectrum	3
1.2 Transmission Method.....	10
1.3 Attenuated Total Reflection (ATR) Method	15
1.4 Water and its mixture with acetonitrile	18
1.5 References	20
 Chapter 2 The Refractive Index of Colourless Liquids in the Visible and Infrared: Contributions from the Absorption of Infrared and Ultraviolet Radiation and the Electronic Molar Polarizability below 20,500 cm ⁻¹	22
2.1 Introduction.....	22
2.2 Equations.....	26
2.3 Compounds and Data.....	28
2.3.1 Determination of Experimental Values of the Coefficient a_2 in Equation (2.3).....	32
2.4 Results	36
2.4.1 Equations 2.2, 2.2a and 2.3 Fitted to the Visible Refractive Indices	36
2.4.2 Correction of the Published Infrared Real Refractive Indices	40
2.4.3 The Electronic Polarizability Between 0 and 25000 cm ⁻¹	41
2.5 Summary	42
2.6 Appendix: Expansion of the Kramers-Kronig transform	43
2.7 References:	45
 Chapter 3 Infrared Intensities of Liquids XVIII: Accurate Optical Constants and Molar Absorption Coefficients Between 6500 and 800 cm ⁻¹ of Dichloromethane at 25°C, from Spectra Recorded in Several Laboratories	48
3.1 Introduction.....	48
3.2 Methods and Results.....	49
3.2.1 Absorption Index Spectrum.....	51
3.2.2 The Real Refractive Index Spectrum.	63

3.2.3 The Molar Absorption Coefficient Spectrum.....	66
3.3 The Accuracy of the Results	66
3.3.1 Accuracy of Absorption Indices, k , and Molar Absorption Coefficients, E_m	69
3.3.2 Accuracy of Areas.....	73
3.3.3 Accuracy of Real Refractive Indices.....	74
3.4 Summary	74
3.5 References.....	75

Chapter 4 An Accurate Modified Kramers-Kronig Transformation from Reflectance to Phase Shift on Attenuated Total Reflection.....	77
4.1 Introduction.....	77
4.2 Method	88
4.2.1 The Simulated Optical Constant Spectra.....	88
4.2.2 Calculation of Phase Shift, Reflectance R_s and ATR from Simulated Optical Constants, n and k	90
4.2.3 The Equations Used to Recover Optical Constants from Reflectance R_s and Phase Shifts θ_s	99
4.2.4 The Transformation of R_s to θ_s	99
4.3 Results and Discussion.....	102
4.3.1 Constant Phase Shift Correction.....	102
4.3.2 Non-Constant Phase Shift Correction.....	107
4.3.3 The Use of Experimental pATR Spectra.....	112
4.4 Conclusion.....	115
4.5 Appendix.....	117
4.5.1 Conditions for the KK Transform.....	117
4.5.2 Derivation of a New Modified Kramers-Kronig Transform between the Reflectance and the Phase Shift on Reflection.....	118
4.6 References.....	119

Chapter 5 Infrared Intensities of Liquids XX: The intensity of the OH stretching band of liquid water revisited, and the best current values of the optical constants of $H_2O(\ell)$ at 25°C between 15,000 and 1 cm^{-1}.....	121
5.1 Introduction.....	121
5.2 Methods and Results.....	125
5.2.1 Experimental and Computational Improvements.....	125

5.2.2 Exploration of the Non-Reproducibility of the OH Stretching Band	126
5.2.3 Recent Spectra with Improved Methods	128
5.2.4 Comparison with Our Previous Spectra	129
5.2.5 Dipole Moment Derivatives of $\text{H}_2\text{O}(\ell)$	132
5.3 The Best Current Refractive Index Spectra of Water at 25°C	133
5.3.1 The Region 15000 to 4000 cm^{-1}	133
5.3.2 The Region 4000 to 3715 cm^{-1}	136
5.3.3 The Region 3715 to 2982 cm^{-1}	138
5.3.4 The Region 2982 to 2800 cm^{-1}	139
5.3.5 The Region 2800 to 2320 cm^{-1}	139
5.3.6 The Region 2320 to 713 cm^{-1}	141
5.3.7 The Region 713 to 590 cm^{-1}	142
5.3.8 The Region 590 to 30 cm^{-1}	142
5.3.9 The Region 30 to 10 cm^{-1}	144
5.3.10 The Region 10 to 6 cm^{-1}	144
5.3.11 The Region 5 to 1 cm^{-1}	144
5.3.12 The Recommended k and n Spectra	145
5.4 The Effect of Temperature	145
5.5 Conclusions	152
5.6 References	153

Chapter 6 The Absolute Intensities of Infrared Spectra of Water-Acetonitrile Mixtures at 25°C and their Application to Investigate the Structure of the Mixtures.	156
6.1 Introduction.....	156
6.2 Experimental.....	159
6.3 Intensity Quantities	161
6.4 Results and Discussion.....	175
6.4.1 The band shapes and peak positions in the $\tilde{\nu}\alpha_m''$ spectra.....	175
6.4.2 Area C_j under bands in the $\tilde{\nu}\alpha_m''$ spectrum	177
6.4.3 The Methyl Group Vibrations of Acetonitrile	178
6.4.4 The Areas under the $\tilde{\nu}\alpha_m''$ Spectra in the O-H Stretching Region.....	180

6.4.5 The areas under the $\tilde{\nu}\alpha''_m$ spectra in the C \equiv N stretching region...	181
6.4.6 The population of hydrogen bonded acetonitrile	185
6.4.7 The Population of Water and Acetonitrile Bonded O-H Groups	187
6.4.8 Discussion.....	193
6.4.9 The bond moments.....	198
6.5 Conclusions	200
6.6 References:	200

Chapter 7 Conclusion	203
----------------------------	-----

Chapter 1 Introduction

Infrared spectroscopy has been one of the most useful analysis methods for chemists for 40 years. However, its application is usually limited to the frequency or wavenumber information contained in the spectra because of the difficulty of determining accurate intensity information and the lack of a model to correlate the intensity information with the structure of the sample. This thesis describes work done to obtain accurate absolute intensities in infrared spectra, to develop a method to convert infrared spectra to fundamental measures of intensity, and to apply the resulting intensities to obtain scientific information in practically useful cases.

The absolute intensities in an infrared spectrum result from the redistribution of electrons in molecules caused by the atomic displacement during molecular vibrations. Like the wavenumbers at which molecules absorb, the intensities of absorption are properties of the sample. Therefore, they should be independent of the experimental conditions under which the spectrum is measured. The developments over the past 20 years in Fourier Transform Infrared (FTIR) spectroscopy and computers now make it possible for spectroscopists to measure very precise infrared spectra. Thus intensities can be measured very precisely, but it is still not easy to determine their accuracy. Accordingly, it is desirable to have intensity standards to help spectroscopists obtain accurate infrared intensity by calibrating their instrument and experiment. Work to develop absolute intensity standards is described in Chapter 3 of this thesis, with liquid dichloromethane as the compound.

The infrared spectra measured by a spectrometer are specific to the particular experiment. Thus the peak wavenumbers in transmission spectra do not coincide with those in attenuated total reflection, ATR, spectra, and the loss of intensity due to reflection from the cell windows affects transmission spectra in a way that is absent from reflection and ATR spectra. Thus fast and accurate procedures are required to correct the measured spectra for experiment-specific features and to convert them to fundamental properties of the sample. A new procedure to achieve this for ATR spectra is described in Chapter 4.

In the long term it is desired to make the intensity information in a spectrum as useful to scientists as the wavenumber information. To explore this, one application of absolute infrared intensities is described in Chapter 6. The system selected for this purpose is the liquid water-acetonitrile mixture which is interesting to both theoretical and experimental chemistry.

Water is perhaps the most important chemical. Several quantitative studies of liquid water have been made of its ability to absorb infrared radiation. Chapter 5 of the thesis describes measurements of the absolute infrared absorption intensities of water between 4000 and 700 cm^{-1} , and examines the recent literature to recommend values of the absorption intensities of liquid water at 25 °C between 15000 and 1 cm^{-1} . Probable errors in the intensity quantities are presented, based on the quality of the spectra and agreement between different workers.

All of the methods used to convert experimental infrared spectra to fundamental intensity properties of the sample require a knowledge of the real refractive index of the

sample at high infrared wavenumbers, usually, about 8000 cm^{-1} . Until recently, it was the practice to use the real refractive index measured at sodium D line (16965 cm^{-1}) for this purpose. However, the real refractive index varies markedly with wavenumber below 16965 cm^{-1} . So an improved method of determining the real refractive index at about 8000 cm^{-1} is required for work of good accuracy. Such a method is described in Chapter 2 of this thesis. In fact, the best procedure requires knowledge of the infrared absorption intensities to improve the accuracy of the value at 8000 cm^{-1} , so a two stage procedure is required, and is described.

In this chapter the exact meaning of absolute intensities is discussed in section 1.1. Then, follow the description of the measurement of intensities by the transmission method in section 1.2, and by the attenuated total reflection (ATR) method in section 1.3. Finally, the background to the application of the absolute intensities to water and its mixtures is presented in section 1.4.

1.1 The Absolute Intensities of the IR Spectrum

As has been noted above, there are many different types of infrared spectrum. The type obtained depends on whether the interaction of the radiation with the sample is measured by transmission, reflection, ATR, or other sampling method. Further, for each of these types of experiment several types of spectrum can be calculated, and the type used depends on which is most convenient for the specific purpose. For example, from a transmission experiment it may be best to look at a transmittance spectrum, or an absorbance spectrum, or a spectrum of the Beer-Lambert absorption coefficient.

Absolute infrared absorption intensities can be calculated from any well defined infrared experiment and it is necessary to describe them by a fundamental intensity quantity that is independent of the experiment used for the measurement. The spectra of the complex refractive index, $\hat{n}(\tilde{\nu}) = n(\tilde{\nu}) + i k(\tilde{\nu})$, are the fundamental quantities that are first calculated from the experimental spectrum in this laboratory. Here $n(\tilde{\nu})$ is the real part of the refractive index and $k(\tilde{\nu})$ is the imaginary part.

If the spectra of the real and imaginary refractive indices are known, all other types of infrared spectra can be calculated. In particular any experimental infrared spectrum can be calculated to the extent that the experimental geometry is well defined. Conversely, the spectra of the real and imaginary refractive indices can be calculated from any well defined infrared experiment. The imaginary refractive index $k(\tilde{\nu})$ is a measure of the absorption ability of a sample at wavenumber $\tilde{\nu}$. Therefore, it is also called the absorption index. The real refractive index, $n(\tilde{\nu})$, is usually called the refractive index. It determines the phase shift of the light wave traveling in the sample. As examples, the k and n spectra of liquid water in the IR region are presented in figure 1.1.

The variation of the n spectrum with wavenumber is a consequence of the absorption of light by the sample. Therefore, the k and n spectra are related to each other by the dispersion relations, which are also called the Kramers-Kronig transforms. In the IR region, it is relatively easier to measure the k spectrum of a liquid.

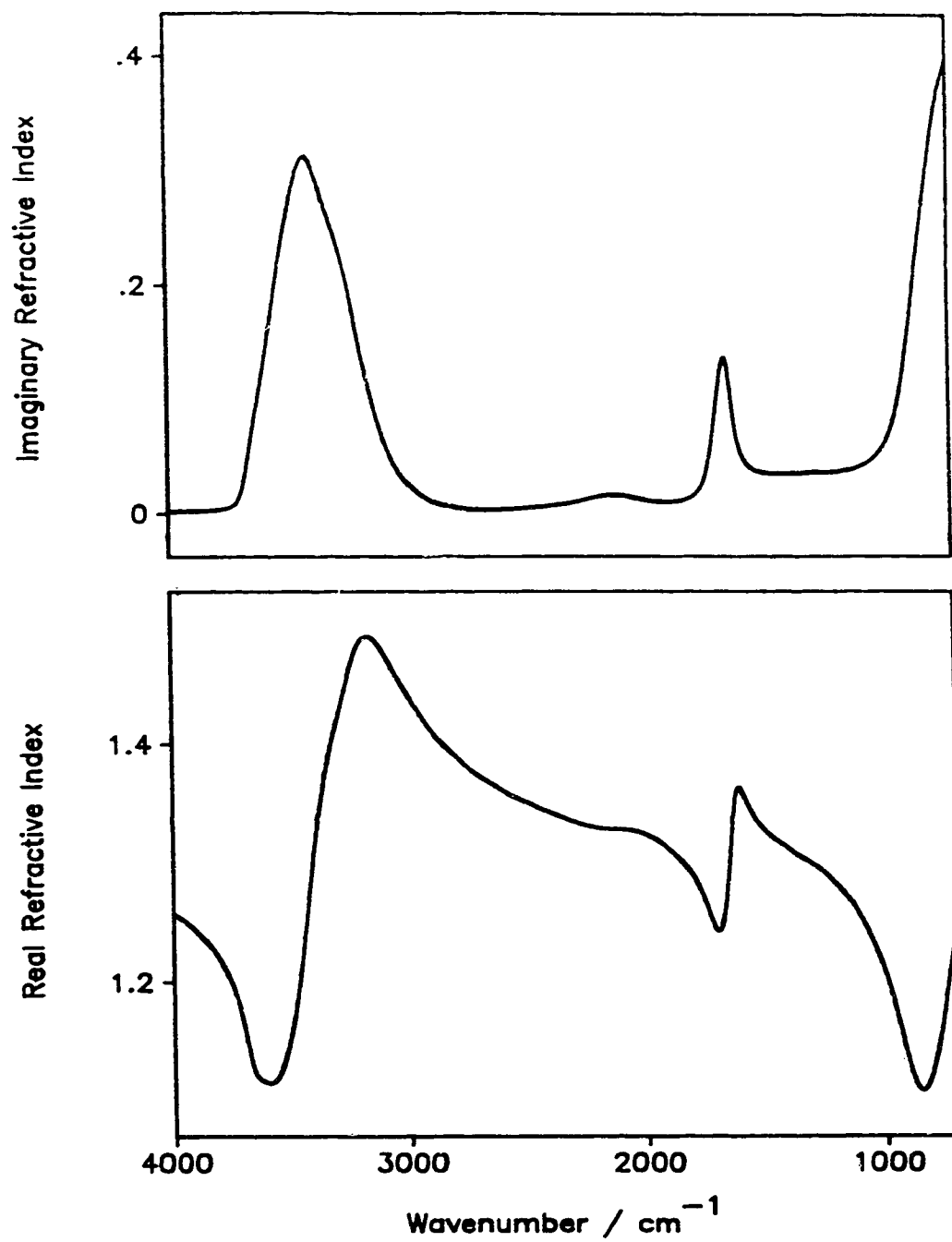


Figure 1.1 Refractive index spectra between 4000 and 700 cm^{-1} of liquid water at 25 °C

Accordingly, the corresponding n spectrum is calculated by the Kramers-Kronig (KK) transform ⁶

$$n(\tilde{\nu}_a) = n_{el}(\tilde{\nu}_a) + \frac{2}{\pi} P \int_0^{\tilde{\nu}_{\max}} \frac{\tilde{\nu} k(\tilde{\nu}) d\tilde{\nu}}{\tilde{\nu}^2 - \tilde{\nu}_a^2} \quad (1.1)$$

where P means the principal value of the integral. $\tilde{\nu}_{\max}$ is the high wavenumber limit of the measured spectrum and is taken well above the significant absorption in the infrared region and well below the significant absorption in the visible or ultraviolet region.

$\tilde{\nu}_{\max}$ is 8000 cm^{-1} in this work.

The real refractive index $n_{el}(\tilde{\nu}_a)$ is determined by electronic absorption in the ultraviolet (UV) region for a colorless sample because the integration is over the near IR, IR and far IR regions ⁷. Thus, $n_{el}(\tilde{\nu}_a)$ is different from the real refractive index measured experimentally at wavenumber $\tilde{\nu}_a$. From the values reported for the visible region, $n_{el}(\tilde{\nu}_a)$ can be obtained by a fitting procedure. In Chapter 2, the principle used for the calculation is described and the method is applied to ten common pure liquids. The determined electronic contributions to the refractive index are presented and discussed in that chapter.

Another type of infrared spectrum that is often used, particularly by analytical spectroscopists, is the molar absorption coefficient spectrum. This is usually defined as

$$E_m(\tilde{\nu}) = \frac{-1}{Cd} \log_{10} I(\tilde{\nu}) / I_o(\tilde{\nu}) \quad (1.2)$$

where I and I_o are the transmitted and incident intensities, d is the path length through

the sample and C is the molar concentration of the sample. It can be shown from electromagnetic theory that $E_m(\tilde{\nu})$ is related to k by

$$E_m(\tilde{\nu}) = \frac{4\pi\tilde{\nu}k(\tilde{\nu})}{2.303C} \quad (1.2a)$$

$E_m(\tilde{\nu})$ is the absorbance spectrum produced by unit molar concentration of sample in unit path length. Like the refractive indices, it is an intensive property. The E_m spectrum of liquid water is displayed in the top box of figure 1.2.

The refractive indices and the molar absorption coefficient are all macroscopic properties of the liquid. They reflect the properties of the molecules in the liquid and their short-range interactions, but they also reflect long-range effects that arise from the polarization of the liquid by the oscillating dipoles that absorb the infrared radiation. These long-range effects are conveniently referred to as macroscopic dielectric effects. These macroscopic dielectric effects change when the composition of, say, a binary mixture is changed, with the consequence that the spectral differences observed for different mixtures are partly due to the different dielectric effects and partly due to changes in the short-range environment of the molecules. It is the short-range environment that is of interest to chemists, so it is desirable to use spectra of a quantity that does not include the macroscopic dielectric effects.

There is no exact solution to this problem, but there is a solution that is very simple and can be shown to be effective. To sample the short-range environment, it is necessary to know the (average) local electric field that acts on each molecule in the liquid and to see how this polarizes the molecule through the (mean) molecular

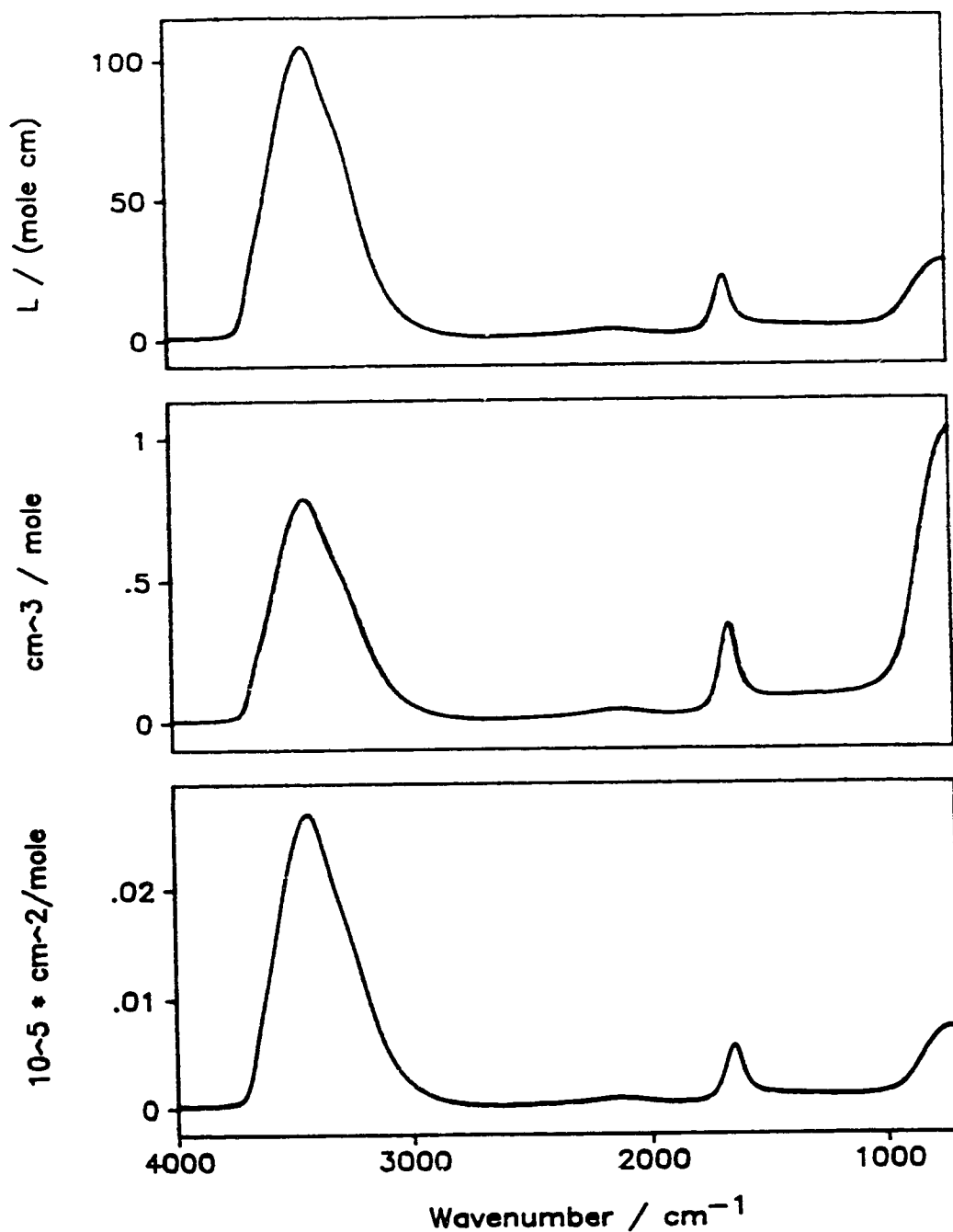


Figure 1.2 Three different spectra between 4000 and 700 cm^{-1} of liquid water at 25 °C. Top box: Molar absorption coefficient $E_m(\tilde{\nu})$, Middle box: Imaginary molar polarizability $\alpha''_m(\tilde{\nu})$; Bottom box: $\tilde{\nu}\alpha''_m(\tilde{\nu})$.

polarizability $\hat{\alpha}(\tilde{\nu})$. The Lorentz local field ⁸ provides a simple expression for calculating this from the macroscopic electric field of the radiation and relates the molar polarizability (or the mean molecular polarizability) to the refractive index through the Lorentz relation:

$$\hat{\alpha}_m = \frac{3V_m}{4\pi} \frac{\hat{n}^2 - 1}{\hat{n}^2 + 2} \quad (1.3)$$

where V_m is molar volume of the sample.

The polarizability in eq. (1.3) is a complex quantity $\hat{\alpha}_m(\tilde{\nu}) = \alpha'_m(\tilde{\nu}) + i\alpha''_m(\tilde{\nu})$. Its imaginary part describes the absorption of radiation and the real part describes the polarization of the molecule. Thus, eq. (1.3) applies to all wavenumbers and to absorbing samples as well as its usual application to non-absorbing samples.

In practical application, the spectrum of the imaginary part, $\alpha''_m(\tilde{\nu})$, and the $\tilde{\nu}\alpha''_m$ spectrum ⁸ are used for the study of the interaction between molecules in the liquid phase. Again, with liquid water as the example, α''_m and $\tilde{\nu}\alpha''_m$ spectra are displayed in the bottom boxes of figure 1.2.

The α''_m , E_m and k spectra look the same qualitatively. In fact there are considerable differences between them. The peak wavenumbers and the band shapes are different in the three spectra. This is illustrated for the O-H stretching band in figure 1.2. Two points should be noted.

First, the peak wavenumber, $\tilde{\nu}_{\text{MAX}}$ in the α''_{m} spectrum is the wavenumber of the mechanical oscillator according to the Classical Damped Harmonic Oscillator, CDHO, theory. It differs from the peak wavenumbers in the k and E_{m} spectra, which depend on the wavenumber of the mechanical oscillator and also on the absorption intensity of the band. The greater the intensity the larger the difference from $\tilde{\nu}_{\text{MAX}}$ in the α''_{m} spectrum.

Second, the band in the α''_{m} spectrum is essentially symmetric. The bands in the E_{m} and k spectra are definitely asymmetric, each with a tail to high wavenumbers. Clearly analysis of the spectrum is simpler with the undistorted bands of the α''_{m} spectrum, and the α''_{m} spectrum is preferred for this reason as well as because it gives the correct wavenumber of the mechanical oscillator. More detailed discussion about this point is given in Chapter 6. Therefore, the imaginary polarizability spectrum is used in this work to obtain physico-chemical information about the liquid phase.

1.2 Transmission Method

The conventional method to measure IR spectra is by transmission. Figure 1.3 illustrates this method. The light passes through the cell window and the sample at 0° incidence, then reaches the detector.

The basic spectroscopic measurement is the transmittance, $t(\tilde{\nu})$, of the sample and cell. This is the ratio $t(\tilde{\nu}) = (I(\tilde{\nu})/I_0(\tilde{\nu}))$ of the radiant intensity transmitted through the sample and cell to that incident on cell. The corresponding decadic absorbance is

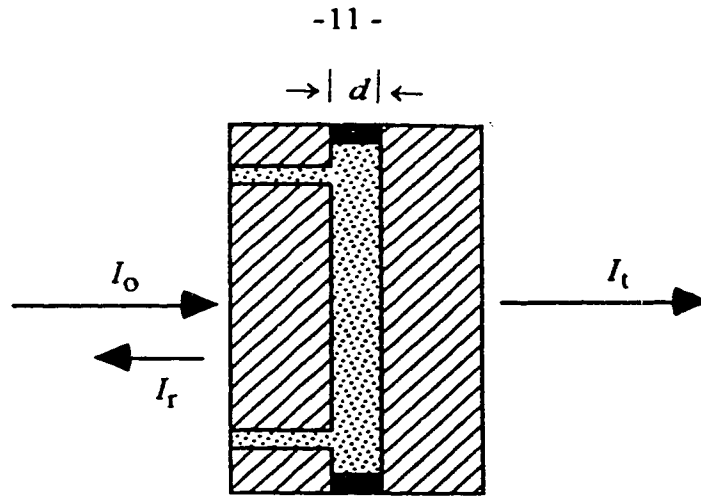


Figure 1.3 Schematic of a transmission cell. I_o is the incident energy flux, I_r is the reflected energy flux and I_t the transmitted energy flux.

$$EA(\tilde{\nu}) = -\log_{10}(I_r(\tilde{\nu})/I_o(\tilde{\nu})) = -\log_{10} t(\tilde{\nu}) \quad (1.4)$$

An EA spectrum of liquid water that was calculated from the known refractive indices for a cell with CaF_2 windows and $10 \mu\text{m}$ path length is presented in the upper box of figure 1.4. The OH stretching peak is too intense to measure, and a path length of about $1 \mu\text{m}$ would be needed to measure it well. Such a cell is extremely difficult to make and use, which illustrates the limitation of the transmission method for the measurement of samples with very strong absorption.

EA spectrum is different from the absorbance, $A(\tilde{\nu})$, spectrum which is defined as the absorption by the sample only, because of the radiant intensity lost on the cell windows. According to Fresnel equations¹, the reflected light and the multiple reflection effect at each interface can be calculated^{3,9}, provided that the real refractive

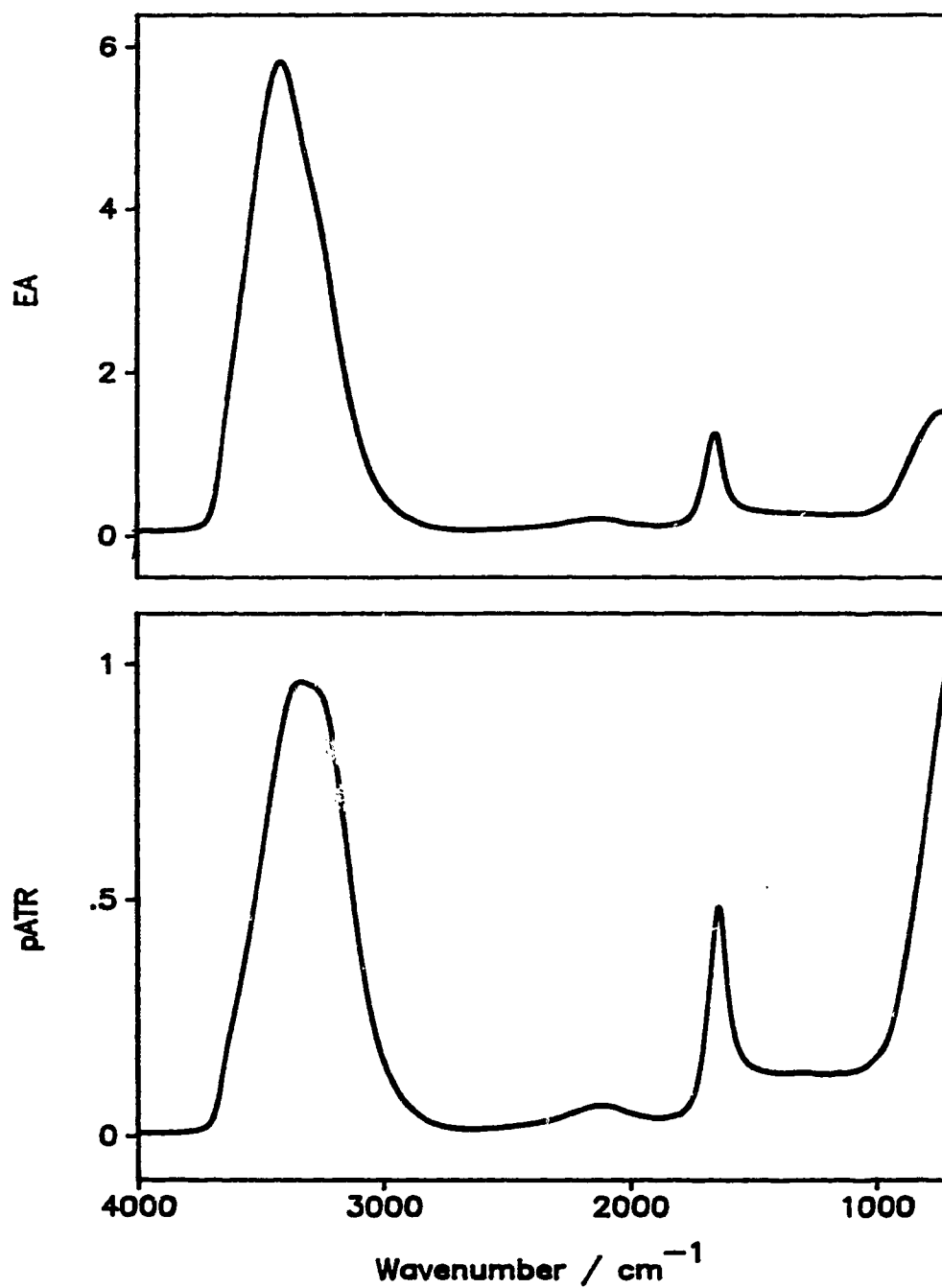


Figure 1.4 Two simulated spectra between 4000 and 700 cm⁻¹ of liquid water at 25 °C. Top box: $EA(\tilde{\nu})$ with CaF₂ as window and $d=10\mu\text{m}$. Bottom box: $pATR(\tilde{\nu})$ with ZnSe as rod and NRF=3

indices of the window and the sample are known. Therefore, the absorbance, $A(\tilde{\nu})$ of the sample can be determined from the experimentally measured spectrum $EA(\tilde{\nu})$. The equations used for the calculation can be found in the references cited.^{3,9}

From electromagnetic theory the absorbance $A(\tilde{\nu})$ of the sample is related to the absorption index $k(\tilde{\nu})$ by equation (1.5)

$$A(\tilde{\nu}) = \frac{4\pi\tilde{\nu}k(\tilde{\nu})d}{2.303} \quad (1.5)$$

Also, it is related to the molar absorption coefficient defined in eq. (1.2) as

$$A(\tilde{\nu}) = C d E_m(\tilde{\nu}) \quad (1.5a)$$

and linear absorption coefficient $K(\tilde{\nu})$ as

$$K(\tilde{\nu}) = 2.303 A(\tilde{\nu})/d \quad (1.6)$$

where d is the path length through the sample and C is the molar concentration of the sample.

In order to measure intensity well in this laboratory, the EA spectrum is measured with an FTIR spectrometer and the cell thickness is adjusted to give peak EA values between 0.5 and 2^{3,9,10}. Accordingly, the intensities in the baseline of the spectra are too weak to measure accurately. A baseline correction method was developed by Bertie, Keefe and Jones^{3,9} to improve the accuracy of the spectra. They proposed that two wavenumbers called anchor points be chosen in the baseline at each side of the band being measured. The experimental absorbances can be measured accurately at these anchor points by using very thick cells. From them, the absorbance per unit path length can be calculated after correcting for the reflection at the window

surfaces and the path length of the cell. The anchor points are then taken as references when processing spectra in cells of normal thickness because their absorbances can be calculated from the known path length. The difference between the experimental absorbance and that calculated at the anchor points is found, and the experimental absorbance spectrum is corrected by subtracting this difference, linearly interpolated between the anchor points.

Once the baseline-corrected absorbance spectrum is known, the approximate imaginary refractive index spectrum of the sample is determined by equation (1.5) and, the real refractive index spectrum is calculated from it by equation (1.1). The EA spectrum is then calculated from these initial k and n spectra and compared with the experimental spectrum. The k spectrum is then adjusted, the n spectrum is recalculated, and the process iterated until the k and n spectra converge.

Overall, the transmission measurement is simple and precise if the sample does not have very strong absorption in the region examined. However, the refining procedure is complex. Therefore, it is desirable to have secondary intensity standards for spectroscopists to use to calibrate their measurement of absorption intensities. In 1993 the International Union of Pure and Applied Chemistry (IUPAC) ¹¹ approved 43 bands from four liquids as secondary intensity standards. Dichloromethane (CH_2Cl_2) is one of the liquids. Chapter 3 describes the measurement of the absolute infrared intensities of dichloromethane at 25 °C by the transmission method and the values obtained, several of which form part of the IUPAC standards.

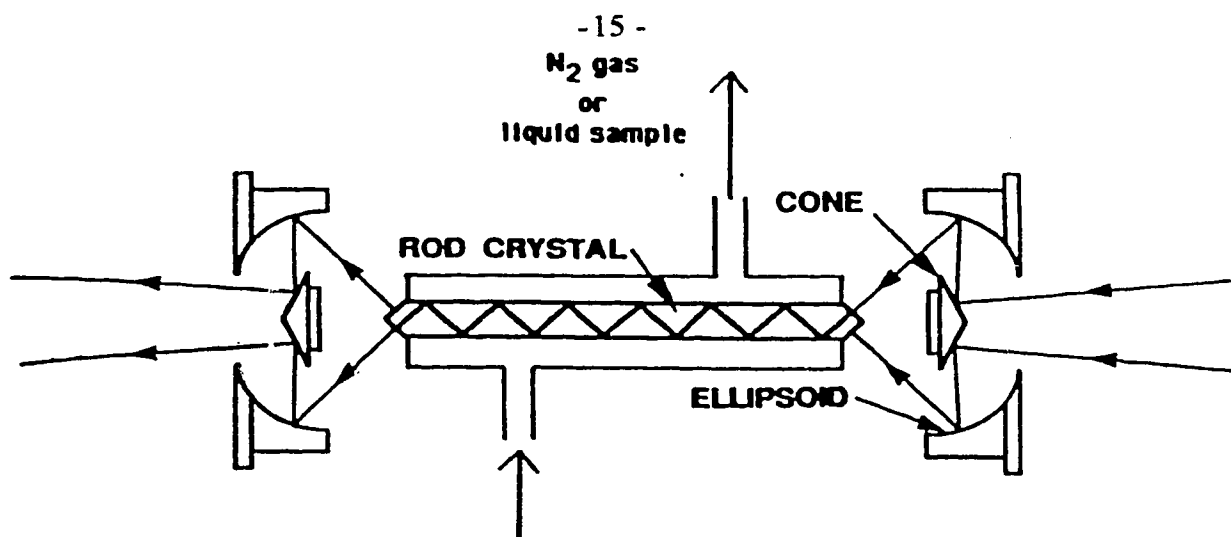


Figure 1.5 Schematic of an ATR CIRCLE cell.

1.3 Attenuated Total Reflection (ATR) Method

Attenuated total reflection (ATR) is an alternative method to measure IR spectra. In late 1950s spectroscopists ^{12,13,14} realized that the total internal reflection at the interface between a liquid sample and an incident phase of high refractive index could supply IR spectra of the sample. The CIRCLE ATR cell that is used in this laboratory is shown in figure 1.5. The sample is placed on the surface of the transparent phase which is a crystal with high real refractive index n_o . The light travels in the transparent phase and reflects from the interface. If the liquid medium does not absorb at a particular wavenumber, the light at this wavenumber is completely reflected, provided that the incident angle is greater than the critical angle. Absorption by the sample causes loss of intensity of the reflected light, because the light penetrates the interface to some extent and is absorbed by the sample. The mechanism is different

from that of the transmission method ¹ and allows very good measurement to be made of bands that are too strong to measure accurately in transmission.

The spectrum obtained in this laboratory from the ATR method is usually the negative decadic logarithm of the ratio of the intensity $I(\tilde{\nu})$ reflected from the cell full of sample to the intensity $I_o(\tilde{\nu})$ reflected from the cell full of N₂ gas.

$$\text{pATR}(\tilde{\nu}) = -\log_{10} (I(\tilde{\nu})/I_o(\tilde{\nu})) \quad (1.7)$$

This spectrum looks like its counterpart from the transmission method, but they differ in terms of peak position, band shapes and intensity. This is illustrated by the spectra in figure 1.4. Unfortunately, spectroscopists frequently compare pATR spectra with transmission spectra without recognizing these inherent differences.

The intensities in the pATR spectrum are determined by the number of reflections (NRF), the incident angle β_o , the refractive index of the transparent phase, n_o , and the complex refractive index of the sample ¹³. The equations for the intensities are given in Chapter 4. If the absorption by a sample is weak, a single reflection does not give a satisfactory spectrum and a number of reflections at the interface are required. This is called multiple attenuated total reflection (ATR) ¹³. In this laboratory, multiple ATR spectra are recorded with the CIRCLE cell shown in figure 1.5. The transparent phase is a rod with conical ends. For the work reported in Chapters 5 and 6 this cell was used. The incident angle in the cell is 45 ° which ensures total internal reflection and also simplifies the calculation used to obtain the real and imaginary refractive index spectra from the measured pATR spectra. ⁵.

The value of NRF can be determined by calibration ^{5,15}. Liquid benzene is used as the calibration standard in our laboratory because its real and imaginary refractive index spectra have been accurately determined by the transmission method ³. The intensities in the pATR spectrum of liquid benzene are calculated for different values of NRF by Fresnel equations from these known n and k values, and are compared with those determined experimentally. The value of NRF is the value that gives the smallest difference between the observed and calculated pATR spectra.

Each pATR spectrum is converted into the real and imaginary refractive index spectra of the liquid sample. This can be done by two approaches. The first one was developed by Eysel and Bertie ^{5,16}. They assumed that pATR intensity always increases with the absorption index, k . Consequently, a correction to an approximate k spectrum can be obtained from the ratio of the experimental pATR to that calculated from the approximate k spectrum and the accompanying n spectrum which is calculated from the k spectrum. In this way an iterative method is used to obtain refractive index spectra. Under the experimental conditions of this work, this method has been shown to give k values with errors <3% for most liquids ¹⁷. However, the underlying assumption may not be valid when a sample has a very strong and sharp band in the region being examined ¹⁸. When the assumption is not valid the iteration diverges ¹⁶ and is not useful.

Plaskett and Shatz ² initially proposed the second approach. They considered the complex reflectivity $\hat{r}(\tilde{\nu}) = r(\tilde{\nu}) \exp(i\theta(\tilde{\nu}))$ from the interface. The experimentally

measured reflectance $I(\tilde{\nu})/I_o(\tilde{\nu})$ is just the square of the amplitude of $\hat{r}(\tilde{\nu})$. Two Kramers-Kronig (KK) transformations were developed to calculate the phase shift $\theta(\tilde{\nu})$ from the measured reflectance^{2,18}. The real and imaginary refractive indices can be calculated from the amplitude and phase shift of reflection through Fresnel equations. The advantages of this approach are that there is no convergence problem and the calculation time is much shorter because no iteration is required. However, the accuracy of the results in published reports of this approach is usually worse than from Eysel and Bertie's method^{18,19}. The desire to determine the source of the inaccuracy and to improve this approach led to the work described in Chapter 4.

1.4 Water and its mixture with acetonitrile

One of the most useful applications of the ATR method is to measure the absorption intensities of water and its solutions, because of the very strong absorption by water in the IR region. However, reproducible results for water could not be obtained by previous workers. The precision of the spectra of liquid water was usually 5% or worse, especially in the O-H stretching region around 3500 cm^{-1} ²⁰. This precision is less than 2.5% for other pure liquids^{17,20}. In Chapter 5, the cause of this poor reproducibility is explored and markedly improved results are presented.

In 1973 Hale and Querry²² reported the refractive index spectra of liquid water from 50000 to 50 cm^{-1} and their values have been widely used. Recent developments in FT spectrometers and computers have led to more accurate spectra in the near, mid and far infrared regions. Water is such a fundamentally important liquid that it is desirable

to summarize the best results. The real and imaginary refractive index spectra of liquid water between 15000 and 1 cm^{-1} that are believed to be the most reliable are also presented in Chapter 5 based on work in this laboratory and comparison with the literature.

The structure and other properties of mixed solvents in which water is one of the components have for a long time been of considerable interest because of the importance of these solvents in many branches of chemistry. Water-acetonitrile mixtures are relatively simple systems to investigate by IR spectroscopy because of the small size of acetonitrile. The CN group is a good sensor of its environment³⁰. The interaction between water and acetonitrile is mainly due to hydrogen bonding and the structure of the system is expected to be mainly decided by this interaction and the molecular shapes in the mixture. However, the reported observations²³⁻³⁰ of the inter-molecular interaction and its effect on the structure of the mixtures, are either not convincing or are controversial. In addition, the IR investigations^{27,28,30} of these mixtures were done by examining peak positions or band shapes because of the difficulty of determining the absolute intensities. Therefore, it was considered of interest to reexamine these mixtures by measuring and interpreting their absolute intensities.

In Chapter 6, the absolute intensities of $\text{H}_2\text{O}+\text{CH}_3\text{CN}$ mixtures determined by the ATR method are presented as the real and imaginary refractive index spectra. These refractive index spectra were converted to imaginary molar polarizability spectra

under the Lorentz local field, and the intensities for different compositions were interpreted in terms of the extent and nature of the hydrogen bonding in the mixtures. The method used and the results obtained are described and discussed in Chapter 6.

1.5. References

1. G. R. Fowles, Introduction to Modern Optics (Holt Rinehart, Winston, New York, 1975)
2. J. S. Plaskett and P. N. Schatz, J. Chem. Phys., **38**, 612 (1963)
3. J. E. Bertie, R. N. Jones and C. D. Keefe, Appl. Spectrosc. **47**, 891 (1993)
4. N. J. Harrick, Internal Reflection Spectroscopy (Interscience, New York, 1967)
5. J. E. Bertie and H. H. Eysel, Appl. Spectrosc., **39**, 392 (1985)
6. J. E. Bertie and Z. Lan, J. Chem. Phys. **103**, 10152 (1995)
7. M. Born and E. Wolf, Principles of Optics, 6th Edition, page 95 (Pergamon, Oxford 1980)
8. J. E. Bertie, S. L. Zhang and C. D. Keefe, J. Mol. Struct., **324**, 157 (1994)
9. J. E. Bertie, C. D. Keefe and R. N. Jones, Can. J. Chem. **69**, 1609 (1991)
10. P. R. Griffiths and J. A. de Haseth, Fourier Transform Infrared Spectrometry, page 339 (A Wiley-Interscience Publication, John Wiley & Sons 1986)
11. J. E. Bertie, C. D. Keefe and R. N. Jones, Tables of Intensities for the Calibration of Infrared Spectroscopic Measurements in the Liquid Phase, International Union of Pure and Applied Chemistry (Blackwell Science Ltd., Oxford, 1995)
12. N. J. Harrick, J. Phys. Chem. Solids, **14**, 60 (1960)

13. W. N. Hansen, *Spectrochimica Acta*, **21**, 815 (1965)
14. J. Fahrenfort, *Spectrochim Acta*, **17**, 698 (1961)
15. J. E. Bertie, S. L. Zhang, R. N. Jones, Y. Apelblat and C. D. Keefe, *Appl. Spectrosc.*, **49**, 1821 (1995)
16. J. E. Bertie, S. L. Zhang and R. Manji, *Appl. Spectrosc.*, **46**, 1660 (1992)
17. J. E. Bertie, S. L. Zhang, H. H. Eysel and S. Baluja, *Appl. Spectrosc.*, **47**, 1100 (1993)
18. J. B. Huang and M. W. Urban, *Appl. Spectrosc.*, **46**, 1666 (1992)
19. J. A. Bardwell and M. J. Dignam, *J. Chem. Phys.*, **83**, 5468 (1985)
20. J. E. Bertie, M. K. Ahmed and H. H. Eysel, *J. Phys. Chem.*, **93**, 2210 (1989)
21. V. M. Zolotarev and A. V. Demin, *Opt. Spectrosc.*, **43**, 157 (1977) (*Opt. Spektrosk.*, **43**, 271, 1977)
22. G. M. Hale and M. R. Querry, *Appl. Opt.*, **121**, 555 (1973)
23. H. Kovacs and A. Laaksonen, *J. Am. Chem. Soc.*, **113**, 5596 (1991)
24. E. Goldammer, H. G. Herz, *J. Phys. Chem.*, **74**, 3734 (1970)
25. G. Z. Kabish, *Z. Phys. Chem., Leipzig*, **263**, 48 (1982)
26. C. Moreau and G. Douheret, *Thermochim. Acta*, **13**, 385 (1975)
27. D. A. Armitage, M. J. Blandamer, M. J. Foster, N. J. Hidden, K. W. Morcom, M. C. R. Symons and M. J. Wootten, *Trans. Faraday Soc.*, **64**, 1193 (1968)
28. B. Z. Gorbunov and Y. I. Naberukhin, *Zh. Strukt. Khim*, **16**, 816 (1975)
29. J. Y. Huang and M. H. Wu, *Phys. Rev. E*, **50**, 3737 (1994)
30. D. Jamroz, J. Stangret and J. Lindgren, *J. Am. Chem. Soc.*, **115**, 6165 (1993)

Chapter 2 The Refractive Index of Colourless Liquids in the Visible and Infrared: Contributions from the Absorption of Infrared and Ultraviolet Radiation and the Electronic Molar Polarizability below 20,500 cm⁻¹ *

2.1 Introduction

The real and imaginary refractive indices of liquids, $n(\tilde{\nu})$ and $k(\tilde{\nu})$, are essential properties for calculating and understanding light propagation, reflection and absorption in all practical situations. This paper is relevant to the determination of the real refractive index in the infrared spectral region. Specifically it discusses the separation of the contributions to the visible refractive indices of colourless liquids from the vibrational (infrared) and electronic (ultraviolet) absorptions, and explores which extrapolation into the near infrared gives the best accuracy when combined with the results of infrared measurements. The real refractive index that results solely from the electronic absorption, n_{el} , and the electronic molar polarizability, α_{el} , are given for 10 colorless liquids between 20,500 and 0 cm⁻¹.

The infrared imaginary refractive index spectrum, the k spectrum, is relatively easy to obtain from transmission¹⁻⁴ or attenuated total reflection⁵⁻⁸ spectra. The real refractive index spectrum, the n spectrum, is obtained¹⁻⁸ from the k spectrum through the Kramers-Kronig (K-K) transform (Ref. 9 and citations therein)

$$n(\tilde{\nu}_a) = n_\infty + \frac{2}{\pi} P \int_0^\infty \frac{\tilde{\nu} k(\tilde{\nu}) d\tilde{\nu}}{\tilde{\nu}^2 - \tilde{\nu}_a^2} \quad (2.1)$$

where P indicates the principal value of the integral. In this laboratory the experimental

* A version of this chapter has been published. Bertie and Lan, J. Chem. Phys., **103**, 10152 (1995)

k values are measured to above 6000 cm^{-1} . Further, without introducing any error into the first four decimal places of the real refractive index, k can usually be set to zero between 6000 cm^{-1} and 8000 cm^{-1} because the near infrared absorption is very weak. Thus, the upper limit of the integral in Eq. (2.1) is usually taken to be 8000 cm^{-1} . The error in the value of n_∞ that is used in Eq. (2.1) contributes significantly to the error in the n values obtained^{3,4,10,11}. The evaluation of n_∞ is the subject of this chapter.

A typical real refractive index spectrum of a colourless liquid is illustrated in Fig. 2.1. The spectrum approximates that of benzene¹² in its salient features. The visible region extends approximately from 25000 to $14,500\text{ cm}^{-1}$. The refractive index in the visible region is on the distant low-wavenumber tail of the anomalous dispersion caused by the electronic absorption in the ultraviolet and is on the distant high-wavenumber tail of the anomalous dispersion caused by the (weaker) vibrational absorption in the infrared. Thus, n is approximately constant in the visible region on the scale of the upper box.

In KK transforms of infrared absorption spectra, n_∞ has been taken to mean the value of the real refractive index far below the electronic absorption and far above the infrared absorption. Because of the near constancy of the refractive index in the visible, it has been common practice to set n_∞ equal to the value of n at the sodium-D line (16965 cm^{-1}). This was done in the first work from this laboratory⁵. The lower box in Figure 2.1 shows that the refractive index is not quite constant in the visible. The value

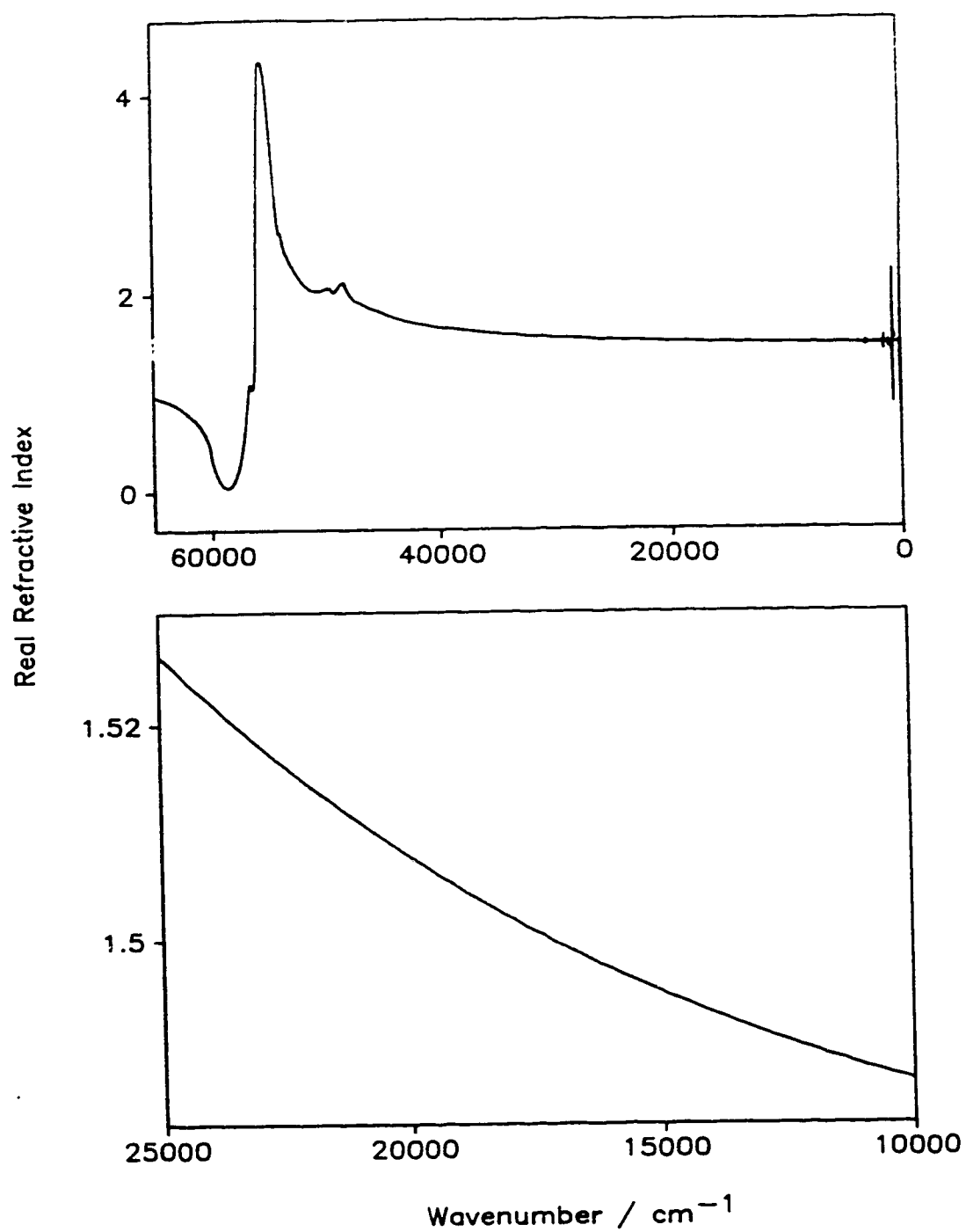


Figure 2.1 A real refractive index spectrum of a colorless liquid, based approximately on that of benzene. The visible and near infrared region is expanded in the lower box.

is lower at $10,000\text{ cm}^{-1}$ than at the sodium-D line by 2.5%. Accordingly the practice in this laboratory changed⁶ to the current practice, namely to set n_r equal to the extrapolated value of n at 8000 cm^{-1} . This extrapolated value is obtained from the equation

$$n^2(\tilde{\nu}) \approx b_0 + b_2 \tilde{\nu}^2 + b_4 \tilde{\nu}^4 \quad (2.2)$$

after the coefficients have been determined from a linear least-squares fit to the experimental values at visible wavenumbers. The latter are usually given to at least 4 decimal places¹³⁻¹⁹, and the extrapolated value is believed to be within about ± 0.004 of the correct value for H_2O ⁶ and 0.0004 for benzene³ and its derivatives^{10,11}. In both of these practices a constant value of n_∞ is used in the K-K transform of the infrared k spectrum to the infrared n spectrum.

The value of n_∞ that is required in the KK transform to calculate n at wavenumber $\tilde{\nu}_a$ is the value of n that results from all absorption except that accounted for in the integral. To high accuracy, for colourless liquids it is the ultraviolet absorption that determines the required value of n_∞ when the integration is over the region below 8000 cm^{-1} . In other words, n_∞ in Eq. (2.1) should be set equal to the value of n at wavenumber $\tilde{\nu}_a$ that results solely from the electronic absorption. We shall call this quantity n_{el} or $n_{el}(\tilde{\nu})$ in general, or $n_{el}(\tilde{\nu}_a)$ when a specific wavenumber is implied.

The only data that are usually available to calculate this value of n_{el} are the refractive indices at several wavenumbers in the visible. However, the visible refractive indices are influenced to some extent by the infrared absorption as well as by the

dominant ultraviolet absorption. Thus a method is required to separate the electronic (ultraviolet) and vibrational (infrared) contributions to the visible refractive indices, so that the ultraviolet contribution can be extrapolated into the infrared to provide the required value of n_{el} .

This chapter describes a method for determining the electronic and vibrational contributions to the visible refractive index, and for determining the correct value of $n_{\infty} = n_{el}$ to use in Eq. (2.1), the Kramers-Kronig transform which calculates $n(\tilde{\nu}_a)$. It is shown that n_{∞} should change with wavenumber $\tilde{\nu}_a$. Equations for the real refractive index as a function of visible and near infrared wavenumbers are given for ten molecular liquids, based on their known visible refractive indices and infrared absolute absorption intensities. Similar equations are also given for $n_{el}(\tilde{\nu})$, the hypothetical real refractive index that results from electronic absorption alone, and the electronic molar polarizability is given for wavenumbers between 20,500 and 0 cm^{-1} .

2.2 Equations

A well known²⁰ improvement on equation (2.2) to fit the visible refractive indices of liquids is

$$n^2(\tilde{\nu}) - 1 = A + B\tilde{\nu}^2 + C\tilde{\nu}^4 + \dots - B'\tilde{\nu}^{-2} - C'\tilde{\nu}^{-4} - \dots$$

Without the last term this equation is the Schott equation, which is used to describe the visible refractive index in the optical glass industry²¹ and in liquid-lens materials research.²² Born and Wolfe²⁰ note that for gases $n^2 - 1$ can be replaced by $2(n - 1)$. An analogous equation in n instead of n^2 also holds for liquids, as is shown in the appendix

by expansion of the Kramers-Kronig transform at wavenumbers in the visible. The appendix also demonstrates that the terms in $\tilde{\nu}^{2m}$ (m integral) arise from the contribution of the ultraviolet electronic absorption and those in $\tilde{\nu}^{-2m}$ arise from the infrared vibrational absorption, and that the coefficients are all positive and independent of wavenumber. Thus, it is shown in the appendix that the refractive index of a colourless liquid in the visible is given by Eq. (A2.6) of the appendix, namely

$$n(\tilde{\nu}) \approx a_0 + a_2 \tilde{\nu}^2 + a_4 \tilde{\nu}^4 - \frac{a_{-2}}{\tilde{\nu}^2} \quad (2.3)$$

where extra terms in $\tilde{\nu}^{2m}$ and / or $\tilde{\nu}^{-2m}$ may be needed for high accuracy. If the infrared contribution to the visible refractive index is negligible, this equation reduces to

$$n(\tilde{\nu}) \approx a_0 + a_2 \tilde{\nu}^2 + a_4 \tilde{\nu}^4 \quad (2.2a),$$

which describes both $n(\tilde{\nu})$ in the visible and $n_{el}(\tilde{\nu})$ from the visible to 0 cm^{-1} . If the infrared contribution to the visible refractive index is *not* negligible, Eq. (2.2a) describes $n_{el}(\tilde{\nu})$ from the visible to 0 cm^{-1} if the coefficients are those which result from the fit of Eq. (2.3) to the visible refractive indices.

It is also shown in the Appendix, Eq. (A2.7), that the Kramers-Kronig transform which gives n at infrared wavenumbers by integrating only over infrared absorption should be written:

$$n(\tilde{\nu}_a) \approx (a_0 + a_2 \tilde{\nu}_a^2 + a_4 \tilde{\nu}_a^4) + \frac{2}{\pi} P \int_{\text{IR}} \frac{\tilde{\nu} k(\tilde{\nu}) d\tilde{\nu}}{\tilde{\nu}^2 - \tilde{\nu}_a^2} \quad (2.4)$$

thus replacing n_∞ in Eq. (2.1) by the power series that describes the electronic contribution to the refractive index at visible and infrared wavelengths.

Results obtained with these different equations are compared in the following sections. In addition, the contributions to the visible refractive index from electronic and vibrational absorption are calculated for 10 common neat liquids, and the power series that replaces n_∞ in Eq. (2.4) is given for these liquids.

2.3 Compounds and Data

Experimental results for ten neat liquids are used in this work. Four of the liquids, water, heavy water, methanol and acetic acid, show strong broad absorption bands in the infrared between 2000 and 4000 cm^{-1} due to the OH or OD stretching vibrations of hydrogen-bonded hydroxyl groups. Three of the liquids, benzene, chlorobenzene and toluene, have only weak infrared absorption but have strong electronic absorption in the ultraviolet near 56,000 cm^{-1} . The other three liquids, acetone, dichloromethane and acetonitrile, are intermediate cases.

The reported values of the real refractive indices of these liquids in the visible region at 25°C are listed in Table 2.1. Except for heavy water and acetone, the refractive index is known at five or more visible wavenumbers, thus allowing the four parameters of Eq.(2.3) to be determined. The reported precision of these refractive

Table 2.1 The real refractive indices of ten liquids in the visible region and their temperature dependence at 25°C.

$-dn/dT$ /°K ^k	H ₂ O ^a	D ₂ O ^b	CH ₃ COOH ^c	CH ₃ OH ^d	(CH ₃) ₂ CO ^e	CH ₃ CN ^f	CH ₂ Cl ₂ ^g	C ₆ H ₆ ^h	C ₆ H ₅ Cl ⁱ	C ₆ H ₅ CH ₃ ^j
$\tilde{\nu}$ /cm ⁻¹	1.1x10 ⁻⁴	9.2x10 ⁻⁵	3.8x10 ⁻⁴	3.9x10 ⁻⁴	5x10 ⁻⁴	4.6x10 ⁻⁴	5.5x10 ⁻⁴	6.5x10 ⁻⁴	5.5x10 ⁻⁴	5.7x10 ⁻⁴
	real refractive index n									
14970.0			1.36751			1.33969	1.41893	1.49262	1.51632	1.48903
15232.7			1.36795		1.35469	1.33997	1.41926		1.51702	
15233.1	1.330672	1.326306		1.32496				1.49327		1.48966
16964.6	1.332503	1.327919	1.36980	1.32652	1.35657	1.34164		1.49792		1.49413
		1.32761								
17013.7	1.332556		1.37012		1.35676	1.34163	1.42171		1.52199	
17267.4				1.32685						
18307.5	1.333977	1.329242		1.32792				1.50197		1.49803
19931.9	1.335860							1.50748		1.50334
20564.8	1.336628		1.37471	1.33034	1.36134	1.34561	1.42747	1.50982	1.53415	1.50559
22357.7	1.338925		1.37752			1.34800	1.43144		1.54185	
22938.0	1.339710			1.33320				1.51964		1.51506
23031.8			1.37887			1.34902				
24710.1				1.33613						
Estimated Accuracy of n	<0.0001	0.0003	<0.0009	0.0006	<0.0009	0.0004	m	<0.0002	m	<0.001

^a Reference 13. ^b References 14 and 15. ^c Reference 16. ^d Reference 17. ^e Page 356 of Reference 16.

^f Page 529 of Reference 16. ^g Page 216 of Reference 16. ^h Reference 18. ⁱ Page 285 of Reference 16. ^j Page 100 of Reference 18. ^k The average of $-dn/dT$ values reported for the region 14970-24710 cm⁻¹; the dn/dT values included in the average differed by less than 5%. ^m Only one set of values exists so the accuracy can not be estimated.

index values is $\pm 1 \times 10^{-5}$ or better. The accuracy of these refractive indices was estimated when values from different sources¹³⁻¹⁹ were available. The accuracy was found to vary as shown in Table 2.1, but is better than 0.001 in all cases.

The other required data that are available for these neat liquids are the absolute intensities of the infrared absorption bands. The infrared imaginary refractive index spectra of the liquids have been determined in this laboratory^{3, 4, 10, 11, 23-27} from the near-infrared to the far-infrared, with an estimated accuracy of a few percent. Thus the infrared contribution to the real refractive index at visible wavenumber $\tilde{\nu}_a$, $\Delta n_{\text{IR}}(\tilde{\nu}_a)$, can be evaluated to comparable accuracy through the Kramers-Kronig transform.

$$\Delta n_{\text{IR}}(\tilde{\nu}_a) = \frac{2}{\pi} \int_{\text{IR}} \frac{\tilde{\nu} k(\tilde{\nu}) d\tilde{\nu}}{\tilde{\nu}^2 - \tilde{\nu}_a^2} \quad (2.5)$$

where the integration is over all infrared absorption of significant intensity. For each liquid, $\Delta n_{\text{IR}}(\tilde{\nu}_a)$ has been calculated by Eq. (2.5) at 10 visible and near infrared wavenumbers between 20501-10472 cm^{-1} , by integrating between 8000 and 1065 cm^{-1} for acetone and between 8000 cm^{-1} and $\leq 700 \text{ cm}^{-1}$ for all other liquids, as given in Table 2.2. These are the experimental values of Δn_{IR} . They are presented in Table 2.2.

These infrared contributions to the visible refractive index are all negative, and only for the four hydrogen-bonded liquids does their magnitude exceed 0.0007 in the red (14985 cm^{-1}) and 0.0003 in the blue (20500 cm^{-1}). The contributions for H_2O are -0.002 in the red and -0.001 in the blue, twice the size of the next largest contributions, those for acetic acid.

Table 2.2 The contribution, $\Delta n_R(\tilde{\nu}_a)$, of infrared absorption to the visible and near-infrared refractive indices of ten liquids at 25°C

$\tilde{\nu}_a/\text{cm}^{-1}$	H_2O^b	D_2O^c	CH_3COOH^d	CH_3OH^e	$(\text{CH}_3)_2\text{CO}^f$	CH_3CN^g	CH_2Cl_2^h	C_6H_6^i	$\text{C}_6\text{H}_5\text{Cl}^j$	$\text{C}_6\text{H}_5\text{CH}_3^k$
$\Delta n_R(\tilde{\nu}_a)^a$										
10472.5	-0.0040227	-0.0015610	-0.0019109	-0.0014951	-0.0003369	-0.0000982	-0.0001585	-0.0001382	-0.0001604	-0.0001617
11475.3	-0.0033049	-0.0012882	-0.0015762	-0.0012285	-0.0002787	-0.0000811	-0.0001315	-0.0001145	-0.0001330	-0.0001335
12979.5	-0.0025461	-0.0009971	-0.0012194	-0.0009465	-0.0002162	-0.0000629	-0.0001025	-0.0000890	-0.0001034	-0.0001034
13982.3	-0.0021786	-0.0008550	-0.0010455	-0.0008100	-0.0001857	-0.0000540	-0.0000881	-0.0000765	-0.0000889	-0.0000888
14985.1	-0.0018862	-0.0007415	-0.0009066	-0.0007013	-0.0001612	-0.0000468	-0.0000766	-0.0000665	-0.0000772	-0.0000770
15987.9	-0.0016495	-0.0006493	-0.0007939	-0.0006133	-0.0001414	-0.0000411	-0.0000672	-0.0000583	-0.0000676	-0.0000675
16990.7	-0.0014551	-0.0005735	-0.0007011	-0.0005410	-0.0001249	-0.0000362	-0.0000595	-0.0000515	-0.0000600	-0.0000596
17993.5	-0.0012934	-0.0005102	-0.0006237	-0.0004809	-0.0001112	-0.0000323	-0.0000530	-0.0000459	-0.0000534	-0.0000530
18996.3	-0.0011570	-0.0004569	-0.0005585	-0.0004303	-0.0000997	-0.0000289	-0.0000475	-0.0000411	-0.0000479	-0.0000475
20500.5	-0.0009908	-0.0003915	-0.0004785	-0.0003684	-0.0000855	-0.0000249	-0.0000408	-0.0000353	-0.0000411	-0.0000407
Integration Range/cm ⁻¹	8000 - 10	8000 - 700	8000 - 700	8000 - 2	8000 - 1065	8000 - 700	8000 - 440	8000 - 500	8000 - 10	8000 - 450
$a_2 \times 10^{-4}^m$	43.2(3) ^p	16.87(7)	20.6(1)	16.0(1)	3.65(1)	1.063(4)	1.729(3)	1.503(4)	1.746(4)	1.749(7)
Maximum deviation in Δn_R	0.00009	0.00002	0.00003	0.00003	0.000004	0.000001	0.000001	0.000001	0.000001	0.000002

^a $\Delta n_R(\tilde{\nu}_a)$ was calculated from the known infrared k spectrum through the Kramers-Kronig transform of Eq. (5).

^b k spectrum from Refs. 23, 27 & 28. ^c k spectrum from Ref. 23. ^d k spectrum from Ref. 26. ^e k spectrum from Ref. 24. ^f k spectrum from Ref. 25.

^g k spectrum from Ref. 27. ^h k spectrum from Refs. 4 & 27. ⁱ k spectrum from Ref. 3. ^j k spectrum from Refs. 11, 29, 30' & 31. ^k k spectrum from Ref. 10.

^m The value of a_2 was obtained by fitting the experimental values of Δn_R to the equation $\Delta n_R(\tilde{\nu}) \equiv \frac{a_2}{\tilde{\nu}^2}$. The number in parentheses is the standard deviation in the last digit.

^p For H_2O the values $a_2 = 40.70(2) \times 10^4$ and $a_4 = 3.73(3) \times 10^{12}$ were also obtained, by fitting the experimental values of Δn_R to the equation $\Delta n_R(\tilde{\nu}) \equiv \frac{a_2}{\tilde{\nu}^2} - \frac{a_4}{\tilde{\nu}^4}$.

The numbers in parentheses are the standard deviations in the last digit.

It is noteworthy that this infrared contribution to the visible refractive index is of recent interest in connection with liquid lens design³². To this end, Volynkin and Petrova³³ have correlated the effect of infrared absorption on the dispersion of the visible refractive index for aqueous solutions of strong acids at various concentrations.

It is usually considered that almost all of the infrared contribution to the visible refractive index comes from the intense absorption above 2500 cm⁻¹. This is not the case. For H₂O, D₂O, CH₃OH, CH₃COOH, (CH₃)₂CO and C₆H₆, Table 2.3 shows the contributions to the real refractive index at three wavelengths in the visible and near infrared from absorption in different parts of the infrared. For H₂O, the region 8000 to 2660 cm⁻¹ contributes -0.0011 to the refractive index near 16,000 cm⁻¹, which is only 70% of the total infrared contribution of -0.0016 from the region 8000 to 10 cm⁻¹. Similarly for methanol and acetic acid, the OH and CH stretching bands contribute only 75% and 60%, respectively, of the total infrared contribution. For acetone, 40% of the -0.000141 contribution from the region 8000 to 1065 cm⁻¹ arises from the absorption between 1600 and 1065 cm⁻¹.

2.3.1 Determination of Experimental Values of the Coefficient a_2 in Equation (2.3)

The development of Eq. (2.3) given in the appendix shows that $\Delta n_R(\tilde{\nu})$ can be described by

$$\Delta n_R(\tilde{\nu}) \equiv -\frac{a_{-2}}{\tilde{\nu}^2} \quad (2.6)$$

with the possible inclusion of higher terms to improve the fit. The coefficient a_2 in

Table 2.3 Contribution to the Visible Refractive Index From Different Infrared Regions

$\tilde{\nu}_s / \text{cm}^{-1}$	Integration Range and $\Delta n_{\text{IR}}(\tilde{\nu}_s)$ from Eq. (2.5)		
H₂O	8000 - 2660 cm⁻¹	8000-1250 cm⁻¹	8000 - 10 cm⁻¹
10472.5	-0.002754	-0.003179	-0.004023
15987.9	-0.001108	-0.001288	-0.001650
20500.5	-0.000662	-0.000771	-0.000991
D₂O	8000 - 1930 cm⁻¹	8000 - 700 cm⁻¹	
10472.5	-0.001371	-0.001561	
15987.9	-0.000568	-0.000649	
20500.5	-0.000342	-0.000392	
CH₃COOH	8000 - 2100 cm⁻¹	8000 - 1580 cm⁻¹	8000 - 700 cm⁻¹
10472.5	-0.001089	-0.001503	-0.001911
15987.9	-0.000445	-0.000620	-0.000794
20500.5	-0.000267	-0.000373	-0.000479
CH₃OH	8000 - 2660 cm⁻¹	8000 - 900 cm⁻¹	8000 - 2 cm⁻¹
10472.5	-0.001123	-0.001372	-0.001495
15987.9	-0.000454	-0.000560	-0.000613
20500.5	-0.000272	-0.000336	-0.000368
(CH₃)₂CO	8000 - 2660 cm⁻¹	8000 - 1600 cm⁻¹	8000 - 1065 cm⁻¹
10472.5	-0.000055	-0.000202	-0.000337
15987.9	-0.000022	-0.000084	-0.000141
20500.5	-0.000013	-0.000051	-0.000086
C₆H₆	8000 - 2740 cm⁻¹	8000 - 1300 cm⁻¹	8000 - 500 cm⁻¹
10472.5	-0.000034	-0.000061	-0.000138
15987.9	-0.000014	-0.000025	-0.000058
20500.5	-0.000008	-0.000015	-0.000035

Eq. (2.6) (without higher terms) was fitted to the values of $\Delta n_{\text{IR}}(\tilde{\nu})$ given in Table 2.2. The resulting values of a_2 are included at the bottom of Table 2.2 with their standard deviations.

Fig. 2.2 shows for benzene, methanol and water the Δn_{IR} values calculated by Eq. (2.5) and the (solid) curves given by Eq. (2.6) with the fitted values of a_2 . The agreement is clearly very good, but suggests that an accurate fit for water requires higher terms in Eq. (2.6). The high quality of the fit is shown numerically by the deviations between the tabulated values of $\Delta n_{\text{IR}}(\tilde{\nu})$ and those given by the curves. These are given in Table 2.2 below the coefficients a_2 . For the hydrogen bonded liquids these are all between 9×10^{-5} and 2×10^{-5} and for the other liquids they are all $< 4 \times 10^{-6}$. The high quality of the fit is also shown by the standard deviations of the coefficients a_2 . These are all less than 0.7% of the coefficient, and are of the order expected from the truncation of the power series (Eq. (A2.5) of the appendix) at the first term.

For water, the experimental $\Delta n_{\text{IR}}(\tilde{\nu})$ values were also fitted to $\Delta n_{\text{IR}}(\tilde{\nu}) \equiv -\frac{a_2}{\tilde{\nu}^2} - \frac{a_4}{\tilde{\nu}^4}$. The coefficients so determined are given in footnote p of Table 2.2. In Figure 2.2 the dashed line given by this fit is in excellent agreement with the data, substantially better than the solid line from the one-parameter fit. In the following, the values of a_2 and a_4 in Table 2.2 are called the *experimental* values of these coefficients. They are

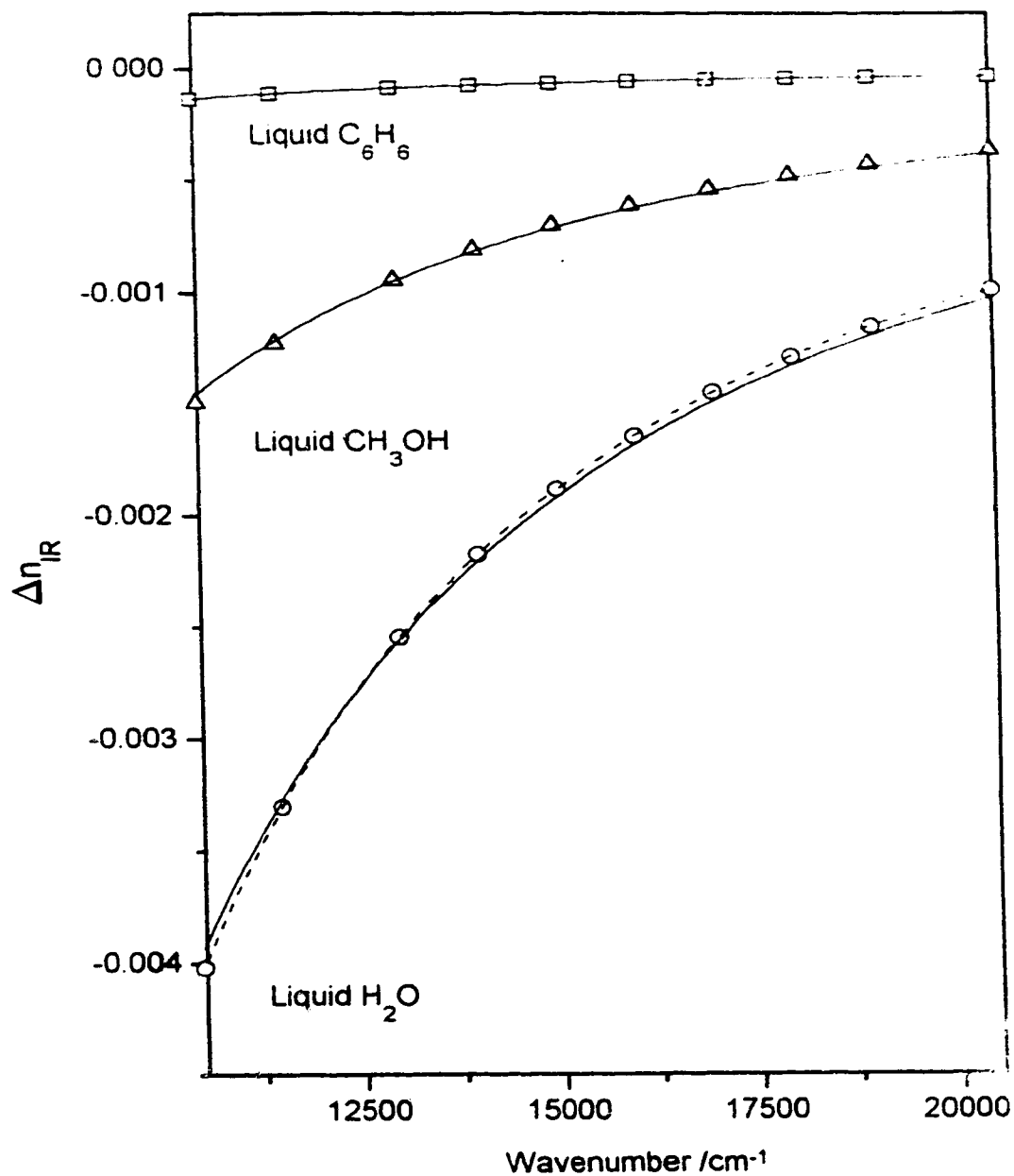


Figure 2.2 The contribution Δn_{IR} to the visible refractive index from infrared absorption between 8000 and 500 cm⁻¹ (C₆H₆), 2 cm⁻¹ (CH₃OH) or 10 cm⁻¹ (H₂O). The points □, Δ, and ○ were calculated from the infrared imaginary refractive index spectra through the Kramers-Kronig transform, Eq. (2.5). The solid and dashed lines are the functions $-\frac{a_2}{\nu^2}$ and $-\frac{a_2}{\nu^2} - \frac{a_4}{\nu^4}$, respectively, with the experimental values of the parameters a_2 and a_4 taken from Table 2.2.

used in the next section to assess the accuracy of directly fitting Eq. (2.3) to the visible refractive indices.

2.4 Results

2.4.1 Equations 2.2, 2.2a and 2.3 Fitted to the Visible Refractive Indices

The only information available before the infrared intensities are measured are the visible refractive indices. Thus it is necessary to obtain the best possible values of n_{el} in the near infrared by extrapolating these values. To evaluate the accuracy with which this can be done, Eqs. (2.2), (2.2a) and (2.3) were fitted to the visible real refractive indices by the linear least square method. The results are tabulated in Table 2.4 as the values of the coefficients, with their standard deviations in parentheses, the standard deviation of each fit, σ , and the values of n_{el} calculated at 8000 cm^{-1} , 4000 cm^{-1} and zero cm^{-1} from the fitted terms in $\tilde{\nu}^{+2m}$. Because the amount of data was sufficiently limited to make many standard deviations very large, the most practical comparison of two fits was judged to be the agreement between the extrapolated values of the refractive index at these wavenumbers.

The first comparison was to confirm that Eqs. (2.2) and (2.2a) are essentially equivalent. The coefficients in the two equations are very different of course, but the extrapolated values agree to better than 0.0001 in all cases. Clearly, these two equations can be used interchangeably, but the question remains whether they give a satisfactory approximation to the correct values of n_{el} . Eq. (2.2a) is slightly preferred on the grounds that it gives n_{el} directly if the vibrational contribution is sufficiently small to be neglected.

Table 2.4 Fits of Equations (2.2), (2.2a) and (2.3) to the Visible Real Refractive Indices of Ten Liquids^a

Liquids	c_0^b	c_2^b $\times 10^{12}$	c_4^b $\times 10^{21}$	a_2^b $\times 10^{-4}$	σ^c $\times 10^5$	n_d at 8000 cm^{-1}	n_d at 4000 cm^{-1}	n_d at 0 cm^{-1}
H₂O								
Eq.(2.2)	1.75000 (42)	92.88 (226)	-14.8 (29)		6.5	1.32509	1.32343	1.32288
Eq.(2.2a)	1.32288 (15)	35.03 (83)	-5.9 (11)		2.4	1.32510	1.32344	1.32288
Eq.(2.3)	1.32702 (25)	23.46 (71)	4.50 (65)	47.3 (29)	0.33	1.32854	1.32740	1.32702
Eq.(2.3)+ ^e	1.32665 (2)	24.56 (10)	3.47 (13)	43.2	0.11	1.32824	1.32704	1.32665
Eq.(2.3)+ ^f	1.32663 (2)	24.39 (14)	3.74 (18)	40.70 (2)	0.31	1.32821	1.32702	1.32663
D₂O^g								
Eq.(2.2)	1.752 (17)	1.07 (1)	131 (220)		58	1.324	1.324	1.324
Eq.(2.2a)	1.3235 (66)	0.7 (471)	49 (83)		22	1.3238	1.3235	1.3235
Eq.(2.3)+ ^e	1.3252 (66)	-5 (47)	55 (83)	16.87	22	1.3251	1.3251	1.3252
CH₃COOH								
Eq.(2.2)	1.8496 (24)	90 (14)	13 (18)		38	1.3621	1.3605	1.3600
Eq.(2.2a)	1.35999 (86)	33.1 (50)	4.4 (66)		14	1.36213	1.36052	1.35999
Eq.(2.3)	1.3719 (92)	-1 (27)	36 (25)	132 (102)	13	1.3720	1.3719	1.3719
Eq.(2.3)+ ^e	1.36185 (81)	27.8 (47)	9.2 (62)	20.6	13	1.36366	1.36230	1.36185
CH₃OH								
Eq.(2.2)	1.7409 (18)	58.8 (91)	22 (11)		36	1.3209	1.3198	1.3194
Eq.(2.2a)	1.31937 (64)	22.7 (33)	7.5 (38)		13	1.32085	1.31973	1.31937
Eq.(2.3)	1.3290 (45)	-2 (12)	28 (10)	117 (54)	9.7	1.3290	1.3290	1.3290
Eq.(2.3)+ ^e	1.32075 (58)	19.1 (29)	10.4 (35)	16.04	12	1.32201	1.32105	1.32075
(CH₃)₂CO^h								
Eq.(2.2)	1.8131 (38)	95 (24)	-0.7 (351)		25	1.3488	1.3471	1.3465
Eq.(2.2a)	1.3466 (14)	35.2 (86)	-0.6 (128)		9.3	1.3488	1.3471	1.3466
Eq.(2.3)+ ^e	1.3469 (14)	34.1 (86)	0.7 (128)	3.65	9.3	1.3491	1.3475	1.3469
CH₃CN								
Eq.(2.2)	1.77822(71)	71.4(41)	13.1(54)		11	1.33523	1.33393	1.33350
Eq.(2.2a)	1.33350(27)	26.8(15)	4.6(20)		4.3	1.33523	1.33393	1.33350
Eq.(2.3)	1.3384(21)	12.7(62)	17.4(57)	54(23)	3.0	1.3393	1.3386	1.3384
Eq.(2.3)+ ^e	1.33359(26)	26.6(15)	4.7(20)	1.063	4.2	1.33531	1.33402	1.33359
CH₂Cl₂								
Eq.(2.2)	1.9924(26)	79(16)	69(22)		34	1.4134	1.4120	1.4115
Eq.(2.2a)	1.41149(91)	28.2(56)	23.3(78)		12	1.41339	1.41194	1.41149
Eq.(2.3)	1.4284(25)	-21.4(72)	69.6(69)	183(27)	2.4	1.4273	1.4281	1.4284
Eq.(2.3)+ ^e	1.41163(90)	27.8(55)	23.6(77)	1.729	12	1.41351	1.41208	1.41163
C₆H₆								
Eq.(2.2)	2.17846(22)	200.1(13)	92.2(17)		4.5	1.48042	1.47705	1.47596
Eq.(2.2a)	1.47589(7)	68.45(40)	27.93(54)		1.3	1.48038	1.47699	1.47589
Eq.(2.3)	1.47795(28)	62.61(79)	33.18(72)	23.0(31)	0.36	1.48209	1.47896	1.47795
Eq.(2.3)+ ^e	1.47602(8)	68.12(42)	28.19(57)	1.503	1.26	1.48049	1.47712	1.47602
C₆H₅Cl								
Eq.(2.2)	2.2485(15)	202(9)	111 (135)		20	1.5040	1.5006	1.4995
Eq.(2.2a)	1.49941(50)	68.1 (31)	33.5(43)		6.4	1.50391	1.50051	1.49941
Eq.(2.3)	1.50877(63)	40.7(19)	59.2(18)	102 (7)	0.61	1.51161	1.50943	1.50877
Eq.(2.3)+ ^e	1.49958(48)	67.6(30)	34.0(41)	1.746	6.3	1.50405	1.50067	1.49958
C₆H₅CH₃								
Eq.(2.2)	2.16984(22)	191.4(12)	89.7(17)		4.3	1.47731	1.47408	1.47304
Eq.(2.2a)	1.47296(7)	65.63(38)	27.31(52)		1.3	1.47727	1.47402	1.47296
Eq.(2.3)	1.47494(24)	60.03(66)	32.35(61)	22.1(26)	0.3	1.47891	1.47591	1.47494
Eq.(2.3)+ ^e	1.47314(6)	65.08(34)	27.84(47)	1.749	1.2	1.47742	1.47419	1.47314

Footnotes of Table 2.4

^a The visible refractive indices at 25°C are given in Table 2.1.

^b c_{2m} ($m=0,1,2$) is the coefficient of the term $\tilde{\nu}^{2m}$ in Eqs. (2.2), (2.2a) and (2.3). For Eq. (2.2), $c_{2m}=b_{2m}$, while, for equations (2.2a) and (2.3), $c_{2m}=a_{2m}$. The number in parentheses is the standard deviation in the last digit.

^c The standard deviation of the fit, σ , is the positive root of $\sigma^2 = \frac{\sum_{j=1}^N (f(\tilde{\nu}_j) - y_j)^2}{N - m}$, where N is the number of observations, m is the number of parameters fitted, $f(\tilde{\nu})$ is the fitting function, and $\tilde{\nu}_j$ and y_j are the wavenumber and experimental refractive index

n_e is the refractive index that results solely from electronic absorption. The values were calculated by $n_e = a_0 + a_2 \tilde{\nu}^2 + a_4 \tilde{\nu}^4$ for Eqs. (2.2a) and (2.3), or $n_e = \sqrt{b_0 + b_2 \tilde{\nu}^2 + b_4 \tilde{\nu}^4}$ for Eq. (2.2).

^d The coefficient a_2 was constrained to the experimental value given in Table 2.2, and only a_0 , a_2 and a_4 were fitted to the visible refractive indices.

^e Equation (2.3) was used with the addition of a term $-\frac{a_4}{\tilde{\nu}^4}$ on the right hand side. The coefficients a_2 and a_4 were constrained to the experimental values given in footnote p of Table 2.2, and only a_0 , a_2 and a_4 were fitted to the visible refractive indices.

^f Insufficient data exist to allow Eq. (2.3) to be fitted for D₂O and acetone.

Eq. (2.3) includes both the electronic and the vibrational contributions to the visible refractive index, but at the expense of an additional term to be fitted. For lack of data, this equation could not be fitted to the visible refractive indices of D₂O or (CH₃)₂CO. The fitted coefficients and the extrapolated n_e values calculated from the fitted terms in $\tilde{\nu}^{2m}$ are given in Table 2.4 for the other eight liquids.

The n_e values extrapolated through Eq. (2.3) differ substantially from those extrapolated through Eqs. (2.2) and (2.2a). To determine whether those from Eq. (2.3) are actually better, as theory suggests that they should be if the coefficients are sufficiently well determined, Eq. (2.3) was used again to fit the visible refractive indices, but using the *experimental* value of a_2 given in Table 2.2 instead of determining it in the fitting process. The results of this procedure are given in Table 2.4 on the lines labelled "Eq.(2.3)+", again with the values of n_e calculated from the terms in $\tilde{\nu}^{2m}$. For water this procedure was repeated with the inclusion of the term

$-a_4/\tilde{\nu}^4$ in the fitting procedure, in which the values of a_2 and a_4 were kept fixed at the values in footnote p of Table 2.2. The results are included in Table 2.4 on the line labelled "Eq. (2.3)*". The extrapolated n_{el} values are within 0.00003 of those from Eq. (2.3)+. Thus, the additional term improves markedly the fit of the experimental Δn_{IR} values (Figure 2.2) but changes the value of n_{el} only in the 5th decimal place.

For all liquids except water, the n_{el} values extrapolated through Eq. (2.3)+ agree well with those from Eq. (2.2a), and those from Eq. (2.3) are in poorer agreement. Keeping in mind that Eq. (2.3)+ should give the best values of $n_{el}(\tilde{\nu})$, since it uses the experimentally determined contribution from the vibrational absorption, it is clear that the visible refractive indices currently available are not sufficiently extensive or accurate to permit the use of Eq. (2.3) to determine $n_{el}(\tilde{\nu})$, the refractive index at infrared wavenumbers that results solely from electronic absorption. Eq. (2.2a) should be used to calculate n_{el} if the infrared absorptivity intensities are not known.

For liquid H₂O, however, the infrared contribution is sufficiently large, and the available refractive index data are sufficiently extensive, to make Eq. (2.3)+ and Eq. (2.3)* superior to Eq. (2.2a). For liquid D₂O, only Eq. (2.2a) is available, for lack of data, and it gives $n_{el}(8000\text{ cm}^{-1})$ and $n_{el}(0\text{ cm}^{-1})$ within 0.002 of those calculated from the experimental data (Eq. (2.3)+ in Table 2.4). Note that the increase in n_{el} for D₂O under Eq. (2.3)+ from 1.3251 at 8000 cm⁻¹ to 1.3252 at 0 cm⁻¹ is not significant and arises because a_2 (c_2 in Table 2.4) is very poorly determined.

For all liquids, once the infrared absorption intensities are known, even if uncertain by ~10%, the best values of n_{el} are obtained from Eq. (2.3) fitted while constraining a_2 , and a_4 when required, to the experimental value.

2.4.2 Correction of the Published Infrared Real Refractive Indices

It has been shown above that during the determination of the infrared absorption intensities as the real and imaginary refractive indices, the integration in Eq. (2.1) is over the infrared region and n_{∞} should be replaced by $n_{el}(\tilde{\nu}_a)$, i.e. by the power series obtained by fitting Eq. (2.2a) to the visible refractive indices. Thus Eq. (2.4) should be used with the coefficients a_{2m} obtained from Eq. (2.2a). For H₂O, the coefficients a_{2m} obtained from Eq. (2.3) should be used. It is only after the infrared intensities are known that Eq. (2.3)+ or Eq (2.3)* (Table 2.4) can be used.

Infrared real and imaginary refractive index spectra have been reported for liquid water, methanol, benzene, toluene and chlorobenzene^{22,23,3,10,11}. The real refractive indices were calculated through Eq. 2.1 with a constant value of n_{∞} . These reported infrared real refractive index values can now be improved slightly by adding Eq. (2.7) to the value of n at $\tilde{\nu}$.

$$\Delta n(\tilde{\nu}) = g + a_2 \tilde{\nu}^2 + a_4 \tilde{\nu}^4 \quad (2.7)$$

The required values of the three coefficients are given in Table 2.5. Because the infrared absorption intensities are known, the values of a_2 and a_4 are from the rows labelled Eq. (2.3)+ in Table 2.4. Eq. (2.3)* was used for H₂O. The value of g for each liquid is the difference between c_0 from the row labelled Eq. (2.3)+ in Table 2.6 and the

Table 2.5 The coefficients of the polynomial required to correct the published infrared refractive indices and the size of the correction at 8000, 4000 and 0 cm⁻¹

	H ₂ O ²³	CH ₃ OH ²⁴	C ₆ H ₆ ³	C ₆ H ₅ Cl ¹¹	C ₆ H ₅ CH ₃ ¹⁰	CH ₂ Cl ₂ ⁴
g^a	0.00163	-0.00425	-0.00438	-0.00472	-0.00416	-0.00137
a_2^b	2.44×10^{-11}	1.91×10^{-11}	6.81×10^{-11}	6.76×10^{-11}	6.51×10^{-11}	2.78×10^{-11}
a_4^c	3.74×10^{-21}	1.0×10^{-20}	2.8×10^{-20}	3.4×10^{-20}	2.8×10^{-20}	2.36×10^{-20}
$\Delta n(8000 \text{ cm}^{-1})^d$	0.00321	-0.00299	0.00009	-0.00025	0.00012	0.00051
$\Delta n(4000 \text{ cm}^{-1})^d$	0.00202	-0.00394	-0.00328	-0.00363	-0.00311	-0.00092
$\Delta n(0 \text{ cm}^{-1})^d$	0.00163	-0.00425	-0.00438	-0.00472	-0.00416	-0.00137

^a This value is the difference between c_0 from "Eq. (2.3) +" in Table 2.4 and the value of n_∞ used in the Kramers-Kronig transform (1) for that liquid in the reference cited with the chemical formula.

^b This is the c_2 from "Eq. (2.3) +" in Table 2.4. For H₂O, c_2 from "Eq. (2.3)*" was used.

^c This is the c_4 from "Eq. (2.3) +" in Table 2.4. For H₂O, c_4 from "Eq. (2.3)*" was used.

^d The correction to be made to the published values at 8000, 4000 and 0 cm⁻¹, calculated by Eq. (2.7)

value of n_∞ used in the original Kramers-Kronig transform for that liquid. The corrections calculated for 8000, 4000 and 0 cm⁻¹ are included in Table 2.5. The corrections range from plus to minus 0.005 and, we believe, improve the accuracy of the published infrared real refractive indices to approximately 0.001, in all cases.

2.4.3 The Electronic Polarizability Between 0 and 25000 cm⁻¹

The values of n_{el} , the refractive index that results solely from the electronic absorption, calculated as in Table 2.4 can be used to calculate the electronic contribution to the molar polarizability, α_{el} , through the well known equation

$$\frac{n^2 - 1}{n^2 + 2} = \frac{4\pi}{3V_m} \alpha. \text{ Selected values of the electronic polarizability are given in}$$

Table 2.6. Between 8000 and 0 cm⁻¹ α_{el} decreases by 1.1% for acetone, 0.75% for the

Table 2.6. Electronic Molar Polarizabilities Between 20,500 and 0 cm^{-1} of Ten Liquids at 25°C

	$V_m(\text{ml})$	$\alpha_{el} (\text{cm}^3/\text{mole})$ at given wavenumber (cm^{-1}) ^a						
		20500	15987.9	13982.3	11475.3	8000	4000	0
H ₂ O	18.07	0.898	0.888	0.884	0.880	0.876	0.873	0.872
D ₂ O	18.09	0.888	0.875	0.872	0.870	0.869	0.869	0.869
CH ₃ COOH	57.24	3.129	3.088	3.073	3.058	3.043	3.033	3.030
CH ₃ OH	40.50	1.976	1.952	1.945	1.937	1.929	1.924	1.922
(CH ₃) ₂ CO	73.53	3.887	3.832	3.812	3.791	3.768	3.752	3.747
CH ₃ CN	53.02	2.692	2.658	2.646	2.633	2.620	2.611	2.608
CH ₂ Cl ₂	64.38	3.950	3.892	3.873	3.855	3.837	3.825	3.821
C ₆ H ₆	89.41	6.380	6.228	6.176	6.123	6.069	6.032	6.021
C ₆ H ₅ Cl	102.21	7.585	7.407	7.347	7.287	7.226	7.185	7.172
C ₆ H ₅ CH ₃	106.86	7.572	7.396	7.336	7.275	7.214	7.172	7.158

^a α_{el} was calculated from n_{el} which was calculated by $n_{el} = a_0 + a_2 \tilde{\nu}^2 + a_4 \tilde{\nu}^4$, where the coefficients are from Table 2.4 for Eqn. (2.3) * for H₂O and Eq. (2.3)+ for all other compounds.

aromatic liquids, and by 0 to 0.5% for the remaining liquids, about three times greater than the percentage decreases in n_{el} .

2.5 Summary

For ten liquids examined in this work, the vibrational contributions to the visible real refractive index, Δn_R , were calculated from known infrared absorption intensities, and were well described by the function $-a_2/\tilde{\nu}^2$ with the single parameter, a_2 . For water the addition of the term $-a_4/\tilde{\nu}^4$ improved the description. Knowledge of these contributions allowed n_{el} , the refractive index in the visible and infrared due solely to electronic absorption, to be calculated as a power series in $\tilde{\nu}^{2m}$. For liquids other than H₂O, the vibrational contribution is very small and the power series for $n_{el}(\tilde{\nu})$ also

accurately describes the total visible-to-near-infrared real refractive index spectra of these liquids. Consequently, before the vibrational intensities are known n_x in Eq. (2.1) should be replaced by n_{el} calculated from the fit of Eq. (2.2a) to the visible refractive indices. The electronic molar polarizability has been calculated for the ten liquids at wavenumbers between 20,500 and 0 cm^{-1} from the n_{el} values.

2.6 Appendix Expansion of the Kramers-Kronig transform

In this appendix the expansion

$$\frac{1}{1-x^2} = 1 + x^2 + x^4 + \dots = \sum_{i=0}^{\infty} x^{2i} \quad \text{for } x < 1 \quad (\text{A2.1})$$

is applied to the Kramers-Kronig (KK) transform

$$n(\tilde{\nu}_a) - n_{\infty} = \frac{2}{\pi} P \int_0^{\infty} \frac{\tilde{\nu} k(\tilde{\nu}) d\tilde{\nu}}{\tilde{\nu}^2 - \tilde{\nu}_a^2}$$

Consider $\tilde{\nu}_a$ to be in the visible spectral region defined by the limits ν_{UVI} , the lower limit of the ultraviolet, and ν_{IRu} , the upper limit of the infrared. The K-K transform can be written to highlight this region as:

$$n(\tilde{\nu}_a) - n_{\infty} = \frac{2}{\pi} \left[\int_{\nu_{UVI}}^{\infty} \frac{\tilde{\nu} k(\tilde{\nu}) d\tilde{\nu}}{\tilde{\nu}^2 - \tilde{\nu}_a^2} + P \int_{\nu_{IRu}}^{\nu_{UVI}} \frac{\tilde{\nu} k(\tilde{\nu}) d\tilde{\nu}}{\tilde{\nu}^2 - \tilde{\nu}_a^2} + \int_0^{\nu_{IRu}} \frac{\tilde{\nu} k(\tilde{\nu}) d\tilde{\nu}}{\tilde{\nu}^2 - \tilde{\nu}_a^2} \right] \quad (\text{A2.2})$$

Colourless compounds do not absorb in the visible. Thus $k \approx 0$ in the second integral and Eq (A2.2) simplifies to

$$n(\tilde{\nu}_a) - n_{\infty} = \frac{2}{\pi} \left[\int_{\nu_{UVI}}^{\infty} \frac{\tilde{\nu} k(\tilde{\nu}) d\tilde{\nu}}{\tilde{\nu}^2 - \tilde{\nu}_a^2} + \int_0^{\nu_{IRu}} \frac{\tilde{\nu} k(\tilde{\nu}) d\tilde{\nu}}{\tilde{\nu}^2 - \tilde{\nu}_a^2} \right] \quad (\text{A2.3})$$

The expansion (A2.1) can be applied to the integrand in the first term in Eq.

(A2.3), recalling that $\tilde{\nu} > \tilde{\nu}_a$,

$$\begin{aligned} \frac{2}{\pi} \int_{\nu_{uvl}}^{\infty} \frac{\tilde{\nu} k(\tilde{\nu}) d\tilde{\nu}}{\tilde{\nu}^2 - \tilde{\nu}_a^2} &= \frac{2}{\pi} \int_{\nu_{uvl}}^{\infty} \frac{\tilde{\nu} k(\tilde{\nu}) d\tilde{\nu}}{\tilde{\nu}^2 [1 - (\tilde{\nu}_a^2 / \tilde{\nu}^2)]} = \frac{2}{\pi} \int_{\nu_{uvl}}^{\infty} \frac{k(\tilde{\nu})}{\tilde{\nu}} \left[1 + \left(\frac{\tilde{\nu}_a}{\tilde{\nu}} \right)^2 + \left(\frac{\tilde{\nu}_a}{\tilde{\nu}} \right)^4 + \dots \right] d\tilde{\nu} \\ &= a_0 - n_{\infty} + a_2 \tilde{\nu}_a^2 + a_4 \tilde{\nu}_a^4 + \dots \end{aligned} \quad (\text{A2.4})$$

and to the integrand in the second term, recalling that $\tilde{\nu} < \tilde{\nu}_a$,

$$\begin{aligned} \frac{2}{\pi} \int_0^{\nu_{uvl}} \frac{\tilde{\nu} k(\tilde{\nu}) d\tilde{\nu}}{\tilde{\nu}^2 - \tilde{\nu}_a^2} &= \frac{2}{\pi} \int_0^{\nu_{uvl}} \frac{-\tilde{\nu} k(\tilde{\nu}) d\tilde{\nu}}{\tilde{\nu}_a^2 [1 - (\tilde{\nu}^2 / \tilde{\nu}_a^2)]} = \frac{2}{\pi} \int_0^{\nu_{uvl}} \frac{-\tilde{\nu} k(\tilde{\nu})}{\tilde{\nu}_a^2} \left[1 + \left(\frac{\tilde{\nu}}{\tilde{\nu}_a} \right)^2 + \left(\frac{\tilde{\nu}}{\tilde{\nu}_a} \right)^4 + \dots \right] d\tilde{\nu} \\ &= -\frac{a_{-2}}{\tilde{\nu}_a^2} - \frac{a_{-4}}{\tilde{\nu}_a^4} - \frac{a_{-6}}{\tilde{\nu}_a^6} - \dots \end{aligned} \quad (\text{A2.5})$$

The coefficients $\{a_{2m}\}$ in Eq (A2.4) and $\{a_{-2m}\}$ in Eq (A2.5) are positive and independent of wavenumber.

For practical calculation, expansion to the term $\tilde{\nu}_a^4$ in Eq (A2.4) and to the term $\tilde{\nu}_a^{-2}$ in Eq (A2.5) is usually sufficient (see text). Thus, the real refractive index of colourless liquids in the visible region is given by

$$n(\tilde{\nu}_a) \approx a_0 + a_2 \tilde{\nu}_a^2 + a_4 \tilde{\nu}_a^4 - \frac{a_{-2}}{\tilde{\nu}_a^2} \quad (\text{A2.6})$$

where the terms in $\tilde{\nu}_a^{2m}$, $m = 0, 1$ and 2 , arise from the ultraviolet electronic absorption and the term in $\tilde{\nu}_a^{-2}$ arises from the infrared vibrational absorption.

If the wavenumber $\tilde{\nu}_a$ is in the infrared region, between ν_{IRu} and zero, Eq (A2.4) still applies but Eq (A2.5) does not. Thus the K-K transform for the calculation of n values of colorless liquids in the infrared region should be written

$$n(\tilde{\nu}_a) \approx (a_0 + a_2 \tilde{\nu}_a^2 + a_4 \tilde{\nu}_a^4) + \frac{2}{\pi} P \int_0^{\nu_{IRu}} \frac{\tilde{\nu} k(\tilde{\nu}) d\tilde{\nu}}{\tilde{\nu}^2 - \tilde{\nu}_a^2} \quad (A2.7)$$

where the coefficients a_0 , a_2 and a_4 arise from the contribution by the ultraviolet electronic absorption.

2.7 References:

1. T. G. Goplen, D. G. Cameron, and R. N. Jones, *Appl. Spectrosc.* **34**, 657 (1980).
2. J. E. Bertie, V. Behnam, and R. N. Jones, *Appl. Spectrosc.* **39**, 401 (1985).
3. J.E.Bertie, R.N.Jones and C.D.Keefe, *Applied Spectrosc.* **47** , 891 (1993).
4. J. E. Bertie, Z. Lan, R. N. Jones and Y. Apelblat, *Applied Spectrosc.* in press.
5. J. E. Bertie and H. H. Eysel, *Appl. Spectrosc.* **39**, 392 (1985).
6. J. E. Bertie, H. Harke, M. K. Ahmed and H. H. Eysel, *Croatica Chemica Acta* **61**, 391 (1988).
7. J.E.Bertie, S.L.Zhang and R. Manji, *Applied Spectrosc.* **46**, 1660 (1992).
8. J.B. Huang and M.W. Urban, *Applied Spectrosc.* **46**, 1666 (1992).
9. J.E. Bertie and S.L. Zhang, *Can. J. Chem.* **70**, 520 (1992).
10. J.E.Bertie, R.N.Jones, Y. Apelblat and C.D.Keefe, *Applied Spectrosc.* **48**, 127 (1994).
11. J.E.Bertie, R.N.Jones and Y. Apelblat, *Applied Spectrosc.* **48**, 144 (1994).

12. *Organic Electronic Spectral Data*. Ed: M. J. Kamlet, Interscience, New York, volume 1, page 83 (1953).
13. L. W. Tilton and J. K. Taylor, *J. Res. Natl. Bur. Std.* **20**, 419 (1938).
14. V. P. Frontas'ev and L. S. Shraiber, *Zh. Strukt. Khim.* **6**, 512 (1965).
15. J. Timmermans, *Physico-Chemical Constants of binary systems*, **4**, page 472 (Interscience, New York, 1961).
16. J. Timmermans, *Physico-Chemical Constants of Pure Organic Compounds*, **1**, page 382 (Elsevier, New York, 1950).
17. S. E. Wood, S. Langys and R. Battino, *J. Chem. Phys.*, **32** 1389 (1960).
18. J. Timmermans, *Physico-Chemical Constants of Pure Organic Compounds*, **2**, page 98 (Elsevier, Amsterdam, 1965).
19. *International Critical Tables Of Numerical Data, Physics, Chemistry and Technology*. (McGraw-Hill, New York 1930), 1st. Edition, Vol. 7, p. 12 & 34
20. M. Born and E. Wolf, *Principles of Optics*, 6th Edition, page 95 (Pergamon, Oxford 1980).
21. *Schott Optical Glass catalog*, Schott Optical Glass Inc., Duryea, Pa 18642.
22. R. D. Sigler, *Appl. Opt.* **29**, 2451 (1990).
23. J. E. Bertie and M. K. Ahmed, *J. Phys. Chem.* **93**, 2210 (1989).
24. J. E. Bertie and S. L. Zhang, *Appl. Spectrosc.* **47**, 1100 (1993).
25. J. E. Bertie and S. O. Paul, unpublished work.
26. J. E. Bertie and M. K. Ahmed, unpublished work.
27. J. E. Bertie and Z. Lan, unpublished work.

28. H. D. Dowling and D. Williams, J. Geophys. Res. **80**, 1656 (1975)
29. T. G. Goplen, D. G. Cameron and R. N. Jones, Appl. Spectrosc. **34**, 657 (1980)
30. M. N. Afsar, D. D. Honijk, W. F. Passchier and J. Goulan, IEEE Trans. Micro. Theory and Tech. MTT-25, 505 (1977)
31. D. D. Honijk, W. F. Passchier, M. Mandel and M. N. Afsar, Infrared Phys. **17**, 9 (1977)
32. V. M. Volynkin, M. V. Petrova, G. T. Petrovskii, M. N. Tolstoi and A. A. Tokarev, Sov. J. Opt. Technol. **58**, 431 (1991)
33. V. M. Volynkin, M. V. Petrova, G. T. Petrovskii and M. N. Tolstoi, *Zhurnal Fizicheskoi Khimii* **64**, 1560 (1990).

Chapter 3 Infrared Intensities of Liquids XVIII: Accurate Optical Constants and Molar Absorption Coefficients Between 6500 and 800 cm^{-1} of Dichloromethane at 25°C, from Spectra Recorded in Several Laboratories *

3.1 Introduction

This paper completes the publication of the detailed measurements and results obtained in the project¹ that led to the acceptance of secondary infrared absorption intensity standards for liquids² by the International Union of Pure and Applied Chemistry. These standards² are based on bands of liquid benzene³, toluene⁴ and chlorobenzene⁵ and on the bands of liquid dichloromethane reported in this paper.

The methods used have been described in detail^{3,4,6}. The spectra, measured in transmission, are the experimental absorbance, EA, spectra⁶, which are frequently called absorbance spectra even though they are influenced by energy losses other than absorption.^{3,6} The quantities calculated from these spectra and reported previously were the spectra of the real and imaginary refractive indices, which are usually called the refractive index, $n(\tilde{\nu})$, and the absorption index, $k(\tilde{\nu})$, respectively, the spectrum of the molar absorption coefficient, $E_m(\tilde{\nu})$, and the areas under bands in the absorption index and molar absorption coefficient spectra. In this paper the same quantities are reported for liquid dichloromethane at 25°C between 6500 and 800 cm^{-1} .

In this work, EA spectra⁶ of liquid dichloromethane at 25°C were measured by two different spectroscopists on the same instrument in this laboratory, one in the current work and one previously^{7,8}, and also by three spectroscopists in three other

* A version of this chapter has been published. Bertie, Lan, Jones and Apelblat, *Appl. Spectrosc.*, 49, 840 (1995)

laboratories. From these EA spectra, the real refractive index and absorption index spectra were calculated in this laboratory by the methods described previously^{3,6}.

As was found for other compounds previously^{3,5}, the absorption index spectra from different workers agreed well in their peak heights and areas beneath band groups. The five average spectra from the different spectroscopists were themselves averaged, unweighted, to yield the absorption index spectrum that is presented as the best currently available. This absorption index spectrum, was used to calculate^{3,6} the molar absorption coefficient spectrum and, through the Kramers-Kronig transformation, the real refractive index spectrum. In order to obtain a more accurate real refractive index spectrum, an approximate earlier^{7,8} spectrum of the very intense band at 738 cm^{-1} , which was not measured in this work, was appended to the absorption index spectrum before the Kramers-Kronig transform.

3.2 Methods and Results

The dichloromethane used in this laboratory was of spectroscopic or reagent grade. Samples were purified by fractional freezing one to three times. They were found to be >99.95% pure by gas chromatography, and no impurities were detected by infrared spectroscopy. The purified liquid was kept over molecular sieve to maintain dryness.

The experimental and instrumental details of this work have been described^{3,6} and are summarised briefly here. The spectra from this laboratory were measured with a Bruker IFS 113V spectrometer. A Globar source, 10 mm aperture, and deuterated triglycine sulfate, DTGS, detector were used for all spectra measured in this laboratory. The slow, room temperature, DTGS detector was used to ensure that the phase

correction was small during the Fourier transformation of the one-sided interferograms. The interferograms were recorded with 0.665 cm s^{-1} optical retardation velocity and 1 cm maximum path difference. Trapezoidal apodization, multiplicative phase correction and one level of zero-filling were used in the Fourier transform.

Cells with KBr or CaF_2 windows and fixed path lengths between 11 and $1500 \mu\text{m}$ were used, as well as cells with NaCl or CaF_2 windows and variable path lengths up to 5 mm. The path lengths of the cells were determined from the fringe patterns in the experimental absorbance spectra of the empty cells by program RNJ22A^{3,6}. For the variable path cells, path lengths greater than $700 \mu\text{m}$ could not be determined in this way because the fringe patterns were too weak. They were found by calibrating the cell micrometer readings from the fringe patterns at path lengths up to $700 \mu\text{m}$, and assuming the calibration held for greater thicknesses.

In addition to the EA spectra recorded for this work, EA spectra recorded previously in this laboratory by V. Behnam^{7,8} were also used. Behnam's methods were as described above except that he used triangular apodization. The refractive indices reported here from Behnam's spectra differ from those reported previously^{7,8} because they were re-computed using the recently developed baseline correction procedure⁶.

Additional EA spectra were kindly supplied by three spectroscopists in other laboratories. They were recorded with good analytical laboratory technique at 1 or 2 cm^{-1} nominal resolution under normal conditions. No additional information is available about one of these three sets of spectra. The other two sets were recorded on a Digilab

and a Nicolet 510P instrument, with DTGS detectors and triangular or Happ-Genzel apodization. Dichloromethane used in other laboratories was of reagent or spectro-grade. The spectra were used if they showed no unexpected peaks.

3.2.1 Absorption Index Spectrum

The linear (decadic) absorption coefficient, $K(\tilde{\nu})$, is the absorbance per unit length⁹, and is needed at anchor points in the baseline in order to correct the baselines^{3,6}. The values were determined from EA spectra recorded in this laboratory. They are given in Table 3.1, with their 95% confidence limit, the corresponding value of the absorption index, k , and its 95% confidence limit, the wavenumber of the anchor point, and the path lengths of the cells used to obtain the anchor point information.

The EA spectra from all sources were converted individually to absorption index, k , spectra by program RNJ46A^{3,6}, with baselines corrected through the anchor point K values. Table 3.2 shows the spectral regions that were used in the calculations, together with the cell path lengths used, the value of n_{∞} , and the number of spectra from each spectroscopist. Each spectrum was only used in those regions where the peak EA values were between 0.3 and 1.9. The spectra recorded in this laboratory are labeled ZL and VB, identifying Z. Lan and V. Behnam. The other collaborators are identified by A, B or C. The value of n_{∞} for each region is needed by the Kramers-Kronig transform in program RNJ46A^{3,6}, and was obtained either from the graphs in reference 10 or from tables of $n(\tilde{\nu})$ calculated from the k spectra of reference 8.

The peak heights, peak wavenumbers, and areas above zero ordinate under band groups between specified integration limits, were measured for each k spectrum. For

Table 3.1. Linear absorption coefficients and imaginary refractive indices at anchor points for liquid dichloromethane at 25°C.

Wave-number (cm ⁻¹)	Cell pathlengths (mm)	$K(\tilde{\nu})$ (cm ⁻¹)	95% Confidence limit (cm ⁻¹)	$k(\tilde{\nu})^a$	95% Confidence limit in $k(\tilde{\nu})^a$
6313.8	3.7-5.0	0.031	0.008	9×10^{-7}	2×10^{-7}
5688.5	3.7-5.0	0.090	0.008	2.9×10^{-6}	2×10^{-7}
4980.0	3.7-5.0	0.071	0.006	2.6×10^{-6}	2×10^{-7}
4618.2	3.0-5.0	0.238	0.005	9.4×10^{-6}	2×10^{-7}
4343.3	3.0-5.0	1.252	0.009	5.29×10^{-5}	4×10^{-7}
4072.9	3.0-5.0	0.551	0.005	2.48×10^{-5}	2×10^{-7}
3854.0	3.0-5.0	0.855	0.015	4.07×10^{-5}	7×10^{-7}
3480.4	2.7-5.0	0.245	0.007	1.29×10^{-5}	4×10^{-7}
2755.7	3.0-5.0	0.704	0.006	4.68×10^{-5}	4×10^{-7}
2382.1	2.7-5.0	1.887	0.007	1.45×10^{-4}	5×10^{-7}
2193.1	3.0-5.0	0.672	0.005	5.62×10^{-5}	4×10^{-7}
1923.6	3.0-5.0	0.113	0.005	1.08×10^{-5}	4×10^{-7}
1685.9	3.7-5.0	0.273	0.004	2.97×10^{-5}	4×10^{-7}
1532.6	1.5-5.0	2.701	0.010	3.23×10^{-4}	1×10^{-6}
1356.6	1.5-3.0	5.547	0.024	7.50×10^{-4}	3×10^{-6}
1186.0	0.5-1.5	7.789	0.038	1.204×10^{-3}	6×10^{-6}
1053.9	1.5-4.7	1.604	0.003	2.79×10^{-4}	5×10^{-7}
965.7	1.5-4.7	3.355	0.008	6.37×10^{-4}	2×10^{-6}
853.8	0.5-4.7	3.777	0.019	8.11×10^{-4}	4×10^{-6}
509.6	~1.5	0.411	0.041	1.48×10^{-4}	1.5×10^{-5}

^a $k(\tilde{\nu})=2.303K(\tilde{\nu})/(4\pi\tilde{\nu})$; The 95% confidence limit of k , Δk , was calculated from the 95% confidence limit of K , ΔK , by $\Delta k=2.303 \Delta K/(4\pi\tilde{\nu})$.

Table 3.2. Pathlengths, high-wavenumber refractive index, and number of spectra from each spectroscopist, for the region processed.

Region (cm ⁻¹)	Path- lengths used (μm)	n_{∞} ^a	ZL	A	B	C	VB	Total
6500-5685	~500	1.413	6				2	8
5695-4600	3700-5000	1.412	6					6
4620-4345	100-200	1.412	6			1	8	15
4365-4075	100-530	1.412	8	2	4	1	7	22
4085-3845	470-520	1.412	5	2	2		7	16
3860-3470 ^b	500-1500	1.412	13	1	2		6	22
3490-2860	30-150	1.411	5		6		11	22
2870-2745	500-1500	1.412	8				6	14
2765-2375	100-520	1.411	5	2	2		7	16
2385-2200	50-150	1.410	5		2		1	8
2210-1915	1200-5000	1.410	16					16
1925-1575 ^b	4200-5000	1.408	5					5
1580-1525	1500-2700	1.403	6					6
1535-1354	~50	1.402	6		4		7	17
1356-1175	~11	1.396	5				1	6
1200-960	~1500	1.413	5					5
968-800	30-60	1.386	6		9		13	28

^a n_{∞} is the real refractive index at the highest wavenumber in the region.

^b The influence of impurity water was seen between 3741 and 3531 cm⁻¹ and between 1685 and 1560 cm⁻¹. Only the spectra from the driest samples were used in these regions.

each region the k spectra were averaged to give a single spectrum for each spectroscopist. Tables 3.3 and 3.4 give the average areas and peak heights obtained by the different spectroscopists. Table 3.3 specifies the integration limits. Table 3.4 contains only those peaks that were measured by more than one spectroscopist, and includes the peak wavenumbers which were determined, with the peak heights, from the maximum of the parabola fitted to the top three points of the band.

The areas and peak heights from the different spectroscopists in Tables 3.3 and 3.4 agree very well. As was found for the liquids reported previously²⁻⁴, the agreement between spectroscopists sometimes exceeds the combined 95% confidence limits by a few percent, up to about 3% for CH_2Cl_2 , partly due to inadequate statistics and partly due to the systematic errors inherent in the use of one instrument by one spectroscopist. There was, however, clear evidence of water absorption in some samples, at 3692, 3600 and 1600 cm^{-1} . The high quality of the agreement between the areas is shown pictorially in Figure 3.1 for the regions 4345.3 to 4075.3 cm^{-1} , 2750.5 to 2625.1 cm^{-1} , and 2480.0 to 2380.2 cm^{-1} .

For each region in Table 3.2, the average k spectra from the different spectroscopists were averaged to yield an unweighted overall average k spectrum. To check for distortion in the unweighted average because two spectroscopists, ZL and VB, used the same instrument and ran the majority of the spectra, an overall weighted-average k spectrum was also calculated from the spectroscopist-average spectra, with the weighting factor equal to the number of spectra which contributed to the spectroscopist average (Table 3.2). The spectra in the different regions were then merged to give an

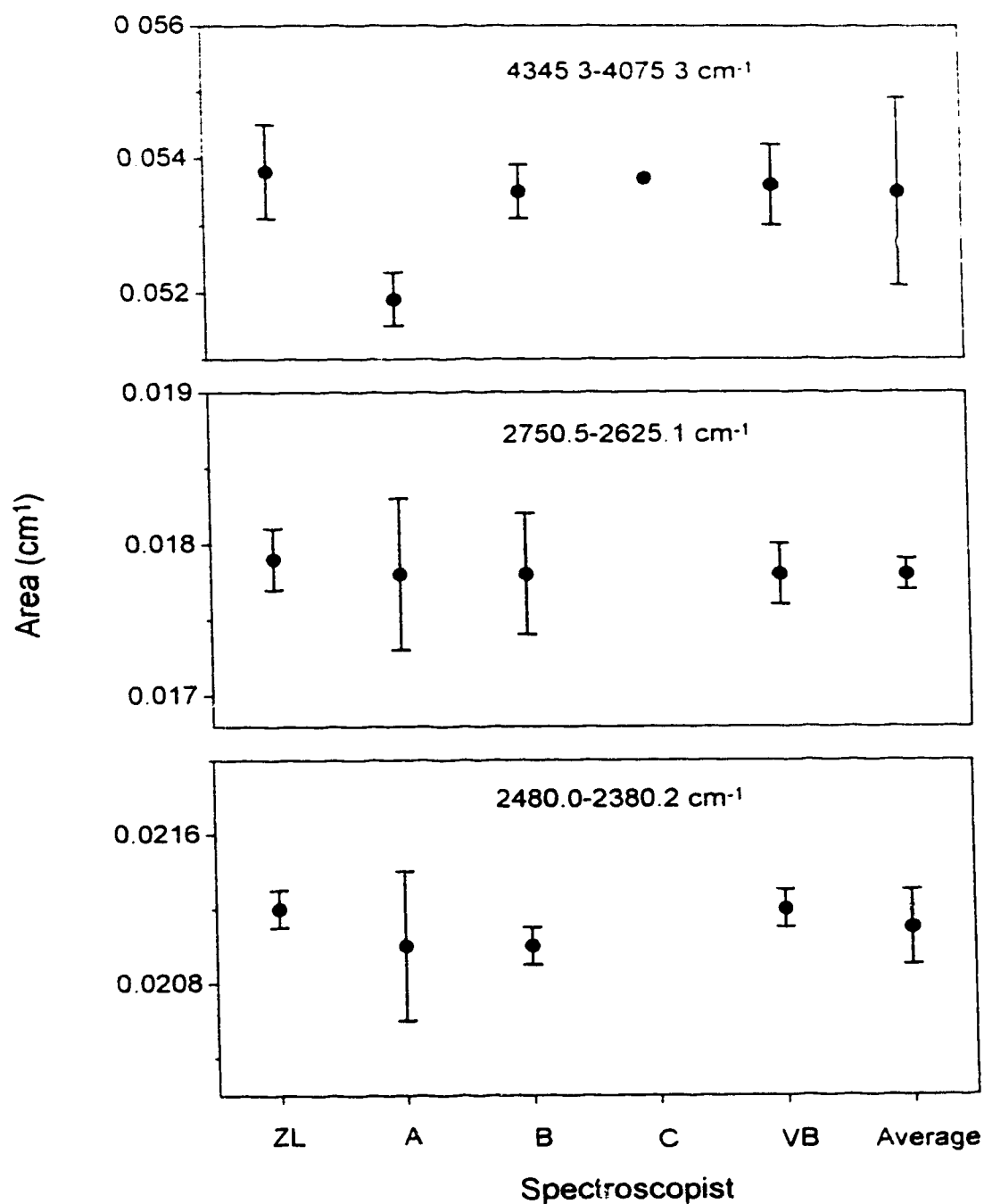


Figure 3.1. Average areas under the absorption index spectra (dots) and their 95% confidence limits (vertical error bars) for the five spectroscopists in three spectral regions from Table 3.3. Also shown for each region above the label 'Average' is the unweighted average area from Table 3.5 (dot) and the maximum deviation from it.

Table 3.3 Spectroscopist average areas under the absorption index bands.^a

Region (cm ⁻¹)	ZL	A	B	C	VB
6200.0-5725.1	0.0303(13)				0.0321(28)
4625.4-4345.3	0.0657(25)			0.0635	0.0677(24)
4345.3-4075.3	0.0538(7)	0.0519(4)	0.0535(4)	0.0537	0.0536(6)
4075.3-3855.0	0.0225(2)	0.0221(1)	0.0224(2)		0.0225(2)
3855.0-3620.2	0.0260(6)	0.0274	0.0260(2) ^b		0.0275(2)
3330.5-2870.0	0.401(4)		0.405(6)		0.411(5)
2750.5-2625.1	0.0179(2)	0.0178(5)	0.0178(4)		0.0178(2)
2615.0-2480.0	0.0147(1)	0.0147(1)	0.0145(1)		0.0146(2)
2480.0-2380.2	0.0212(1)	0.0210(4)	0.0210(1)		0.0212(1)
2380.2-2215.3	0.0734(6)		0.0721(1)		0.0734
2190.3-2085.2	0.0142(1)				
2085.2-2030.2	0.00442(2)				
1530.2-1355.2	0.370(2)		0.372(3)		0.374(2)
1355.2-1185.0	2.696(30)				2.697
965.2-860.1	0.299(6)		0.301(6)		0.303(4)

^a The unit of area is cm⁻¹. The numbers in parentheses are the 95% confidence limits in the last digit. In some cases only one spectrum was available, so that no 95% confidence limit could be calculated, and in others no spectrum was available from that spectroscopist for that region.

^b The result from the driest sample, in which the 3600 cm⁻¹ water peak was essentially absent.

Table 3.4. Spectroscopist average absorption index peak heights, k_{\max}^a

$\tilde{\nu}(\text{cm}^{-1})$	ZL	A	B	C	VB
6063.2	0.000131(5)				0.000136(13)
5915.1	0.000268(12)				0.000277(31)
5899.2	0.000275(12)				0.000279(24)
5834.5	0.000146(6)				0.000152(20)
4452.7	0.00231(10)			0.00217	0.00232(13)
4253.1	0.000524(11)	0.000508(9)	0.000513(9)	0.000519	0.000520(6)
4196.6	0.00127(5)	0.00112(2)	0.00123(2)	0.00123	0.00125(4)
3944.0	0.000615(7)	0.000586(4)	0.000605(5)		0.000611(6)
3878.0	0.0000644(9)	0.0000629(52)	0.0000632(4)		0.0000636(10)
3825.9	0.0000739(3)	0.0000725	0.0000741(5)		0.0000744(9)
3757.2	0.000275(2)	0.000269	0.000273(2)		0.000276(2)
3729.2	0.000180(2)	0.000183	0.000182(1)		0.000186(1)
3691.9	0.000330(12)	0.000352	0.000323(1) ^b		0.000354(4)
3054.1	0.00716(9)		0.00703(6)		0.00733(17)
2987.0	0.00383(2)		0.00383(2)		0.00392(5)
2830.7	0.000313(3)				0.000311(1)
2685.5	0.000870(8)	0.000871(6)	0.000867(i)		0.000870(9)
2521.4	0.000355(2)	0.000352(1)	0.000350(1)		0.000352(2)
2410.5	0.000658(3)	0.000647(9)	0.000643(11)		0.000652(4)
2305.6	0.00292(2)		0.00283(2)		0.00287
1422.0	0.00983(3)		0.00952(20)		0.00988(6)
1265.2	0.244(5)				0.244
896.1	0.0184(1)		0.0176(2)		0.0183(2)

^a The numbers in parentheses are the 95% confidence limits in the last digit. In some cases only one spectrum was available, so that no 95% confidence limit could be calculated, and in others no spectrum was available from that spectroscopist for that region.

^b The result from the driest sample, in which the 3600 cm^{-1} water peak was essentially absent.

unweighted-average k spectrum and a weighted-average k spectrum over the full spectral range. The overall average areas and the overall average peak heights for both the weighted and the unweighted average k spectra are presented in Tables 3.5 and 3.6. The weighted and unweighted averages all agree to 1.8% or better; only a few cases exceed 1% and the average agreement over all bands equals 0.4% for the areas and 0.6% for the peak heights. The unweighted average k spectrum, areas and peak heights were taken as the primary absorption intensity results of this work. The k spectrum is shown graphically in Fig. 3.2 and is tabulated in the Compact Table¹¹ format in Table 3.7.

Because the different integration ranges have different widths, the height of the strongest peak of each band group is included in Table 3.5 to indicate the prominence of the absorption. The agreement between spectroscopists is shown in Table 3.5 by the maximum deviation of the averages of the different spectroscopists from each unweighted average area. The quality of the agreement is illustrated in Figure 3.1, where each box includes, above the label 'Average', the unweighted average area and the maximum deviation from it. Numerically, the average agreement is $\pm 1.5\%$ over the 11 unstarred band groups in Table 3.5, band groups for which good data were available from more than one spectroscopist. Below 3600 cm^{-1} , the agreement averages $\pm 0.8\%$ over the 7 unstarred band groups and is always better than $\pm 1.5\%$. Above 3600 cm^{-1} it lies between 1.3 and 3.2%. This good agreement between spectra measured in different laboratories on instruments by different manufacturers is similar to that found for benzene³, toluene⁴ and chlorobenzene⁵.

Table 3.5. Overall average areas under the absorption index bands.

Region (cm ⁻¹)	k_{\max} ^a	Weighted average area	Unweighted average area	Maximum deviation ^{b,c}	Anchor point uncertainty ^{b,d}	Percent estimated error ^e
6200.0-5725.1	0.000277	0.0307	0.0312	±0.0009	±0.00011	3.3
4625.4-4345.3	0.00227	0.0666	0.0656	±0.0021	±0.000080	3.3
4345.3-4075.3	0.00122	0.0535	0.0533	±0.0014	±0.000082	2.8
4075.3-3855.0	0.000604	0.0224	0.0224	±0.0003	±0.00010	1.8
3855.0-3620.2	0.000323	0.0260	0.0260	±0.0002*	±0.00013	~2
3330.5-2870.0	0.00717	0.407	0.405	±0.006	±0.00017	1.5
2750.5-2625.1	0.000870	0.0178	0.0178	±0.0001	±0.00006	0.9
2615.0-2480.0	0.000352	0.0146	0.0146	±0.0001	±0.00006	1.1
2480.0-2380.2	0.000650	0.0211	0.0211	±0.0001	±0.000044	0.7
2380.2-2215.3	0.00287	0.0731	0.0730	±0.0009	±0.000076	1.3
2190.3-2085.2	0.000272	0.0142	0.0142	±0.0001*	±0.000044	1.0
2085.2-2030.2	0.000249	0.00442	0.00442	±0.00002*	±0.000023	1.0
1530.2-1355.2	0.00974	0.372	0.372	±0.002	±0.00039	0.64
1355.2-1185.0	0.244	2.696	2.697	±0.030*	±0.00078	1.1
965.2-860.1	0.0181	0.302	0.301	±0.002	±0.00029	0.76

^a Height of the strongest peak in the region.

^b The unit of area is cm⁻¹.

^c The maximum deviation of the average of any one spectroscopist from the unweighted average, except for the starred values for the regions 3855.0-3620.2, 2190.3-2085.2 and 2085.2-2030.2, and 1355.2-1185.0 cm⁻¹. The values given for the middle two regions are the 95% confidence limit of the average area of ZL (Table 3.3), the only spectroscopist who had spectra in these regions. For the last region, the maximum deviation is 0.001, but five of the six spectra came from ZL so the value given is ZL's 95% confidence limit. For 3855.0-3620.2 cm⁻¹ the value is the 95% confidence limit for the driest sample, in which the 3600.0 cm⁻¹ water peak was essentially absent.

^d The anchor point uncertainty is the integration range multiplied by the average of the 95% confidence limits in k (Table 3.1) at the two anchor points used for that range.

^e The percent estimated error is the sum of the maximum deviation and the anchor point uncertainty as a percentage of the unweighted average area for all regions except 3855.0-3620.2 cm⁻¹. For this region the error so calculated was rounded up to the next digit to acknowledge the extra uncertainty due to water impurity.

Table 3.6. Overall average peak heights in the absorption index spectra.

$\nu(\text{cm}^{-1})$	Weighted average	Unweighted average ^a	Anchor point uncertainty ^b	Percent estimated error ^c	Reference 7 & 8 ^d	Reference 10 ^e
6063.2	0.000132	0.000134(3)	2.4×10^{-7}	2.4		
5915.1	0.000270	0.000272(5)	2.4×10^{-7}	1.9		
5899.2	0.000276	0.000277(2)	2.4×10^{-7}	0.8		
5834.5	0.000149	0.000149(3)	2.4×10^{-7}	2.2		
4452.7	0.00231	0.00227(10)	2.9×10^{-7}	4.4		
4255.1	0.000519	0.000517(9)	3.1×10^{-7}	1.8		
4196.6	0.00124	0.00122(10)	3.1×10^{-7}	8.2		
3944.0	0.000609	0.000604(18)	4.8×10^{-7}	3.1	0.000606(5)	0.000610(36)
3878.0	0.0000638	0.0000635(9)	4.8×10^{-7}	2.2	0.000063(6) ^f	0.000064(05)
3825.9	0.0000740	0.0000737(12)	5.4×10^{-7}	2.4		0.000075(06)
3757.2	0.000275	0.000273(4)	5.4×10^{-7}	1.7		0.000268(18)
3729.2	0.000182	0.000183(3)	5.4×10^{-7}	2.0		0.000176(11)
3691.9	0.000323 ^g	0.000323 ^g	5.4×10^{-7}	~5 ^g		0.000368(20)
3054.1	0.00720	0.00717(16)	3.6×10^{-7}	2.2	0.00731(8)	0.00705(16)
2987.0	0.00388	0.00386(6)	3.6×10^{-7}	1.6	0.00390(3)	0.00382(11)
2830.7	0.000312	0.000312(1)	3.6×10^{-7}	0.5		0.000298(19)
2685.5	0.000868	0.000870(3)	4.4×10^{-7}	0.4	0.000856(6)	0.000911(40)
2521.4	0.000352	0.000352(3)	4.4×10^{-7}	1.0	0.000346(5)	0.000338(22)
2410.5	0.000651	0.000650(8)	4.4×10^{-7}	1.3	0.000644(6)	0.000700(35)
2305.6	0.00288	0.00287(5)	4.6×10^{-7}	1.8	0.00277(2) ^f	0.00288(11)
*2155.5	0.000247	0.000247(1)	4.2×10^{-7}	0.6		0.000237(16)
*2126.0	0.000272	0.000272(2)	4.2×10^{-7}	0.9		0.000266(17)
*2054.8	0.000249	0.000249(2)	4.2×10^{-7}	1.0		0.000240(16)
*1998.3	0.0000697	0.0000697(4)	4.2×10^{-7}	1.2		0.000073(5)
*1970.0	0.0000960	0.0000960(4)	4.2×10^{-7}	0.9		0.000101(6)
*1884.1	0.0000326	0.0000326(3)	4.1×10^{-7}	2.2		0.000040(4)
*1789.0	0.0000656	0.0000656(5)	4.1×10^{-7}	1.4		0.000075(5)
*1707.7	0.0000449	0.0000449(1)	4.1×10^{-7}	1.2		0.000057(4)
*1600.0	0.00023 ^g	0.00023 ^g	7.9×10^{-7}	~5 ^g		0.000354(20)
*1550.8	0.000804	0.000804(6)	7.9×10^{-7}	0.9		0.000842(31)
1422.0	0.00978	0.00974(22)	2.3×10^{-6}	2.3	0.00973(4)	0.00974(20)
1265.2	0.245	0.244(1)	4.6×10^{-6}	0.5		0.246(5)
*1156.2	0.00181	0.00181(1)	3.2×10^{-6}	0.8		0.00185(7)
*1020.0	0.000514	0.000514(1)	1.1×10^{-6}	0.5		0.000584(4)
*985.9	0.000966	0.000966(2)	1.1×10^{-6}	0.4		0.000958(6)
896.1	0.0181	0.0181(5)	2.8×10^{-6}	2.8	0.0184(1)	0.0182(4)

^a In this column the number in parentheses is the maximum deviation from the unweighted average, except where the starred wavenumbers identify peaks recorded only by ZL. In these cases the number is the 95% confidence limit in ZL's average value.

^b The uncertainty due to the anchor points is the average of the uncertainties in the k values at the closest anchor points either side of the peak (Table 3.1).

^c The percent estimated error is the sum of the maximum deviation and the uncertainty due to the anchor points as a percentage of the unweighted average.

^d In this column the number in parentheses is the 90% confidence limit in the last digit.

^e In this column the number in parentheses is the evaluated uncertainty in the value.

^f The exponent of this value was erroneously shown as 10^{-4} in Table 3.3 of Ref. 7.

^g At 3691.9 and 1600.0 cm^{-1} (also at 3600 cm^{-1}) some spectra showed clear effects of impurity water in the sample used. The value given is from the dried sample with a % estimated error of ~5%.

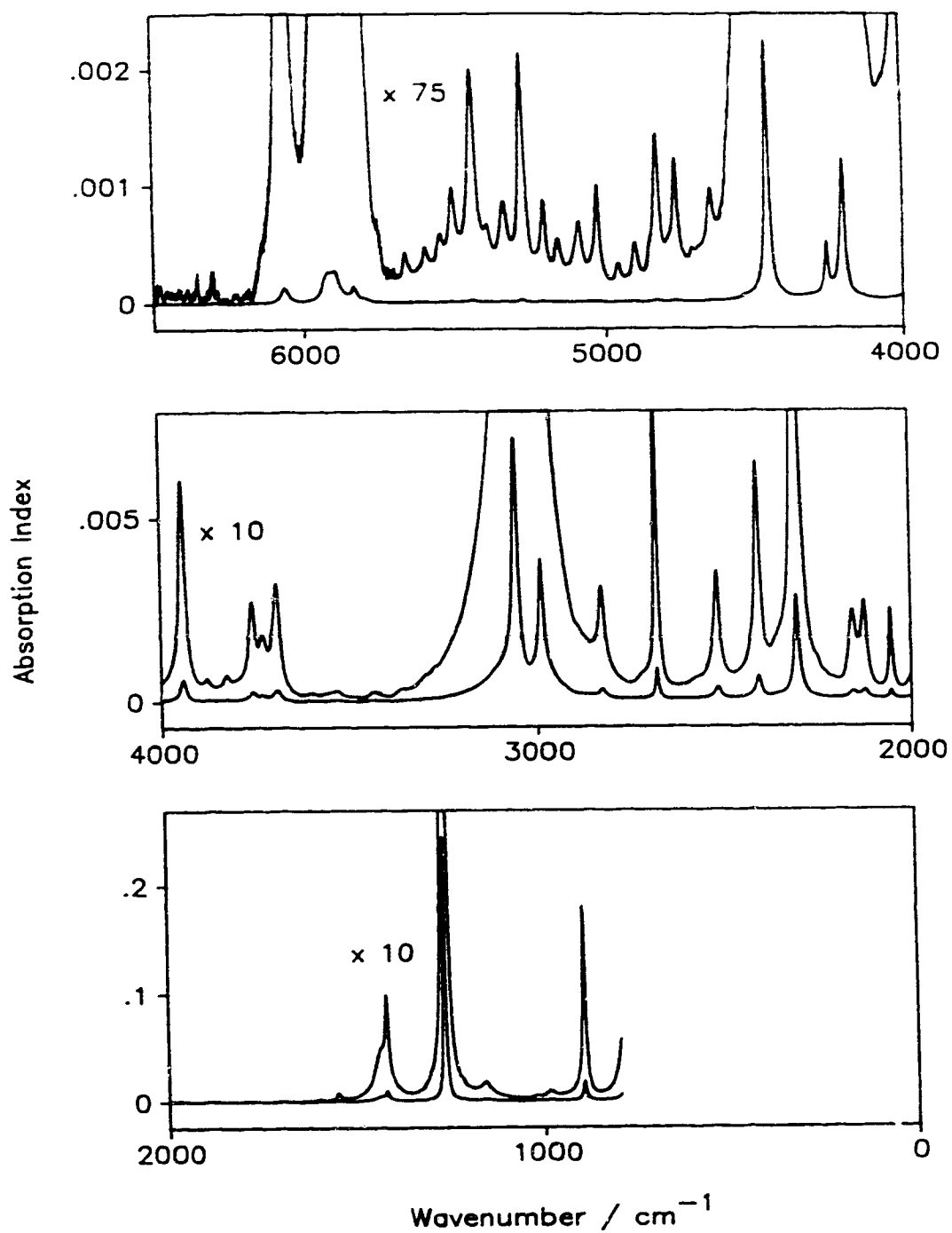


Figure 3.2. Absorption index (imaginary refractive index), k , spectrum between 6500 and 800 cm^{-1} of dichloromethane at 25°C. The ordinate labels are for the lower spectrum in each box; they must be divided by 75 or 10, as shown, for the upper spectrum in the box.

Table 3.7. Absorption indices between 6500 and 800 cm^{-1} for liquid dichloromethane at 25 $^{\circ}\text{C}$.^{a,b}

cm^{-1}	XE	YE	0	1	2	3	4	5	6	7	8	9	10	11	12	13	14	15	16
6499.90	4	-7	0	12	10	15	12	8	8	12	4	20	9	2	14	37	7	3	5
6237.63	4	-7	2	10	1	11	5	27	56	68	114	198	451	1210	891	361	207	165	195
5975.35	4	-7	301	489	1022	2252	2678	2739	1808	988	796								
5848.08	2	-7	864	1002	1231	1451	1422	1207	965	759	614								
5809.51	3	-7	454	422	377	278	201	128	99	70	76	54	40	35	35	31	34	31	31
5678.37	3	-7	31	41	58	50	42	37	35	37	40	44	53	63	55	49	48	53	66
5547.23	3	-7	78	75	67	69	84	117	129	103	86	79	81	93	123	185	258	242	168
5416.10	3	-7	117	93	83	87	88	77	67	62	65	78	102	116	100	80	71	74	93
5284.96	3	-7	157	278	236	154	102	73	59	56	57	61	81	116	89	58	48	48	63
5153.83	3	-7	72	58	47	43	44	46	54	65	82	92	75	57	47	45	52	62	99
5022.69	3	-7	128	75	48	36	29	27	26	30	40	44	34	29	29	31	35	49	68
4891.56	3	-7	58	43	36	37	46	67	83	137	192	147	99	74	68	72	77	88	138
4760.42	3	-7	152	97	70	58	52	52	59	62	60	61	65	67	71	82	109	129	110
4629.28	3	-7	95	93	99	110	136	190	220	252	284	331	378	461	543	648	746	817	945
4498.15	3	-6	113	146	203	308	558	1334	2234	1156	550	304	198	151	124	104	84	71	61
4367.01	3	-7	558	532	532	527	543	565	612	653	698	729	779	900	1145	1753	3552	4960	2714
4235.88	3	-6	197	199	236	350	694	1213	792	369	201	130	97	77	65	59	50	41	36
4104.74	3	-7	319	291	256	246	246	251	257	265	278	299	331	379	440	491	546	633	757
3979.39	1	-7	793	834	882	934	991	1061	1146	1241	1361	1511	1700	1940	2262	2685	3238	3938	4755
3946.61	1	-7	5536	6000	5922	5353	4565	3790	3125	2579	2146	1806	1549	1353	1198	1071	966	880	809
3913.82	1	-7	751	704	663	630	604	579	559	549	536	525	519	521	520	525	538	557	576
3881.04	1	-7	604	631	630	602	567	529	495	470	451	437	421	414	410	407	400	408	414
3848.25	1	-7	418	425	436	451	467	490	522	556	602	652	700	731	733	707	666	630	597
3815.47	1	-7	574	562	558	558	563	573	579	588	603	611	622	634	646	661	677	696	
3782.69	2	-7	749	831	962	1176	1532	2066	2609	2691	2276	1814	1546	1502	1621	1770	1819	1734	1561
3717.12	2	-7	1432	1398	1508	1770	2164	2674	3139	3148	2569	1866	1330	980	762	601	500	417	360
3651.55	2	-7	317	278	256	226	215	198	190	184	172	181	179	198	216	227	230	203	194
3585.98	2	-7	176	174	176	177	194	200	221	224	234	246	250	264	261	282	281	260	222
3520.42	2	-7	189	165	151	140	135	130	130	129	128	129	128	118	112	106	105	109	123
3454.85	2	-7	121	145	186	228	243	251	250	242	228	220	180	162	153	142	131	141	139
3389.28	2	-7	149	164	191	229	261	305	321	340	352	356	342	337	343	356	359	372	389
3323.71	2	-7	419	449	486	532	575	619	678	711	738	752	787	824	888	947	964	966	1004
3258.14	2	-7	1040	1101	1166	1235	1274	1376	1449	1517	1594	1674							
3215.72	3	-6	184	203	224	251	284	320	361	403	453	507	564	630	709	804	897	995	1126
3090.37	1	-6	1168	1215	1268	1328	1396	1474	1564	1672	1800	1956	2150	2393	2711	3124	3670	4374	5236
3057.58	1	-6	6175	6940	7158	6631	5609	4509	3575	2864	2345	1964	1681	1472	1318	1206	1124	1066	1026
3024.80	1	-6	1001	986	980	982	992	1010	1037	1072	1114	1167	1229	1303	1399	1520	1686	1923	2265
2992.02	1	-6	2745	3325	3778	3822	3491	3032	2602	2239	1946	1710	1518	1362	1232	1126	1036		
2957.30	3	-7	7838	6198	5066	4281	3611	3027	2534	2205	2072	1968	1827	1719	1614	1572	1642	1930	
2839.67	1	-7	206	2300	2567	2852	3065	3101	2943	2670	2371	2098	1865	1674	1514				
2808.81	3	-7	1112	859	740	641	566	509	477	468	484	539	644	751	817				
2714.32	1	-7	839	869	908	956	1015	1093	1192	1324	1511	1787	2210	2887	3968	5648	7709	8694	7380
2681.53	1	-7	5311	3743	2769	2168	1779	1490	1252	1057									
2660.32	3	-7	656	513	448	418	408	411	423	447	488	553	604	646	673	715	809	1005	1417
2534.97	1	-7	1575	1763	1996	2282	2627	3009	3359	3522	3371	2967	2493	2073	1743	1495	1317	1179	1074
2502.18	1	-7	1000	941	888	846	818	793	771	759	752	742	737	737	738	738	744	751	758
2467.47	2	-7	782	809	847	891	944	1016	1103	1226	1386	1616	1946	2442					
2423.12	1	-7	2783	3213	3745	4389	5139	5888	6416	6443	5901	5034	4158	3423	2867	2457	2163	1949	
2390.33	2	-7	1668	1517	1452	1436	1477	1559	1642	1720	1812	1915	2018	2131	2260	2469	2753	3142	3743
2326.69	1	-6	414	462	523	600	703	845	1045	1330	1726	2224	2696	2876	2635	2159	1684	1303	1027
2293.91	1	-7	8317	6918	5837	4939	4190	3589	3131	2770	2478	2241	2042	1867	1709	1583	1477	1396	1340
2259.20	2	-7	1265	1221	1149	1047	937	850	808	776	749	696	662	635	628	611	597	585	572
2193.63	2	-7	563	561	577	621	708	854	1098	1412	1836	2287	2462	2237	1911	1702	1646	1771	2135
2128.06	2	-7	2613	2636	2063	1442	1031	780	623	523	462	425	402	388	388	402	428	468	548
2064.42	1	-7	628	710	1026	1479	2122	2481	2157	1595	1200	943	763	632	540	475	427	393	368
2031.64	1	-7	351	341	337	337	342	352	363	377	394	415	440	470	505	545	590	636	674
1998.85	1	-7	693	688	660	617	572	530	497	475	466	475	504	562	659	788	910	959	906
1966.07	1	-7	779	632	503	404	330	274	232	200	176								
1942.93	3	-7	127	113	106	109	125	157	213	291	310	247	215	200	196	215	233	234	244
1817.58	1	-7	249	255	262	269	278	289	304	318	337	363	398	442	501	571	632	653	620
1784.79	1	-7	561	502	452	412	378	352	332	316	301	290	278	267	261				
1753.94	3	-7	246	243	250	275	351	375	446	355	300	298	313	340	381	439	505	598	
1634.37	2	-7	656	717	784	868	990	1170	1424	1754	2094	2309	2199	1901	1672	1561	1543	1594	1701
1570.73	1	-7	1776	1871	1985	2134	2340	2544	3123	3945	5311	7035	7993	7856	6946	5742	4780	4113	3699
1532.17	3	-6	323	335	371	418	492	615	773	992	1273	1714	2526						
1453.10	1	-6	2796	3084	3387	3702	4020	4324	4593	4795	4921	4984	5030	5128	5373	5912	6964	8613	9840
1420.31	1	-6	9042	7204	5655	4580	3850	3340	2951	2631	2366	2153	1977						
1393.32	3	-6	1491	1220	979	838	761	734	779	856	1021	1189	1637	2248					
1307.50	0	-6	2339	2410	2504	2595	2698	2783	2897	3022	3146	3291	3439	3603	3795	3996	4211	4447	4702
1291.11	0	-5	499	527	563	600	642	685	738	798	867	947	1042	1156	1290	1455	1660	1917	2246
1274.71	0	-4	267	323	399	503	650	856	1146	1527	1959	2325	2446	2240	1827	1415	1083	835	653
1258.32	0	-5	5207	4239	3523	2973	2536	2168	1863	1614	1412	1244	1107	992	896	813	744	685	631

Table 3.7. Continued.

cm ⁻¹	XE	YE	0	1	2	3	4	5	6	7	8	9	10	11	12	13	14	15	16
1241.93	0	-6	5872	5464	5135	4835	4551	4317	4120	3890	3704	3547	3364	3205	3084	2949	2822	2716	2625
1225.54	0	-6	2539	2440	2381	2324	2263	2225	2189	2141	2106	2065	1998	1910					
1211.08	2	-6	1698	1484	1379	1314	1276	1216	1221	1206	1227	1266	1350	1425	1554	1712	1804	1756	1679
1145.51	2	-6	1372	1192	1049	925	823	742	676	620	571	528	491	458	429	403	380	363	350
1079.94	2	-7	3287	3135	3025	2934	2862	2816	2790	2792	2829	2903	3052	3306	3655	4128	4677	5090	5109
1014.37	2	-7	4848	4599	4561	4846	5585	7074	8882	9611	9486	8594	7490	6742	6423	6310	6391	6491	6756
950.73	1	-6	693	716	737	760	787	815	849	887	926	973	1028	1081	1147	1224	1311	1408	1524
917.95	1	-5	166	182	202	227	260	306	373	476	641	917	1348	1768	1680	1219	821	572	427
885.16	1	-6	3300	2554	2033	1681	1435	1253	1115	1015	946	898	858	832	813	802			
856.24	2	-6	800	816	862	953	997	1058	1163	1305	1465	1670	2005	2414	2978	3821	4858	6080	

Note: Footnotes follow Table 3.9

Table 3.6 contains the peak heights in the average k spectra based on the data in Table 3.4. However the peaks whose wavenumbers are starred were not included in Table 3.4 because they were only observed by Z. Lan. These peaks are omitted from consideration of the agreement between workers. As is usual, this agreement is slightly worse than for the areas, and averages 2.3% over the full 23 peaks and about 1.9% over the 16 peaks below 4000 cm⁻¹. There was no evidence that the nominal resolution affected this agreement. For the peaks at 3691.9 and 1600 cm⁻¹ which were clearly changed by water in some samples, only the spectra from the driest sample were used.

3.2.2 The Real Refractive Index Spectrum.

The real refractive index spectrum, $n(\tilde{\nu})$, was determined by Kramers-Kronig transformation of the k spectrum, with n_{∞} taken as 1.4130 ± 0.0004 at 8000 cm⁻¹. This value was obtained by fitting the literature¹² values of the refractive index at six wavelengths in the visible region to $n^2(\tilde{\nu}) = a\tilde{\nu}^4 + b\tilde{\nu}^2 + c$, and extrapolating to 8000 cm⁻¹. In the KK transform it was assumed that k is exactly zero between 6500 and 8000 cm⁻¹. The real refractive index spectrum is shown in Figure 3.3 and the values are given in Table 3.8 in the Compact Table format.¹¹

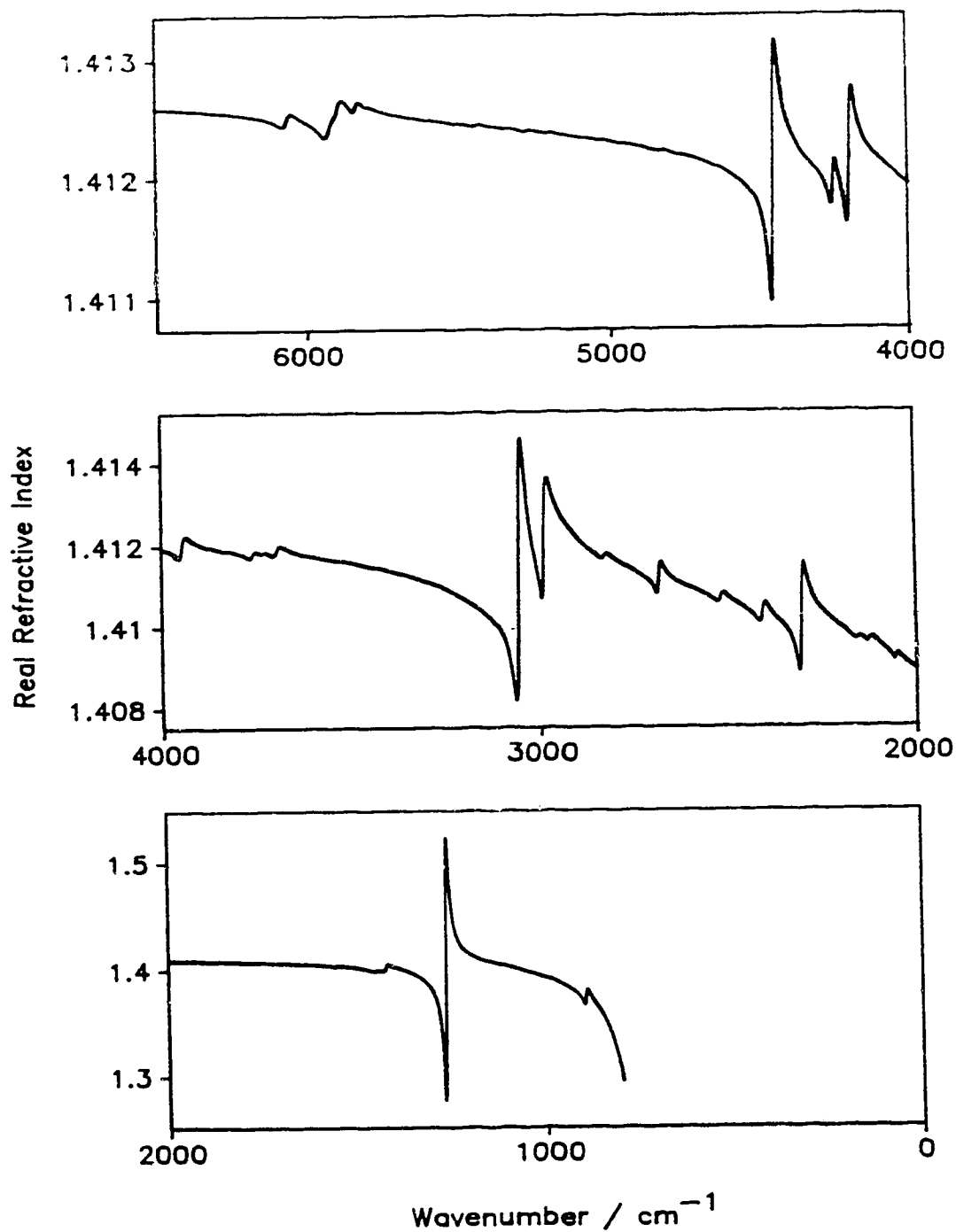


Figure 3.3. Real refractive index, n , spectrum between 6500 and 800 cm^{-1} of dichloromethane at 25°C.

Table 3.8. Real refractive index between 6500 and 800 cm^{-1} of liquid dichloromethane at 25 $^{\circ}\text{C}$.^{a,b}

cm^{-1}	χ_F	0	1	2	3	4	5	6	7	8	9	10	11	12	13	14	15	16
6499.90	4	14125	14125	14125	14125	14125	14125	14125	14125	14125	14125	14125	14125	14125	14125	14125	14125	14125
6237.63	4	14125	14125	14125	14125	14125	14125	14125	14124	14124	14124	14124	14124	14125	14125	14125	14124	14124
5975.35	4	14124	14123	14123	14123	14124	14125	14126	14126	14125								
5848.08	2	14125	14125	14125	14125	14126	14126	14126	14126	14126								
5809.51	3	14126	14126	14125	14125	14125	14125	14125	14125	14125	14125	14125	14125	14125	14125	14125	14125	14125
5678.37	3	14125	14125	14125	14125	14125	14124	14124	14124	14124	14124	14124	14124	14124	14124	14124	14124	14124
5547.23	3	14124	14124	14124	14124	14124	14124	14124	14124	14124	14124	14124	14124	14124	14124	14124	14124	14124
5416.10	3	14124	14124	14124	14124	14124	14124	14124	14124	14124	14124	14124	14124	14124	14124	14123	14123	14123
5284.96	3	14123	14123	14123	14124	14123	14123	14123	14123	14123	14123	14123	14123	14123	14123	14123	14123	14123
5153.83	3	14123	14123	14123	14123	14123	14123	14123	14123	14123	14123	14123	14123	14123	14123	14123	14123	14123
5022.69	3	14123	14123	14123	14123	14122	14122	14122	14122	14122	14122	14122	14122	14122	14122	14122	14122	14122
4891.56	3	14122	14122	14122	14122	14122	14122	14122	14122	14122	14122	14122	14122	14122	14121	14121	14121	14121
4760.42	3	14121	14121	14121	14121	14121	14121	14121	14121	14121	14121	14121	14121	14121	14120	14120	14120	14120
4629.28	3	14120	14120	14120	14120	14120	14120	14119	14119	14119	14119	14119	14119	14118	14118	14118	14118	14117
4498.15	3	14117	14116	14115	14113	14111	14109	14122	14131	14129	14127	14126	14125	14124	14123	14123	14123	14122
4367.01	3	14122	14122	14121	14121	14121	14121	14120	14120	14120	14120	14119	14119	14118	14118	14117	14120	14121
4235.88	3	14120	14119	14118	14117	14116	14120	14127	14126	14125	14124	14123	14123	14122	14122	14122	14122	14121
4104.74	3	14121	14121	14121	14121	14120	14120	14120	14120	14120	14120	14119	14119	14119	14119	14119	14119	14118
3979.39	1	14118	14118	14118	14118	14118	14118	14118	14118	14117	14117	14117	14117	14117	14117	14117	14117	14117
3946.61	1	14118	14119	14120	14121	14122	14122	14122	14122	14122	14122	14121	14121	14121	14121	14121	14121	14120
3913.82	1	14120	14120	14120	14120	14120	14120	14120	14120	14120	14120	14120	14119	14119	14119	14119	14119	14119
3881.04	1	14119	14119	14119	14119	14119	14119	14119	14119	14119	14119	14119	14119	14119	14119	14119	14119	14119
3848.25	1	14119	14118	14118	14118	14118	14118	14118	14118	14118	14118	14118	14118	14118	14118	14118	14118	14118
3815.47	1	14118	14118	14118	14118	14118	14118	14118	14118	14118	14118	14118	14118	14118	14117	14117	14117	14117
3782.69	2	14117	14117	14117	14117	14116	14116	14117	14118	14118	14118	14118	14118	14118	14118	14118	14118	14118
3717.12	2	14118	14117	14117	14117	14117	14117	14118	14119	14119	14119	14119	14119	14119	14119	14118	14118	14118
3651.55	2	14118	14118	14118	14118	14118	14117	14117	14117	14117	14117	14117	14117	14117	14117	14117	14117	14117
3585.98	2	14117	14116	14116	14116	14116	14116	14116	14116	14116	14116	14116	14116	14116	14116	14116	14116	14116
3520.42	2	14116	14115	14115	14115	14115	14115	14115	14115	14115	14115	14115	14115	14115	14115	14115	14114	14114
3454.85	2	14114	14114	14114	14114	14114	14114	14114	14114	14114	14114	14114	14114	14113	14113	14113	14113	14113
3389.28	2	14113	14113	14113	14113	14112	14112	14112	14112	14112	14112	14112	14112	14112	14112	14112	14111	14111
3323.71	2	14111	14111	14111	14111	14111	14111	14110	14110	14110	14110	14110	14110	14110	14110	14109	14109	14109
3258.14	2	14109	14109	14109	14108	14108	14108	14108	14108	14108	14108	14107						
3215.72	3	14107	14106	14106	14106	14105	14105	14104	14104	14103	14102	14102	14101	14100	14100	14099	14098	14096
3090.37	1	14096	14095	14094	14094	14093	14092	14091	14090	14089	14088	14087	14085	14084	14082	14081	14081	14084
3057.58	1	14090	14101	14117	14131	14141	14145	14145	14144	14141	14139	14136	14134	14131	14129	14128	14126	14124
3024.80	1	14123	14122	14121	14120	14119	14118	14117	14116	14115	14114	14113	14112	14111	14110	14108	14107	14106
2992.02	1	14106	14109	14115	14124	14130	14134	14135	14136	14136	14135	14134	14134	14133	14133	14132	14132	
2957.30	3	14129	14128	14126	14125	14124	14123	14122	14121	14120	14120	14119	14118	14118	14117	14117	14116	
2839.67	1	14116	14116	14116	14116	14116	14116	14117	14117	14117	14117	14117	14117	14117	14117	14117	14117	
2808.81	3	14116	14116	14115	14115	14114	14114	14113	14113	14113	14112	14112	14111	14111				
2714.32	1	14111	14111	14110	14110	14110	14110	14109	14109	14109	14108	14108	14107	14107	14109	14111	14114	
2681.53	1	14115	14115	14114	14114	14114	14113	14113	14113	14113								
2660.32	3	14112	14111	14111	14110	14110	14109	14109	14109	14108	14108	14108	14107	14107	14107	14106	14106	14105
2534.97	1	14105	14105	14105	14105	14105	14105	14106	14106	14107	14107	14107	14107	14107	14107	14107	14107	14106
2502.18	1	14106	14106	14106	14106	14106	14106	14105	14105	14105	14105	14105	14105	14105	14105	14105	14104	14104
2467.47	2	14104	14103	14104	14103	14103	14103	14102	14102	14102	14101	14101	14101					
2423.12	1	14100	14100	14100	14100	14100	14101	14102	14103	14104	14105	14105	14105	14105	14104	14104	14104	
2390.33	2	14103	14103	14102	14102	14101	14101	14100	14100	14100	14099	14099	14098	14098	14097	14097	14096	14095
2326.69	1	14094	14094	14093	14092	14091	14090	14089	14088	14088	14090	14095	14102	14109	14113	14115	14115	14114
2293.91	1	14113	14112	14111	14111	14110	14109	14108	14108	14107	14107	14106	14106	14106	14105	14105	14105	14104
2259.20	2	14104	14103	14103	14103	14102	14102	14101	14101	14101	14101	14100	14100	14100	14099	14099	14099	14099
2193.63	2	14098	14098	14098	14097	14097	14096	14096	14096	14096	14096	14096	14096	14096	14096	14096	14095	14095
2128.06	2	14095	14096	14096	14096	14096	14096	14095	14095	14095	14094	14094	14094	14093	14093	14092	14092	14092
2064.42	1	14091	14091	14091	14091	14091	14092	14092	14092	14092	14092	14092	14092	14091	14091	14091	14091	14091
2031.64	1	14091	14090	14090	14090	14090	14090	14090	14089	14089	14089	14089	14089	14089	14089	14088	14088	14088
1998.85	1	14088	14088	14088	14088	14088	14088	14088	14087	14087	14087	14087	14087	14087	14087	14087	14087	14087
1966.07	1	14087	14087	14086	14086	14086	14086	14086	14086	14086	14085							
1942.93	3	14085	14084	14084	14083	14082	14082	14081	14080	14080	14079	14079	14078	14077	14077	14076	14075	14074
1817.58	1	14074	14074	14074	14074	14073	14073	14073	14073	14073	14072	14072	14072	14072	14072	14072	14071	14071
1784.79	1	14071	14071	14071	14071	14070	14070	14070	14070	14070	14069	14069	14069	14069				
1753.94	3	14068	14067	14066	14065	14064	14063	14062	14061	14060	14059	14057	14056		14054	14052	14051	
1634.37	2	14050	14049	14048	14048	14047	14046	14045	14044	14044	14043	14043	14042	14041	14040	14039	14038	14037
1570.73	1	14036	14035	14035	14034	14033	14032	14031	14030	14030	14030	14030	14030	14030	14030	14030	14030	14030
1532.17	3	14028	14024	14021	14018													

Table 3.8. Continued.

cm ⁻¹	XE	0	1	2	3	4	5	6	7	8	9	10	11	12	13	14	15	16
1241 93	0	14383	14368	14355	14343	14331	14321	14311	14302	14293	14284	14277	14269	14262	14255	14249	14243	14237
1225 54	0	14231	14226	14221	14216	14211	14207	14203	14199	14195	14191	14188	14184					
1211 08	2	14172	14159	14148	14138	14130	14122	14114	14107	14101	14095	14089	14084	14080	14076	14074	14073	14071
1145 51	2	14068	14064	14060	14056	14052	14048	14044	14040	14036	14033	14029	14025	14021	14018	14014	14010	14006
1079 94	2	14003	13999	13995	13991	13987	13984	13980	13976	13971	13967	13963	13959	13954	13950	13946	13942	13938
1014 37	2	13934	13929	13924	13918	13913	13907	13903	13899	13895	13891	13885	13879	13872	13866	13858	13851	13844
950 73	1	13840	13836	13832	13827	13823	13819	13814	13810	13805	13800	13795	13790	13784	13779	13773	13767	13760
917 95	1	13754	13746	13739	13730	13721	13710	13699	13685	13671	13660	13663	13706	13772	13803	13800	13786	13771
885 16	1	13757	13744	13730	13718	13706	13694	13683	13672	13661	13650	13639	13628	13617	13605			
856 24	2	13582	13558	13532	13505	13476	13445	13411	13374	13335	13290	13242	13189	13129	13062	12990	12910	

Note: Footnotes follow Table 3.9

3.2.3 The Molar Absorption Coefficient Spectrum.

To present the data in a form preferred by chemists, the molar absorption coefficient spectrum was calculated from the unweighted average k spectrum by $E_m(\tilde{\nu}) = 4\pi\tilde{\nu}k(\tilde{\nu})/(2.303 C)$. The molar concentration, C , of liquid dichloromethane at 25°C is 15.532 mol/L, as calculated from its density of 1.3191 g/ml.¹² The E_m spectrum is shown in Figure 3.4 and tabulated in Table 3.9. The areas under the band groups in the E_m spectrum are given in Table 3.10, with their estimated errors. The values of the molar absorption coefficient at the peaks of the bands are listed in Table 3.11.

3.3 The Accuracy of the Results

As discussed previously³⁻⁵, the estimated error in the k values is taken as the sum of the maximum deviation from the unweighted average (in parenthesis in column 3 of Table 3.6) plus the anchor point uncertainty. For the peak heights, the latter is taken as the average of the 95% confidence limits of the k values at the anchor points immediately to either side of the band, and is listed in column 4 of Table 3.6. For the areas, it is taken as the integration range times the average of the 95% confidence limits of the k values at

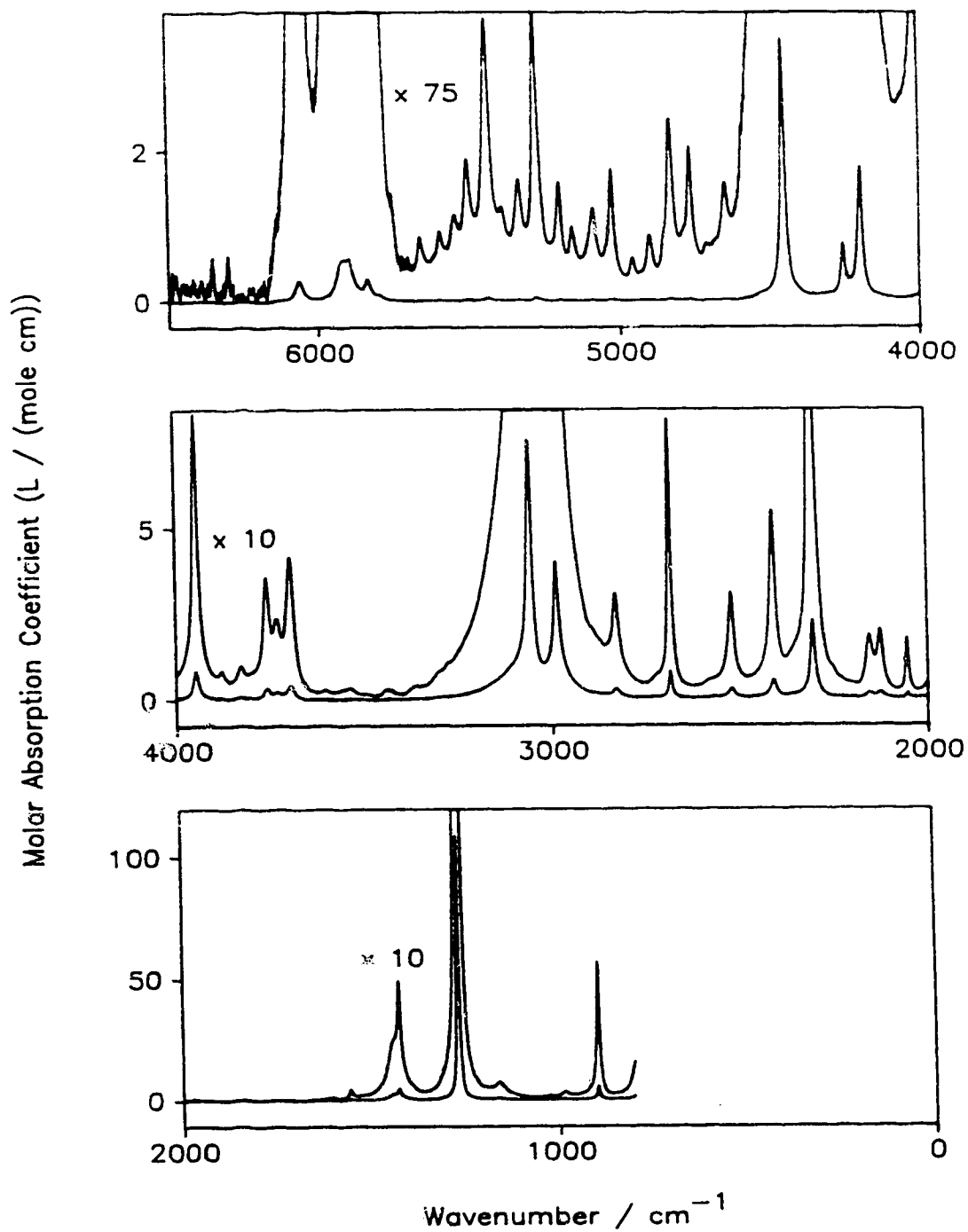


Figure 3.4. Molar absorption coefficient, E_m , spectrum between 6500 and 800 cm⁻¹ of dichloromethane at 25°C. The ordinate labels are for the lower spectrum in each box; they must be divided by 75 or 10, as shown, for the upper spectrum in the box.

Table 3.9 Molar absorption coefficients between 6500 and 800 cm^{-1} of liquid dichloromethane at 25 °C.^{a,b,c}

cm^{-1}	XE	YE	0	1	2	3	4	5	6	7	8	9	10	11	12	13	14	15	16
6499.90	4	-5	0	2687	2182	3436	2604	1871	1789	2673	851	4379	2035	549	3174	8122	1480	535	1070
6237.63	4	-4	5	22	2	23	12	59	121	146	246	424	945	2580	1895	765	438	348	411
5975.35	4	-4	632	1025	2135	4691	5564	5675	3737	2037	1636								
5848.08	2	-4	1776	2058	2527	2975	2913	2472	1975	1553	1255								
5809.51	3	-5	9272	8600	7683	5648	4085	2605	2004	1813	1544	1097	799	707	706	627	672	622	617
5678.37	3	-5	621	808	1150	990	825	728	694	723	792	866	1038	1248	1071	954	947	1036	1279
5547.23	3	-5	1529	1453	1307	1339	1621	2259	2488	1997	1653	1525	1555	1790	2355	3546	4935	4621	3210
5416.10	3	-5	2223	1760	1584	1541	1669	1457	1261	1174	1226	1465	1911	2174	1862	1486	1321	1381	1722
5284.96	3	-5	2912	5162	4374	2844	1891	1347	1094	1031	1051	1120	1475	2124	1621	1651	866	876	1142
5153.83	3	-5	1306	1050	853	768	792	832	966	1169	1473	1644	1346	1020	835	806	919	1094	1758
5022.69	3	-5	2263	1324	844	624	517	465	458	516	692	761	598	502	504	540	609	836	1162
4891.56	3	-5	1000	731	617	630	778	1140	1416	2328	3252	2497	1682	1258	1146	1208	1302	1470	2318
4760.42	3	-5	2540	1622	1160	967	859	855	974	1029	989	1012	1063	1102	1168	1345	1784	2107	1793
4629.28	3	-4	155	150	160	178	220	307	354	405	455	531	604	737	866	1048	1185	1296	1495
4498.15	3	-3	179	230	320	484	876	2090	3494	1805	858	473	307	234	192	161	130	109	94
4367.01	3	-4	856	816	813	805	827	859	929	990	1055	1100	1173	1353	1720	2628	5315	7409	4047
4235.88	3	-3	293	295	350	518	1026	1789	1166	542	295	191	142	112	95	85	73	60	51
4104.74	3	-4	461	418	367	353	353	358	366	378	395	424	469	535	620	691	766	887	1058
3979.39	1	-4	1108	1165	1231	1304	1382	1480	1597	1729	1895	2103	2366	2698	3144	3730	4496	5466	6597
3946.61	1	-4	7676	8315	8203	7411	6317	5243	4320	3563	2964	2493	2138	1866	1651	1476	1331	1211	1113
3913.82	1	-4	1032	967	911	865	829	794	766	752	734	719	711	713	711	717	735	760	786
3881.04	1	-5	8238	8596	8587	8700	7715	7189	6734	6382	6128	5936	5709	5616	5554	5510	5417	5516	5601
3848.25	1	-5	5653	5743	5887	6090	6299	6603	7043	7485	8105	8781	9414	9828	9857	9495	8942	8448	8002
3815.47	1	-5	7693	7535	7473	7471	7527	7667	7734	7850	8056	8155	8290	8454	8614	8798	9013	9265	
3782.69	2	-4	995	1104	1276	1559	2028	2731	3446	3551	3000	2389	2034	1974	2128	2321	2382	2270	2040
3717.12	2	-4	1870	1824	1965	2304	2815	3474	4075	4082	3327	2414	1719	1266	983	774	643	536	463
3651.55	2	-5	4073	3560	3279	2892	2751	2530	2418	2343	2189	2300	2271	2511	2733	2875	2903	2564	2446
3585.98	2	-5	2218	2195	2208	2224	2436	2512	2762	2798	2922	3070	3120	3286	3251	3501	3485	3227	2748
3520.42	2	-5	2342	2034	1863	1730	1663	1604	1592	1578	1574	1575	1564	1440	1366	1288	1252	1326	1498
3454.85	2	-5	1470	1757	2252	2759	2940	3025	3014	2910	2739	2648	2161	1940	1828	1700	1562	1677	1660
3389.28	2	-5	1770	1955	2264	2719	3095	3616	3794	4022	4154	4191	4029	3965	4029	4174	4207	4350	4548
3323.71	2	-4	489	523	567	619	668	719	786	824	854	869	908	950	1023	1089	1107	1108	1150
3258.14	2	-4	1191	1259	1331	1407	1474	1559	1647	1722	1807	1896							
3215.72	3	-3	207	229	252	282	318	357	402	448	502	561	622	693	778	880	980	1084	1223
3090.37	1	-3	1268	1319	1375	1439	1512	1595	1692	1807	1945	2112	2320	2581	2921	3365	3949	4705	5628
3057.58	1	-3	6633	7451	7680	7110	6010	4829	3826	3063	2506	2098	1795	1571	1405	1284	1196	1134	1091
3024.80	1	-3	1064	1048	1040	1042	1052	1070	1098	1134	1178	1233	1298	1375	1475	1602	1776	2024	2383
2992.02	1	-3	2885	3493	3967	4010	3660	3177	2725	2343	2035	1787	1586	1422	1285	1174	1079		
2957.30	3	-4	8144	6423	5237	4413	3713	3104	2592	2249	2108	1997	1849	1735	1624	1578	1644	1927	
2839.67	1	-4	2084	2293	2557	2840	3049	3083	2924	2651	2353	2081	1848	1658	1498				
2808.81	3	-4	1097	875	726	627	553	496	463	453	467	519	618	719	779				
2714.32	1	-4	800	828	865	910	966	1039	1132	1256	1432	1694	2093	2732	3751	5337	7279	8203	6958
2681.53	1	-4	5004	3524	2605	2038	1672	1399	1174	991									
2660.32	3	-4	613	478	417	388	377	379	389	410	445	504	549	584	607	643	726	899	1263
2534.97	1	-4	1403	1569	1775	2028	2332	2669	2978	3120	2984	2625	2203	1831	1538	1318	1161	1038	945
2502.18	1	-5	8791	8270	7790	7417	7173	6943	6749	6637	6570	6480	6433	6427	6429	6424	6473	6527	6582
2467.47	2	-4	678	701	732	769	813	874	947	1051	1187	1381	1661	2081					
2423.12	1	-4	2369	2733	3183	3728	4362	4993	5436	5455	4992	4255	3512	2889	2417	2070	1821	1639	
2390.33	2	-4	1401	1272	1216	1201	1232	1299	1366	1428	1502	1585	1667	1758	1861	2030	2260	2575	3062
2326.69	1	-3	339	378	427	489	573	688	850	1081	1401	1804	2185	2330	2133	1746	1360	1052	828
2293.91	1	-4	6703	5571	4696	3970	3366	2881	2510	2220	1984	1793	1632	1490	1364	1262	1176	1111	1065
2259.20	2	-4	1004	967	909	827	739	669	635	609	586	544	516	495	488	475	462	453	442
2193.63	2	-4	434	432	443	476	542	660	837	1075	1395	1734	1864	1691	1442	1282	1237	1329	1599
2128.06	2	-4	1954	1967	1537	1072	765	578	461	386	340	313	295	285	284	294	312	341	398
2064.42	1	-4	455	558	743	1069	1533	1791	1542	1149	864	678	548	454	388	341	306	281	263
2011.64	1	-5	2504	2430	2398	2400	2434	2498	2575	2672	2792	2938	3113	3322	3563	3845	4158	4478	4740
1998.85	1	-5	4870	4826	4625	4324	4004	3707	3468	3314	3250	3306	3503	3908	4574	5467	6308	6637	6264
1966.07	1	-5	5383	4360	3466	2782	2270	1886	1595	1374	1210								
1942.93	3	-5	869	768	716	734	843	1050	1418	1929	2048	1623	1410	1307	1273	1389	1501	1500	1558
1817.58	1	-5	1590	1629	1667	1713	1769	1838	1928	2014	2137	2298	2513	2791	3158	3599	3978	4101	3890
1784.79	1	-5	3520	3144	2831	2573	2361	2198	2067	1965	1873	1802	1727	1657	1617				
1753.94	3	-5	1517	1488	1524	1671	2128	2259	2676	2123	1792	1765	1841	1996	2224	2549	2923	3443	
1634.37	2	-4	377	411	448	495	563	664	806	991	1180	1298	1233	1064	933	869	857	883	940
1570.73	1	-4	980	1031	1093	1174	1285	1450	1711	2158	2902	3840	4357	4277	3777	3118	2592	2228	2001
1532.17	3	-3	174	179	198	222	259	323	403	515	658	881	1292						
1453.10	1	-3	1427	1572	1725	1882	2041	2193	2326	2425	2486	2514	2534	2580	2699	2966	3489	4310	4917
1420.31	1	-3	4512	3590	2814	2276	1911	1655	1461	1300	1168	1061	973						
1393.32	3	-3	730	594	474	403	364	350	369	403	478	553	757	1033					
1307.50	0	-3	1074	1106	1149	1190	1236	1274	1325	1381	1437	1502	1568	1642	1728	1818	1915	2020	2134
1291.11	0	-2	226	239	255	272	290	310	333	360	391	427	469	520	580	654	745	860	1007
1274.71	0	-1	120	145	178	225	290	382	511	680	872	1034							

Table 3.9. Continued.

cm ⁻¹	AE	YE	0	1	2	3	4	5	6	7	8	9	10	11	12	13	14	15	16
1241 93	0	-3	2562	2382	2237	2105	1980	1876	1789	1688	1606	1537	1457	1387	1333	1274	1218	1171	1131
1225 54	0	-3	1093	1050	1024	998	971	954	938	917	901	883	864	846					
1211 08	2	-4	7227	6293	5829	5538	5361	5091	5096	5018	5088	5232	5478	5852	6359	6942	7334	7113	6375
1145 51	2	-4	5521	4780	4192	3685	3270	2936	2665	2435	2236	2062	1910	1775	1657	1551	1459	1388	1331
1079 94	2	-4	1247	1185	1140	1101	1071	1049	1036	1033	1043	1066	1117	1205	1327	1493	1686	1828	1828
1014 37	2	-4	1728	1633	1613	1708	1960	2473	3093	3334	3278	2958	2568	2302	2185	2151	2156	2181	2261
950 73	1	-4	2316	2388	2451	2525	2607	2694	2803	2922	3043	3191	3366	3531	3738	3982	4253	4561	4926
917 95	1	-3	536	587	648	728	833	977	1189	1512	2032	2901	4257	5570	5281	3823	2570	1788	1330
885 16	1	-3	1026	793	629	520	442	385	342	311	289	274	261	253	246	242			
856 24	2	-3	241	244	257	283	295	311	340	380	425	482	576	690	848	1082	1369	1706	

Footnotes to Tables 3.7, 3.8 and 3.9

- The column headed cm⁻¹ contains the wavenumber of the first ordinate value in the row. The columns headed AE and YE contain the X-exponent and the Y-exponent, respectively, for the row. The columns headed 0,1,2,...,16, contain the ordinate values, and the headings give the indices of the ordinate values in the row. In a row which starts with $\tilde{\nu}(0)$, the wavenumber corresponding to the ordinate indexed J is $\tilde{\nu}(J) = \tilde{\nu}(0) - \frac{15798.002}{16384} \cdot J \cdot 2^{XE}$. In Tables 3.7 and 3.9, the $k(\tilde{\nu})$ and $E_m(\tilde{\nu})$ values in that row are the ordinate value shown times 10^{YE} . In Table 3.8 the $n(\tilde{\nu})$ values are given directly with the decimal point implicitly after the first digit. Thus the entry indexed 16 in the second row of Tables 3.7, 3.8 and 3.9 shows that at $\tilde{\nu} = 6237.63 - \frac{15798.002}{16384} \cdot 16 \cdot 2^4 = 5990.79 \text{ cm}^{-1}$ the ordinate values are $k = 195 \times 10^{-7} = 1.95 \times 10^{-5}$, $n = 1.4124$ and $E_m = 411 \times 10^{-4} = 4.11 \times 10^{-2} \text{ L mole}^{-1} \text{ cm}^{-1}$.
- The 4-point spline interpolation program TRECOVER¹¹ interpolated the $k(\tilde{\nu})$ and $E_m(\tilde{\nu})$ values in the table to the original wavenumber spacing, 0.482117 cm^{-1} , and yielded the original values accurate to 1% below 4000 cm^{-1} , 2% between 4000 and 6000 cm^{-1} and 5% above 5000 cm^{-1} . The original $n(\tilde{\nu})$ values were similarly recovered accurate to 0.1%.
- The unit of E_m is $\text{L mole}^{-1} \text{ cm}^{-1}$. Multiply the values by 1000 to change the unit to $\text{cm}^2 \text{ mole}^{-1}$.

the anchor points immediately to either side of the integration range, and is listed in

Table 3.5. For the starred peaks in Table 3.6, which were recorded only by ZL, the 95% confidence limit is used instead of the maximum deviation. In the earlier papers the term 'accuracy' was used instead of 'error'.

3.3.1 Accuracy of Absorption Indices, k , and Molar Absorption Coefficients, E_m

The estimated percent errors in the peak k values are given in Table 3.6. They average 1.9% over the 36 peaks in the Table, and 2.3% over the 23 peaks that were studied by more than one spectroscopist. The latter value, 2.3%, is taken to be the

Table 3.10. Overall average areas under molar absorption coefficient bands of liquid dichloromethane at 25 °C.

Region (cm ⁻¹)	Area ^a	Estimated error in area ^{a,b}	Area above baseline ^{a,c}	Estimated error in area above baseline ^{a,d}
6200.0-5725.1	65.1	2.1	63.0	1.8
4625.4-4345.3	102.5	3.5	89.1	2.9
4345.3-4075.3	79.0	2.3	63.4	1.7
4075.3-3855.0	31.0	0.5	21.2	0.3
3855.0-3620.2	34.2	~1*	25.1	~0.5*
3330.5-2870.0	332.2	7.0	382.8	5.7
2750.5-2625.1	16.84	0.16	11.60	0.08
2615.0-2480.0	13.02	0.15	6.07	0.04
2480.0-2380.2	17.94	0.12	8.72	0.08
2380.2-2215.3	59.1	0.8	45.2	0.8
2190.3-2085.2	10.7	0.1*	6.93	0.05*
2085.2-2036.2	3.19	0.03*	1.74	0.01*
1530.2-1355.2	186.8	1.3	141.2	0.8
1355.2-1185.0	1198	13*	1126	13*
965.2-860.1	95.2	0.7	73.1	0.5

^a The unit of area is L mol⁻¹ cm². Divide the values by 100 to obtain areas in the unit km mole⁻¹.

^b Calculated from the percent estimated error in the area, which is the same for the $E_m(\tilde{\nu})$ and $k(\tilde{\nu})$ (Table 3.5) bands. The starred values are less reliable (Footnote c of Table 3.5)

^c The baseline is a straight line through the ordinate values at each end of the integration range. In fact the average of the five E_m values centered on the integration limit was used.

^d The percent estimated error in the area under E_m above baseline equals the maximum deviation from the unweighted average k area expressed as a percentage of the k area (Table 3.5). This percentage multiplied by the entries in column 4 above give the entries in this column. The starred values are less reliable (Footnote c of Table 3.5).

Table 3.11. Overall average peak heights in the molar absorption coefficient spectrum of liquid dichloromethane at 25 ° C.

$\tilde{\nu}(\text{cm}^{-1})$	$E_m(\tilde{\nu})^a$	$\tilde{\nu}(\text{cm}^{-1})$	$E_m(\tilde{\nu})^a$
6063.2	0.282(7)	2410.5	0.551(7)
5915.1	0.564(9)	2305.6	2.33(5)
5899.2	0.570(5)	2155.5	0.187(2)
5834.5	0.302(7)	2126.0	0.203(2)
4452.7	3.53(16)	2054.8	0.179(2)
4253.1	0.773(14)	1998.3	0.0488(6)
4196.6	1.80(15)	1970.0	0.0664(6)
3944.0	0.837(3)	1884.1	0.0214(5)
3878.0	0.0865(2)	1789.0	0.0411(6)
3825.9	0.0990(24)	1707.7	0.0268(4)
3757.2	0.361(7)	1600.0	0.130(7)
3729.2	0.240(5)	1550.8	0.438(4)
3691.9	0.419(20)	1422.0	4.93(12)
3054.1	1.70(2)	1265.2	108.5(6)
2987.0	1.05(7)	1156.2	0.734(6)
2830.7	0.310(2)	1020.0	0.184(1)
2685.5	0.821(3)	985.9	0.335(2)
2521.5	0.312(4)	896.0	5.70(16)

^a The unit of E_m is $\text{L mole}^{-1} \text{cm}^{-1}$. Multiply the values by 1000 to change the unit to $\text{cm}^2 \text{mole}^{-1}$. The number in parentheses is the estimated error in the last digit. The percent estimated error is the same as that of the corresponding k value.

better estimate. The peak heights of the 29 peaks below 4000 cm^{-1} all exceed 3×10^{-5} , and their percent errors average 1.6% over all and 2% over the unstarred peaks, which were studied by more than one worker. Again, the latter value, 2%, is taken to be the better estimate. Above 4000 cm^{-1} the error averages 3.1% over the 7 peaks. As noted above, the accuracy of the peaks at 3691.9 and 1600.0 cm^{-1} is an estimate because they were influenced by water in some samples. Only one other medium peak has an unusually high error, that at 4196.6 cm^{-1} . This error resulted from one low value from the five spectroscopists who studied it..

The k values in the baseline are not known as accurately as those in regions of significant absorption, except at the anchor points. From the agreement between different workers and the 95% confidence limits of the values at the anchor points (Table 3.1), the accuracy of the baseline k values is estimated to be about 1% below 4500 cm^{-1} and about 8% above 4500 cm^{-1} rising to 25% at the 6300 cm^{-1} where the absorption is too weak for our measurement techniques.

The percent error in the molar absorption coefficient is the same as that in the corresponding absorption index. The actual, not percent, errors are listed for the peaks in Table 3.11.

The peak k values are compared in Table 3.6 with the results published previously from the work of VB and with the only calibrated results available, those of Jones and coworkers in Ref. 10. The values from Ref. 7 at 3878.0 and 2305.6 cm^{-1} have been corrected for a typographical error in the exponent. Of the 29 k_{max} values in Table 3.6 for which there is a calibrated value, 7 lie outside the limits set by the combined

estimated accuracy of this work plus the evaluated uncertainty of Ref. 10. They are at 3691.9, 2410.5, 1884.1, 1789.0, 1707.7, 1600.0 and 1020.0 cm^{-1} . The bands at 1884.1, 1789.0 and 1707.7 cm^{-1} are extremely weak (Fig. 3.2) and that at 1884.1 cm^{-1} was only studied in excessively thin cells for Ref. 10. The bands at 3691.9 and 1600 cm^{-1} appears to be influenced by rather more water in the samples used for Ref 10 than in those of ZL. The band at 1020 cm^{-1} is weak, broad, and nearly a shoulder. It is, in fact, not visible in Fig. 3.5 of reference 10.

Figs. 3.2 and 3.4 and Tables 3.7 and 3.9 include all regions between 6500 and 800 cm^{-1} . Above 4600 cm^{-1} many bands have $k_{\text{max}} < 2 \times 10^{-5}$ (Fig. 3.2) and were measured only by ZL. We estimate the accuracy of the k values in these bands to be about 5%. These bands were omitted from Tables 3.4 and 3.6.

3.3.2 Accuracy of Areas.

The percent estimated errors in the areas under the $k(\tilde{\nu})$ bands are given in Table 3.5. The percent error in the area under an $E_m(\tilde{\nu})$ band equals that of the corresponding $k(\tilde{\nu})$ band. The percent error averages 1.0% over the 10 band groups below 3600 cm^{-1} , 1.5% over all 15 band groups, and never exceeds 3.3%. The estimated error under the E_m bands, not the percent estimated error, is given in Table 3.10.

Table 3.10 includes the preferred area for a secondary standard, namely the area under $E_m(\tilde{\nu})$ band groups above a linear baseline drawn between the E_m values at the integration limits. In fact, the average of the 5 E_m values centered on the integration limit is used. This area does not depend on the anchor points, so its error is calculated

from the maximum deviation of the spectroscopist average from the unweighted average area under k bands. The error is less than 1.5% for all band groups below 4000 cm^{-1} .

3.3.3 Accuracy of Real Refractive Indices.

Three factors contribute to the accuracy of the n values. First, the Kramers-Kronig transform procedure has an intrinsic error of about 0.05%¹³. Second, $n(8000 \text{ cm}^{-1})$ was calculated to be 1.4130 ± 0.0004 , an error of 0.03%. Third, the approximately 2% error in the absorption indices yields an approximately 2% error in the values of $\Delta n = n(\tilde{\nu}) - n(8000 \text{ cm}^{-1})$ from the Kramers-Kronig transform, which corresponds to an error of $\sim 0.08\%$ in $n(\tilde{\nu})$. The sum of these contributions gives $\sim 0.2\%$ as the estimated error in the values of the real refractive index.

3.4 Summary

Transmission measurements on dichloromethane have been made by five spectroscopists in four different laboratories. The spectra have been converted to absorption index spectra which were compared and averaged, and the real refractive index and molar absorption coefficient spectra have been calculated from the average. The imaginary refractive index, k , and molar absorption coefficient, E_m , values are believed accurate to an average $\pm 2.3\%$ over the 36 measured bands. The baseline k values are believed accurate to $\sim 8\%$ below 6000 cm^{-1} , $\sim 1\%$ below 4500 cm^{-1} , and $\sim 25\%$ above 6000 cm^{-1} where the absorption is extremely weak. The areas under band groups in the k and E_m spectra are believed accurate to 1.5% averaged over the 15 measured band groups and to 1.0% over the 10 band groups below 3600 cm^{-1} . The real refractive index, n , values are believed accurate to 0.2%.

For long-term reference, the complete numerical data are presented in Compact Table format¹¹, which is readable and allows the original spectra to be recovered by interpolation without loss of accuracy. The complete final k , n , and E_m spectra obtained in this work are available on diskette from the authors. To provide continuity over the longer term, it is anticipated that they will be made available in the future on an internationally accessible data base.

3.5 References

1. J.E. Bertie, C.D. Keefe, R.N. Jones, H.H. Mantsch, and D.J. Moffatt, Appl. Spectrosc. **45**, 1233 (1991).
2. J.E. Bertie, C.D. Keefe and R.N. Jones, *Tables of Intensities for the Calibration of Infrared Spectroscopic Measurements in the Liquid Phase*: International Union of Pure and Applied Chemistry (Blackwell Scientific Publications, Oxford, 1995).
3. J.E. Bertie, R.N. Jones, and C.D. Keefe, Appl. Spectrosc. **47**, 891 (1993).
4. J.E. Bertie, R.N. Jones, Y. Apelblat and C.D. Keefe, Appl. Spectrosc. **48**, 127 (1994)
5. J.E. Bertie, R.N. Jones, and Y. Apelblat, Appl. Spectrosc. **48**, 144 (1994).
6. J.E. Bertie, C.D. Keefe, and R.N. Jones, Can. J. Chem. **69**, 1609 (1991).
7. J.E. Bertie, R.N. Jones, and V. Behnam, Appl. Spectrosc. **39**, 401 (1985).
8. J.E. Bertie, R.N. Jones, and V. Behnam, Appl. Spectrosc. **40**, 427 (1986).

9. I.M. Mills, T. Cvitas, K. Homann, N. Kallay and K. Kuchitsu, *Quantities Units and Symbols in Physical Chemistry*: International Union of Pure and Applied Chemistry (Blackwell Scientific Publications, Oxford, 1988).
10. T.G. Goplen, D.G. Cameron, and R.N. Jones, *Appl. Spectrosc.* **34**, 657 (1980).
11. J.E. Bertie, R.N. Jones and Y. Apelblat, *Appl. Spectrosc.*, **47**, 1989 (1993).
12. J. Timmermans. *Physico-Chemical Constants of Pure Organic Compounds*, (Elsevier, New York, 1950), Vol. 1, pp. 215 - 216.
13. J.E. Bertie and S.L. Zhang. *Can. J. Chem.* **70**, 520 (1992).

Chapter 4 An Accurate Modified Kramers-Kronig Transformation from Reflectance to Phase Shift on Attenuated Total Reflection.

4.1 Introduction

One way to obtain infrared optical constants of the sample from attenuated total reflection (ATR) spectra is to use the Kramers-Kronig (KK) transformation from attenuated total reflectance, $R(\tilde{\nu})$, to the phase change on reflection, $\theta(\tilde{\nu})$ ^{1,4}. The optical constants, namely the real refractive index $n(\tilde{\nu})$ and the absorption index or imaginary refractive index $k(\tilde{\nu})$, can then be calculated from $(R(\tilde{\nu}), \theta(\tilde{\nu}))$. This method is more direct than the iterative procedure that is used^{5,6} in this laboratory to convert pATR spectra to the refractive index spectra, and Urban and Huang have incorporated it into their procedure⁴.

Currently experimental ATR spectra are capable of yielding imaginary refractive index spectra of liquids with errors in the k values estimated to be as small as $\sim 3\%$ ^{7,8}. Thus, it is important that the calculations introduce no comparable error into the optical constants, and we take computational errors $\leq \sim 0.1\%$ of the k values as a suitable current goal. This paper describes a procedure that improves the accuracy with which the optical constants can be calculated from attenuated total reflection spectra via the Kramers-Kronig transform from $R(\tilde{\nu})$ to $\theta(\tilde{\nu})$. The results are pleasing for ATR elements made of materials like Si which have real refractive indices $n \approx 3.5$ or more, but are not sufficiently good for the commonly used ZnSe, $n \approx 2.4$, to enable the

method to be used without being followed by the currently used iteration procedures^{4,6} to achieve the best fit to the experimental spectra.

The Kramers-Kronig transforms, or dispersion relations as they are sometimes⁹ called, derive from causality^{9,10}. Their mathematical derivation involves the theory of complex functions of complex variables^{9,10}. Under the conditions summarized in the appendix, the real, f_R , and imaginary, f_I , parts of a complex function \hat{f} of real wavenumber $\tilde{\nu}$ are related by the Kramers-Kronig transforms, Eqs. (4.1a) and (4.1b).

$$f_R(\nu_a) = \frac{2}{\pi} \text{P} \int_0^{\infty} \frac{\nu f_I(\nu)}{\nu^2 - \nu_a^2} d\nu \quad (4.1a)$$

$$f_I(\nu_a) = \frac{-2\nu_a}{\pi} \text{P} \int_0^{\infty} \frac{f_R(\nu)}{\nu^2 - \nu_a^2} d\nu \quad (4.1b)$$

These relations hold for the real and imaginary refractive indices^{11,12} as functions of frequency, ν , or vacuum wavenumber of the radiation, $\tilde{\nu}$, when $f_R(\nu) = n(\tilde{\nu}) - n(\infty) = n(\tilde{\nu}) - 1$ and $f_I(\nu) = k(\tilde{\nu})$. They also hold for the real and imaginary parts of the dielectric constant as functions of frequency or vacuum wavenumber, when $f_R(\nu) = \epsilon'(\tilde{\nu}) - \epsilon'(\infty) = \epsilon'(\tilde{\nu}) - 1$ and $f_I(\nu) = \epsilon''(\tilde{\nu})$.

The simplest example of reflection at the surface of an absorbing medium of refractive index \hat{n} is reflection at normal incidence of light that propagates in a non-absorbing medium of real refractive index, n_o . In turn, the simplest case of this is when $n_o = 1$. This is the case commonly treated in text books, and will be referred to as reflection at normal incidence from air. In this case, the reflectance,

$R(\tilde{\nu})$, the complex coefficient of reflection, $\hat{r}(\tilde{\nu})$, and the phase shift on reflection, $\theta(\tilde{\nu})$, are related by:

$$R(\tilde{\nu}) = \hat{r}(\tilde{\nu}) \hat{r}^*(\tilde{\nu}), \quad \text{where} \quad \hat{r}(\tilde{\nu}) = \rho(\tilde{\nu}) e^{i\theta(\tilde{\nu})} \quad \text{and} \quad \rho(\tilde{\nu}) = \sqrt{R(\tilde{\nu})}.$$

$$\text{Thus} \quad \ell n \hat{r}(\tilde{\nu}) = \ell n [R(\tilde{\nu})]^{1/2} + i\theta(\tilde{\nu}).$$

The Kramers-Kronig relations 1a) and 1b) also hold in this case when^{1,3,9-12}

$$f_R(\nu) = \ell n [R(\tilde{\nu})]^{1/2} - \ell n [R(\infty)]^{1/2} = \frac{1}{2} \ln [R(\tilde{\nu})/R(\infty)] \quad \text{and} \quad f_I(\nu) = \theta(\tilde{\nu}).$$

In these three situations there is only one singularity to be resolved in the Kramers-Kronig transform, that at $\tilde{\nu} = \tilde{\nu}_a$.

In a reflection experiment in which the angle of incidence is not normal, several situations arise. The reflection may be external ($n > n_o$) or internal ($n < n_o$), or the special case^{1,3} of internal reflection when the angle of incidence β_o is greater than the critical angle, β_{crit} , total internal reflection if $k = 0$ and attenuated total reflection if $k \neq 0$ where k is the imaginary refractive index of the sample. There is no distinction between total internal reflection, TIN, and attenuated total reflection, ATR, in the theory in this paper^{3,13}, and ATR will be used throughout.

The following discussion is restricted to ATR with a non-absorbing incident medium. In this situation, two cases exist, the case of ATR with *constant* n_o and the case of ATR with *varying* n_o , i.e., the cases when the refractive index n_o of the incident medium does not change with the wavenumber of the radiation and when it does. The

former case has been discussed in the literature^{1,3,14}, but the latter, realistic, case has not.

For the case of ATR with *constant* n_0 , Plaskett and Schatz¹ have given a modified Kramers-Kronig transform, Eq. (4.2), that is exactly correct.

$$\theta(\tilde{\nu}_a) = -\frac{2\tilde{\nu}_a^2}{\pi} P \int_0^\infty \frac{\ln[R(\tilde{\nu})]^{1/2}}{\tilde{\nu}(\tilde{\nu}^2 - \tilde{\nu}_a^2)} d\tilde{\nu} + \theta(0) \quad (4.2)$$

where the constant $\theta(0)$ is the phase shift at zero wavenumber. This integrand is singular at $\tilde{\nu} = 0 \text{ cm}^{-1}$ as well as at $\tilde{\nu} = \tilde{\nu}_a$, the usual singularity in the KK transform. This extra singularity at zero wavenumber can be expected to introduce extra numerical error in practical calculations. The constant $\theta(0)$ is given by

$$\theta(0) = -2 \arctan\left\{ \frac{\sqrt{(n_0^2 \sin^2 \beta_0 - n^2)}}{n^2 \cos \beta_0} \cdot n_0 \right\} \quad \text{for p-polarized light} \quad (4.2a)$$

$$\text{and} \quad \theta(0) = -2 \arctan\left\{ \frac{\sqrt{(n_0^2 \sin^2 \beta_0 - n^2)}}{n_0 \cos \beta_0} \right\} \quad \text{for s-polarized light.} \quad (4.2b)$$

where β_0 is the angle of incidence in the incident medium of refractive index n_0 and n is the refractive index of the sample at 0 cm^{-1} .

Plaskett and Schatz noted that their derivation is only valid if the refractive index of the transparent phase is independent of wavenumber. Further, they did not discuss the errors introduced by the availability of spectral data over only a finite wavenumber range, and did not illustrate the accuracy of their equation in practice.

Plaskett and Schatz¹ also showed that the usual KK transform holds for all cases of reflection from an incident medium of constant n_o , provided that it is corrected by an additive term, $I(\tilde{\nu}_a)$, as shown in Eq. 4.3.

$$\theta(\tilde{\nu}_a) = -\frac{2\tilde{\nu}_a}{\pi} P \int_0^{\infty} \frac{\ln[R(\tilde{\nu})]^{1/2}}{(\tilde{\nu}^2 - \tilde{\nu}_a^2)} d\tilde{\nu} + I(\tilde{\nu}_a) \quad (4.3)$$

Here "all cases" means for all angles of incidence and for all combinations of external reflection and internal reflection, including the special case of ATR. The different cases differ in having different expressions for $I(\tilde{\nu}_a)$. Plaskett and Schatz¹ did not derive the value of $I(\tilde{\nu}_a)$ for TIN and ATR, but Bardwell and Dignam³ gave it for s-polarized light as

$$I(\tilde{\nu}_a) = -\pi + M(\infty) + \frac{2}{\pi} \arctan \frac{\tau'(\tilde{\nu}_a) [M(0) - M(\infty)]}{\tilde{\nu}_a} \quad (4.3a)$$

$$\text{where } M(\tilde{\nu}_n) = 2 \arctan \frac{\sqrt{(n_o^2 \sin^2 \beta_o - n^2(\tilde{\nu}_n))}}{n_o \cos \beta_o} \quad (4.3b).$$

Where $\tilde{\nu}_n$ is zero or infinity in Eq. (4.3a).

It is convenient to make a number of points here for clarity.

First, equations related to this work are different in different references, because they depend on the definition of \hat{r}_s , $\hat{\epsilon}$ and \hat{n} . The definitions used in this work and those used by Plaskett and Schatz¹ and Bardwell and Dignam³ are summarised in Table 4.1, with the equations that result from these definitions and the range of the primary values of θ . Note that Eq. (4.3) has a plus sign before the integral with Bardwell and Dignam's definitions³.

Table 4.1. Different definitions of the reflection coefficient, \hat{r}_s , and dielectric constant, $\hat{\epsilon}$, the phase shift for s-polarised light, θ_s .

Physical Quantity	Plaskett & Shatz ^a	Bardwell & Dignam ^b	This work
\hat{r}_s	$\frac{n_o \cos \beta_o - \hat{n} \cos \hat{\beta}}{n_o \cos \beta_o + \hat{n} \cos \hat{\beta}}$	$\frac{\hat{n} \cos \hat{\beta} - n_o \cos \beta_o}{\hat{n} \cos \hat{\beta} + n_o \cos \beta_o}$	$\frac{\hat{n} \cos \hat{\beta} - n_o \cos \beta_o}{\hat{n} \cos \hat{\beta} + n_o \cos \beta_o}$
$\hat{\epsilon}$ ^c	$\epsilon_1 + i\epsilon_2$	$\epsilon_1 - i\epsilon_2$	$\epsilon_1 + i\epsilon_2$
ϵ_2 ^d	$-c \sin \theta_s$	$-c \sin \theta_s$	$c \sin \theta_s$
Region of θ_s ^e	$[-\pi, 0]$	$[-\pi, 0]$	$[0, \pi]$
θ_s ^f	$-\frac{2}{\pi} P \int_0^\infty \frac{F(\tilde{\nu}) d\tilde{\nu}}{\tilde{\nu}^2 - \tilde{\nu}_a^2} - \theta_0$	$\frac{2}{\pi} P \int_0^\infty \frac{F(\tilde{\nu}) d\tilde{\nu}}{\tilde{\nu}^2 - \tilde{\nu}_a^2} - \pi + \theta_0$	$-\frac{2}{\pi} P \int_0^\infty \frac{F(\tilde{\nu}) d\tilde{\nu}}{\tilde{\nu}^2 - \tilde{\nu}_a^2} + \pi - \theta_0$
$\theta_s(\tilde{\nu}_n)$ ^{f, g}	$-M(\tilde{\nu}_n)$	$-\pi + M(\tilde{\nu}_n)$	$\pi - M(\tilde{\nu}_n)$

^a. Reference 1.

^b. Reference 3.

^c. ϵ_2 is always greater than zero. ϵ_1 and ϵ_2 are called ϵ' and ϵ'' in the text of this paper.

^d. $c = \frac{4n_o^2 \cos^2 \beta_o R_s^{1/2} (1 - R_s)}{(1 + R_s + 2R_s^{1/2} \cos \theta_s)^2}$ for Plaskett & Shatz and $c = \frac{4n_o^2 \cos^2 \beta_o R_s^{1/2} (1 - R_s)}{(1 + R_s - 2R_s^{1/2} \cos \theta_s)^2}$ for Bardwell & Dignam and this work (see Eq. (4.15b) and Eq. (4.11) of Ref. 3).

^e. The value of the phase shift can be shifted by $2\pi j$ ($j=0, \pm 1, \pm 2, \dots$).

^f. Function $F(\tilde{\nu}) = \tilde{\nu}_a^2 \ln[R(\tilde{\nu})]^{1/2} / \tilde{\nu}$ and $\theta_0 = M(0)$ for modified KK transform (2),

$F(\tilde{\nu}) = \tilde{\nu}_a \ln[R(\tilde{\nu})]^{1/2}$ and $\theta_0 = M(\infty) + \frac{2}{\pi} \arctan \frac{\tau[M(0) - M(\infty)]}{\tilde{\nu}_a}$ for KK transform (3), and $F(\tilde{\nu}) = \tilde{\nu}$

$\ln[R(\tilde{\nu})]^{1/2}$ and $\theta_0 = M(\infty)$ for modified KK transform (16); where $M(a) = 2 \arctan \frac{\sqrt{n_o^2 \sin^2 \beta_o - n^2(a)}}{n_o \cos \beta_o}$.

^g. The exact phase shift at $\tilde{\nu}_n$, usually taken as the highest wavenumber in the spectrum, at which $k=0$ and total internal reflection condition is met. The function $M(a)$ is defined in f.

Second, note that $M(\tilde{\nu}_n)$ in Eq. (4.3b) and $\theta(0)$ in Eq. (4.2b) are the same except for a sign difference that results from different definitions (Table 4.1). Subject to the addition of π for certain definitions (Table 4.1), they are the phase shift of s-polarised light on total internal reflection at the surface of a sample that does not absorb at that wavenumber, i.e., they are the correct phase shift at wavenumber $\tilde{\nu}_n$ when $n_o \sin \beta_o > n(\tilde{\nu}_n)$ and $k(\tilde{\nu}_n) = 0$. This can be shown by expanding Eq. (4.4) for $k = 0$, i.e., $\hat{n}(\tilde{\nu}) = n(\tilde{\nu})$, and using the relation between $\tan \theta$ and $\tan \theta/2$, as has been described recently by Yamamoto, Masui and Ishida¹⁴.

$$\hat{r}_s(\tilde{\nu}) = \frac{\hat{n}(\tilde{\nu}) \cos \hat{\beta} - n_o \cos \beta_o}{\hat{n}(\tilde{\nu}) \cos \hat{\beta} + n_o \cos \beta_o} \quad (4.4)$$

It is convenient to note here the phase shift under these conditions for the definitions used in this paper

$$\theta_o(\tilde{\nu}_n) = \pi - 2 \arctan \frac{\sqrt{(n_o^2 \sin^2 \beta_o - n^2(\tilde{\nu}_n))}}{n_o \cos \beta_o} \quad (4.5)$$

where the subscript zero on θ_o indicates that it is the phase shift when $k = 0$ at wavenumber $\tilde{\nu}_n$.

Third, the correction terms in Eqs. (4.2a), (4.2b), and (4.3a) are appropriate for the infinite integrals in Eqs. (4.2) and (4.3), but the latter can not be found in practice so the correction terms can not be used as they stand. In practice for infrared spectroscopy, the integration in Eqs. (4.2) and (4.3) is best taken over the entire region of intense infrared absorption. This can usually be achieved to high wavenumber, because it is easy to obtain spectra to $\geq 4500 \text{ cm}^{-1}$, but it is frequently not possible to

include strong absorption below 700 cm^{-1} because of absorption by the incident medium. Some assumption has to be made to allow for this, which remains a source of error that can not be removed easily for samples that absorb strongly at low wavenumbers. However this is done, the integration is then taken over the wavenumber range of the available reflectance spectrum. The phase spectrum so obtained is then corrected by comparing it with $\theta_o(\tilde{\nu}_n)$ calculated through Eq. (4.5) at wavenumbers where n is known.

Bardwell and Dignam³ have presented a detailed discussion of equation (4.3) for s-polarized light. Very recently, Yamamoto, Masui and Ishida¹⁴ have also applied Eq. (4.3) for s-polarized light. However their study is very similar to that of Bardwell and Dignam and is not considered further here.

To test these equations Bardwell and Dignam³ synthesised real and imaginary refractive index, n and k , spectra from the Classical Damped Harmonic Oscillator (CDHO) model, and used these n and k spectra to calculate the attenuated total reflectance spectrum, $R(\tilde{\nu})$, and phase shift spectrum, $\theta(\tilde{\nu})$, for ATR with constant n_o . They calculated the R spectrum from 4000 to 400 cm^{-1} only, and assumed the reflectance above 4000 cm^{-1} and the reflectance below 400 cm^{-1} equalled the values at these limits. They used $\ln[R/R_\infty]$ instead of $\ln[R]$ in eqs.(4.2) and (4.3). They initially looked at the difference between the phase shift spectrum calculated from the original refractive index spectra and that given by the KK and modified KK integrals without the correction terms, $\theta - \theta'$.

Bardwell and Dignam³ tested three methods of using Eqs. (4.2) and (4.3). In Method 1, they used the exact equation of Plaskett and Schatz¹, Eq. (4.2).

Unfortunately, they do not describe their use of Eq. (4.2b) clearly, but they do compare the phase shift calculated by Eq. (4.2) without $\theta(0)$ with the known, synthesized, phase shift.

In Method 2, they used Eqs. (4.3) and (4.3a), but assumed that $\tau'(\nu_a)$ is independent of wavenumber. They determined it and the two parameters $M(\infty)$ and $M(0)$ in Eq. (4.3a), through Eqs. (4.3b) and (4.5), from values of the real refractive index of the sample at three wavenumbers at which k is very small.

In Method 3, they again used Eqs. (4.3) and (4.3a), but simply set the third term in the right hand side of Eq. (4.3a) to zero, so that $I(\tilde{\nu}_a) = -\pi + M(\infty)$. They determined^{3,13} the value of $M(\infty)$ from the real refractive index of the sample at one wavenumber where k is very small, through Eqs. (4.3b) and (4.5).

Bardwell and Dignam tested these three methods on ATR spectra calculated from two sets of model real and imaginary refractive index spectra.

The first set simulated a very strongly absorbing inorganic compound, which has $n(\infty) = 2$ and three huge infrared absorption peaks which have peak k values of about 8, 40 and 16. The refractive index of the incident medium was taken to be constant at 6.00. The differences between the correct, synthesized, phase shifts and those calculated from the integrals in Eqs. (4.2) and (4.3) (without the correction terms) vary with wavenumber, so a constant phase correction is not adequate for these

cases. Method 2 gave phase errors of less than 0.02 and gave the CDHO parameters accurate to $\leq 0.5\%$ for the intensity and 1.5% for the bandwidth. Both Methods 1 and 3 gave errors up to 25% of the CDHO parameters.

The second set of model spectra simulated benzene, with $n(\infty) = 1.475$ and 8 peaks with $k < 1.5$. Method 2 was not applied to this case, because the similar but simpler Method 3 gave phase errors less than 0.004 and errors in the CDHO intensity and bandwidth parameters of less than 1% of the values. Method 1 gave errors in the CDHO intensity and bandwidth parameters of less than 2% of the values. Bardwell and Dignam concluded that for normal organic systems like benzene their simple Method 3 is the preferred method, being simpler than Method 2 and more accurate than Method 1.

It should be noted that Bardwell and Dignam³ implemented all of these methods through their double Fourier transform algorithm for the Kramers-Kronig transform. This procedure is not correct for Method 1, which uses Eq. (4.2) and therefore has a singularity at 0 cm^{-1} , and this may contribute to the poor accuracy Bardwell and Dignam found for Method 1.

In this paper a new modified KK transform for ATR spectra is derived which does not have the extra singularity point at zero wavenumber. The new transform is compared with the methods used by Bardwell and Dignam for real and imaginary refractive index spectra that were simulated from the CDHO model to be like liquid methanol and benzene. Very strongly absorbing systems like Bardwell and Dignam's "inorganic" system are extreme cases that are not considered in this paper. In contrast

to Bardwell and Dignam's use of the double Fourier transform, or Hilbert transform¹⁵, to evaluate the Kramers-Kronig transform, all methods were implemented by us through the direct calculation of the KK transform. This was for two reasons. First, because work in this laboratory has shown¹⁵ literature implementations of the double FFT method of evaluating the Hilbert transform to be subject to error, and has shown that our best implementation of this method is slightly less accurate than the directly programmed KK transform¹⁵. Second, because the Hilbert transform is not equivalent to the modified KK transforms, since f_R in Eq. (4.1a) is not an even function of wavenumber in the modified transforms.

In all previous work on the relation between $R(\tilde{\nu})$ and $\theta(\tilde{\nu})$ in ATR spectroscopy, the refractive index of the incident medium has been assumed to be independent of wavenumber. In reality this is never true. The real refractive indices of all materials change significantly with wavenumber through the infrared region. For silicon, Si, n varies from 3.56 at 10,000 cm^{-1} to 3.42 at 500 cm^{-1} . For zinc selenide, ZnSe, n varies from 2.485 at 10,000 cm^{-1} to 2.373 at 500 cm^{-1} . The ATR elements are used only in those regions where they are essentially non-absorbing, but n_o always changes with wavenumber.

This real situation is the second case of attenuated total reflection that was mentioned earlier, the case of ATR with varying n_o . The variation in n_o causes the transforms described above to be approximate, and no exact transform, or correction to the KK transform or to a modified KK transform, has been presented for this case. The effect of the wavenumber dependence of n_o on the accuracy of the spectra

recovered by the methods designed for constant n_0 is explored in this paper. A very simple non-constant correction of the phase shift is shown to greatly improve the accuracy given by our implementation of Bardwell and Dignam's Method 3, which uses a one constant correction of the phase shift.

4.2 Method

The method used to test the accuracy of the different transforms and phase corrections was based on that of Bardwell and Dignam³. Attenuated total reflection $R_s(\tilde{\nu})$ and $\theta_s(\tilde{\nu})$, spectra of liquids similar to methanol and benzene were calculated from simulated optical constant, n and k , spectra for both constant and non-constant refractive index of the incident medium. The phase shift and optical constant spectra were then recovered from ATR spectra by the different transforms and phase corrections. The differences between the original and recovered phase shift and optical constant spectra indicated the accuracy of a transform and phase correction.

4.2.1 The Simulated Optical Constant Spectra

The vibrational contribution to the mean molecular polarizability of randomly oriented molecules in the liquid is given by the Classical Damped Harmonic Oscillator (CDHO) model⁷. The polarizability is a complex quantity, and if the mean molecular polarizability is multiplied by Avogadro's number to give the molar polarizability the expression for $\hat{\alpha}_m$ is

$$\hat{\alpha}_m = \frac{N_A}{4\pi^2 c^2} \sum_j \frac{(\mu_j^2/3)}{[\tilde{\nu}_j^2 - \tilde{\nu}^2 - i\tilde{\nu}\Gamma_j]}$$

In order to include the electronic polarization, which is due to absorption processes at higher than infrared wavenumbers, it is standard practice to use the real dielectric constant, $\varepsilon'_\infty = n_\infty^2$ at a wavenumber sufficiently far above the strong infrared absorption and sufficiently far below the strong visible and ultraviolet absorption that anomalous dispersion due to these absorptions is extremely small and the real refractive index is essentially constant. It may be noted in passing, that an improvement on this procedure has been developed in this work and is reported elsewhere¹⁶. For the present simulation, ε'_∞ was used with the Lorentz local field, which corrects for the fact that the local electric field which acts on a molecule in the liquid differs from the macroscopic field, to obtain the molar polarizability at infrared wavenumbers as Eq.

(4.6)

$$\hat{\alpha}_m(\tilde{\nu}) = \frac{(\varepsilon_\infty - 1)}{(\varepsilon_\infty + 2)} \frac{3N_A}{4\pi N} + \frac{N_A}{4\pi^2 c^2} \sum_j \frac{\mu_j^2 / 3}{[\tilde{\nu}_j^2 - \tilde{\nu}^2 - i \tilde{\nu} \Gamma_j]} \quad (4.6)$$

Here N is the number of molecules in unit volume and N_A is Avogadro number. The sum is over all vibrations, and vibration j has wavenumber $\tilde{\nu}_j$, damping factor Γ_j , and dipole moment derivative with respect to the normal coordinate $\delta\mu/\delta Q_j$, which is written as μ_j for brevity.

Under the Lorentz local field the dielectric constant is related to the molar polarizability by Eq. (4.7)

$$\hat{\varepsilon}(\tilde{\nu}) = \frac{3V_m + 8\pi\hat{\alpha}_m(\tilde{\nu})}{3V_m - 4\pi\hat{\alpha}_m(\tilde{\nu})} \quad (4.7)$$

where the molar volume, $V_m = N_A/N$ has been used. The real and imaginary parts of this equation are separated in practice to give Eqs. (4.7a) and (4.7b)

$$\varepsilon'(\tilde{\nu}) = \frac{\left[1 - \frac{4\pi}{3V_m} \alpha'_m(\tilde{\nu})\right] \left[1 + \frac{8\pi}{3V_m} \alpha'_m(\tilde{\nu})\right] - 2 \left[\frac{4\pi}{3V_m} \alpha''_m(\tilde{\nu})\right]^2}{\left[1 - \frac{4\pi}{3V_m} \alpha'_m(\tilde{\nu})\right]^2 + \left[\frac{4\pi}{3V_m} \alpha''_m(\tilde{\nu})\right]^2} \quad (4.7a)$$

$$\varepsilon''(\tilde{\nu}) = \frac{\left[\frac{4\pi}{3V_m} \alpha''_m(\tilde{\nu})\right]}{\left[1 - \frac{4\pi}{3V_m} \alpha'_m(\tilde{\nu})\right]^2 + \left[\frac{4\pi}{3V_m} \alpha''_m(\tilde{\nu})\right]^2} \quad (4.7b).$$

At each wavenumber the complex refractive index, $\hat{n} = n + ik$, is related to the complex dielectric constant $\hat{\varepsilon} = \varepsilon' + i\varepsilon''$ by equation 4.8

$$\hat{\varepsilon}(\tilde{\nu}) = \hat{n}^2(\tilde{\nu}) \quad (4.8)$$

so the real and imaginary refractive index spectra, $n(\tilde{\nu})$ and $k(\tilde{\nu})$, can be calculated from the dielectric constant spectra through Eqs. (4.8a) and (4.8b).

$$n(\tilde{\nu}) = \sqrt{(\sqrt{(\varepsilon'(\tilde{\nu}))^2 + (\varepsilon''(\tilde{\nu}))^2} + \varepsilon'(\tilde{\nu})) / 2} \quad (4.8a)$$

$$k(\tilde{\nu}) = \sqrt{(\sqrt{(\varepsilon'(\tilde{\nu}))^2 + (\varepsilon''(\tilde{\nu}))^2} - \varepsilon'(\tilde{\nu})) / 2} \quad (4.8b).$$

The parameters μ_j , I_j and $\tilde{\nu}_j$, used to simulate the spectra of liquid methanol and benzene are given in Table 4.2. The simulated n and k spectra are shown in Fig. 4.1 for methanol between 7800 and 2 cm^{-1} and in Fig. 4.2 for benzene between 8000 and 2 cm^{-1} .

4.2.2 Calculation of Phase Shift, Reflectance R_s and ATR from Simulated Optical Constants, n and k

The equations in this section apply at each wavenumber.

Table 4.2. Classical Damped Harmonic Oscillator Parameters for Simulated Spectra of "Benzene" and "Methanol"

j	μ_h (Debye Å amu ^{-1/2})	$\bar{\nu}_{j,1}$ (cm ⁻¹)	$\Gamma_{j,1}$ (cm ⁻¹)
"Benzene" ^a			
1	0.16129	849.998	22.257
2	0.22288	851.809	144.027
3	0.47999	1035.56	9.86736
4	0.14453	1011.76	24.1246
5	0.04619	991.872	7.51311
6	0.23185	973.107	63.9954
7	0.06939	1249.36	11.8006
8	0.18753	1177.26	22.7901
9	0.27674	1167.12	149.92
10	0.10846	1147.48	19.74
11	0.16027	1393.24	11.9
12	0.09058	1307.92	31.56
13	0.55332	1692.22	230.17
14	0.24566	1527.96	17.93
15	0.65962	1479.07	6.0747
16	0.31176	1959.96	15.5583
17	0.3828	1815.2	16.134
18	0.12687	2324.92	9.79
19	0.09335	2210.2	9.076
20	0.07315	2652.92	9.086
21	0.05682	2614.24	10.93
22	0.07465	2595.04	9.376
23	0.4968	3091.01	8.8421
24	0.37297	3071.48	7.629
25	0.13008	3061.39	8.503
26	0.73908	3035.66	11.086
27	0.14007	4082.52	34.798
28	0.24608	4056.62	14.656
"Methanol" ^b			
1	4.15155	3356.001	250
2	1.84544	2947.271	100
3	1.1820	2833.979	50
4	1.35024	1452.45	100
5	0.40576	1115.283	30
6	1.43738	1033.928	22
7	1.49813	663.7399	200
8	1.58014	676.105	8.294

^a The spectra were calculated between 8000 and 2 cm⁻¹, data points are 0.964 cm⁻¹ apart, and $n(\infty)=1.4804$.

^b The spectra were calculated between 7800 and 2 cm⁻¹, data points are 0.964 cm⁻¹ apart, and $n(\infty)=1.325$.

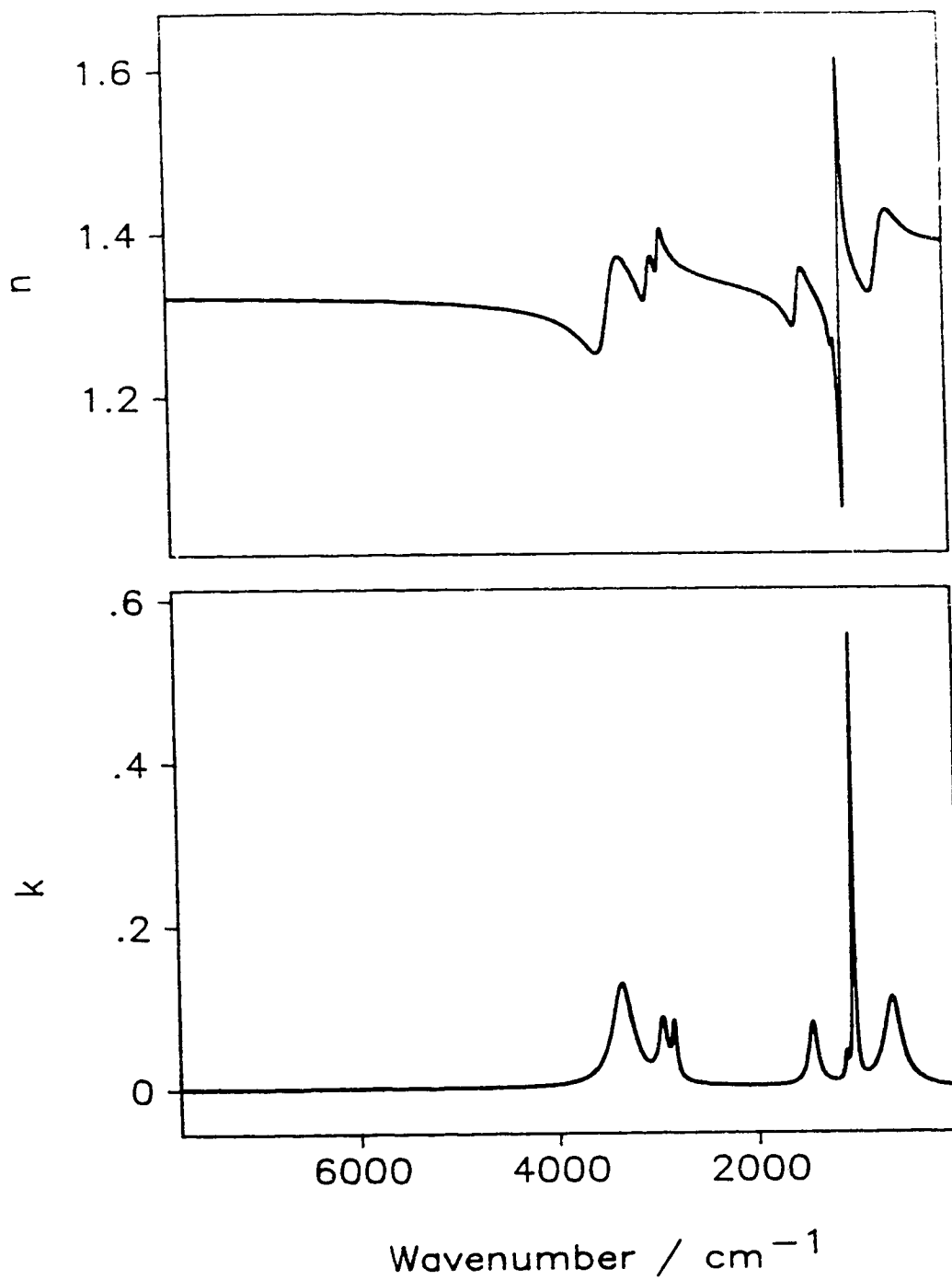


Figure. 4.1. The simulated refractive index spectra of liquid methanol, 7800 to 2 cm⁻¹. Lower box: k , Upper box: n

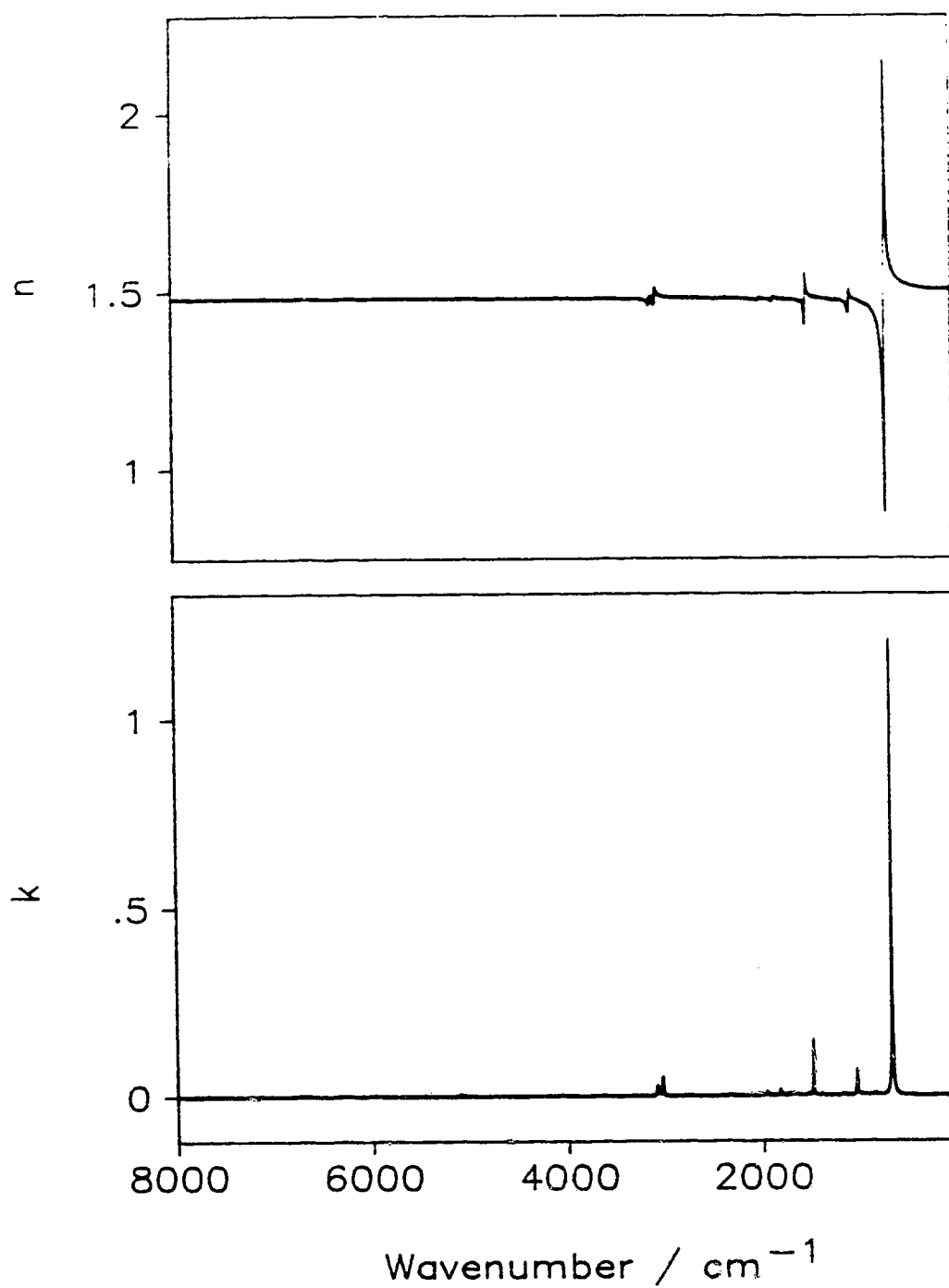


Figure 4.2. The simulated refractive index spectra of liquid benzene, 8000 to 2 cm^{-1} Lower box: k , Upper box: n .

For s-polarized light whose vector \hat{E}_s is parallel to the reflecting surface, the complex Fresnel reflection coefficient \hat{r}_s is related to the reflectance R_s and phase shift θ_s through equation (4.9a)

$$\hat{r}_s = R_s^{1/2} \exp(i\theta_s) \quad (4.9a)$$

The reflection coefficient is given¹⁷ in terms of the refractive indices by Eq. 4.4, and the complex angle of refraction, $\hat{\beta}$, is related to β_o through Snell's law¹⁷,

$$n_o \sin \beta_o = \hat{n} \sin \hat{\beta} \quad (4.9b)$$

From equations (4.9a), (4.9b) and (4.4) one can obtain

$$R_s^{1/2} \cos \theta_s = \frac{-n_o^2 \cos^2 \beta_o + A^2 + B^2}{(A + n_o \cos \beta_o)^2 + B^2} \quad (4.10a)$$

$$R_s^{1/2} \sin \theta_s = \frac{2Bn_o \cos \beta_o}{(A + n_o \cos \beta_o)^2 + B^2} \quad (4.10b)$$

where $A = ((a^2 + b^2)^{1/2} + a)^{1/2} / \sqrt{2}$ and $B = ((a^2 + b^2)^{1/2} - a)^{1/2} / \sqrt{2}$

with $a = n^2 - k^2 - n_o^2 \sin^2 \beta_o$ and $b = 2nk$.

Equations (4.10a) and (4.10b) yield the reflectance R_s as Eq. (4.11)

$$R_s = \frac{(-n_o^2 \cos^2 \beta_o + A^2 + B^2)^2 + 4B^2 n_o^2 \cos^2 \beta_o}{[(A + n_o \cos \beta_o)^2 + B^2]^2} \quad (4.11).$$

The phase shift, θ_s , is obtained through θ'_s , the principal value of the arctan function of Eq. (4.12)

$$\theta'_s = \arctan\left(\frac{2Bn_o \cos \beta_o}{-n_o^2 \cos^2 \beta_o + A^2 + B^2}\right) \quad (4.12)$$

This θ_s' lies in the range $-\pi/2 < \theta_s' < \pi/2$. In fact, the positive root is taken in Eq. (4.10b) so $\sin \theta_s$ is ≥ 0 , as is required by our definition of \hat{r} and $\hat{\varepsilon}$ (Table 4.1), therefore θ_s lies between 0 and π . The sign of $\cos \theta_s$ is the sign of the right-hand side of Eq. (4.10a). Thus, θ_s and θ_s' are related by Eqs. (4.12)

$$\theta_s = \pi + \theta_s' \quad \text{if } \cos \theta_s < 0 \quad (4.12a)$$

$$\theta_s = \pi/2 \quad \text{if } \cos \theta_s = 0 \quad (4.12b)$$

$$\theta_s = \theta_s' \quad \text{if } \cos \theta_s > 0 \quad (4.12c)$$

In this laboratory, the pATR spectrum is measured through the CIRCLE cell with effectively natural light at incident angle $\beta_o = \pi/4$. The quantity pATR is defined by

$$pATR = -\log_{10} (ATR) = -\log_{10} (I_R/I_0) \quad (4.13)$$

The pATR can be calculated from the R_s spectrum alone, because s and p polarizations are equally intense at each reflection in a well aligned CIRCLE cell⁵ and the reflectance of p-polarized light at 45° incidence is $R_p = R_s^2$. Therefore, for m reflections in the CIRCLE cell

$$pATR = -\log_{10} [(R_s^m + R_s^{2m})/2] \quad (4.14)$$

The pATR spectra were all calculated in this work with $m = 1$. Spectra simulated for liquid methanol are shown in Fig. 4.3 for constant $n_o = 2.38$, approximately that of ZnSe, and also for the actual $n_o(\tilde{\nu})$ values of ZnSe and of Si. Note that the spectrum for actual ZnSe ends at 700 cm^{-1} . Spectra simulated for liquid benzene are shown in Fig. 4.4 for constant $n_o = 3.5$, approximately that of Si, and for

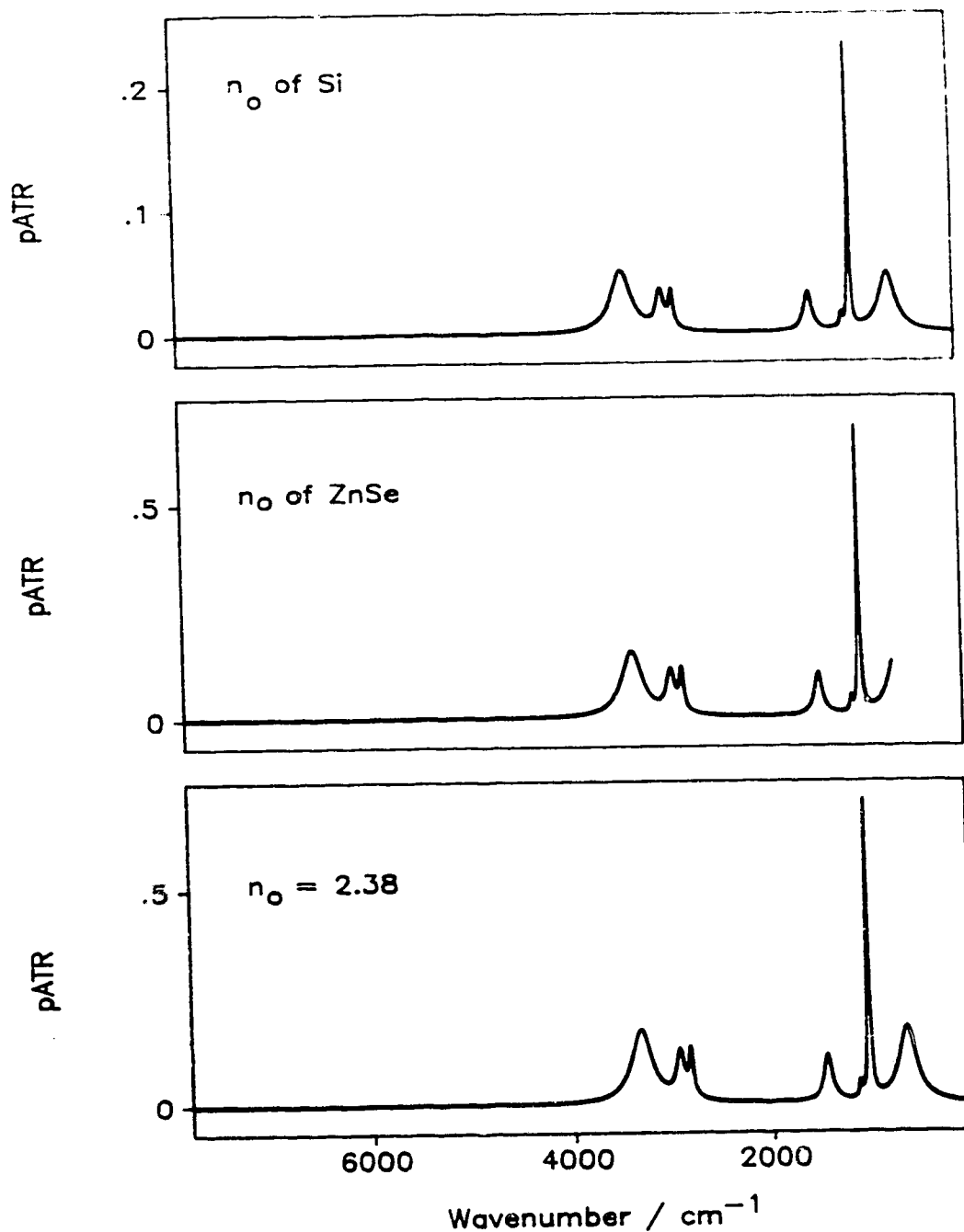


Figure 4.3. The simulated single-reflection pATR spectra of methanol calculated for the CIRCLE cell (Eq. 4.14.) with different sets of n_o values. **Lower box:** constant $n_o=2.38$, approximates ZnSe; **Middle box:** $n_o(\tilde{\nu})$ values of ZnSe; **Upper box:** $n_o(\tilde{\nu})$ values of Si. Note that the spectrum in the middle box stops at 700 cm⁻¹..

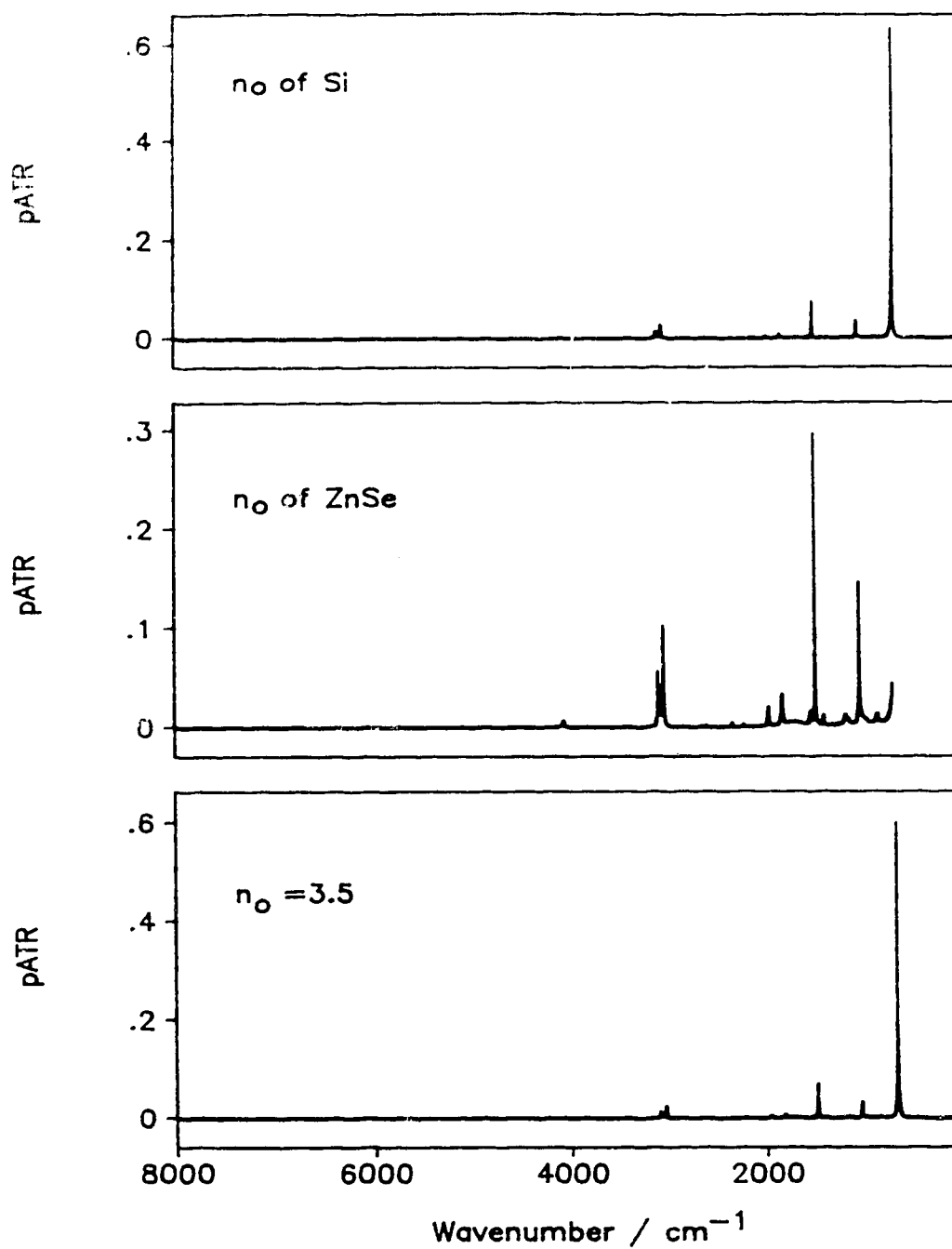


Figure 4.4. The simulated single-reflection pATR spectrum of benzene calculated for the CIRCLE cell (Eq. 4.14) with **Lower box** constant $n_o=3.5$, approximates Si; **Middle box:** $n_o(\tilde{\nu})$ values of ZnSe; **Upper box:** $n_o(\tilde{\nu})$ values of Si. Note that the spectrum in the middle box stops at 700 cm^{-1} .

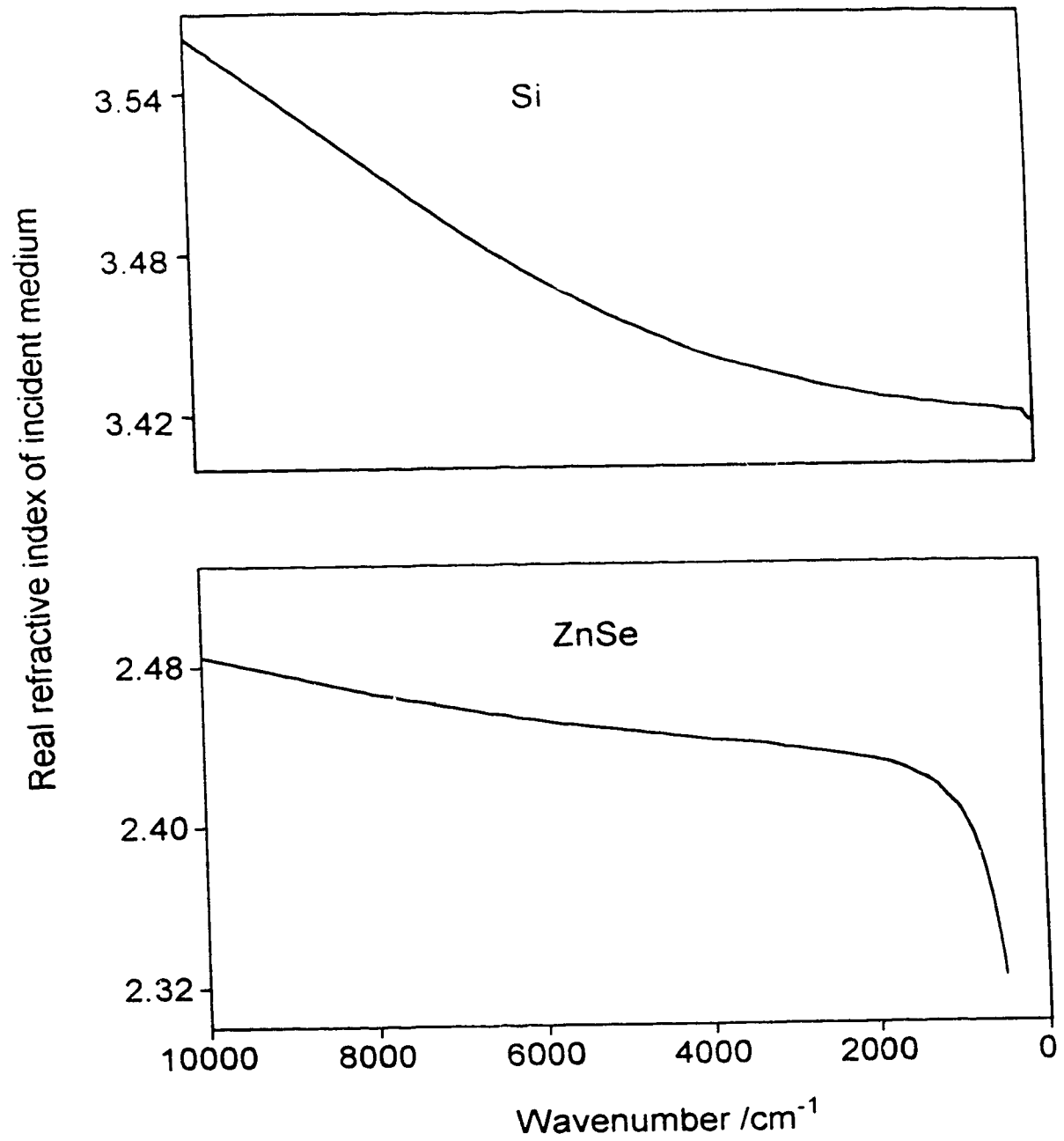


Figure 4.5. The real refractive indices of Si¹⁸⁻²⁰ and ZnSe²¹ at room temperature 25°C.

the actual $n_o(\tilde{\nu})$ values of ZnSe and Si. The actual n_o spectra of ZnSe and Si are shown in Fig. 4.5.

4.2.3 The Equations Used to Recover Optical Constants from Reflectance R_s and Phase Shifts θ_s

The various transforms and phase corrections used to calculate the phase shift spectrum from the reflectance spectrum are discussed in the next section. Once the phase shift and reflectance had been calculated, the dielectric constants were calculated through Eqs. (4.15a) and (4.15b), which can be derived from Eqs. (4.4), (4.9a) and (4.9b).

$$\varepsilon'/n_o^2 = \sin^2 \beta_o + \cos^2 \beta_o [(1-R_s)^2 - 4R_s \sin^2 \theta_o] / (1+R_s-2R_s^{1/2} \cos \theta_o)^2 \quad (4.15a)$$

$$\varepsilon''/n_o^2 = 4 \sin \theta_s \cos^2 \beta_o (1-R_s) R_s^{1/2} / (1+R_s-2R_s^{1/2} \cos \theta_o)^2 \quad (4.15b)$$

The optical constants were then calculated from the dielectric constants through Eqs. (4.8)

Bardwell and Dignam³ gave the same equations except that Eq. (4.10) of Ref. 3 differs in form from Eq. (4.15a) and the right hand side of Eq. (4.11) of Ref. 3 is the negative of Eq. (4.15b), as is required by their different definition of $\hat{\varepsilon}$ (Table 4.1).

4.2.4 The Transformation of R_s to θ_s

The spectrum of R_s^m can be determined from a pATR spectrum measured in, or calculated for, a CIRCLE cell by the solution of Eq. (4.14), namely

$$R_s^m = \frac{1}{2} [1 + 8ATR]^{1/2} - \frac{1}{2} \quad (4.16)$$

The transformation of the $\ln[R_s]$ spectrum to the θ_s spectrum was carried out with three different transforms.

The first two transforms were those of Plaskett and Schatz¹, given above as Eqs. (4.2) and (4.3). The correction factors $\theta(0)$ in Eq. (4.2) and $I(\tilde{\nu}_a)$ in Eq. (4.3) were not used, and the correction of the θ spectrum calculated by the transform was carried out as described below.

The third transform is a modified KK transform developed during this work for the case of ATR by using a different integrand and a different integral contour from those of Plaskett and Schatz¹. The derivation is given in the appendix and the transform is Equation (4.17)

$$\theta(\tilde{\nu}_a) = -\frac{2}{\pi} P \int_0^{\infty} \frac{\tilde{\nu} \ln|R(\tilde{\nu})|^{1/2}}{\tilde{\nu}^2 - \tilde{\nu}_a^2} d\tilde{\nu} + \theta_{\infty} \quad (4.17)$$

The transform is identical for s and p polarizations. Again, the correction θ_{∞} was calculated as described below.

The remainder of this paper deals entirely with the s-polarized reflectance and phase shift, so the subscript 's' is omitted for simplicity. If the correction to the phase shift spectrum is neglected for the moment, these three transforms can be summarized in practical terms by Eq. (4.18)

$$\theta_t(\tilde{\nu}_a) = -\frac{2}{\pi} P \int_0^{\tilde{\nu}_u} \frac{F(\tilde{\nu})}{\tilde{\nu}^2 - \tilde{\nu}_a^2} d\tilde{\nu} \quad (4.18)$$

where function $F(\tilde{\nu})$ is $\tilde{\nu}_a^2 \ln[R(\tilde{\nu})]^{1/2} / \tilde{\nu}$ for the modified KK transform of Eq. (4.2), $\tilde{\nu}_a \ln[R(\tilde{\nu})]^{1/2}$ for the KK transform of Eq. (4.3) and $\tilde{\nu} \ln[R(\tilde{\nu})]^{1/2}$ for the modified KK transform of Eq. (4.17). The subscript 't' on θ shows that the phase shift is obtained from the transform without the application of correction terms.

The phase shift spectrum, $\theta(\tilde{\nu})$, calculated by the transform differs from the correct spectrum $\theta(\tilde{\nu})$ by the required correction $\Delta\theta(\tilde{\nu})$. Bardwell and Dignam's work³ suggests that a constant phase correction will prove satisfactory for molecular liquids. In our view, this is particularly likely to be the case if the correction is determined at a high-wavenumber where the reflectance is essentially constant. The upper integration limit $\tilde{\nu}_u$, is 7800 or 8000 cm^{-1} for the spectra synthesized for this study. It is, thus, sufficiently far above the strong infrared absorption and below the strong visible and ultraviolet absorption that $k(\tilde{\nu}_u) \approx 0$ and the real refractive index, and hence the reflectance, is approximately constant. Thus, $\Delta\theta$ was calculated through Eq. (4.5) as

$$\Delta\theta = \theta_o(\tilde{\nu}_u) - \theta(\tilde{\nu}_u) \quad (4.19a)$$

where $\tilde{\nu}_u$ is the highest wavenumber in the spectrum and $k(\tilde{\nu}_u) \approx 0$. The corrected phase shift spectrum was then calculated as

$$\theta(\tilde{\nu}) = \theta(\tilde{\nu}) + \Delta\theta \quad (4.19b)$$

Three FORTRAN programs REPH1.FOR, REPH2.FOR and REPH3.FOR were developed to calculate the phase shift and optical constants from pATR spectra measured with the CIRCLE cell at 45° incidence by the transformations of Eqs. (4.3), (4.2) and (4.17) with the constant phase shift correction, Eqs. (4.19). The programs create spectral files of the phase shift and the real and imaginary refractive indices. These spectra were compared with the synthesized spectra to evaluate the accuracy of the different transforms.

The upper integration limit is usually 4500 cm^{-1} or more for individual ATR spectra recorded in this laboratory. However, spectra recorded with KBr and CaF_2 beamsplitters are usually merged and averaged to give an experimental spectrum to 6500 cm^{-1} before they are processed. The $\ln[R_s]$ spectrum is essentially zero between 6500 and 8000 cm^{-1} , so the spectrum is filled with zero points up to 8000 cm^{-1} before it is transformed. The real refractive index of the sample can be determined¹⁶ to good accuracy at 8000 cm^{-1} so the phase correction can be well determined at 8000 cm^{-1} .

4.3 Results and Discussion

4.3.1 Constant Phase Shift Correction

The constant phase shift correction, Eqs. (4.19a) and (4.19b) was applied with all three transformations to the *pATR* spectra simulated for liquid methanol (7800 to 2 cm^{-1}) and benzene (8000 to 2 cm^{-1}) with constant $n_o=2.38$ or 3.5 , which approximate those of ZnSe or Si. $\ln[R_s(\tilde{\nu})]$ was extrapolated linearly from its value at 2 cm^{-1} to zero at 0 cm^{-1} . Above $\tilde{\nu}_u = 7800$ or 8000 cm^{-1} $\ln[R_s(\tilde{\nu})]$ is essentially zero throughout the near infrared and visible and was assumed to be accounted for by the correction to the phase shift. Thus, the integration was taken between $\tilde{\nu}_u$ and 0 cm^{-1} .

Consider first the results obtained for the synthesized spectrum of methanol with an incident medium of constant refractive index, $n_o = 2.38$. Figure 4.6 shows the synthesized phase shift (Top) , imaginary refractive index (Middle) and real refractive index (Bottom) spectra. The different boxes in Fig. 4.6 also contain the corresponding

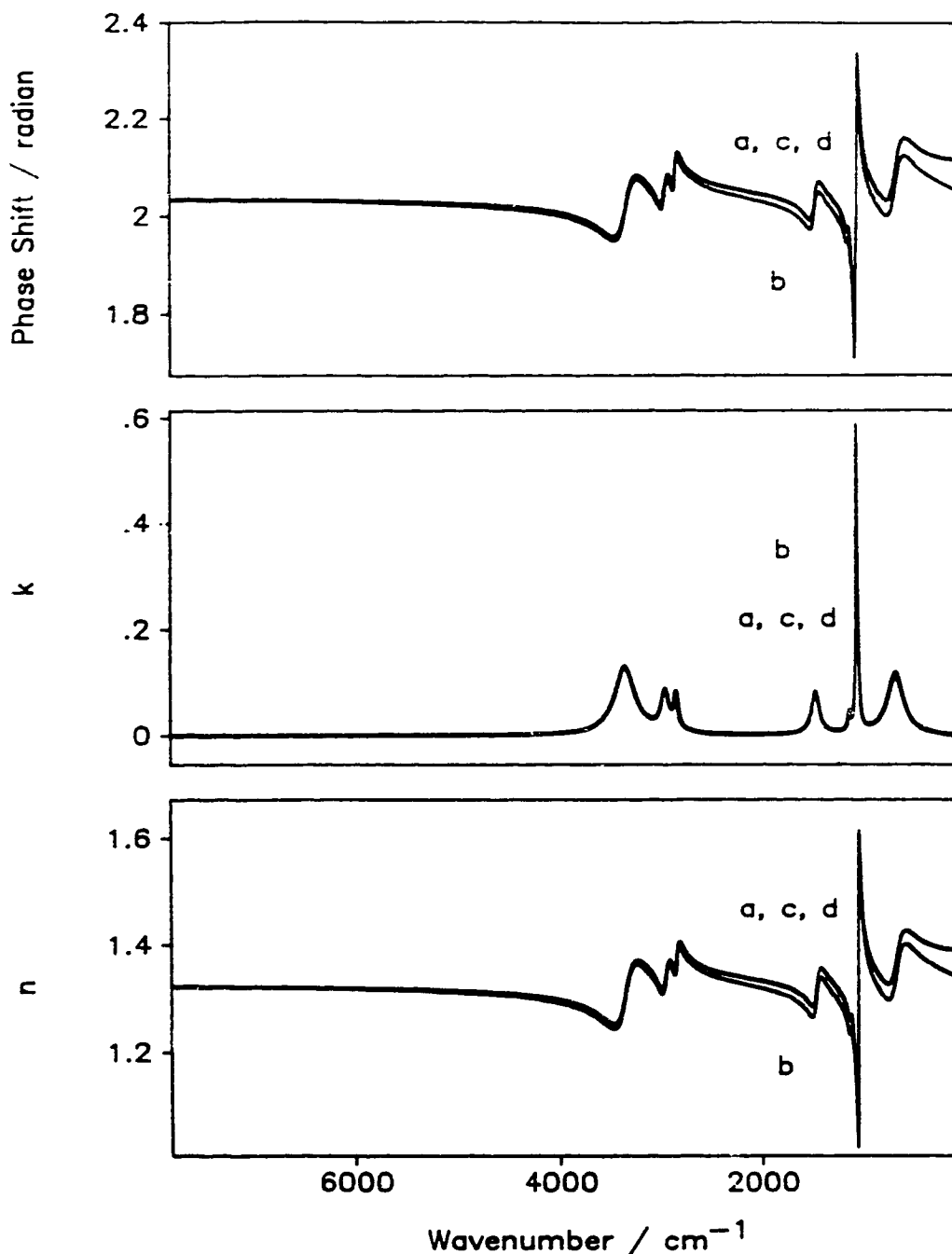


Figure 4.6. Results for the phase shift (top), imaginary refractive index (middle) and real refractive index (bottom) of "methanol" with constant $n_o = 2.38$ and recovered with constant phase correction. Curves a are Synthesized spectra; Curves b were recovered with Eqs. (4.3) and (4.19); Curves c were recovered with Eqs. (4.2) and (4.19); Curves d were recovered with Eqs. (4.17) and (4.19). The curves a to d in the middle box, and a, c and d in the top and bottom boxes, overlap

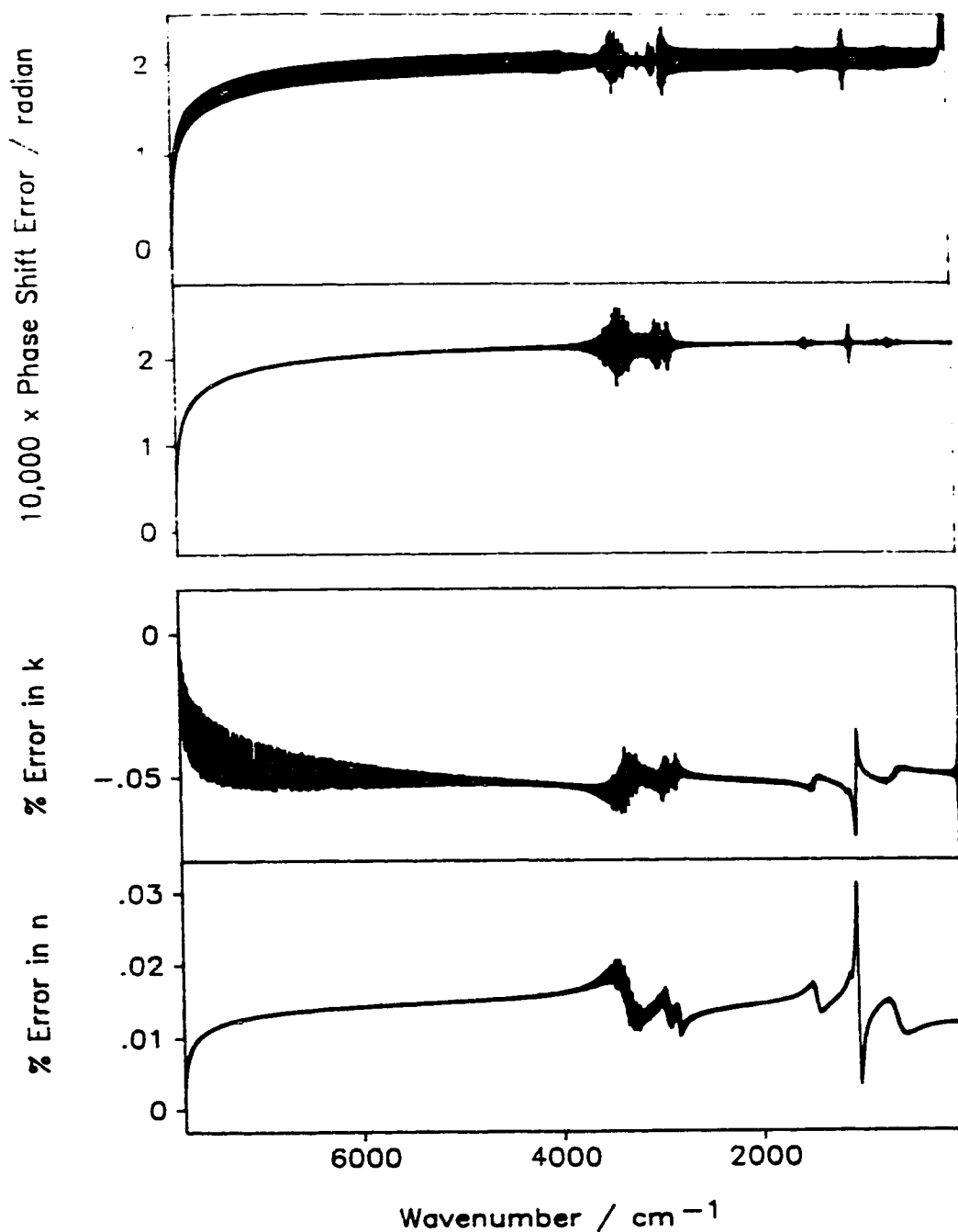


Figure 4.7. Errors in the phase shifts and refractive indices of "methanol" with constant $n_0 = 2.38$ and recovered with constant phase correction. Top box: Error in phase shift; *curve c* minus *curve a* of the top box of Fig. 4.6. Upper Middle box: Error in phase shift; *curve d* minus *curve a* of the top box of Fig. 4.6. Lower Middle box: % error in k from Eqs. (4.17) and (4.19); $(\text{Curve } d \text{ minus Curve } a) \div \text{Curve } a \times 100\%$ from middle box of Fig. 4.6. Bottom box: % error in n from Eqs. (4.17) and (4.19); $(\text{Curve } d \text{ minus Curve } a) \div \text{Curve } a \times 100\%$ from bottom box of Fig. 4.6.

spectra recovered, from the synthesized pATR spectrum, by Eqs. (4.3), (4.2) and (4.17) with the constant phase shift correction of Eqs. (4.19). The spectra overlap on the scale shown except for those recovered by the normal KK transform, Eq. (4.3) (curves b in Figs. 4.6). Thus, it is clear that the well known Kramers-Kronig transform, Eq. (4.3) is by far the least accurate. It yields phase shifts in error by 0 to -0.06 radian, and these yield errors from 0 to +15% and from 0 to -4% in the optical constants, k and n , respectively. In contrast, the two modified KK transforms, Eqs. (4.2) and (4.17), both yield errors that are about 100 times smaller.

For the same system Fig. 4.7 shows the error spectra of the phase shift calculated with the two modified KK transforms, from Eq. (4.17) in the upper box and from Eq. (4.2) in the upper middle box. It is clear that the two methods are about equally accurate on average, but the new equation, (4.17) gives far less numerical noise, undoubtedly because it does not have the singularity at 0 cm^{-1} . The same result was found for the error spectra of the refractive indices. Accordingly, the bottom two boxes in Fig. 4.7 show only the results for Eq. (4.17). They show the percent error spectra of the recovered k and n values. The percent errors average 0.05 % and 0.01% for k and n , respectively. The noise at high wavenumbers in the lower middle box is numerical noise of magnitude 10^{-7} , which distorts the percent error spectrum for k values $\leq 10^{-5}$ which, in any case, are not reliably determined by the pATR method.

The same calculations yielded similar results for the synthesized spectrum of methanol with an incident medium of constant refractive index, $n_0 = 3.5$, which is close to that of silicon. Again, the normal KK transform, Eq. (4.3) was inaccurate and the

two modified KK transforms had equal accuracy on average and Eq. (4.17) gave far less numerical noise. The phase shifts recovered with Eq. (4.17) in this case were about 80% of those with $n_o = 2.35$, and the errors in the recovered phase shifts were about $2\frac{1}{2}$ times smaller. Thus, the relative error in the phase shift is smaller with $n_o = 3.5$ than with $n_o = 2.38$. Similarly, the percentage errors in the recovered real and imaginary refractive indices were slightly smaller than for $n_o = 2.38$.

Refractive index, phase shift, and pATR spectra were simulated, and phase shift, and refractive index spectra were recovered, in the same way for simulated benzene (Table 4.2) with the same qualitative results as for simulated methanol. Quantitatively the errors in the recovered spectra for benzene were up to a factor of 2 smaller than for methanol.

It should be noted that these results are essentially the reverse of those of Bardwell and Dignam³, who found that the normal KK transform of Eq. (4.3) with constant phase shift correction was more accurate than the modified KK transform of Plaskett and Schatz, Eq. (4.2), again with constant correction. As noted earlier, we believe this is due to Bardwell and Dignam's use of their double Fourier transform procedure to evaluate the integrals, because the singularity in Eq. (4.2) at 0 cm^{-1} invalidates that procedure.

It is clear that Eqs. (4.2) and (4.17) with the constant phase correction of Eqs. (4.19) give optical constants that are more accurate than current experimental spectra when n_o is constant. Unfortunately, the real refractive index of the incident medium

never is constant, as is shown in Fig. 4.5 for ZnSe and Si. To obtain a useful result it is necessary to explore corrections for the case of n_o values that change with wavenumber.

Theoretically, the non-constancy of n_o makes all existing KK transforms approximate, whether they are modified or not. In practice, the constant phase shift correction does not give satisfactory accuracy when used to recover optical constants from ATR spectra. To determine this, the synthesized refractive index spectra of benzene and methanol were used with the actual n_o spectra of ZnSe or Si to calculate four synthesized pATR spectra, and Eq. (4.17) was used with constant phase shift correction of Eqs. (4.19) to recover the θ , n , and k spectra. The results for simulated methanol on silicon are shown in Fig. 4.8. The correct phase shifts, imaginary refractive indices, and real refractive indices, are shown as curves C in the top, middle and bottom box, respectively, and those recovered by Eqs. (4.17) and (4.19) are shown as curves R. The errors in the recovered quantities are from 0 to +7% for k , 0 to -5% for n and 0 to -0.01 rad for θ , where $\theta \approx 1.75$ rad. Curves C and R in the three boxes in Figure 4.9 show similar results for simulated benzene on silicon. These errors given by the constant phase shift correction when n_o is not constant are larger than the probable errors in the experimental data, and a method was sought to reduce them.

4.3.2 Non-Constant Phase Shift Correction

A new, wavenumber-dependent, phase shift correction was based on the constant phase shift correction of Eqs. (4.19). The only difference is to recognize that

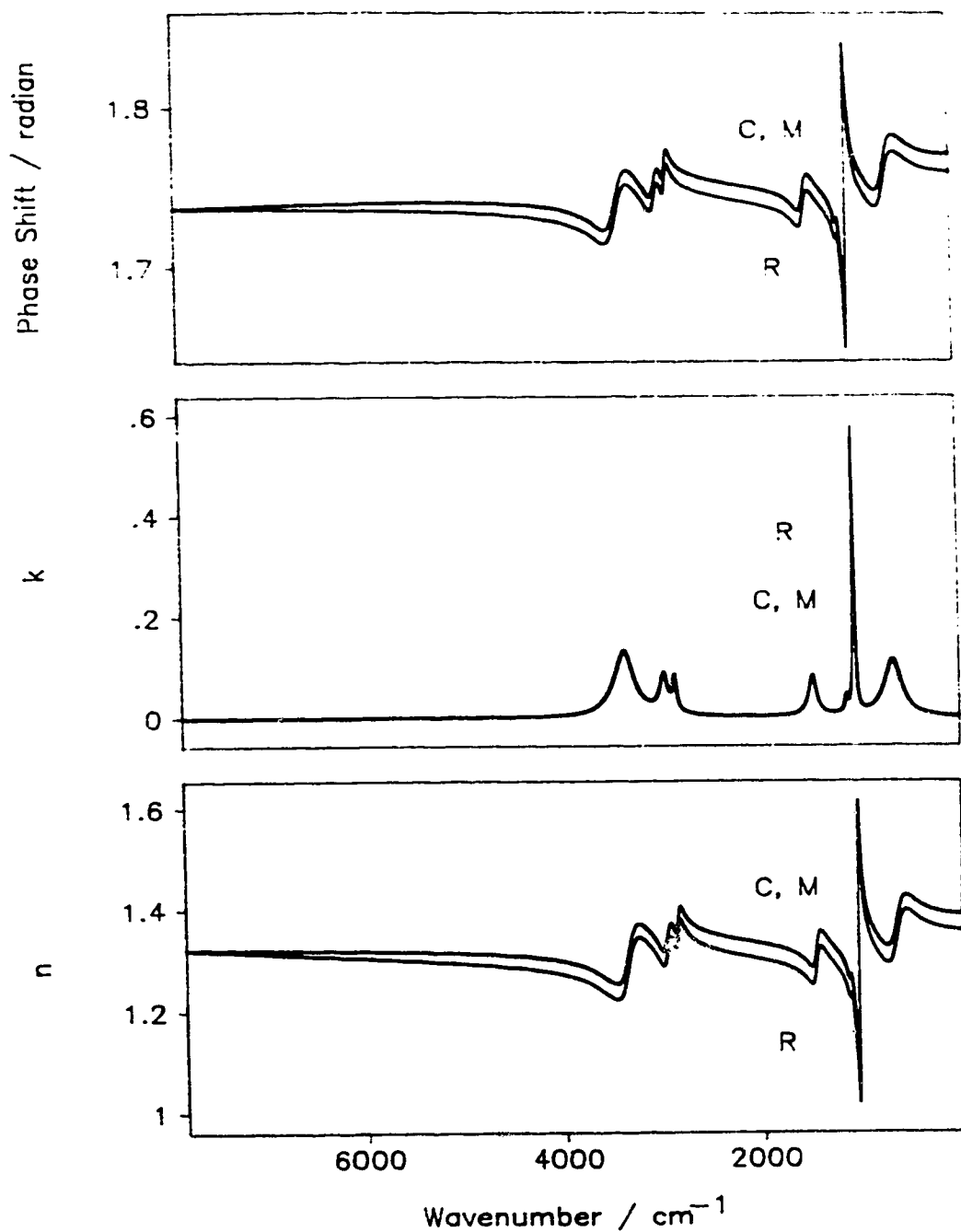


Figure 8. Results for the phase shift (top), imaginary refractive index (middle) and real refractive index (bottom) of "methanol" with $n(\tilde{\nu})$ of Si, recovered with constant and with non-constant phase correction. In each box, C indicates the correct (synthesized) spectrum, R indicates recovery with Eqs. (4.17) and (4.19), and M indicates recovery with Eqs. (4.17) and (4.20)

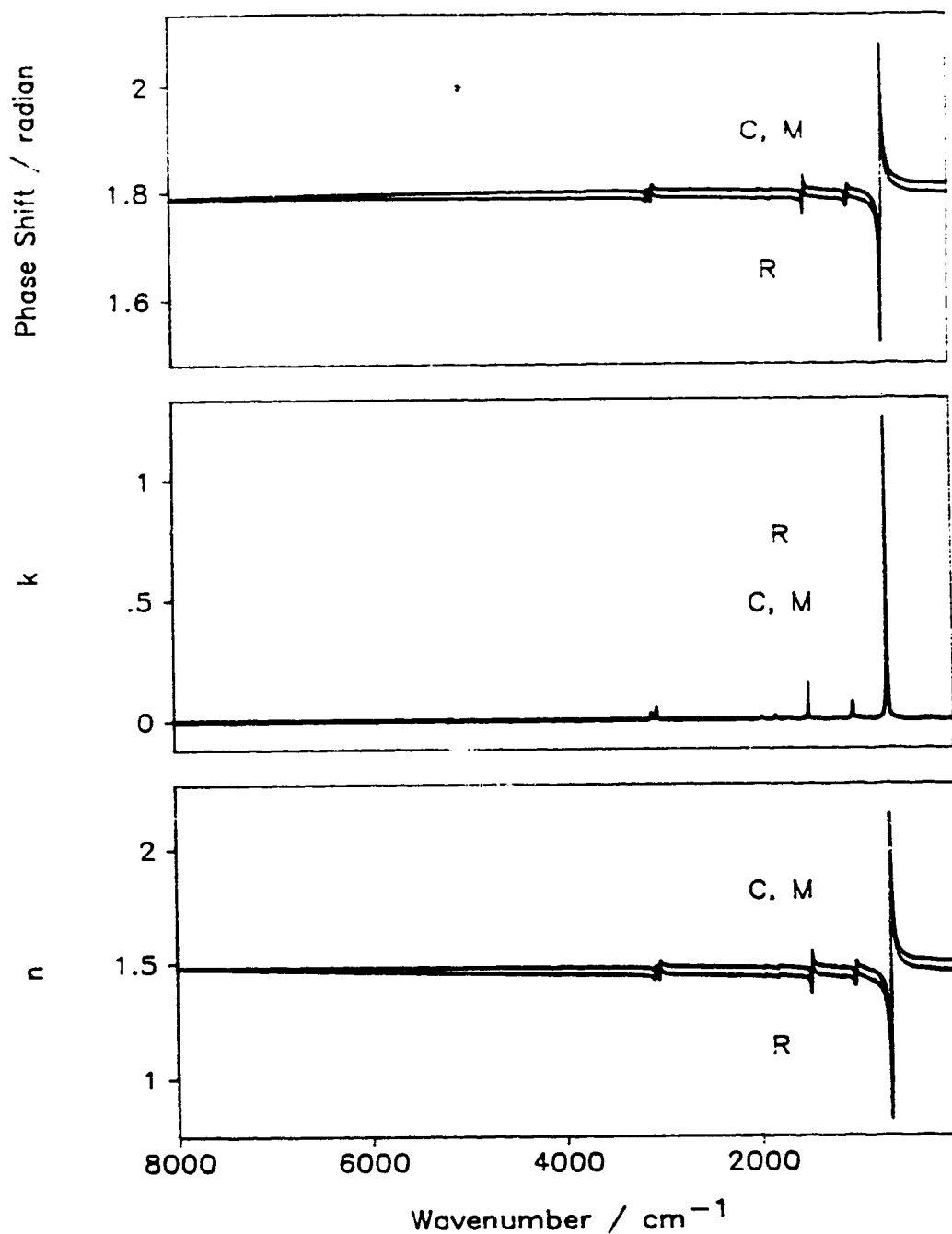


Figure 4.9. Results for the phase shift (top), imaginary refractive index (middle) and real refractive index (bottom) of "benzene" with $n(\tilde{\nu})$ of Si, recovered with constant and with non-constant phase correction. In each box, C indicates the correct (synthesized) spectrum, R indicates recovery with Eqs. (4.17) and (4.19), and M indicates recovery with Eqs. (4.17) and (4.20). All curves in the middle box, and curves C and M in the top and bottom boxes, overlap.

the refractive index of the incident medium depends on wavenumber. Thus, the non-constant correction is defined by Eqs. (4.20a) and (4.20b).

$$\Delta\theta(\tilde{\nu}) = \pi - 2 \arctan \frac{\sqrt{(n_o^2(\tilde{\nu}) \sin^2 \beta_o - n^2(\tilde{\nu}_u))}}{n_o(\tilde{\nu}) \cos \beta_o} - \theta(\tilde{\nu}_u) \quad (4.20a)$$

$$\theta(\tilde{\nu}) = \theta(\tilde{\nu}) + \Delta\theta(\tilde{\nu}) \quad (4.20b)$$

The programs MREPH1.FOR, MREPH2.FOR and MREPH3.FOR calculate the phase shift and optical constants from pATR spectra through Eqs. (4.3), (4.2) and (4.17), respectively, each with the non-constant phase correction of Eqs. (4.20). Again, it was found that Eqs. (4.2) and (4.17) are more accurate than Eq. (4.3) by a factor of about 100, and that Eq. (4.17) gives less numerical noise than Eq. (4.2). The spectra recovered by Eq. (4.17) with Eqs. (4.20) (program MREPH3) for synthesized methanol on silicon incident medium are included in Fig. 4.8 as curves M. The use of the new, non-constant, phase shift correction yields spectra that can not be distinguished from the correct spectra, curves C, on the scale shown.

Figure 4.9 shows that results of the same quality were obtained for synthesized benzene on silicon, and Fig. 4.10 shows, for synthesized methanol on Si, an expanded view of the deviation of the calculated θ spectrum from the correct one and the percent error spectra for k and n . The new transform with the non-constant phase shift correction allows the phase shift and refractive indices to be recovered from pATR, or R_s spectra with an accuracy of better than 0.1%, as was sought.

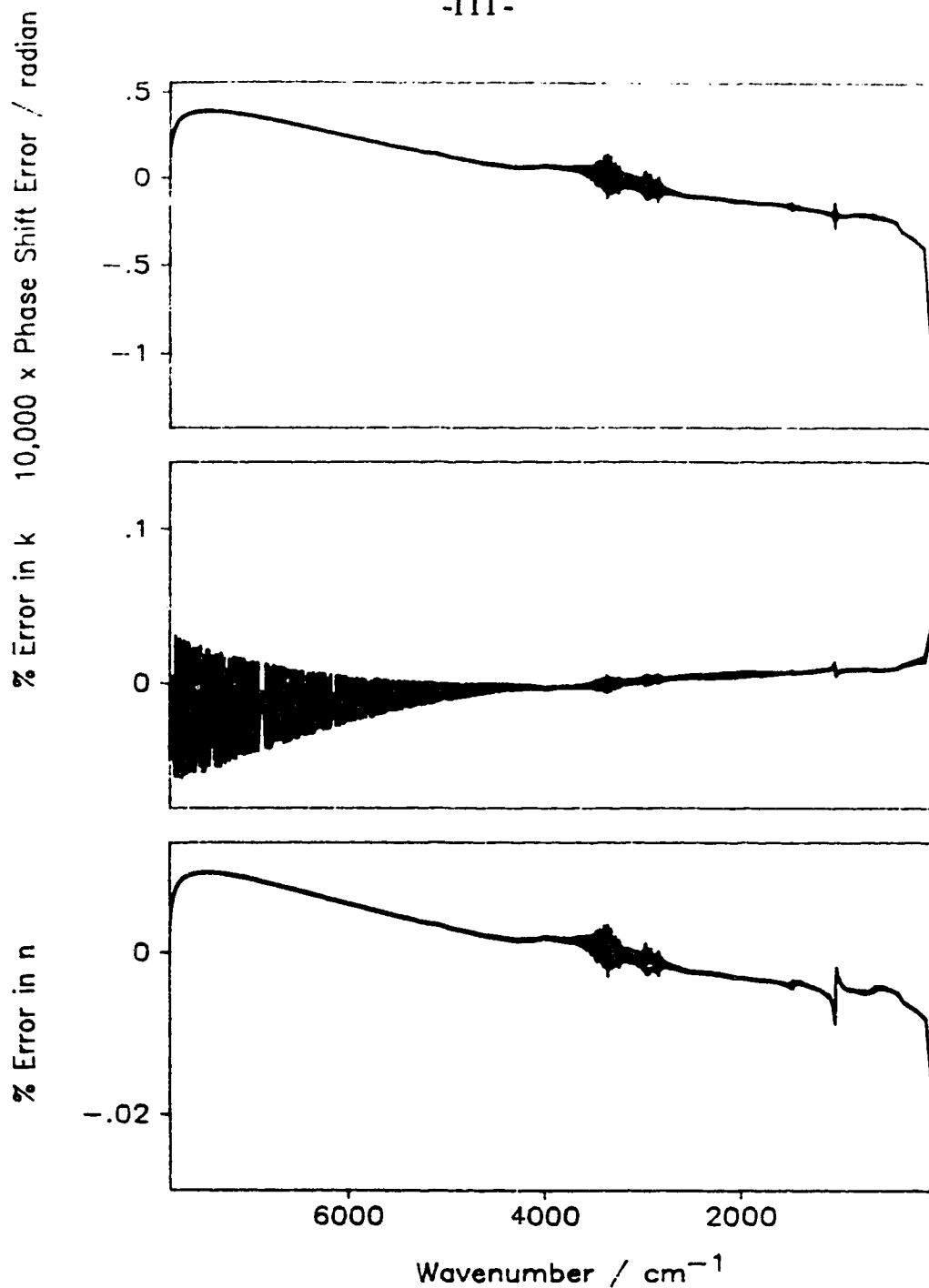


Figure 4.10. Error in the phase shift (top) and percent errors in the imaginary refractive index (middle) and real refractive index (bottom) of "methanol" with $n(\tilde{\nu})$ of Si, recovered with non-constant phase correction, Eqs. (4.17) and (4.20). Top Box: *Curve M* minus *Curve C* from the top box of Fig. 4.8. Middle box: $\% \text{ error in } k$ from Eqs. (4.17) and (4.20); $(\text{Curve } M \text{ minus Curve } C) + \text{Curve } C \times 100\%$ from middle box of Fig. 4.8. Bottom box: $\% \text{ error in } n$ from Eqs. (4.17) and (4.20); $(\text{Curve } M \text{ minus Curve } C) + \text{Curve } C \times 100\%$ from bottom box of Fig.4.8..

4.3.3 The Use of Experimental pATR Spectra.

It has been shown above that Eqs. (4.17) and (4.20) allow the accurate recovery of θ , n , and k spectra, provided the reflection spectra run from $\tilde{\nu}_u$ to 2 cm^{-1} . This is almost never the case, and pATR spectra in this laboratory have 700 cm^{-1} as the lowest wavenumber. To show the effect of this, the simulated n and k spectra of methanol were used with the real n_o spectrum of ZnSe to calculate a phase shift spectrum and a pATR spectrum (still for a single reflection in a CIRCLE cell) between 7800 and 700 cm^{-1} . These synthesized θ , k and n spectra are shown as curves C in Fig. 4.11. Eqs. (4.17) and (20) were used to recover the θ , n , and k spectra from the pATR spectrum, using linear extrapolation of $\ln[R]$ between its value at 700 cm^{-1} and zero at 0 cm^{-1} . The error in θ and the percent errors in k and n are shown as curves M in Fig. 4.11. The errors pass through a maximum or minimum near 1000 cm^{-1} and have maximum size at 700 cm^{-1} where they are 0.015 rad in θ ($\theta \approx 2\text{ rad}$), -3% in k and $+1\%$ in n . These errors are much greater than those in Figs. 4.9 and 4.10, simply due to the omission of part of the spectrum from the transform.

A similar error is present in all methods that use the KK transform or a modification of it with truncated spectra. These methods include the use of the k to n transform in the iterative procedure used in this laboratory⁶ and also the use of the $\ln[R]$ to θ and k to n transforms used in Huang and Urban's iterative procedure⁴. In the present case, the error can be minimized by following the initial recovery of the θ

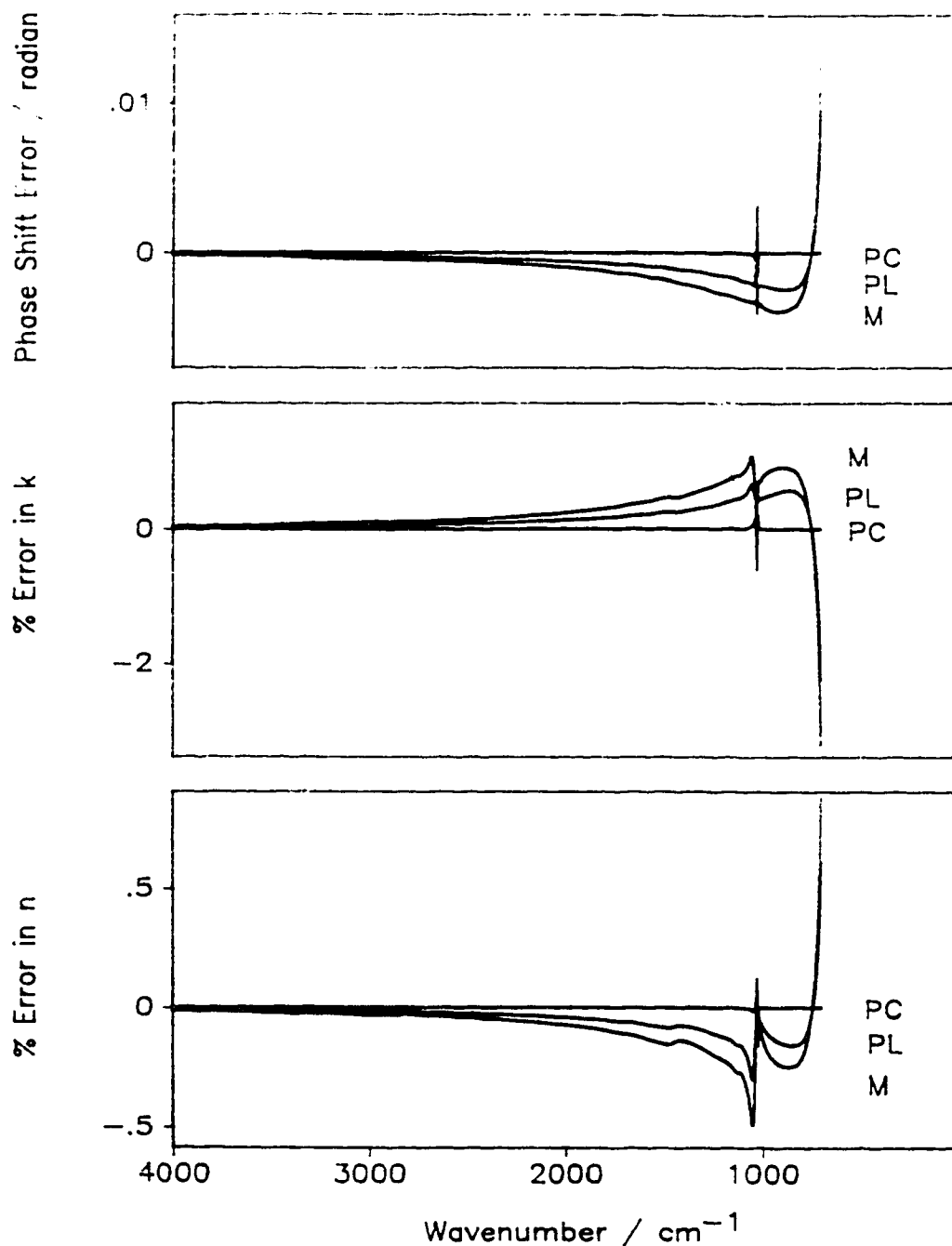


Figure 4.11. The effect of a truncated reflectance spectrum on the recovered phase shift (top), imaginary refractive index (middle) and real refractive index (bottom) spectrum of "methanol" on ZnSe. In each box, Curve M shows the errors or percent errors in the spectrum recovered with Eqs. (4.17) and (4.20), Curve PL shows smaller errors in the spectrum obtained from Curves M by refinement with the linear extension of the k spectrum, and Curve PC shows the very small errors in the spectrum obtained from Curves M by refinement with the exact extension of the k spectrum.

and k spectra, as described above, by a modification of Huang and Urban's iterative refinement.

In Huang and Urban's refinement⁴, the k_1 spectrum is used to calculate the n_1 spectrum via the normal KK transformation of k to n ¹⁵, and these k and n spectra are used to calculate the phase spectrum, θ_1 . This phase spectrum and the experimental R spectrum are used to calculate a second k spectrum, k_2 , which yields a second n spectrum, n_2 , via the KK transform. At this stage the error test is done, but Huang and Urban's test is unclear in their paper⁴. In our implementation of their method, the error test is to calculate the pATR spectrum from the k_2 and n_2 spectra and compare it with the experimental spectrum. The calculation is stopped if the root-mean-squared-percent-deviation and the sum of squared deviations have reduced to their pre-set limits. If the limits have not been reached a second phase spectrum, θ_2 , is calculated from the k_2 and n_2 spectra, and the " θ plus R to k to n to pATR" cycle is repeated until the limits are reached.

The modification of Huang and Urban's procedure is to minimize the truncation error by extending the k spectrum to 0 cm^{-1} in one of several ways before it is used to calculate the n spectrum by the KK transform. The simplest extension has to be used when there is absolutely no knowledge of the missing part of the k spectrum, and consists of the linear extrapolation of the value of k from its value at the lowest wavenumber to zero at 0 cm^{-1} . The converged results from use of this extension are included in Fig. 4.11 as curves PL. The best extension consists of the correct k

spectrum when this is known from other sources. The converged results of using this extension are curves PC in Fig. 4.11. The errors in curves PC are essentially zero, except for $\pm 1\%$ at the strong sharp CO stretching band near 1000 cm^{-1} . Intermediate, and quite helpful, extensions are qualitative estimates of the missing k spectrum when the absorption spectrum is qualitatively known to low wavenumber of the ATR spectrum.

Such procedures have been included in a FORTRAN program PKREF that accepts the pATR spectrum from the CIRCLE cell and the phase shift spectrum calculated by MREPH3, i.e., by Eqs. (4.17) and (4.20), calculates the real and imaginary refractive index spectra from the reflectance and phase shift, and then refines the n and k spectra by Urban and Huang's iterative procedure modified to include extension of the k spectrum.

4.4 Conclusion

A simple procedure has been presented for the calculation of the infrared real and imaginary refractive index spectra from s-polarized ATR spectra by a modified Kramers-Kronig transform of the reflectance to the phase shift on reflection. The new procedure consists of two parts, first a new modified Kramers-Kronig transform and second, a new correction to the phase shift. The procedure has been applied to spectra recorded at 45° incidence for m reflections with equal intensities of s- and p- polarized light and retention of polarization between reflections. Such spectra are recorded in a CIRCLE cell, and yield the R_s spectrum through a simple equation.

The procedure has been applied to the previously studied^{1,3,14}, but unreal, case of constant refractive index of the incident medium n_o . To allow for the fact that the transforms are finite, not infinite, the phase shift at each wavenumber was corrected by a constant which ensured that the correct phase shift was given at the highest wavenumber in the transform, 7800 or 8000 cm^{-1} . In this case of constant n_o , the new transform gave better results than either of two previously studied procedures^{1,3}. It also indicated that the normal KK transform is inferior for this purpose to the new modified KK transform and also to a previous modified KK transform¹. The new modified KK transform has only the usual singularity of a KK transform and this makes it numerically superior to the previous modified transform¹ which has an additional singularity at 0 cm^{-1} . A previous study³ has reported the reverse, namely that the normal KK transform is superior to the previous modified KK transform, and this is believed to arise from their use³ of a double Fourier transform method to calculate the modified KK transform.

For the real case, in which n_o , the refractive index of the incident medium, i.e., the ATR element, changes with wavenumber throughout the infrared, the new transform was used with a new simple wavenumber dependent additive correction to the phase shift. The new correction is initially determined at the highest wavenumber in the transform, 7800 or 8000 cm^{-1} , but the use of the actual value of $n_o(\tilde{\nu})$ at each wavenumber yields the wavenumber dependent correction. It is shown that for molecular liquids such as methanol and benzene the new transform is superior to the previous two transforms. Further, with the new wavenumber dependent correction to

the phase shift, the new transform yields real and imaginary refractive index values that are accurate to better than 0.1%, provided the reflection spectrum is known down to 2 cm^{-1} . This is rarely the case, and the effect of the omission of low wavenumber bands is illustrated. A method to reduce the impact of missing low-wavenumber parts of the reflectance spectrum is described, and its effectiveness is illustrated.

4.5 Appendix

4.5.1 Conditions for the KK Transform

Consider the complex function \hat{f} of a complex variable $\hat{\nu}$, $\hat{f}(\hat{\nu}) = f_R(\hat{\nu}) + i f_I(\hat{\nu})$, where f_R is the real part and f_I is the imaginary part of \hat{f} . The complex variable $\hat{\nu}$ is defined as $\hat{\nu} = \nu_R + i \nu_I$. Then, the KK transform holds for $\hat{f}(\hat{\nu})$ if the function has the following properties^{3,11,12}.

- 1) The poles of $\hat{f}(\hat{\nu})$ are all below the real axis in the complex plane of $\hat{\nu}$.
- 2) The integral of $\hat{f}(\hat{\nu})/\hat{\nu}$ vanishes when taken around an infinite semicircle in the upper half of the complex $\hat{\nu}$ plane. It suffices that $\hat{f}(\hat{\nu})$ tends to zero as the modulus of ν tends to infinity;
- 3) $f_R(\nu)$ is even and $f_I(\nu)$ is odd with respect to ν_R .

Under these conditions, the Kramers-Kronig transforms are:

$$f_R(\nu_a) = \frac{2}{\pi} \text{P} \int_0^\infty \frac{\nu f_I(\nu)}{\nu^2 - \nu_a^2} d\nu \quad (\text{A4.1})$$

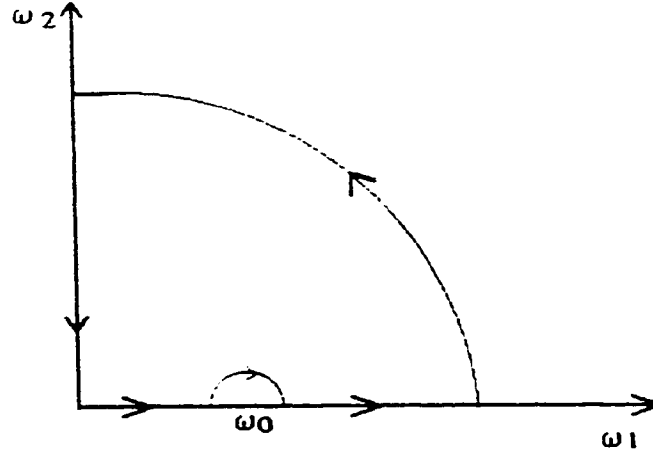


Figure 4.12. The integral contour on the complex frequency plane

$$f_l(\nu_a) = \frac{-2\nu_a}{\pi} \text{P} \int_0^{\infty} \frac{f_R(\nu)}{\nu^2 - \nu_a^2} d\nu \quad (\text{A4.2})$$

4.5.2 Derivation of a New Modified Kramers-Kronig Transform between the Reflectance and the Phase Shift on Reflection.

On the complex frequency plane Cauchy's theorem insures that the integral

$$\int_C \frac{\hat{\omega} \ln \hat{r}(\hat{\omega}) d\hat{\omega}}{\hat{\omega}^2 - \omega_o^2} = 0 \quad (\text{A4.3})$$

where the contour C is shown in Fig. 4.12, $\hat{\omega} = \omega_1 + i\omega_2$ is complex frequency and coefficient of reflection \hat{r} is defined by Eq. (4.9a) and can be described by Fresnel's equation (4.4).

We let the radius of the large circle go to infinity and the radius of the small semicircle about ω_o go to zero, Eq. (A4.3) can be written as

$$P \int_0^{\infty} \frac{\omega_1 \ln \hat{r}(\omega_1) d\omega_1}{(\omega_1^2 - \omega_0^2)} - \frac{i\pi \ln \hat{r}(\omega_0)}{2} - \frac{\pi\theta_{\infty}}{2} + \int_{\infty}^0 \frac{(i\omega_2) \ln \hat{r}(i\omega_2) d(i\omega_2)}{\omega_2^2 - \omega_0^2} = 0 \quad (\text{A4.4})$$

The first term is the integral along the real axis. The second and third terms are the limits of the integrals along the small and large semicircles, respectively. The last integral (real part) in Eq. (A4.4) is easy to evaluate if we note that along the imaginary axis, the magnitude of reflectivity is constant

$|\hat{r}(i\omega_2)| = 1$ because $n(i\omega_2)$ and constant n_0 are always real and the total internal reflection condition is satisfied. We now take the real terms in Eq. (A4.4) and reorganize them

$$\theta(\omega_0) = \theta_{\infty} - \frac{2}{\pi} P \int_0^{\infty} \frac{\omega_1 \ln |r(\omega_1)| d\omega_1}{\omega_1^2 - \omega_0^2} \quad (\text{A4.5})$$

or write it as

$$\theta(\tilde{\nu}_s) = \theta_{\infty} - \frac{2}{\pi} P \int_0^{\infty} \frac{\tilde{\nu}_1 \ln |R(\tilde{\nu}_1)|^{1/2} d\tilde{\nu}_1}{\tilde{\nu}_1^2 - \tilde{\nu}_s^2} \quad (\text{A4.6})$$

For p-polarized light the same relation as (A4.6) can be derived by the same procedure.

4.6 References

1. J. S. Plaskett and P. N. Schatz. J. Chem. Phys. **38**, 612 (1963)
2. A. E. Tshmel and V. I. Vettegren. Spectrochimica Acta **20A**, 1681 (1973)
3. J. A. Bardwell and M. J. Dignam. J. Chem. Phys. **83**, 5468 (1985)
4. J. B. Huang and M. W. Urban. Appl. Spectrosc. **46**, 1666 (1992)
5. J. E. Bertie and H. H. Eysel. Appl. Spectrosc. **39**, 392 (1985)

6. J. E. Bertie, S. L. Zhang and Rizwan Manji. *Appl. Spectrosc.* **46**, 1660 (1992)
7. J. E. Bertie, S. L. Zhang and C. D. Keele. *J. Mol. Struct.* **324**, 157 (1994)
8. J. E. Bertie, S. L. Zhang and C. D. Keele. *Vibrational Spectrosc.* **9**, 215 (1995)
9. J. S. Toll. *Phys. Rev.* **104**, 1769 (1956)
10. C. Kittell. *Introduction to Solid State Physics*. 5th. Edition. J. Wiley and Sons, New York (1976).
11. T. S. Robinson. *Proc. Phys. Soc. (London)* **B65**, 910 (1952)
12. T. S. Robinson and W. C. Price. *Proc. Phys. Soc. (London)* **B66**, 969 (1953)
13. M. J. Dignam. *Applied Spectroscopy Reviews* **24**, 99 (1988)
14. K. Yamamoto, A. Masui and H. Ishida. *Appl. Opt.* **33**, 6285 (1994)
15. J. E. Bertie and S. L. Zhang. *Can. J. Chem.* **70**, 520 (1992)
16. J. E. Bertie and Z. Lan. *J. Chem. Phys.* **103**, ??? (1995)
17. G. R. Fowles. *Introduction to Modern Optics* (Holt Rinehart, Winston, New York, 1975)
18. C. D. Satzberg and J. J. Villa. *Journal of Optical Society of America* **47**, 244 (1957)
19. E.V. Loewenstein, D. R. Smith and R. L. Morgan. *Appl. Optics*; **12**, 398 (1973)
20. D. F. Edwards and E. Ochoa. *Appl. Optics* **19**, 4130 (1980)
21. W. J. Wolfe and G. J. Zissis. *The Infrared Handbook*; page 7-65; (1978)

Chapter 5 **Infrared Intensities of Liquids XX: The intensity of the OH stretching band of liquid water revisited, and the best current values of the optical constants of $\text{H}_2\text{O}(\ell)$ at 25°C between 15,000 and 1 cm^{-1}**

5.1 Introduction

In 1989 optical constants of $\text{H}_2\text{O}(\ell)$ at 22°C¹ were reported, based on calibrated multiple ATR measurements in this laboratory. The reported values of the real, n , and imaginary, k , refractive indices of H_2O covered the range 9000 to 1250 cm^{-1} , although above 5300 cm^{-1} the reported k values were all zero, meaning ≤ 0.0003 . The precision of the k values was reported to be “within $\pm 1\%$ of the value below 3300 cm^{-1} , $\pm 3.5\%$ at the peak of the OH stretching band, which is notoriously non-reproducible^{2,3}, and $\sim \pm 5$ -10% for k values between 0.002 and 0.009 in the region above 3700 cm^{-1} ”. It was also noted¹ that k values less than 0.001 were only determined qualitatively.

The non-reproducibility of the OH stretching band was much greater than that observed for other liquids, with methanol⁴ being of particular relevance. This non-reproducibility of the k values had been observed and discussed previously^{2,3,5,6}. Differences of up to 30% have been reported since 1960 (Ref. 3 and citations therein) and differences of up to 8% since 1969 (ref. 1-3, 5-7 and citations therein). Zolotarev and Demin³ have attempted to correlate the differences with the method of measurement used, whether transmission, specular reflection from an air-water interface, or attenuated total reflection (ATR), and have concluded that the three methods yield the same results.

To seek the origin of this non-reproducibility, a further study was made⁸ in 1989 of the effect of impurities, and of dissolved N₂, O₂, Ar, and CO₂ gases, in the water. The result of this study was summarized⁸ as “There is no effect greater than $\pm 1.5\%$ of either the gas content or the water purity on the intensity of the OH stretching band of water”. Here “water” means water with purity ranging from that of Edmonton drinking water to that of water triply distilled from permanganate or deionized water from a Millipore Super-Q system⁸.

Since ~~that~~ time several developments in this laboratory have made it desirable to report additional findings about the optical constants and the integrated area under the OH stretching band of liquid water. First, the experimental methods have been improved. Second, the accuracy of the computation of optical constants from ATR spectra has been improved⁹. Third, several good sets of measurements by different workers now exist in this laboratory, because water is the natural sample to use while learning the technique. Fourth, as part of a study of acetonitrile-water mixtures last year, the current authors measured k values for the OH stretching band that were 5% lower than those measured as part of a study of methanol-water mixtures three years ago. It was clearly necessary to resolve the difficulty, and this has been achieved. The results obtained, and the best current values of the optical constants of the OH stretching band of water are reported in this paper.

There have been four other significant studies of the optical constants of water since 1990. Marechal¹⁰ has determined the dielectric constant spectra of liquid H₂O, D₂O, and their mixtures, at temperatures between -5 and +80°C from ATR spectra

between 5000 and 750 cm^{-1} . Marechal presented an extensive analysis of his spectra, but reported no numerical optical or dielectric constants.

Kou, Labrie and Chylek¹¹ have determined the optical constants of H_2O at 22°C from transmission measurements between 4000 and 15000 cm^{-1} at 16 cm^{-1} resolution. They also reported values for water at -8 °C and ice at -25°C, which will not be discussed further. They used long-path transmission cells because the absorption is very weak in this region, and compared their results with those reported previously by Palmer and Williams¹², Downing and Williams⁶, and Hale and Querry¹³. Good agreement was reported with the results of Palmer and Williams, who also used transmission measurements with long-path cells. It should be noted that Downing and Williams⁶ reported the values of Palmer and Williams¹² above $\sim 3850 \text{ cm}^{-1}$ and those of Robertson and Williams¹⁴ for those regions between 3850 and 1700 cm^{-1} where the absorption is weak.

Marley, Gaffney and Cunningham¹⁵ used a combination of calibrated ATR measurements and transmission measurements to re-examine the weak absorption between 3300 cm^{-1} and 934 cm^{-1} . They reported the Lambert absorption coefficients, from which the k values can be obtained. It is of particular note that these workers have found much smaller values of k near 2500 cm^{-1} than any previous worker, in particular, much smaller than those of Robertson and Williams¹⁴, who also used transmission cells with long path lengths.

Zelmann¹⁶ measured the transmission spectrum of $\text{H}_2\text{O}(\ell)$ at temperatures between -5.6 and +81.4 °C over the wavenumber range 450-25 cm^{-1} . He used a cell

with thick silicon windows, and used $\sim 2 \text{ cm}^{-1}$ resolution which is sufficiently low to average over the interference fringes from multiple reflections within the windows. As is done in this laboratory¹⁷, he used the methods of Jones et al¹⁸ to compute the optical constants from the transmission spectra. In order to compute the real refractive index by Kramers-Kronig transformation, and to fit his k spectrum with four Gaussian bands, he added values reported by Afsar and Hasted¹⁹ to the low-wavenumber end of his measurements and those of Draeger, Stone, Curnutte and Williams²⁰ to extend the high-wavenumber end to $\sim 987 \text{ cm}^{-1}$. He tabulated values of k and n between 20 and 600 cm^{-1} . Unfortunately, the tabulated k values are the fitted values not the experimental ones.

Water is such a fundamentally important liquid that it is desirable to present the best results obtained in this laboratory over a period of ten years. This importance is illustrated by the fact that much of the recent interest in its infrared optical constants has been stimulated by the need for accurate calculation of radiative energy balances through the atmosphere. Accordingly, this paper contains a brief account of our recent ATR measurements and conclusions with respect to the OH stretching band. It also contains an evaluation of the literature values of the real and imaginary refractive indices of water between 15000 and 1 cm^{-1} , and presents the values that are believed to be currently the most reliable. As part of the evaluation process, we have used transmission methods to re-measure the weak absorption between 4000 and 3700 cm^{-1} , as well as that between 3300 and 1700 cm^{-1} where we sought to test the very small k values reported by Marley et al¹⁵.

5.2 Methods and Results

The experimental and computational methods have been described in detail^{1, 4,7,9,21}.

5.2.1 Experimental and Computational Improvements

The most important improvement in the experimental method over that used previously for water^{1,8} is that a shorter sample holder was used. The ~6 mm sample holder used previously yields a pATR value close to 2 at the peak of the OH stretching band. Peak pATR values near 1 are less sensitive to noise and instability, and are now obtained in a 3mm sample holder.

The most important improvement in the computational methods⁹ over those⁷ used in the previous work on water^{1,8} lies in the calculation of the optical constants from the ATR spectrum by an iterative procedure. Part of this procedure^{7,9,21} is to calculate an estimate of the k spectrum from the ATR spectrum and then to Kramers-Kronig transform the k spectrum to obtain the n spectrum. Ideally, the KK transform requires the k spectrum from 0 to infinite wave number. This is never available and, more practically, the KK transform yields an erroneous n spectrum if strong absorption is omitted to low wavenumber of the k spectrum that is available from the ATR spectrum. This is always the case when $\text{H}_2\text{O}(\ell)$ is measured with a ZnSe ATR rod, because the latter only yields a spectrum above 700 cm^{-1} and the intense band due to rotational vibrations in water lies largely below 700 cm^{-1} . To overcome this difficulty it is now possible to extend the k spectrum from ATR, solely for the purpose of the KK transform, by adding the known k spectrum of water below 700 cm^{-1} . Even if the

accuracy of this added k spectrum is uncertain, its addition reduces the error in the n spectrum considerably, and this leads to reduced error in the final k spectrum. During the calculation of the optical constant spectra from ATR spectra in the present work, the k spectrum was always extended for the KK transform by adding the k spectrum of Downing and Williams⁶ between 700 cm^{-1} and 10 cm^{-1} .

A second significant improvement over the computational methods used previously is that the value of n at the high wave number limit of the data is no longer taken to be constant. When, as in the present work, the KK integral includes all of the strong infrared absorption, the value required for the calculation of n at wave number $\tilde{\nu}_a$ is the value the real refractive index would have at $\tilde{\nu}_a$ if it were due solely to electronic polarization.²² A simple dispersion equation that provides this value has been determined for water²² and the appropriate value was used.

5.2.2 Exploration of the Non-Reproducibility of the OH Stretching Band

To explore the non-reproducibility of the OH stretching band of water in our experiments, two factors were studied. First, the sample temperature and second the reproducibility with which the cell was filled with water.

The temperature of the water samples was previously reported as 22°C . In fact, the temperature of the samples when equilibrated with the sample compartment of our Bruker IFS 113V spectrometer is $24.5 \pm 1^\circ\text{C}$, and we now quote 25°C as the sample temperature. The temperature of the sample before it is injected into the cell, which is kept under vacuum *in situ* in the sample compartment, is room temperature, 21 to

22°C. It was thought that the sample temperature may not reliably reach 25°C before the spectra are recorded. This was thought to be a potentially more serious error for water than for other liquids, because the hydrogen bonding is temperature dependent.

To explore this, samples were held at 4°C, 24.5°C or 38°C before use. The initial sample temperature was measured and the sample was immediately injected into the CIRCLE cell (through a 15 cm length of 1.5 mm diameter teflon tubing, 13 cm of which passes through a vacuum). The interferogram collection was started right after the cell was filled, and collection of 64 scans at 4 cm⁻¹ resolution took 1 minute. The resulting k spectra and their areas are not reported in detail because the sample temperature is not well known, but the k value at the peak of the OH stretching band, and the area under the k band between 4000 and 2660 cm⁻¹ was always within 1.9% and 1.5%, respectively, of those for the sample held at 24.5°C. Thus, an initial sample temperature between 20 and 25°C can not influence the peak height and area by more than 1%, and can not be responsible for non-reproducibility of the magnitude observed. This conclusion was confirmed for samples with an initial temperature of 22°C, and is consistent with the measured²³ temperature variation of k . It can be noted that the effect on the molar absorption coefficients and imaginary molar polarizabilities²⁴, is even smaller, because the increase in the molar volume offsets the decrease in the k values with increasing temperature.

The reproducibility with which the CIRCLE cell was filled with water was explored. The inside diameter of the liquid holder is only 1.5 mm larger than outside diameter of the rod, and air bubbles frequently form when the cell is filled with water if

the liquid holder is significantly off center. The remedy, when an air bubble forms regularly in the cell, is to dismantle the cell, clean the rod and polish it with jeweler's rouge and alcohol, and reassemble the cell taking particular care to ensure that the ATR rod and the cylindrical glass liquid holder are coaxial. Once the cell has been assembled correctly, it can be repeatedly re-filled with water without bubble formation, provided that it is dried with alcohol and benzene before it is refilled. When no bubbles were visible, the k values and the area under the OH stretching band were reproducible to ~1%. H. M. Heise and A. Bittner ²⁵ have also identified the formation of bubbles in the cell as an important limitation on the reproducibility of ATR spectra of aqueous solutions.

5.2.3 Recent Spectra with Improved Methods

The improved experimental and computational methods have been used to determine k and n spectra of water at 25°C that are independent of those reported previously¹. Five sets of pATR spectra of water in the short cell obtained in different years by four different workers, were converted to optical constant spectra. In some cases the set was a single pATR spectrum which was the average of several pATR spectra. The average pATR spectrum was transformed in this work to a single pair of n and k spectra. In other cases the set consisted of several pATR spectra, each of which was converted to a pair of n and k spectra and the k spectra were then averaged. Five k spectra resulted from the five sets of pATR spectra, and they were compared to determine the precision of the k values obtained by the ATR method in this laboratory.

The agreement was very good and the five k spectra were averaged, unweighted, to give a single final k spectrum.

The agreement between the k spectra is illustrated by the 95% confidence limits of k_{\max} , the k value at the peak of the OH stretching band, and of the area under the OH stretching band. k_{\max} was 0.312 with a 95% confidence limit of 0.003 and the area under the k spectrum and above zero ordinate between 4000 and 2660 cm^{-1} was 123.7 cm^{-1} with a 95% confidence limit of 0.4 cm^{-1} . For the OH stretching band, the precision of the imaginary refractive index is, thus, 1% and that of the area is 0.33%.

The precision of the other pronounced band, due to $\tilde{\nu}_2$, the HOH bending vibration at 1640 cm^{-1} , was of the same order, 1.7% for the peak height and 0.9% for the area. For the weaker absorption between 2660 and 1890 cm^{-1} the precision is about 6% of the k value. This is significantly worse than was estimated for the spectra previously reported¹, probably partly because of the use of the short cell but mainly because the absorption in this region is too weak to be defined very well by ATR measurements even with the long cell. Transmission measurements through long-path cells should be much superior in this region.

5.2.4 Comparison with Our Previous Spectra

The imaginary refractive index spectrum of water determined with the short ATR cell in this work is plotted in Fig. 5.1 together with the spectra determined with the long cell and reported in 1989^{1,8}. The agreement is generally very good. It is ~2% at the peaks of the three bands above 1200 cm^{-1} , but is only ~20% near 2600 cm^{-1} where k is only 0.003.

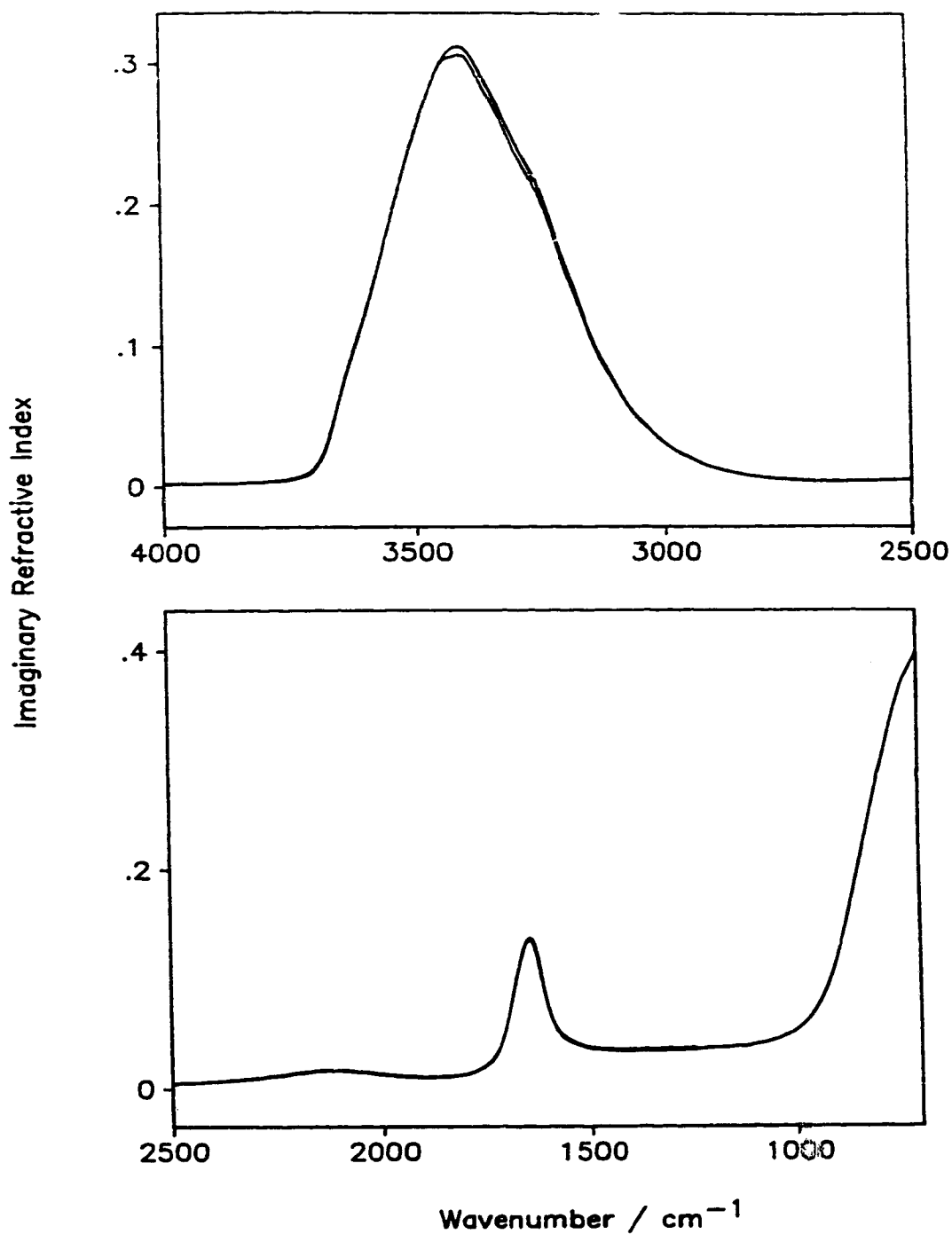


Figure 5.1 Imaginary refractive index spectra of $\text{H}_2\text{O}(\ell)$ at $25 \pm 1^\circ\text{C}$ determined in this laboratory by calibrated multiple attenuated total reflection spectroscopy. Three spectra are shown. Two extend from 4000 to 1250 cm^{-1} and almost coincide. They were reported previously^{1,8} from measurements with the long (6 cm) cell. The spectrum determined in this work with the short (3cm) cell extends from 4000 to 700 cm^{-1} and is the highest curve at the peak of the OH stretching band.

Table 5.1 Peak Height and Integrated Intensity of the OH Stretching Band of H₂O (ℓ) at 25 °C

	<u>Peak Height^a</u>	<u>Area^{a,b}</u>
Imaginary refractive index, k	0.312 (3)	123.7 (4)
Molar Absorption Coefficient, E_m	104.9 (8) ^c	410 (1)
Imaginary Molar polarizability, α_m''	0.787 (5) ^c	
$C_j = \int \tilde{\nu} \alpha_m'' d\tilde{\nu}$		10.20 (3)

^a The number in parentheses is the 95% confidence limit in the last digit.

^b The integration limits are 4000 to 2660 cm⁻¹. The unit is cm⁻¹ for the area under the k spectrum and km mol⁻¹ for the other two areas. The area under E_m is equivalent to 410 x10² L mole⁻¹ cm⁻².

^c The unit of E_m is L mole⁻¹ cm⁻¹. The unit of α_m'' is cm³ mole⁻¹

The new k spectrum is about 2% higher at the OH stretching peak. This is barely significant, but the new spectrum should be the most reliable because the measurements near the peak were less sensitive to noise and instability because the pATR values were near to 1 instead of 2.

For the OH stretching band, the peak heights and areas in the imaginary refractive index and molar absorption coefficient, E_m , spectra are given in Table 5.1, with the peak height in the imaginary molar polarizability^{4,24}, α_m'' , spectrum and the area C_j under the $\tilde{\nu} \alpha_m''$, spectrum.

It should be noted that the integrated intensity of the OH stretching band was previously given as the area under the molar conductivity spectrum, $V_m \int \tilde{\nu} \epsilon'' d\tilde{\nu}$, which was 194 ±4 km mol⁻¹ between 4000 and 2500 cm⁻¹. In order to relate this quantity to the molecular dipole transition moment, one has to use^{1,24} the hypothetical value of the real refractive index that would exist in the region of the band if the band

were not present. This value can not be determined with accuracy²⁴, and for this and other reasons²⁴ the integrated intensity that is the most useful, and is now used in this laboratory, is $C_j = \int \tilde{\nu} \alpha_m'' d\tilde{\nu}$, where the integration is over band j . The value of C_j calculated from the previously reported¹ spectra over the currently used integration range, 4000 to 2660 cm^{-1} , is $10.2 \pm 0.2 \text{ km mol}^{-1}$. The value found in this work is the same, with slightly higher precision, $10.20 \pm 0.03 \text{ km mol}^{-1}$ (Table 5.1).

The intensity of the OH stretching band is not very sensitive to the integration limits used. The value $10.20 \text{ km mol}^{-1}$ for the range 4000 to 2660 cm^{-1} is increased by only 0.3% for the range 4000 to 2500 cm^{-1} and decreased by only 0.4% for the range 3800 to 2700 cm^{-1} .

Based on considerations of our temperature control, precision of calibration, and reproducibility of intensity measurements made with different instruments^{17,26}, we estimate that the uncertainty in the 10.2 km mol^{-1} integrated intensity of the OH stretching band of water is ~2%.

5.2.5 Dipole Moment Derivatives of $\text{H}_2\text{O}(\ell)$

The integrated intensity C_j in km mol^{-1} is multiplied by 1.8686 to convert it^{4,24} to $|\delta\mu/\delta Q_j|^2 = 19.06 (\text{D } \text{\AA}^{-1} \text{ amu}^{-1/2})^2$, 1.5% smaller than reported previously. From the previous analysis, this yields $|\delta\mu/\delta R| = 3.00 \text{ D } \text{\AA}^{-1}$, the same as the value 3.02 ± 0.03 reported previously¹. Here $\delta\mu/\delta Q_j$ is the derivative of the molecular dipole moment with respect to the normal coordinate and $|\delta\mu/\delta R|$ is the derivative of the bond

dipole moment with respect to the OH stretching internal coordinate and is assumed to point along the bond.

Thus, the previous discussion¹ of the dipole moment derivative with respect to OH bond displacement requires no change. It is clear from Fig. 5.1 that the previous discussion¹ for the HOH bending vibration also remains valid.

5.3 The Best Current Refractive Index Spectra of Water at 25°C

The imaginary refractive index values of $\text{H}_2\text{O}(\ell)$ at 25°C reported in the literature are evaluated region by region in this section. The values believed to be the most reliable have been assembled into a single k spectrum which is recommended for use. The likely errors in the values reported in the following sections are intentionally conservative. They indicate the probable maximum percent differences between the values recommended and the correct values. They are, of course, considerably larger than the reproducibility with which the values can be measured in one laboratory.

5.3.1 The Region 15000 to 4000 cm^{-1}

The k values of Kou, Labrie and Chylek¹¹ are recommended for this region. The error in the values is unlikely to exceed 4% below 13,500 cm^{-1} or 20% above 13,500 cm^{-1} .

Numerical data has been tabulated for this region by Hale and Querry¹³ for 25°C, Palmer and Williams¹² for 27°C and Kou, Labrie and Chylek¹¹ for 22°C. Below 5000 cm^{-1} , Downing and Williams⁶ also tabulated Palmer and Williams' values, and

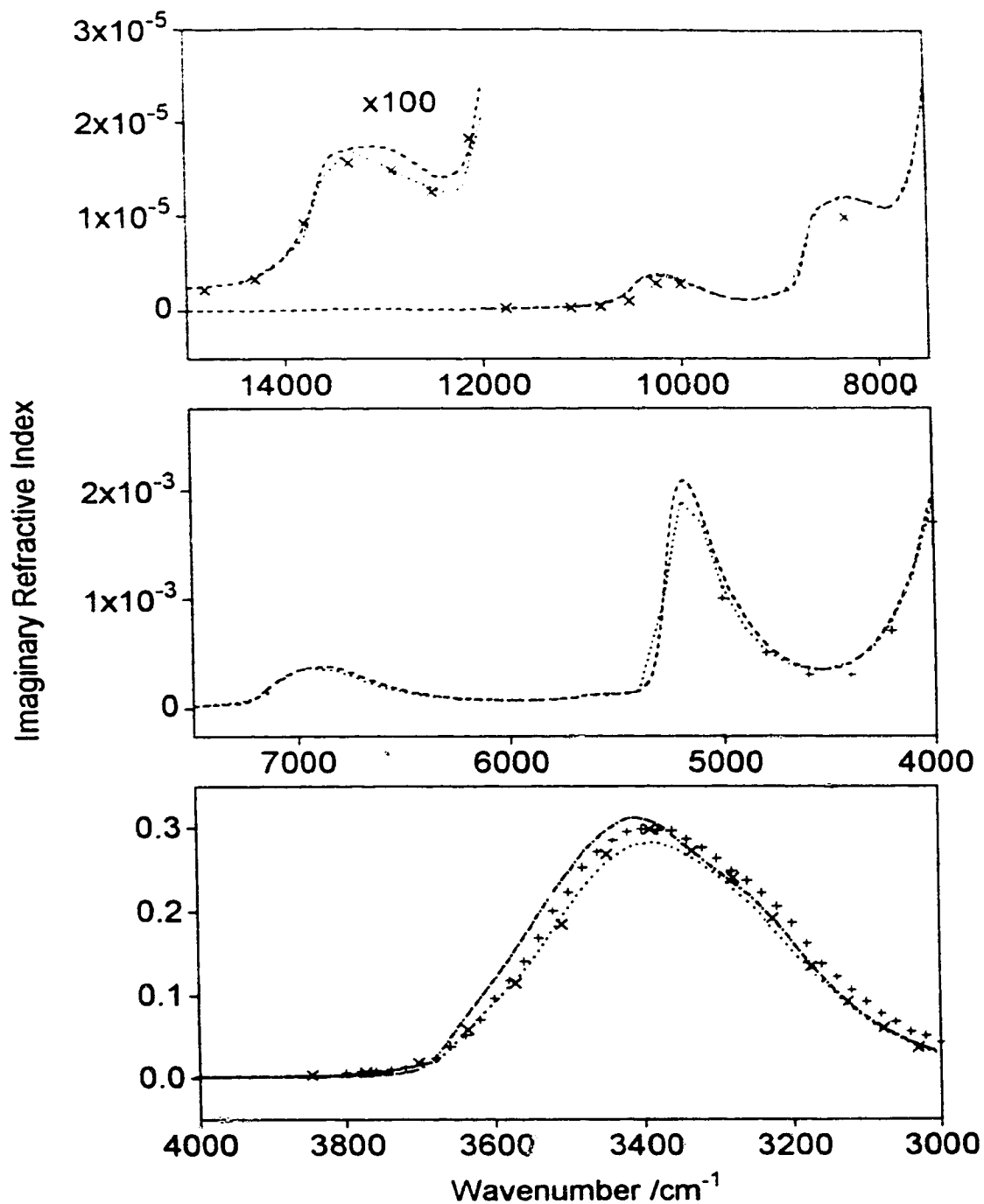


Figure 5.2. Imaginary refractive index spectra of $\text{H}_2\text{O}(\ell)$ between 15,000 and 3000 cm^{-1} determined by different workers. Top two boxes: Dashed line, Kou et al.¹¹ (22 °C); dotted line, Palmer and Williams¹² (27 °C); crosses x, Hale and Querry¹³ (25 °C); plus sign +, Zolotarev and Demin³ (25 °C). Bottom box, as in the other boxes except without Kou et al's spectrum and with: dotted line, Downing and Williams⁶ (27 °C) instead of Palmer and Williams; dash-dotted line, this work by ATR (25 °C).

values interpolated between them. The tabulated values are compared in the top two boxes of Fig. 5.2.

Hale and Querry analysed the literature to the early 1970s, and tabulated the optical constants at large wavelength intervals, as shown by the crosses, x, in Fig. 5.2. Palmer and Williams measured the spectrum by transmission through long path cells, and tabulated values at 100 cm^{-1} intervals. Their spectrum is shown by the dotted line in Fig. 5.2. Their values agreed fairly well with those of Hale and Querry, although distinct differences exist. Kou et al have summarised this earlier literature in their paper¹¹, which presents the most recent study. Kou et al¹¹ used a Fourier transform spectrometer. For the weakest absorption they used cells with path lengths up to 20 cm, significantly longer than the $\leq 5\text{ cm}$ paths used by Palmer and Williams in their study with a dispersive spectrometer. Both Palmer and Williams¹² and Kou et al¹¹ removed the loss of light due to reflection at the window surfaces appropriately. Neither group considered the multiple reflection in the liquid layer between the windows, but this can be ignored safely in cells with long pathlengths. The use by Kou et al of a Fourier transform spectrometer enhances the value of their work, because well aligned FT spectrometers have been shown to be reproducible between laboratories and manufacturers to about 3% with a liquid cell in the beam^{17,26}. Kou et al's k values agree with those of Palmer and Williams to better than 5% between 4000 and $14,500\text{ cm}^{-1}$, except in two regions. Their values are $\sim 10\%$ higher near the 5200 cm^{-1} peak and near 12750 cm^{-1} . In the latter region, the longer paths used by Kou et al were an improvement and the k values of Kou et al¹¹ are considered the most reliable.

Kou et al reported the percent error of their measurements based on the uncertainty in the path lengths and the standard deviation of their data¹¹. The maximum probable error reported above is approximately twice this reported percent error of their measurements.

The existing data give no useful information about the effect of temperature differences between 15 and 35 °C on the absorption intensities of H₂O(*ℓ*).

5.3.2 The Region 4000 to 3715 cm⁻¹

The *k* values obtained by transmission spectroscopy in this work are recommended for this region of weak absorption. The error in the values is unlikely to exceed 5% above 3850 cm⁻¹ and 30% between 3850 and 3720 cm⁻¹.

In the first report on H₂O(*ℓ*) from this laboratory¹, the imaginary refractive indices reported by Downing and Williams⁶ for 21 °C and by Zolotarev and Demin³ for 25°C were considered to be the best in the literature. Those reported by Williams and his coworkers were much preferred because they were more consistent over time than those from Zolotarev and his colleagues¹. The values reported by Downing and Williams are those of Palmer and Williams¹² above 3800 cm⁻¹ and those of Robertson and Williams¹⁴ below 3800 cm⁻¹, both obtained from transmission measurements through thick films and both interpolated to 10 cm⁻¹ intervals. These spectra are shown in the bottom box of Fig. 5.2 with those obtained from the current ATR study in this laboratory. Hale and Querry's values¹³ (25 °C) are included in the figure. It can be seen that below ~3800 cm⁻¹ the earlier workers^{6,3,13} all obtained values about twice as

large as those from our ATR work. Downing and Williams saw a plateau or shoulder between ~ 3850 and 3720 cm^{-1} .

The absorption in this region is weak, and the best intensities should come from transmission measurements through fairly thick liquid films. Transmission measurements were therefore made in this laboratory in order to explore the differences between Downing and Williams's values and our values from ATR.

The transmission methods have been described¹⁷. Cells with CaF_2 windows were used with path lengths of 150, 125, 115, 100 and $85\text{ }\mu\text{m}$. The anchor points¹⁷ are at 4501 and 3727.7 cm^{-1} , where the linear absorption coefficients are $9.29 \pm 0.3\text{ cm}^{-1}$ and $130.9 \pm 0.7\text{ cm}^{-1}$, respectively. The k values obtained agree with our values from ATR near 3715 cm^{-1} , where Downing and Williams' values are about 70% larger, and agree with Downing and Williams' values within 3% above 3850 cm^{-1} and within 1% above 3900 cm^{-1} , where our values from ATR are about 30% lower. The difference between our transmission results and our ATR results is unusually large, much better agreement having been obtained for, *inter alia*, the isotopomers of methanol^{4,27}.

Accordingly, the k values from our transmission measurements are recommended. They connect extremely well at 4000 cm^{-1} to the spectrum of Kou et al¹¹. The large possible error cited above for the lower part of the range reflects the large disagreement with both the values from our ATR spectra and the values of Downing and Williams.

5.3.3 The Region 3715 to 2982 cm^{-1}

The k values determined by ATR measurements of $\text{H}_2\text{O}(\ell)$ at 25 °C in this work are recommended for this region. The error in these values is unlikely to exceed 4 %.

The region is shown in the bottom box of Fig. 5.2. For reasons discussed previously¹ the values obtained from calibrated ATR measurements in this laboratory are preferred to the values in the literature. Our 1989^{1,8} and 1995 spectra are compared in Fig. 5.1 and have been discussed above. Our 1995 spectrum is included in the bottom box of Fig. 5.2, and is the preferred spectrum in this region.

Two features are evident in the Figure and deserve comment. As noted previously¹, Zolotarev and Demin's spectrum³ agrees quite well with ours in intensity, to about 5% with our new spectrum, but is shifted markedly to low wavenumber. The spectrum of Downing and Williams⁶ is significantly less intense than ours, and has a different shape. Thus, while the low-wavenumber end of their band coincides with ours, their peak is at a lower wavenumber and the high wavenumber side of their band is to low wavenumber of even that of Zolotarev and Demin. These differences are undoubtedly due to the instrumental and computational limitations of the early 1970s. Thus, the OH stretching band reported by Downing and Williams spectrum is strongly influenced by that of Rusk, Williams and Querry², which was calculated from a normal incidence reflection spectrum. The percent reflection is less than 5% throughout, and was very difficult to measure well with the dispersive instruments available in the early 1970s. Thus, their reflection spectrum was noisy and gave a noisy real refractive index spectrum as the primary result. Their k spectrum was calculated from the noisy n

spectrum by Kramers-Kronig transformation. The accuracy claimed was of the order of 10%, which is roughly consistent with the agreement with our new spectrum. The agreement that is observed is a tribute to the work of Williams and his colleagues.

5.3.4 The Region 2982 to 2800 cm^{-1}

The average of the k spectra from Downing and Williams⁶ and from the ATR measurements of this work is recommended for this region. The error in the values is unlikely to exceed 10%.

This short region is shown in the top box of Fig. 5.3. The absorption intensity is moderate, so both transmission and ATR methods can give good results. All spectra agree well except those of Zolotarev and Demin³ and of Marley, Gaffney and Cunningham¹⁵. Our transmission measurements between 2867 and 2800 cm^{-1} gave k values 6% below those of Downing and Williams⁶ and 4% above those from our ATR measurements. Thus the average of the latter two spectra is used.

5.3.5 The Region 2800 to 2320 cm^{-1}

The k values of Downing and Williams⁶ are recommended for this region. The error in the values is unlikely to exceed 6%.

The region contains only weak absorption, as shown in the top box of Fig. 5.3. Marley, Gaffney and Cunningham¹⁵ (lower dashed curve) have recently reported k values about a factor of ten lower than those of all previous workers (Fig. 5.3, top box). Transmission measurements were undertaken in this laboratory to see if Marley et al are correct. Cells with CaF_2 windows were used with path lengths of 125, 115, 100 and 85 μm . The anchor points are at 2630 and 1885 cm^{-1} , where the linear

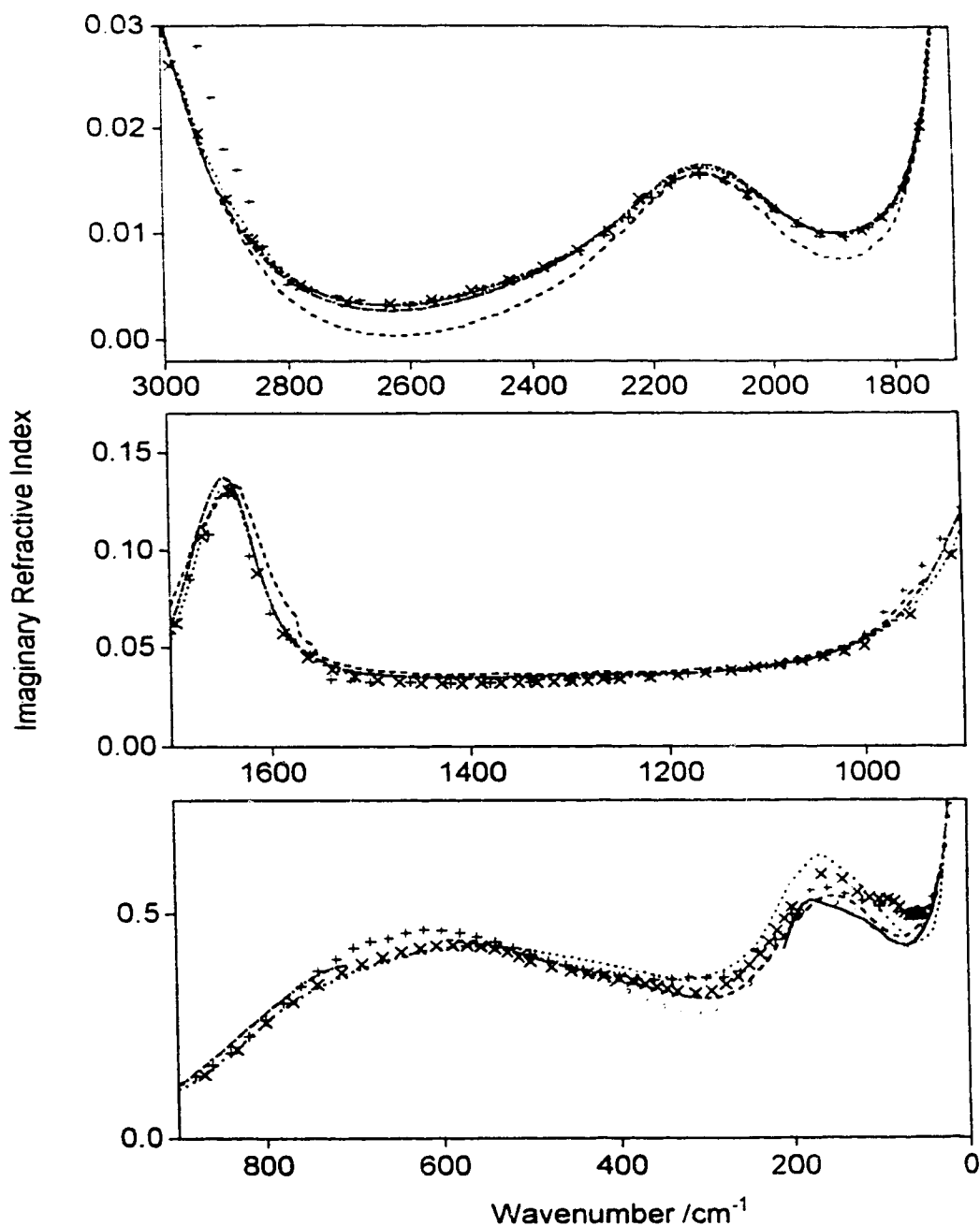


Figure 5.3. Imaginary refractive index spectra of $\text{H}_2\text{O}(\ell)$ between 3000 and 0 cm^{-1} determined by different workers. Top box: Dotted line, Downing and Williams⁶ (27 °C); Crosses x, Hale and Query¹³ (25 °C); Plus sign +, Zolotarev and Demin³ (25 °C); Dash-dotted line, this work by ATR (25 °C); upper dashed line, This work by transmission (25°C); Lower dashed line, Marley, Gaffney and Cunningham¹⁵ (no temperature given). Middle box: As top box except without this work by transmission. Bottom box: As in middle box except without Marley, Gaffney and Cunningham and with: dashed line, Zelsmann¹⁶ (25°C); Open circle o, Afsar and Hasted¹⁹ (19 °C); Solid line, Afsar and Hasted²⁷ (25 °C).

absorption coefficients are $48.6 \pm 0.3 \text{ cm}^{-1}$ and $103.8 \pm 0.4 \text{ cm}^{-1}$, respectively. The anchor point measurements used path lengths up to $325 \text{ }\mu\text{m}$. Our results agree with those of the previous workers, not with those of Marley et al. In fact our transmission measurements agree with those of Downing and Williams to within 4% in this region.

5.3.6 The Region 2320 to 713 cm^{-1}

The k values from our new ATR measurements are recommended in this region. The error in their values is unlikely to exceed 5% above, and 10% below, 1000 cm^{-1} .

This region is shown in Fig. 5.3. Again, the absorption is moderate and both ATR and transmission measurements should be reliable. The k values from the ATR measurements in this work agree with those of Downing and Williams⁶ within 2% for most of this region, except near the 1640 cm^{-1} peak where our measurements should be better. Accordingly, the k values from these ATR measurements are used throughout the region. Our spectrum is higher than that of all workers except Zolotarev and Demin³ below $\sim 1000 \text{ cm}^{-1}$, but was reproducible and is considered reliable. To illustrate this, the greatest difference occurs near 812 cm^{-1} , where our many ATR spectra gave $k = 0.262$ with a maximum deviation of 0.005, while the values of Downing and Williams and Zolotarev are 10% smaller, 0.237 and 0.240, respectively. A final test of our k values from ATR was made at the end of this study. The calculation of the k spectrum from the pATR spectrum was redone by extending the k spectrum for the KK transform by adding the final recommended k spectrum below 700 cm^{-1} instead of adding Downing and Williams' k spectrum (vide infra). The resulting k value at 700

cm^{-1} was higher by 2%, but the difference decreased rapidly with increasing wavenumber and was already virtually zero at 710 cm^{-1} .

5.3.7 The Region 713 to 590 cm^{-1}

The average of the k values reported by Downing and Williams⁶ and by Zolotarev and Demin³ are recommended in this region. These are the most recent sets of measurements in this region and there is no way to judge between them. The maximum deviation from the average is $\sim 7\%$, and the error in the k values is unlikely to exceed this.

5.3.8 The Region 590 to 30 cm^{-1}

A k spectrum based on those reported by Zelsmann¹⁶ is recommended in this region. He reported k spectra at 20.2 and 38.7°C from which a spectrum at 25°C was calculated as described below. The error in the k values is unlikely to exceed 12%

The several spectra reported for this region are shown in the bottom box of Fig. 5.3. They require some explanation.

Zelsmann tabulated his fitted values (See Introduction) at, *inter alia*, 20.2 and 38.7°C . A k spectrum for 25°C was calculated under the assumption that the k values vary linearly with temperature. This spectrum is referred to below as Zelsmann's 25°C spectrum.

Hasted and his colleagues have published three papers relevant to this region^{19, 28, 29}. In 1985 Hasted, Husain, Frescura and Birch²⁹ reported optical constants of $\text{H}_2\text{O}(\ell)$ at 20°C between 4 and 40 cm^{-1} . Although they only reported²⁹ the 20°C values, they said they had obtained values between 4 and 44°C with a new polarizing

interferometer for dispersive FTS studies, and that the results above 15 cm^{-1} agreed with those of Afsar and Hasted¹⁹.

Afsar and Hasted¹⁹ tabulated optical constants of water at 19°C between 6 and 450 cm^{-1} . This is referred to below as A&H's 19°C spectrum.

One year later, Afsar and Hasted²⁸ tabulated optical constants of water at 4°C , 30°C and 57°C in two ranges, namely between 10 and 45 cm^{-1} , measured with a InSb Rollin detector, and between 30 to 220 cm^{-1} , measured with a Golay detector. To obtain data for 25°C , we have interpolated between the 4 and 30°C data, again under the assumption that the imaginary refractive index changes linearly with temperature. These interpolated 25°C spectra are referred to below as A&H's 25°C spectra, and they agree rather well with A&H's 19°C spectrum¹⁹. This is not surprising, because the assumption on which our interpolation was based is unlikely to be valid between 4 and 30°C , but it does mean that the 25°C (interpolated) spectra and the 19°C spectrum are the best that can be obtained from Afsar and Hasted for the present purpose.

Downing and Williams⁶ and Zolotarev and Demin³ have also tabulated optical constants in this region for $\text{H}_2\text{O}(\ell)$ at 27°C and 25°C , respectively.

Zelsmann's 25°C spectrum, Zolotarev's spectrum and A&H's 19°C and 25°C spectra agree within 6% at the peak near 165 cm^{-1} . Downing and Williams' spectrum is about 17% more intense and is not considered further. Downing and Williams estimated their errors to be up to 20%. Zelsmann's spectrum is very nearly the average of the remaining four spectra, so it is convenient to recommend its use even though it is a fitted spectrum¹⁶, not the experimental one. The $\leq 12\%$ probable error in the k values

is slightly larger than the maximum deviation of the remaining spectra from the average.

5.3.9 The Region 30 to 10 cm⁻¹

The average of Zolotarev's spectrum³, A&H's 19°C spectrum¹⁹ and A&H's 25°C spectrum²⁸ is used in this region. Based on the agreement between them, the error in the k values is unlikely to exceed 6%.

5.3.10 The Region 10 to 6 cm⁻¹

In 1987, Hasted, Husain, Frescura and Birch³⁰ published optical constants of H₂O(ℓ) at 10, 20, 30 and 40 °C between 6 and 14 cm⁻¹. They used their new polarizing interferometer and estimated the errors in their values to be no larger than 3%. We have taken the average of the 20 °C and 30 °C values to correspond to 25 °C and recommend these values for this region. The error in the values is unlikely to exceed 5%.

5.3.11 The Region 5 to 1 cm⁻¹

Kaatze and Uhlendorf³¹ have reported the dielectric properties of H₂O(ℓ) at several temperatures including 25°C between 0.5 and 100 GHz, i.e., 0.016 to 3.3 cm⁻¹. They estimated the error in their values to be about 2%. Their data was well described by the Debye relaxation function, and the Debye parameters were reported for each temperature. The values of the imaginary refractive index recommended for this region are those calculated from the dielectric constants calculated from the Debye function for 25°C. The error in the k values is unlikely to exceed 5%.

5.3.12 The Recommended k and n Spectra

The recommended k spectrum was constructed by merging the spectra recommended for the different regions. There were no significant discontinuities to be smoothed. The recommended k spectrum is shown in Fig. 5.4 and is tabulated in Compact Table format³² in Table 5.2. The real refractive index spectrum was calculated by Kramers-Kronig transform of this recommended k spectrum. In the KK transform to calculate the real refractive index at wavenumber $\tilde{\nu}_a$, the value of n_∞ was replaced by $n_{el}(\tilde{\nu}_a)$ calculated from the equation²²

$$n_{el}(\tilde{\nu}_a) = 1.32663 + 2.439 \times 10^{-11} \tilde{\nu}_a^2 + 3.74 \times 10^{-21} \tilde{\nu}_a^4.$$

The recommended n spectrum is shown in Fig. 5.5 and is tabulated in the Compact Table 5.3. The molar absorption coefficient, E_m , spectrum was calculated from the k spectrum as described previously^{4,24}, and is shown in Fig. 5.6 and tabulated in the Compact Table 5.4.

5.4 The Effect of Temperature

For many purposes it is necessary to know the small effect on band positions, shapes and intensities of small changes in temperature near ambient, specifically changes of one or two degrees at temperatures between 20 and 35°C. It has been noted above that the existing data above 4000 cm⁻¹ give no useful information about such effects. The same is essentially true for the mid-infrared region, and for all except the extreme far infrared. Only Williams and his co-workers^{23,33} have specifically studied the effect of temperature on the mid-infrared optical constants of H₂O(ℓ), with

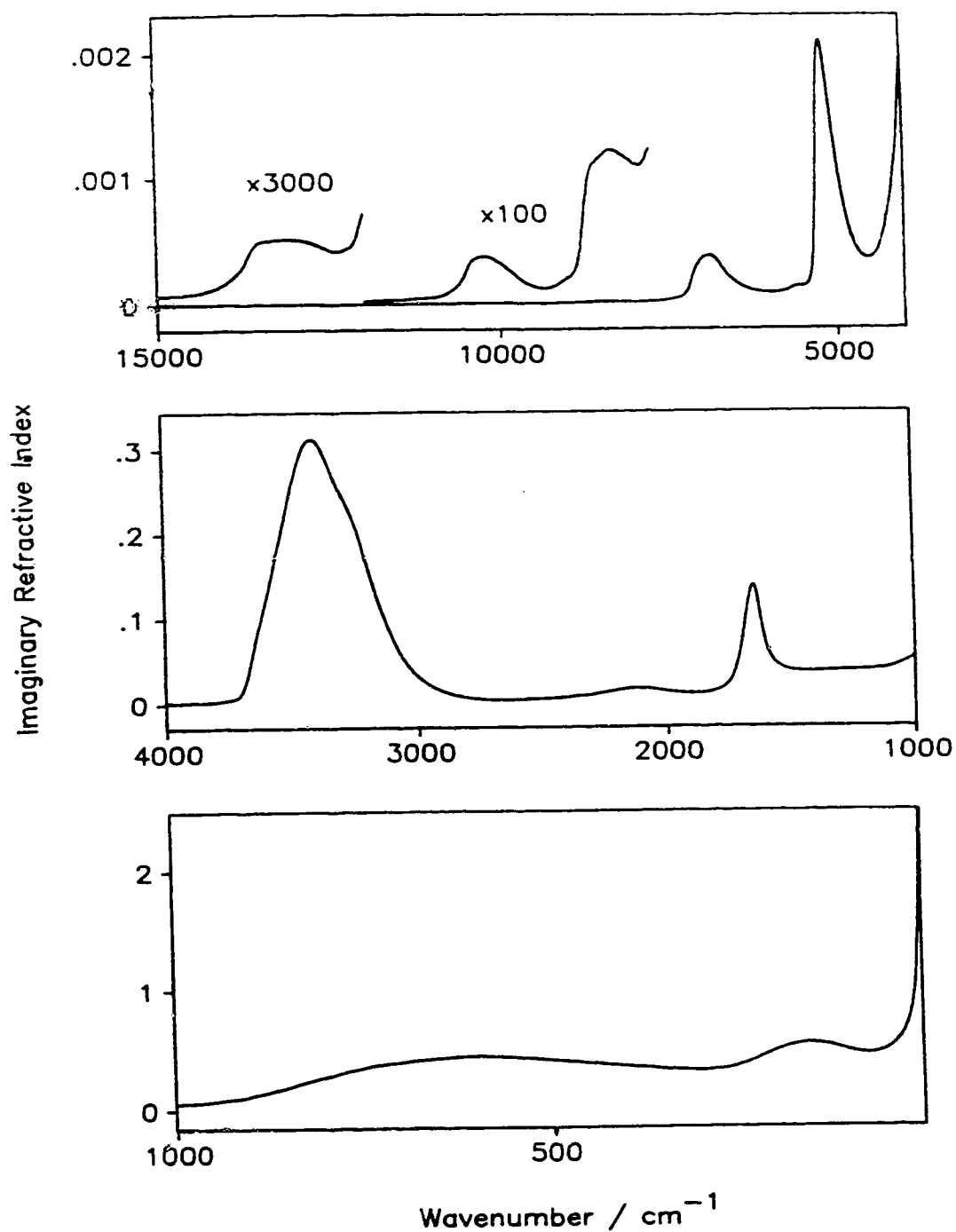


Figure 5.4. The recommended imaginary refractive index spectrum of $\text{H}_2\text{O}(\ell)$ between 15000 and 1 cm^{-1} . For the upper two curves in the top box the ordinate labels must be divided by 100 or 3000 as shown.

Table 5.2. Imaginary refractive indices between 4154.88 and 1 cm^{-1} of liquid water at 25 °C.^{a,b}

cm^{-1}	K_E	I_E	0	1	2	3	4	5	6	7	8	9	10	11	12	13	14	15	16
4154.88	5	-6	1006	1149	1311	1539	1776	1955	2053	2116	2150	2230	2439						
3842.47	2	-6	2474	2515	2559	2605	2659	2709	2769	2830	2897	2965	3039	3119	3205	3289	3386	3486	3589
3776.90	2	-6	3699	3819	3948	4090	4236	4397	4570	4768	4979	5220	5489	5797	6144	6551	7016	7481	7946
3711.33	2	-5	882	985	1109	1253	1426	1627	1864	2135	2450	2803	3195	3623					
3661.19	3	-4	456	555	653	749	839	926	1012	1098	1186	1277	1370	1466	1565	1667	1770	1873	1977
3530.06	3	-4	2079	2179	2277	2371	2463	2551	2635	2714	2790	2861	2925	2983	3031	3071	3098	3115	3120
3398.92	3	-4	3111	3092	3063	3023	2978	2927	2872	2816	2758	2702	2645	2591	2538	2487	2437	2386	2335
3267.79	3	-4	2283	2228	2168	2106	2038	1966	1890	1810	1729	1645	1561	1477	1396	1317	1239	1166	1095
3136.65	3	-4	1028	964	903	846	792	742	694	649	607	567	530	495	463	433	404	377	352
3005.51	3	-5	3289	3072	2867	2678	2529	2388	2221	2083	1945	1816	1694	1588	1489	1395	1309	1230	1151
2874.38	3	-5	1081	1020	953	894	845	795	750	701	665	636	606	577	546	518	493	470	451
2743.24	3	-6	4315	4156	4016	3890	3785	3694	3601	3542	3486	3426	3376	3348	3358	3354	3365	3394	3400
2612.11	3	-6	3461	3507	3546	3639	3695	3745	3821	3911	3990	4066	4160	4253	4330	4463	4594	4706	4804
2480.97	3	-6	4924	5063	5196	5347	5490	5642	5770	5922	6103	6264	6444	6611	6773	6935	7140	7353	7548
2349.83	3	-5	779	801	822	842	868	897	930	961	994	1029	1063	1099	1136	1173	1211	1250	1287
2218.70	3	-5	1326	1366	1403	1442	1479	1512	1545	1573	1600	1622	1639	1652	1660	1663	1662	1656	1645
2087.56	3	-5	1629	1609	1588	1562	1533	1502	1469	1433	1399	1363	1327	1291	1255	1221	1190	1160	1132
1956.43	3	-5	1105	1083	1064	1047	1034	1023	1016	1012	1011	1013	1018	1026	1038	1052	1073	1096	1125
1825.29	3	-5	1160	1200	1249	1307	1377	1462	1567	1692	1846	2035	2273	2574	2960	3455	4079	4862	5821
1694.16	3	-4	696	823	958	1091	1213	1310	1368	1366	1295	1165	1013	871	753	662	593	541	501
1563.02	3	-5	4711	4473	4278	4120	3999	3901	3817	3752	3703	3664	3624	3600	3573	3554	3544	3535	3527
1431.88	3	-5	3518	3514	3509	3506	3508	3511	3516	3520	3527	3534	3543	3553	3562	3574	3584	3596	3604
1300.75	3	-5	3614	3622	3635	3644	3650	3650	3642	3632	3624	3632	3637	3657	3683	3696	3693	3704	3724
1169.61	3	-5	3743	3763	3797	3849	3853	3848	3863	3918	3972	4027	4085	4145	4210	4278	4356	4441	4535
1038.48	3	-4	464	476	490	504	521	540	561	585	612	643	678	720	766	819	880	948	1024
907.34	3	-4	1108	1201	1302	1411	1527	1650	1778	1910	2045	2181	2317	2452	2584	2714	2839	2961	3077
776.21	3	-4	3196	3310	3419	3521	3608	3691	3756	3812	3868	3923	3980	4034	4085	4130	4172	4214	4259
645.07	3	-4	4301	4335	4362	4389	4407	4419	4425	4425	4408	4376	4354	4328	4299	4266	4232	4195	4157
513.93	3	-4	4118	4078	4038	3997	3956	3916	3876	3836	3796	3757	3717	3678	3638	3598	3558	3518	3477
382.80	3	-4	3437	3398	3358	3320	3283	3248	3217	3188	3164	3146	3134	3133	3143	3170	3215	3284	3378
251.66	3	-4	3498	3644	3813	4000	4199	4403	4605	4798	4974	5127	5250	5339	5389	5398	5368	5300	5201
120.53	3	-4	5076	4937	4794	4663	4556	4491	4478	4531	4651	4845							
47.25	2	-3	497	512	530	552	580	612	657	717	802	922	1180	1628	2819				

Note: Footnotes follow Table 5.4

the second paper²³ superseding the first³³. In both cases the measurements were by near-normal reflection from an air-water interface, and the results are valuable guides. However, neither supplies reliable detailed information of the type noted above.

We recommend that this information be obtained by ATR or transmission, using the analytical technique of eliminating as many sources of variation as possible in order to obtain spectra of very high precision. Such spectra are of questionable accuracy, because many variables are fixed so many systematic errors are likely to be fixed with them, but the spectra can be calibrated with a factor determined by scaling the data at 25°C to the values reported in this paper. We believe that only in this way will data be

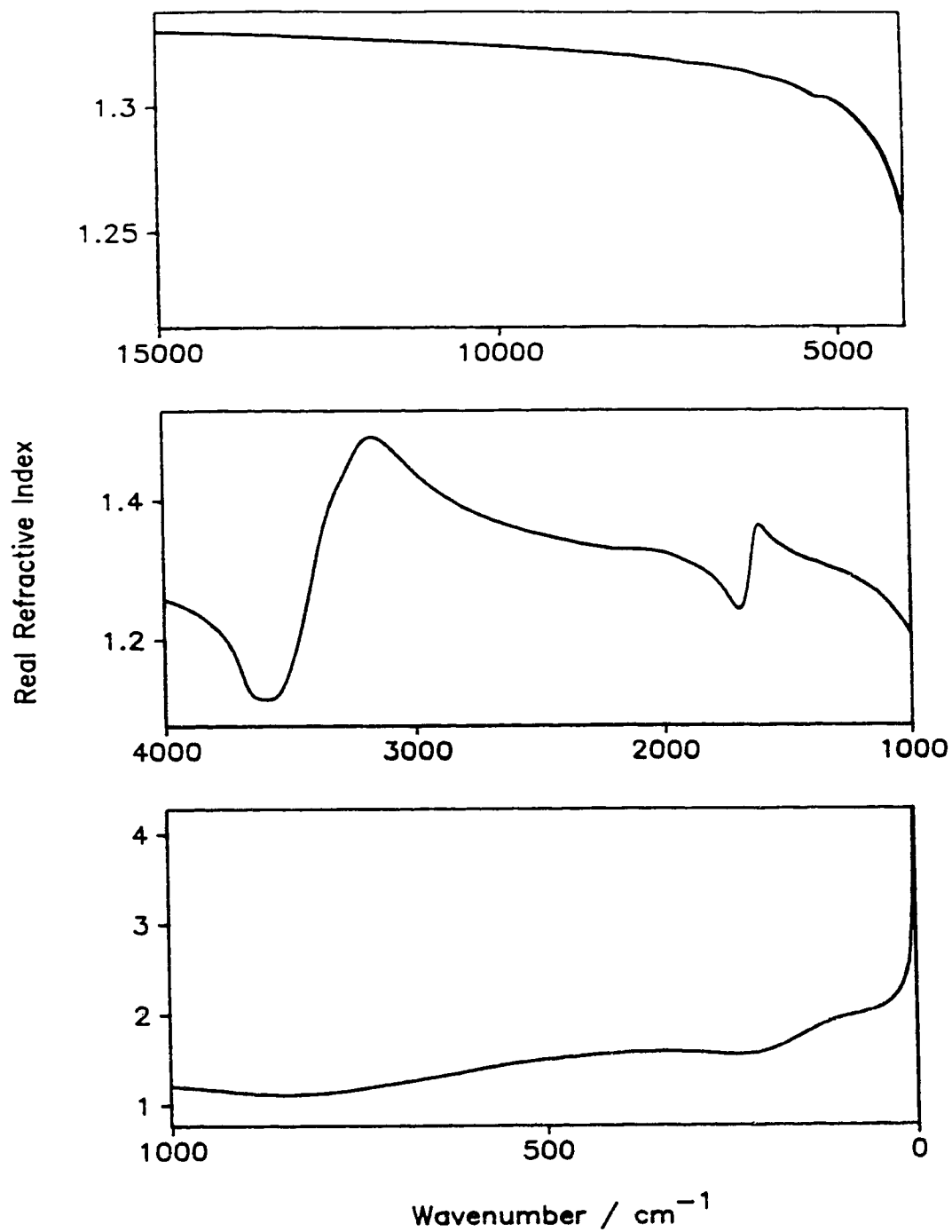


Figure 5.5. The recommended real refractive index spectrum of H₂O(*l*) between 15000 and 1 cm⁻¹.

Table 5.3. Real refractive indices between 15000 and 1 cm⁻¹ of liquid water at 25°C ^{a,b}

cm ⁻¹	XE	0	1	2	3	4	5	6	7	8	9	10	11	12	13	14	15	16
15000.6	5	13304	13303	13303	13303	13302	13302	13302	13301	13301	13301	13300	13300	13300	13299	13299	13299	13298
14476.0	5	13298	13298	13297	13297	13297	13296	13296	13296	13295	13295	13295	13295	13295	13294	13294	13293	13293
13951.5	5	13293	13292	13292	13292	13291	13291	13291	13290	13290	13290	13289	13289	13289	13288	13288	13288	13287
13427.0	5	13287	13287	13286	13286	13286	13285	13285	13284	13284	13284	13283	13283	13283	13282	13282	13282	13282
12902.4	5	13281	13281	13281	13280	13280	13280	13279	13279	13279	13278	13278	13278	13277	13277	13277	13276	13276
12377.9	5	13276	13275	13275	13275	13274	13274	13274	13273	13273	13272	13272	13272	13271	13271	13271	13270	13270
11853.3	5	13270	13269	13269	13269	13268	13268	13267	13267	13267	13266	13266	13266	13265	13265	13264	13264	13264
11328.8	5	13263	13263	13263	13262	13262	13261	13261	13261	13260	13260	13260	13259	13259	13258	13258	13258	13257
10804.2	5	13257	13256	13256	13255	13255	13255	13254	13254	13253	13253	13253	13252	13252	13251	13251	13250	13250
10279.7	5	13250	13249	13249	13248	13248	13247	13247	13246	13246	13245	13245	13244	13244	13243	13243	13242	13242
9755.15	5	13242	13241	13241	13240	13240	13239	13239	13238	13238	13237	13237	13236	13236	13235	13235	13234	13234
9230.61	5	13233	13233	13232	13231	13231	13230	13230	13229	13229	13228	13227	13227	13226	13226	13225	13224	13224
8706.06	5	13223	13222	13222	13221	13221	13220	13219	13219	13218	13217	13217	13216	13215	13214	13214	13213	13212
8181.52	5	13211	13211	13210	13209	13208	13208	13207	13206	13205	13204	13204	13203	13202	13201	13200	13199	13198
7656.98	5	13197	13196	13195	13194	13193	13192	13191	13190	13189	13188	13187	13186	13185	13184	13183	13182	13181
7132.43	5	13178	13177	13176	13176	13175	13174	13173	13172	13171	13170	13169	13168	13167	13166	13165	13164	13163
6607.89	5	13160	13159	13157	13156	13154	13152	13151	13149	13147	13145	13144	13142	13140	13138	13136	13134	13132
6083.35	5	13130	13127	13125	13123	13120	13118	13116	13113	13110	13108	13105	13102	13099	13096	13093	13089	13085
5635.94	4	13092	13090	13089	13087	13085	13084	13082	13080	13078	13077	13075	13073	13071	13068	13066	13064	13061
5373.67	4	13059	13056	13053	13050	13046	13043	13041	13039	13039	13039	13039	13039	13039	13039	13039	13039	13039
5203.97	5	13039	13039	13038	13037	13034	13030	13026	13021	13015	13010	13003	12997	12990	12983	12976	12968	12960
4679.42	5	12952	12943	12934	12924	12914	12903	12892	12880	12867	12854	12840	12825	12809	12792	12774	12755	12734
4154.88	5	12714	12690	12664	12635	12604	12571	12534	12491	12441	12382	12313	12244	12175	12106	12037	11968	11899
3842.47	2	12303	12294	12284	12273	12263	12252	12241	12230	12218	12206	12194	12181	12168	12155	12141	12127	12113
3776.90	2	12098	12082	12066	12050	12032	12015	11996	11977	11956	11935	11913	11890	11866	11841	11814	11786	11756
3711.33	2	11722	11689	11654	11617	11580	11541	11502	11462	11423	11386	11350	11317	11284	11251	11218	11185	11152
3661.19	3	11261	11221	11194	11177	11166	11158	11151	11145	11142	11141	11144	11150	11162	11181	11206	11238	11279
3530.06	3	11326	11381	11443	11511	11586	11666	11753	11845	11944	12049	12161	12279	12404	12531	12665	12802	12936
3398.92	3	13071	13201	13325	13442	13551	13652	13746	13831	13908	13979	14045	14107	14167	14224	14280	14338	14394
3267.79	3	14450	14508	14565	14620	14673	14723	14767	14807	14840	14867	14887	14900	14907	14909	14906	14898	14887
3136.65	3	14873	14855	14836	14814	14791	14766	14740	14714	14687	14660	14632	14604	14577	14549	14521	14494	14467
3005.51	3	14440	14413	14387	14361	14333	14311	14289	14265	14243	14221	14199	14177	14156	14136	14115	14096	14077
2874.38	3	14059	14041	14023	14006	13989	13973	13957	13941	13925	13910	13895	13881	13868	13854	13841	13828	13815
2743.24	3	13802	13790	13778	13766	13754	13743	13732	13721	13710	13700	13690	13679	13669	13660	13650	13641	13631
2612.11	3	13622	13614	13605	13596	13588	13580	13572	13564	13556	13548	13540	13533	13525	13518	13511	13504	13497
2480.97	3	13490	13483	13476	13469	13463	13456	13450	13443	13437	13431	13424	13418	13412	13406	13400	13394	13388
2349.83	3	13382	13376	13370	13364	13358	13352	13347	13341	13336	13331	13326	13321	13317	13313	13308	13303	13301
2218.70	3	13298	13295	13292	13290	13288	13286	13285	13284	13283	13282	13282	13281	13281	13281	13280	13280	13279
2087.56	3	13278	13277	13275	13273	13271	13267	13264	13260	13255	13250	13245	13239	13232	13225	13217	13208	13200
1955.43	3	13190	13181	13171	13160	13149	13138	13126	13114	13101	13088	13075	13060	13046	13030	13014	12998	12980
1825.29	3	12961	12941	12920	12898	12874	12848	12820	12790	12757	12722	12683	12642	12597	12552	12507	12466	12435
1694.16	3	12420	12429	12470	12545	12657	12807	12990	13193	13385	13531	13613	13638	13629	13601	13567	13530	13496
1563.02	3	13464	13434	13408	13382	13359	13338	13318	13299	13282	13266	13250	13236	13222	13209	13196	13184	13173
1431.88	3	13161	13150	13139	13128	13117	13107	13096	13086	13075	13065	13054	13044	13033	13023	13013	13003	12992
1300.75	3	12981	12971	12960	12949	12938	12927	12916	12902	12888	12873	12857	12842	12826	12813	12796	12778	12760
1169.61	3	12741	12722	12701	12683	12665	12643	12616	12590	12565	12539	12512	12484	12455	12424	12392	12359	12324
1038.48	3	12286	12247	12207	12164	12119	12072	12023	11971	11916	11859	11799	11737	11674	11609	11543	11478	11414
907.34	3	11351	11292	11239	11191	11150	11117	11094	11080	11076	11084	11102	11129	11163	11210	11263	11322	11385
776.21	3	11454	11535	11626	11724	11829	11928	12040	12141	12235	12328	12421	12520	12619	12720	12819	12916	13016
645.07	3	13125	13238	13350	13464	13584	13702	13823	13952	14066	14173	14275	14374	14470	14562	14650	14734	14814
513.93	3	14890	14962	15032	15097	15159	15219	15276	15331	15384	15434	15483	15529	15573	15615	15654	15691	15725
382.80	3	15755	15782	15804	15822	15836	15845	15847	15845	15836	15820	15796	15766	15727	15683	15634	15584	15540
251.66	3	15506	15491	15500	15539	15614	15726	15876	16066	16292	16551	16840	17152	17479	17813	18145	18467	18769
120.53	3	19045	19290	19501	19678	19827	19956	20082	20224	20406	20649	20900	21150	21400	21650	21900	22150	22400
47.25	2	20801	20976	21168	21396	21670	21986	22374	22879	23606	24609	25871	31053	48755				

Note: Footnotes follow Table 5.4.

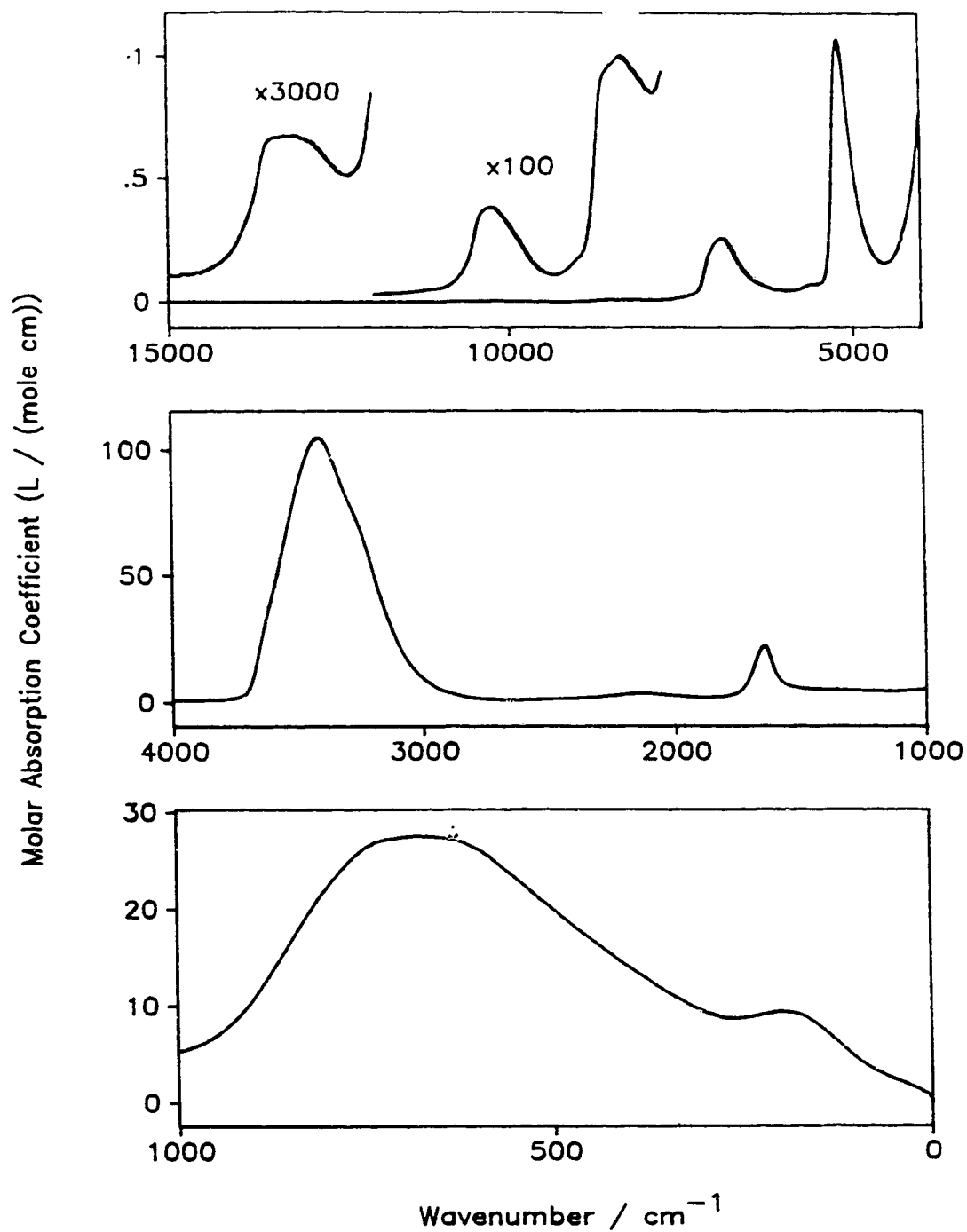


Figure 5.6. The recommended molar absorption coefficient spectrum of $\text{H}_2\text{O}(\ell)$ between 15000 and 1 cm^{-1} . For the upper two curves in the top box the ordinate labels must be divided by 100 or 3000 as shown.

Table 5.4. Molar absorption coefficients between 15000 and 1 cm⁻¹ of liquid water at 25 °C.^{a,b,c}

cm ⁻¹	XE	YE	0	1	2	3	4	5	6	7	8	9	10	11	12	13	14	15	16
15000.6	5	-7	359	358	356	355	355	355	381	380	379	378	378	377	376	402	401	401	399
14476.0	5	-7	426	424	450	449	474	500	498	523	548	573	599	623	647	672	722	746	796
13951.5	5	-7	871	920	995	1044	1118	1191	1264	1388	1510	1658	1779	1950	2020	2115	2159	2180	2200
13427.0	5	-7	2219	2215	2209	2229	2223	2242	2237	2232	2227	2245	2241	2235	2230	2201	2196	2190	2162
12902.4	5	-7	2156	2151	2123	2093	2066	2037	1985	1957	1929	1879	1851	1823	1795	1745	1740	1714	1709
12377.9	5	-7	1705	1701	1719	1737	1755	1795	1836	1899	2005	2156	2350	2587	2779	2904	3005	3063	3121
11853.3	5	-7	3179	3213	3270	3283	3318	3373	3429	3441	3517	3572	3626	3700	3775	3849	3943	4037	4152
11328.8	5	-7	4244	4358	4469	4581	4692	4802	4891	5000	5129	5257	5404	5570	5776	6040	6364	6805	7363
10804.2	5	-6	806	894	996	1108	1218	1375	1543	1729	1958	2262	2623	3027	3334	3542	3656	3728	3764
1079.7	5	-6	3800	3815	3806	3762	3708	3628	3535	3430	3318	3202	3075	2950	2806	2662	2534	2405	2254
9755.15	5	-6	2116	1984	1850	1734	1624	1525	1434	1342	1280	1220	1178	1138	1120	1105	1103	1114	1131
9230.61	5	-6	1171	1225	1280	1346	1435	1522	1613	1715	1820	1866	2011	2188	2475	2963	3731	4823	6041
8706.06	5	-5	725	830	889	924	938	948	965	966	976	985	994	1004	1002	995	986	977	967
8181.52	5	-5	951	939	929	913	905	889	874	863	859	849	848	864	879	912	938	984	1042
7656.98	5	-4	112	122	133	148	164	183	204	226	249	267	286	313	351	418	537	736	1054
7132.43	5	-4	1414	1734	2001	2173	2335	2443	2527	2555	2570	2559	2492	2375	2226	2072	1892	1746	1599
6607.89	5	-4	1453	1325	1220	1130	1022	942	869	804	748	705	664	625	594	569	545	525	506
6083.35	5	-5	4925	4801	4698	4626	4578	4579	4592	4637	4732	4892	5095	5382	5786	6185	6711		
5635.94	4	-5	6884	7034	7147	7207	7205	7182	7145	7236	7182	7217	7238	7320	7473	7682	7909	8505	9372
5373.67	4	-4	1066	1264	1613	2163	2960	4120	5597	7158	8499	9483							
5203.97	5	-3	1050	1071	1029	943	843	746	655	575	508	446	395	351	310	277	249	225	206
4679.42	5	-4	1904	1778	1693	1629	1588	1575	1584	1621	1683	1782	1920	2093	2315	2579	2936	3248	3652
4154.88	5	-4	4120	4672	5290	6166	7060	7713	8034	8216	8284	8526	9248						
3842.47	2	-3	937	952	968	984	1003	1021	1043	1065	1089	1113	1140	1168	1200	1230	1265	1301	1338
3776.90	2	-3	1377	1421	1467	1519	1571	1629	1691	1763	1839	1926	2023	2135	2260	2407	2575	2743	2911
3711.33	2	-2	323	360	405	457	520	592	678	776	889	1016	1157	1311					
3661.19	3	-2	1647	1999	2349	2685	3003	3308	3607	3907	4210	4521	4841	5170	5508	5852	6200	6549	6895
3530.06	3	-1	723	757	789	820	850	878	905	930	954	976	996	1013	1027	1039	1045	1049	1048
3398.92	3	-1	1043	1034	1022	1006	989	970	949	929	908	887	866	847	828	809	791	772	754
3267.79	3	-2	7355	7160	6953	6738	6505	6260	6005	5737	5465	5187	4911	4637	4370	4113	3861	3623	3395
3136.65	3	-2	3179	2973	2780	2598	2426	2265	2114	1972	1839	1715	1599	1491	1390	1295	1206	1123	1046
3005.51	3	-3	9748	9079	8453	7875	7418	6986	6482	6062	5646	5258	4892	4574	4276	3996	3740	3504	3271
2874.38	3	-3	3065	2883	2687	2514	2371	2224	2092	1949	1844	1758	1672	1586	1497	1417	1344	1279	1224
2743.24	3	-3	1167	1121	1080	1043	1012	985	958	939	922	903	887	878	874	874	874	879	878
2612.11	3	-3	891	900	908	929	940	950	967	986	1003	1019	1040	1060	1076	1105	1134	1158	1179
2480.97	3	-3	1205	1235	1263	1296	1326	1359	1385	1417	1456	1490	1527	1562	1595	1628	1670	1715	1755
2349.83	3	-3	1805	1849	1892	1931	1985	2045	2112	2176	2243	2313	2382	2455	2528	2601	2677	2753	2825
2218.70	3	-3	2900	2977	3048	3121	3191	3251	3309	3358	3403	3437	3461	3475	3480	3474	3459	3435	3398
2087.56	3	-3	3354	3300	3245	3180	3108	3035	2957	2874	2794	2712	2630	2549	2469	2393	2322	2255	2192
1956.43	3	-3	2132	2081	2036	1997	1962	1935	1913	1898	1884	1886	1893	1908	1925	1955	1990	2033	
1825.29	3	-3	2087	2151	2228	2322	2437	2575	2748	2955	3210	3523	3918	4417	5058	5876	6907	8195	9768
1694.16	3	-2	1162	1369	1586	1798	1989	2139	2223	2210	2084	1867	1615	1382	1190	1040	927	842	777
1563.02	3	-3	7260	6859	6529	6256	6041	5863	5709	5582	5482	5396	5309	5247	5181	5125	5085	5044	5007
1431.88	3	-3	4967	4934	4900	4870	4845	4824	4803	4783	4765	4748	4733	4719	4704	4693	4679	4666	4650
1300.75	3	-3	4635	4618	4606	4591	4570	4543	4505	4465	4428	4409	4388	4384	4388	4375	4343	4328	4323
1169.61	3	-3	4316	4311	4321	4351	4327	4292	4279	4310	4339	4369	4400	4433	4471	4510	4559	4615	4678
1038.48	3	-3	4751	4838	4939	5049	5176	5322	5486	5678	5897	6146	6428	6767	7149	7580	8071	8626	9235
907.34	3	-2	991	1065	1145	1230	1319	1414	1509	1607	1705	1802	1897	1988	2076	2160	2238	2311	2378
776.21	3	-2	2446	2508	2565	2614	2651	2684	2703	2714	2725	2734	2743	2750	2753	2753	2749	2744	2741
645.07	3	-2	2736	2724	2708	2692	2669	2642	2613	2579	2535	2484	2438	2391	2342	2291	2241	2190	2138
513.93	3	-2	2087	2035	1985	1934	1885	1835	1787	1739	1693	1646	1601	1556	1512	1468	1424	1381	1339
382.80	3	-2	1297	1257	1216	1177	1139	1103	1067	1034	1002	972	945	920	900	883	871	865	864
251.66	3	-3	8680	8765	8882	9013	9143	9250	9326	9351	9316	9212	9035	8781	8453	8057	7604	7105	6576
120.53	3	-3	6032	5492	4968	4478	4028	3629	3278	2972	2697	2441							
47.25	2	-3	2317	2190	2065	1942	1819	1687	1562	1432	1297	1139	1010	774	268				

Footnotes to Tables 5.2, 5.3 and 5.4.

^a The column headed cm⁻¹ contains the wavenumber of the first ordinate value in the row. The columns headed XE and YE contain the X-exponent and the Y-exponent, respectively, for the row. The columns headed 0,1,2,...16, contain the ordinate values, and the headings give the indices of the ordinate values in the row. In a row which starts with $\tilde{\nu}(0)$, the wavenumber corresponding to the ordinate indexed J is $\tilde{\nu}(J) = \tilde{\nu}(0) - \frac{15798.002}{16384} \cdot J \cdot 2^{XE}$. In Tables 5.2 and 5.4, the $k(\tilde{\nu})$ and $E_m(\tilde{\nu})$ values in that row are the ordinate value shown times 10^{YE}. In Table 5.3 the $n(\tilde{\nu})$ values are given directly with the decimal point implicitly after the first digit. Thus the entry indexed 16 in the second row of Table 5.2 shows that at $\tilde{\nu} = 3842.47 - \frac{15798.002}{16384} \times 16 \times 2^2 = 3780.76$ cm⁻¹ the k value is $3589 \times 10^{-6} = 3.589 \times 10^{-3}$; The entry indexed 16 in the second row of

Tables 5.3 and 5.4 show that at $\tilde{\nu} = 14476.0 - \frac{15798.002}{16384} \times 16 \times 2^5 = 13982.3 \text{ cm}^{-1}$ the ordinate values are $n = 1.3292$ and $E_m = 796 \times 10^{-7} = 7.96 \times 10^{-5} \text{ L mole}^{-1} \text{ cm}^{-1}$.

^b The 4-point spline interpolation program TRECOVER³² interpolated the $k(\tilde{\nu})$ and $E_m(\tilde{\nu})$ values in the table to the original wavenumber spacing, 0.964234 cm^{-1} , and yielded the original values accurate to 1%. The original $n(\tilde{\nu})$ values were similarly recovered accurate to 0.1%.

^c The unit of E_m is $\text{L mole}^{-1} \text{ cm}^{-1}$. Multiply the values by 1000 to change the unit to $\text{cm}^2 \text{ mole}^{-1}$.

obtained with sufficient precision to show clearly the small spectral changes caused by temperature changes of a few degrees near 25°C . Heise and Bittner²⁵ have recently published a graph which shows such effects between 2000 and 800 cm^{-1} for a 5 degree change in temperature.

5.5 Conclusions

It has been found that the previously reported nonreproducibility of the intensity of the OH stretching band of water can be eliminated in measurements with the CIRCLE multiple ATR cell by ensuring that the ATR rod is coaxial with the glass liquid holder. Normal laboratory temperature variations of a few degrees change the intensity by less than 1%. A new imaginary refractive index spectrum of water has been determined between 4000 and 700 cm^{-1} as the average of spectra calculated from ATR spectra recorded by 4 workers in this laboratory over the past 7 years. It was obtained under superior experimental and computational conditions to those used previously, but is only marginally different from the spectra reported in 1989^{1,8}. In particular, the integrated intensities of the fundamentals are not changed significantly from those reported previously^{1,8}.

The available imaginary refractive index, k , values between 15,000 and 1 cm^{-1} have been compared. The values that appear to be the most reliable have been combined into a recommended k spectrum of $\text{H}_2\text{O}(\ell)$ at $25\text{ }^\circ\text{C}$ between 15,000 and 1 cm^{-1} , from which the real refractive index spectrum has been calculated by Kramers-Kronig analysis. The recommended values of the real and imaginary refractive indices and molar absorption coefficients of liquid water at $25 \pm 1^\circ\text{C}$ are presented in graphs and tables. The real and imaginary dielectric constants in this wavenumber range can, of course, be calculated from the tabulated values. The probable absolute errors associated with the recommended values are conservative. The relative errors between regions are far smaller, and the recommended values should be of considerable value as (tentative) standard intensities of liquid water, which will facilitate lab-to-lab transfer of intensities.

5.6 References

1. J.E. Bertie, M.K. Ahmed and H.H. Eysel, J. Phys. Chem. **93**, 2210 (1989).
2. A.N. Rusk, D. Williams and M.R. Querry, J. Opt. Soc. Amer. **61**, 895 (1971).
3. V.M. Zolotarev and A.V. Demin, Opt. Spectrosc. **43**, 157 (1977) (Opt. Spektrosk. **43**, 271 (1977)).
4. J.E. Bertie, S.L. Zhang, H.H. Eysel, S. Baluja and M.K. Ahmed, Appl. Spectrosc. **47**, 1100 (1993).
5. W.M. Irvine and J.B. Pollack, Int. J. Solar Syst., ICARUS **8**, 324 (1978).
6. H.D. Downing and D. Williams, J. Geophys. Res. **80**, 1656 (1975).

7. J.E. Bertie, H. Harke, M.K. Ahmed and H.H. Eysel, *Croat Chem. Acta* **61**, 391 (1988).
8. J.E. Bertie, M.K. Ahmed and S.J. Baluja, *Phys. Chem.* **93**, 6660 (1989).
9. J.E. Bertie, S.L. Zhang and R. Manji, *Appl. Spectrosc.* **46**, 1660 (1992).
10. Y. Maréchal, *J. Chem. Phys.* **95**, 5565 (1991); *Idem J. Phys. II France* **3**, 557 (1993); *Idem J. Phys. Chem.* **97**, 2846 (1993).
11. L. Kou, L. Labrie and P. Chylek, *Appl. Optics* **32**, 3531 (1993).
12. K.F. Palmer and D. Williams, *J. Opt. Soc. Amer.* **64**, 1107 (1974).
13. G.M. Hale and M.R. Querry, *Appl. Opt.* **121**, 555 (1973).
14. C.W. Robertson and D. Williams, *J. Opt. Soc. Amer.* **61**, 1316 (1971).
15. N.A. Marley, J.S. Gaffney and M.M. Cunningham, *Appl. Opt.* **33**, 8041 (1994).
16. H.R. Zelsmann, *J. Mol. Struct.* **350**, 95 (1995)
17. J.E. Bertie, Z. Lan and Y. Apelblat, *Appl. Spectrosc.* **49**, 840 (1995).
18. R.N.Jones, T.G. Goplen and D.G. Cameron, *Appl. Spectrosc.* **34**, 652 (1980).
19. M.N. Afsar and J.B. Hasted, *J. Opt. Soc. Amer.* **67**, 902 (1977).
20. D.A. Draegert, N.W.B. Stone, B. Curnutte and D. Williams, *J. Opt. Soc. Amer.* **56**, 64 (1966)
21. J.E. Bertie and H.H. Eysel, *Appl. Spectrosc.* **39**, 392 (1985).
22. J.E. Bertie and Z. Lan, *J. Chem. Phys.* In press (accepted September 15, 1995).
23. L.W. Pinkley, P.P. Sethna and D. Williams, *J. Opt. Soc. Amer.* **67**, 494 (1977).
24. J.E. Bertie, S.L. Zhang and C.D. Keefe, *J. Mol. Struct.* **324**, 157 (1994).

25. H.M. Heise and A. Bittner, J. Mol. Struct. **348**, 21 (1995).
26. J.E. Bertie, S.L. Zhang and C.D. Keefe. Vibrational Spectroscopy **8**, 215 (1995).
27. J.E. Bertie and S.L. Zhang. Appl. Spectrosc. **48**, 176 (1994); J. Chem. Phys. **101**, 8364 (1994).
28. M.N. Afsar and J.B. Hasted, Infrared Phys. **18**, 835 (1978).
29. J.B. Hasted, S.K. Husain, F.A.M. Frescura and J.R. Birch, Chem. Phys. Letters **118**, 622 (1985).
30. J.B. Hasted, S.K. Husain, F.A.M. Frescura and J.R. Birch, Infrared Phys. **27**, 11 (1987).
31. U. Kaatze and V. Uhlendorf, Z. Physik. Chem. NF. **126**, 151 (1981).
32. J.E. Bertie, R.N. Jones and Y. Apelblat, Appl. Spectrosc. **47**, 1989 (1993).
33. G.M. Hale, M.R. Querry, A.N. Rusk and D. Williams, J. Opt. Soc. Amer. **62**, 1103 (1972).

Chapter 6 The Absolute Intensities of Infrared Spectra of Water-Acetonitrile Mixtures at 25°C and their Application to Investigate the Structure of the Mixtures.

6.1. Introduction

Binary solutions in which water is one of the components have been investigated intensively due to their importance for many branches of chemistry. The mixture of water with acetonitrile has a relatively simple structure because the acetonitrile is a small molecule. In addition the $\text{C}\equiv\text{N}$ group of the acetonitrile is a good sensor for its environment in the mixture. However, observations of this binary solution still give controversial results about its microstructure. The molecular dynamic simulation ¹ and dynamic properties ² suggest that there exist clusters consisting entirely of molecules of one type, either CH_3CN or H_2O , when the acetonitrile concentration is high enough, and that the order in the water structure increases at low acetonitrile concentration. Raman spectroscopy ³ and thermodynamic studies ^{4,5} show no such structure-making functionality of acetonitrile at low concentration but do support the formation of clusters at intermediate compositions. In contrast, the IR study by Gorbunov and Naberukhin ⁶ indicated non-existence of clusters at any concentration. Two recent works still give inconsistent observations. Huang and Wu ⁷ used nonlinear optical spectroscopic approach to study the $\text{CH}_3\text{CN}+\text{H}_2\text{O}$ system. They noticed the existence of microheterogeneity due to the formation of clusters in the mixtures at intermediate acetonitrile concentrations, but obtained no information at low acetonitrile concentration.

Jamroz, Stangret and Lindgren ⁸ investigated the CN stretching band of CD₃CN + H₂O mixtures and the OD stretching band of dilute HOD in CH₃CN + H₂O mixtures by infrared transmission spectroscopy. They resolved the CN stretching band of pure CD₃CN into three Lorentzian bands. They resolved the CN stretching band in the mixtures into a single Lorentzian band due to the hydrogen-bonded CD₃CN and the group of three Lorentzian bands due to the non-bonded CD₃CN that they found for the pure liquid. In the fitting, they simply scaled the height of this latter group of three bands and adjusted the single Lorentzian due to the bonded CD₃CN to fit the experimental spectrum. While their statement is not quite clear, it seems that they calculated the concentration of non-bonded CD₃CN in each mixture from the scaling factor for the non-bonded group of bands required for that mixture, then calculated the concentration of bonded CD₃CN by subtraction of this quantity from the total concentration. They compared the percentage of bonded CD₃CN with that calculated from a close packing model. The model predicted far higher percentages of hydrogen bonded CD₃CN. They concluded that this comparison shows that the arrangement in the mixture is remarkably non-random, and strong preferential solvation occurs in the system.

These authors also studied the OD stretching band of dilute HDO in the mixtures. They studied the difference spectra formed by subtracting the absorbance spectrum of "reference solutions containing CH₃CN and H₂O" from those of CH₃CN + H₂O + HDO mixtures. They found for $x_{\text{H}_2\text{O}} < 0.04$ a single OD band at 2631 cm^{-1} . As $x_{\text{H}_2\text{O}}$ increased above 0.04 the band broadened and shifted to lower wavenumber, and a

broad band grew near 2540 cm^{-1} and shifted to low wavenumber with increasing water concentration. They assigned the 2631 cm^{-1} peak to water H-bonded to CH_3CN and the 2540 cm^{-1} band to HDO- H_2O hydrogen bonding. The authors deconvoluted these bands, and presented the deconvoluted and original spectra, but their method of deconvolution was not stated.

From their band deconvolution, Jamroz et al were able to state that two types of each component exist over a wide composition range. The one type consists of molecules that are "in close contact with molecules of the same kind, and the interactions among them are very similar to those in the pure solvent. Molecules of the other type interact strongly through hydrogen bonds with molecules of the other component". Further, they concluded that the shift with concentration of the OD stretching band due to water-water bonding shows that the water molecules form dimers, trimers and other oligomers, because "the formation of spherical clusters of water molecules would result in concentration-independent positions of the CN and OD stretching bands".

In this work the infrared attenuated total internal reflection (ATR) spectra of $\text{H}_2\text{O}+\text{CH}_3\text{CN}$ mixtures were measured. This technique can supply reliable spectroscopic information for regions with strong absorption⁹. The ATR spectra were converted to accurate absolute intensities in terms of real and imaginary refractive indices. The refractive index spectra were then converted to the corresponding complex molar polarizability spectra $\hat{\alpha}_m(\tilde{\nu}) = \alpha'_m(\tilde{\nu}) + i\alpha''_m(\tilde{\nu})$, through the use of the Lorentz local field in the mixtures. The absolute intensities, not just the band

positions and shapes, were examined to measure the interaction between the water and acetonitrile molecules. In the O-H and C \equiv N stretching regions, the areas under the $\tilde{\nu}\alpha''_m(\tilde{\nu})$ spectrum were determined as functions of composition. Accordingly, quantitative information about the structure of the mixtures was obtained and is discussed.

6.2. Experimental

The spectra were recorded with the Bruker IFS 113V FT-IR spectrometer. A DTGS detector was used to keep the phase correction small. A 10-mm aperture, automatic gain selection, and an optical retardation velocity of 0.396 cm s⁻¹ were used with a global source. Ge-on-KBr and Si-on-CaF₂ beam splitters were used, and each transformed interferogram was the average of 512 interferograms. The nominal resolution was 2 cm⁻¹ for water rich mixtures with mole fraction of acetonitrile $x_{\text{CH}_3\text{CN}}$ less than 0.20 and 1 cm⁻¹ for the remainder. All averaged interferograms were Fourier transformed with trapezoidal apodization and one level of zero-filling.

The CIRCLE cell used to contain the sample has been described before ¹⁰. The ATR rod in the cell was ZnSe. For $x_{\text{CH}_3\text{CN}} < 0.4$, the spectra were measured in a short cell with effective number of reflections (NRF) ~ 3.3 because the O-H stretching band is very strong. For $x_{\text{CH}_3\text{CN}} > 0.4$, a long cell with effective number of reflections (NRF) ~ 6 was used. Both cells were used for $x_{\text{CH}_3\text{CN}} = 0.4$. Each ATR spectrum was measured as the ratio of the spectrum of the CIRCLE cell full of the liquid under study

Table 6.1 The volumes used to make 50 grams of CH₃CN+H₂O mixture solution ^a

$x_{\text{CH}_3\text{CN}}$	$V_{\text{CH}_3\text{CN}}/\text{ml}$	$V_{\text{H}_2\text{O}}/\text{ml}$
0.00	0.000	50.118
0.05	6.864	44.751
0.01	12.951	39.992
0.15	18.384	35.745
0.20	23.264	31.930
0.30	31.671	25.356
0.40	38.656	19.895
0.50	44.551	15.286
0.60	49.593	11.344
0.70	53.955	7.934
0.80	57.765	4.955
0.90	61.122	2.330
1.00	64.103	0.00

^a. The densities and molar weights used for the calculation are $d_{\text{CH}_3\text{CN}}=0.7800 \text{ g/cm}^3$ (at 22.5°C) and $W_{\text{CH}_3\text{CN}}=41.05 \text{ g/mole}$ for liquid acetonitrile, and $d_{\text{H}_2\text{O}}=0.99765 \text{ g/cm}^3$ (at 22.5°C) and $W_{\text{H}_2\text{O}}=18.0153 \text{ g/mole}$ for liquid water.

to the spectrum of the cell full of dry nitrogen gas. Its negative decadic logarithm, -
log₁₀ (ATR), called the pATR spectrum, was calculated.

Spectra were obtained between 8000 and 700 cm⁻¹ by merging three spectra in
the following way: The pATR values in the region from 8000 cm⁻¹ to 6500 cm⁻¹ were

set to zero; the spectrum recorded with the Si-on-CaF₂ beam splitter was used from 6500 to 4500 cm⁻¹; the average of the pATR spectra recorded with the two beam splitters was used between 4500 and 1200 cm⁻¹; and the spectrum recorded with the Ge-on-KBr beam splitter was used from 1200 to 700 cm⁻¹.

The liquid water was building distilled water passed through a Millipore water system consisting of a SUPER-C carbon filter, two ION-EX ion-exchange cartridges, and an ORGANEX-Q carbon filter. The acetonitrile used was analytical reagent grade with 99.5% purity. The mixtures were made by volumetric method (Table 6.1). Each mixture was kept in a closed glass bottle.

6.3. Intensity Quantities

The programs used to convert pATR spectra to real and imaginary refractive index spectra have been described ¹⁰. The values of the real refractive index at 8000 cm⁻¹ at 25 °C were found to be 1.325 ± 0.003 for water and 1.325 ± 0.01 for acetonitrile, by fitting the reported values ^{11,12} at visible wavelengths to $n^2 = A + B\tilde{\nu}^2 + C\tilde{\nu}^4$, then extrapolating to 8000 cm⁻¹. There are no available values of the real refractive index at several visible wavelengths for each mixture that allow the fitting procedure to be used for the mixtures. However, the real refractive indices listed in Table 6.2 for sodium D light show that the variation of the real refractive index of the different mixtures ranges from 1.3330 to 1.3479, not over 0.015. Therefore, the value $n_{8000} = 1.325$ was used for all mixtures.

Table 6.2. Properties of H₂O+CH₃CN mixtures ¹⁵

$x_{\text{CH}_3\text{CN}}$	V_m^a at 25°C ml/mole	$x_{\text{CH}_3\text{CN}}$	n_D^b at 20°C	$x_{\text{CH}_3\text{CN}}$	Q_{mix}^c at 20°C cal/mole
0.00	18.0682	0.00	1.3330	0.00	0.00
0.05	19.4649	0.07	1.3414	0.019	-5.34
0.01	21.2077	0.10	1.3430	0.033	-3.94
0.15	22.8642	0.16	1.3459	0.056	+3.54
0.20	24.5611	0.31	1.3478	0.148	+67.60
0.30	28.0215	0.35	1.3479	0.198	+100.46
0.40	31.4983	0.42	1.3479	0.390	+169.83
0.50	35.0462	0.49	1.3478	0.450	+185.07
0.60	38.5940	0.60	1.3473	0.533	+198.63
0.70	42.2345	0.61	1.3472	0.618	+200.93
0.80	45.8561	0.69	1.3470	0.745	+197.4
0.90	49.443	0.79	1.3462	0.907	+125.16
1.00	53.016	1.00	1.3444	1.00	0.0000

^a. V_m is the molar volume of mixture.

^b. n_D is the real refractive index at Sodium-D line.

^c. Q_{mix} is the molar heat of mixing.

For each of the mixtures, at least four imaginary refractive index spectra were obtained and averaged to give the final spectrum. The final real refractive index spectrum was determined by Kramers-Kronig transform of the k spectrum with

$n_{8000}=1.325$. In figures 6.1 and 6.2 these two spectra are displayed for five mixtures, $x_{\text{CH}_3\text{CN}}=0.0, 0.20, 0.50, 0.70, 1.00$. The numerical values of the refractive indices of pure liquid water have been reported ¹³. The numerical values for acetonitrile and the three mixtures are presented in tables 6.3 to 6.6 for the imaginary refractive index and 6.7 to 6.10 for the real refractive index.

From the real and imaginary refractive index spectra, the complex molar polarizability spectra, $\hat{\alpha}_m(\tilde{\nu}) = \alpha'_m(\tilde{\nu}) + i \alpha''_m(\tilde{\nu})$, were determined for all the mixtures under the Lorentz local field assumption ¹⁴. The molar volumes used for the calculation were calculated from the reported densities ¹⁵, and their values are listed in Table 6.2.

The imaginary molar polarizability spectrum $\alpha''_m(\tilde{\nu})$, or the $\tilde{\nu}\alpha''_m(\tilde{\nu})$ spectrum is the best spectrum to use to obtain physico-chemical information, in spite of the fact that it depends on the Lorentz local field approximation but quantities like the absorbance, A_{10} , molar absorption coefficient, E_m , and imaginary refractive index, k , do not ¹⁴. There are several facts which support this statement ¹⁴.

First, very strong bands are essentially symmetrical in the α''_m spectrum and are asymmetric with a high wavenumber tail, in A_{10} , E_m and k spectra. This agrees with the prediction of simple theory ¹⁴ and indicates that the Lorentz local field is a very good approximation that corrects the dielectric effects in the liquid that distort the spectra of macroscopic quantities, A_{10} , E_m and k .

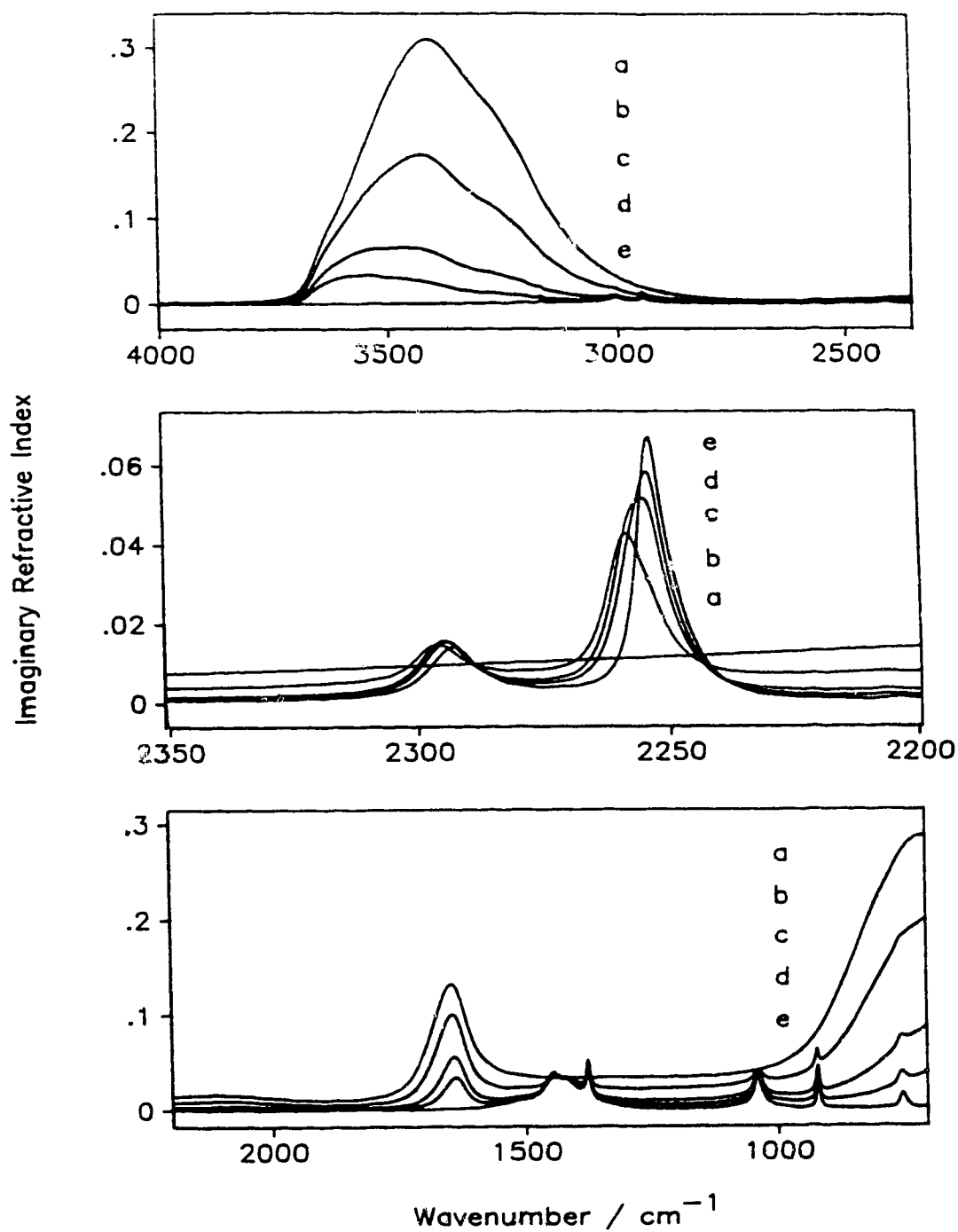


Figure 6.1. Imaginary refractive index spectra of five $\text{CH}_3\text{CN}+\text{H}_2\text{O}$ mixtures at 25°C : a $x_{\text{CH}_3\text{CN}}=0.0$; b $x_{\text{CH}_3\text{CN}}=0.20$; c $x_{\text{CH}_3\text{CN}}=0.50$; d $x_{\text{CH}_3\text{CN}}=0.70$; e $x_{\text{CH}_3\text{CN}}=1.00$.

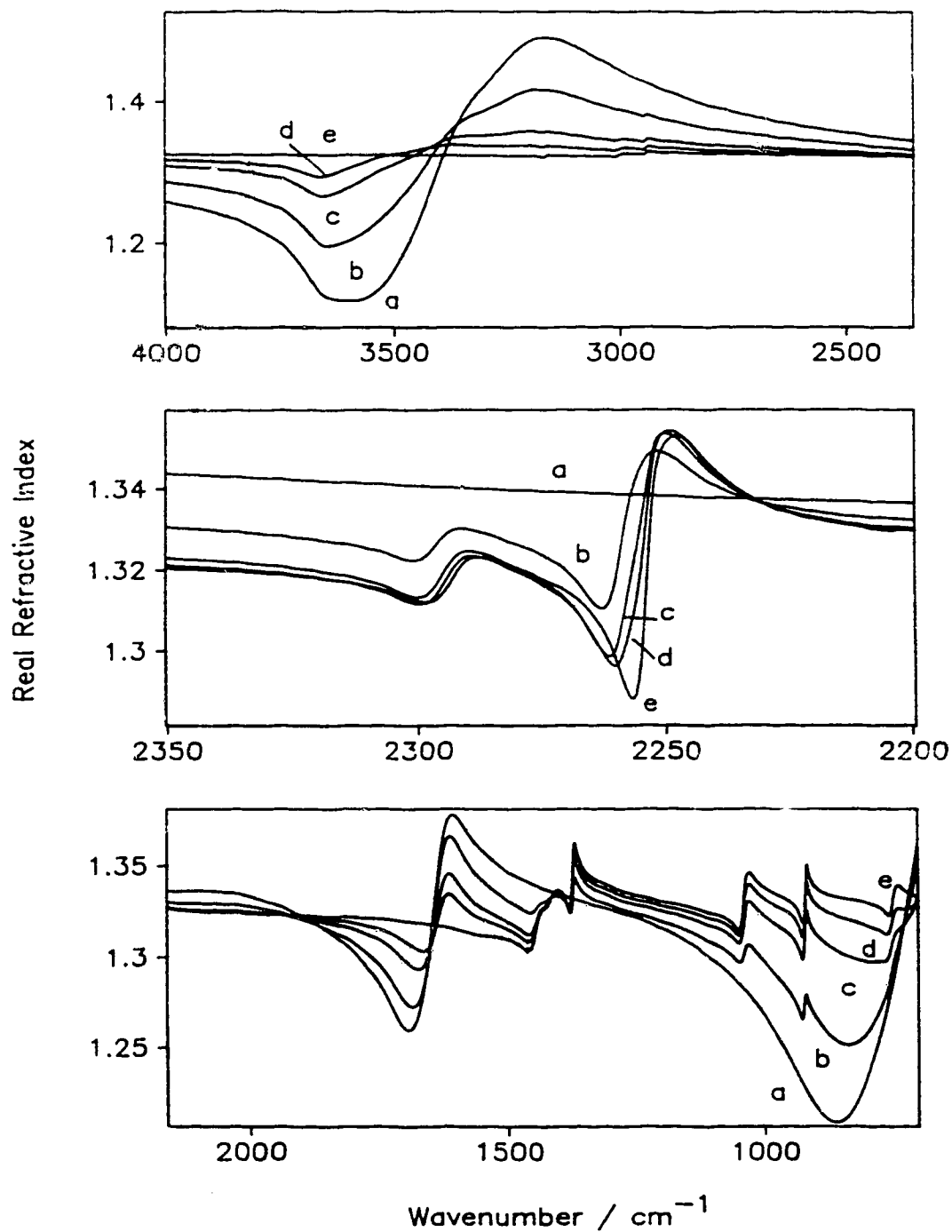


Figure 6.2. Real refractive index spectra of five $\text{CH}_3\text{CN}+\text{H}_2\text{O}$ mixtures at 25 °C: a $x_{\text{CH}_3\text{CN}}=0.0$; b $x_{\text{CH}_3\text{CN}}=0.20$; c $x_{\text{CH}_3\text{CN}}=0.50$; d $x_{\text{CH}_3\text{CN}}=0.70$; e $x_{\text{CH}_3\text{CN}}=1.00$.

Table 6.3. Imaginary refractive indices between 8000.25 and 700 cm^{-1} of liquid mixture water-acetonitrile with $x_{\text{CH}_3\text{CN}}=0.20$ at 25 $^{\circ}\text{C}$.^{a,b}

cm^{-1}	kE	kE	0	1	2	3	4	5	6	7	8	9	10	11	12	13	14	15	16
8000.25	7	0	0	0	0	0	0	0	0	0	0	0	0	0	0	0	0	0	0
6488.33	5	-7	0	0	0	0	0	0	0	0	0	0	0	2948	0	2622	0	0	0
5963.78	5	0	0	0	0	0	0	0	0	0	0	0	0	0	0	0	0	0	0
5439.24	5	-7	0	0	0	0	0	0	305	325	2083	2	0	0	0	0	0	0	0
4914.70	5	-7	0	0	0	0	0	0	0	0	0	0	0	0	0	1574	0	2327	1659
4390.15	5	-7	2690	2556	0	0	0	0	0	0	0	0	110	1550	2748	2269			
3981.32	3	-7	3087	3439	2595	1843	1489	1454	1154	1295	1274	1070	2407	732	790	911	1188	401	564
3850.18	3	-6	90	78	210	117	97	103	187	329	314	434	495	691	731	925	1071	1362	1653
3719.05	3	-5	206	269	369	522	779	1089	1508	1978	2480	2948	3378	3779	4098	4420	4715	4972	5235
3587.91	3	-5	5465	5669	5870	6016	6141	6256	6340	6378	6412	6433	6454	6479	6499	6509	6530	6545	6555
3456.78	3	-5	6557	6551	6529	6485	6417	6322	6207	6072	5900	5715	5518	5308	5111	4902	4709	4540	4381
3325.64	3	-5	4235	4104	4002	3908	3827	3742	3671	3596	3516	3426	3328	3211	3077	2933	2791	2656	2505
3194.50	3	-5	2316	2163	2054	2010	1901	1655	1517	1418	1327	1247	1175	1105	1045	992	943	896	854
3067.23	2	-6	8374	8176	8035	7889	7763	7653	7576	7570	7488	7539	7592	7734	8023	8345	8688	9289	9596
3001.66	2	-5	953	897	822	746	684	628	591	567	549	537	528	529	554	629	851	1013	746
2936.09	2	-6	5741	4775	4173	3746	3434	3209	3060	2913	2784	2616	2512	2402	2305	2199	2109	2027	1934
2870.52	2	-6	1846	1774	1691	1619	1540	1489	1418	1376	1327	1262	1175	1094	1027	968	909	865	819
2804.95	2	-7	7830	7090	6870	6524	6117	5780	5612	5274	5019	4812	4460	4229	4132	4128	3723	3476	3694
2739.39	2	-7	3566	3646	3386	2887	2657	2387	2142	1963	1678	1702	1491	1505	1541	1355	1590	1506	1605
2673.82	2	-7	1516	1324	1137	1045	922	1090	1265	1595	2520	4139	5849	7842	7899	5633	4222	2708	1747
2608.25	2	-7	1301	1026	1001	1084	838	842	862	916	907	1025	1224	1327					
2558.11	3	-6	129	168	185	201	253	293	337	411	476	570	631	639	638	679	770	914	1045
2426.98	3	-6	1201	1500	1827	1762	1457	1215	1121	1109	1144	1221	1390	1551					
2340.19	1	-6	1564	1599	1610	1635	1655	1692	1762	1836	1906	2012	2110	2243	2371	2525	2702	2967	3290
2307.41	1	-5	377	450	556	728	978	1281	1515	1531	1335	1081	881	748	654	597	562	552	559
2274.63	1	-5	576	602	652	741	913	1246	1853	2862	4091	4881	5143	4844	3658	2614	1895	1388	1034
2241.84	1	-6	7903	6261	5158	4408	3922	3602	3388	3290	3193	3102	3030	2977	2930	2892	2918	3026	
2209.06	1	-6	3148	3216	3248	3225	3080	2956	2884	2837	2809	2778	2769	2766	2770	2781	2804	2829	2848
2176.27	1	-6	2868	2896	2901	2928	2940	2944	2975	3007	3033	3044							
2151.20	3	-6	3166	3275	3392	3493	3601	3685	3790	3878	3971	4062	4267	4331	4121	3976	3870	3765	3672
2020.07	3	-6	3563	3457	3341	3218	3096	2961	2853	2762	2639	2517	2435	2334	2261	2183	2143	2088	2037
1888.93	3	-6	2012	1999	2040	2029	2038	2100	2210	2336	2413	2296	2331	2380	2487				
1794.44	1	-6	2510	2689	2639	2617	2637	2767	2724	2778	2786	2850	2902	2925	3070	3071	3118	3203	3265
1761.65	1	-6	3467	3418	3526	3587	3712	3795	3896	4072	4155	4318	4466	4615	4806	5001	5389	5421	5636
1728.87	1	-5	586	613	640	669	698	730	780	810	847	890	935	987	1043	1100	1164	1247	1306
1696.09	1	-5	1397	1472	1562	1665	1767	1876	2006	2122	2253	2391	2542	2705	2855	3025	3214	3377	3565
1663.30	1	-5	3755	3952	4141	4331	4522	4712	4882	5042	5191	5325	5403	5477	5507	5502	5457	5372	5249
1630.52	1	-5	5091	4895	4681	4443	4192	3940	3686	3443	3204	2986	2780	2596	2426	2269	2133	2009	1899
1597.73	1	-5	1799	1711	1631	1560	1498	1441	1393	1349	1311	1276	1247	1226	1201	1180	1164	1154	1146
1564.95	1	-5	1140	1126	1123	1120	1135	1123	1119	1127	1132	1132	1136	1143	1166	1158	1161	1168	1188
1532.17	1	-5	1186	1196	1220	1215	1228	1253	1252	1267	1279	1297	1293	1315	1326	1354	1358	1367	1384
1499.38	1	-5	1401	1418	1445	1456	1476	1507	1525	1555	1592	1641	1665	1712	1773	1818	1885	1956	2035
1466.60	1	-5	2130	2249	2351	2470	2602	2763	2896	3040	3176	3313	3390	3448	3476	3465	3434	3392	3339
1433.81	1	-5	3285	3245	3218	3197	3194	3204	3215	3195	3165	3126	3074	3005	2932	2857	2779	2693	2608
1401.03	1	-5	2533	2465	2396	2341	2304	2280	2285	2322	2386	2529	2794	3260	3983	4669	4537	3639	2827
1368.25	1	-5	2334	2035	1839	1694	1588	1513	1451	1409	1368	1341	1312	1295	1278	1256	1242	1225	1208
1335.46	1	-5	1189	1172	1162	1149	1135	1121	1116	1101	1090	1077	1069	1057	1047	1037	1025	1020	1015
1302.68	1	-5	1008	1000	994	990	982	978	969	970	966	962	956	954	951				
1271.82	3	-5	942	936	929	930	933	931	933	935	934	944	941	955	972	986	999	1010	1030
1146.47	1	-5	1030	1039	1042	1048	1052	1057	1060	1066	1075	1081	1089	1093	1104	1111	1124	1134	1147
1113.69	1	-5	1160	1173	1185	1199	1212	1226	1240	1256	1276	1289	1306	1324	1340	1357	1373	1392	1411
1080.91	1	-5	1433	1454	1475	1500	1529	1562	1599	1634	1675	1727	1786	1847	1928	2018	2139	2287	2474
1048.12	1	-5	2702	2974	3271	3568	3747	3789	3675	3438	3154	2883	2640	2427	2253	2111	1995	1902	1826
1015.34	1	-5	1765	1717	1679	1648	1620	1600	1585	1572	1558	1548	1538	1530	1526	1519	1513	1511	1508
982.55	1	-5	1505	1502	1503	1503	1503	1507	1512	1513	1519	1521	1530	1533	1539	1550	1561	1574	1589
949.77	1	-5	1604	1622	1640	1660	1682	1709	1747	1788	1843	1927	2056	2260	2569	3074	3801	4424	4185
916.99	1	-5	3338	2651	2355	2228	2155	2108	2085	2081	2080	2083	2091	2116	2140	2164	2192		
886.13	2	-5	2237	2286	2355	2432	2525	2607	2683	2764	2861	2964	3070	3169	3278	3398	3524	3642	3765
820.56	2	-5	3896	4032	4183	4330	4478	4631	4785	4957	5114	5292	5461	5652	5857	6101	6362	6698	7106
754.99	2	-5	7513	7715	7713	7601	7571	7599	7655	7764	7882	8013	8120	8244	8366	8486	8586		

Note: Footnotes follow Table 6.10

Table 6.4. Imaginary refractive indices between 8000.25 and 700.0 cm⁻¹ of liquid water-acetonitrile with $x_{\text{CH}_3\text{CN}}=0.50$ at 25 °C.^{a,b}

cm ⁻¹	XE	YE	0	1	2	3	4	5	6	7	8	9	10	11	12	13	14	15	16
8000.25	7	0	0	0	0	0	0	0	0	0	0	0	0	0	0	0	0	0	0
6488.33	5	-7	0	0	0	0	0	0	0	0	65	0	0	2948	0	2622	0	0	0
5963.78	5	0	0	0	0	0	0	0	0	0	0	0	0	0	0	0	0	0	0
5439.24	5	-7	0	0	0	0	0	0	305	325	2083	2	0	0	0	0	0	0	0
4914.70	5	-7	0	0	0	0	0	0	0	0	0	0	0	0	0	1574	0	2327	1659
4390.15	5	-7	2690	2556	0	0	0	0	0	0	0	0	110	1550	2748	2269	1843	1295	732
3865.61	5	-5	4	21	19	49	107	269	1089	2948	4420	5465	6141	6412	6499	6555	6485	6072	5308
3356.50	4	-5	4902	4540	4235	4002	3827	3671	3516	3328	3077	2791	2505						
3200.29	1	-5	2455	2409	2360	2316	2273	2232	2196	2163	2131	2099	2076	2054	2037	2026	2019	2010	2000
3167.51	1	-5	1984	1956	1901	1828	1758	1701	1655	1615	1582	1546	1517	1493	1464	1442	1418	1393	1374
3134.72	1	-5	1350	1327	1307	1284	1264	1247	1227	1212	1192	1175	1155	1138	1123	1105	1089	1073	1059
3101.94	1	-5	1045	1033	1018	1005	992	980	968	956	943	931	920	908	896	886	873	864	854
3069.15	1	-6	8445	8374	8265	8176	8100	8035	7959	7889	7823	7763	7723	7653	7613	7576	7550	7570	7483
3036.37	1	-6	7488	7501	7539	7548	7592	7669	7734	7876	8023	8132	8345	8569	8888	9048	9289	9480	9596
3003.59	1	-6	9660	9532	9279	8972	8616	8225	7823	7463	7113	6835	6553	6282	6099	5911	5792	5669	5593
2970.80	1	-5	549	541	537	529	528	527	529	539	554	581	629	717	851	990	1013	888	746
2938.02	1	-6	6444	5741	5174	4775	4417	4173	3924	3746	3567	3434	3307	3209	3134	3060	2996	2913	2834
2903.31	2	-6	2694	2582	2468	2358	2262	2169	2053	1970	1882	1819	1738	1660	1574	1526	1454	1407	1348
2837.74	2	-6	1295	1221	1143	1069	1002	946	881	829	810	750	695	659	640	586	571	556	528
2772.17	2	-7	4858	4563	4289	4064	3997	3783	3536	3569	3706	3689	3511	3274	2798	2373	2269	2186	1805
2706.60	2	-7	1691	1674	1720	1466	1479	1268	1193	1486	1587	1491	1156	1134	1035	1046	1048	1329	
2646.82	1	-7	1595	1928	2520	3104	4139	5060	5849	6972	7842	8155	7899	6704	5653	4573	4222	3092	2708
2614.04	1	-7	2244	1747	1632	1301	1091	1026	1069	1001	808	1084	783	838	777	842	762	862	884
2581.25	1	-7	916	1079	907	1032	1025	1108	1224	1375	1327								
2558.11	3	-6	129	168	185	201	253	293	337	411	476	570	631	639	638	679	770	914	1045
2426.98	3	-6	1201	1500	1827	1762	1457	1215	1121	1109	1144	1221	1390	1551					
2341.16	0	-6	1577	1564	1585	1602	1610	1619	1635	1637	1655	1676	1692	1729	1762	1794	1836	1865	
2324.77	0	-6	1906	1958	2012	2057	2110	2175	2243	2278	2371	2415	2525	2590	2702	2815	2967	3107	3290
2308.37	0	-5	351	377	408	450	495	556	633	728	844	978	1128	1281	1419	1515	1556	1531	1451
2291.98	0	-5	1335	1206	1081	976	881	806	748	695	654	622	597	578	562	554	552	552	559
2275.59	0	-5	566	576	588	602	625	652	689	741	814	913	1056	1246	1505	1853	2304	2862	3487
2259.20	0	-5	4091	4572	4881	5055	5143	5112	4844	4297	3658	3087	2614	2223	1895	1618	1388	1194	1034
2242.81	0	-6	8985	7903	7015	6261	5658	5158	4744	4408	4136	3922	3751	3602	3489	3388	3338	3290	3236
2226.41	0	-6	3193	3130	3102	3046	3030	3014	2977	2939	2930	2909	2892	2885	2896	2892	2918	2975	3026
2210.02	0	-6	3113	3148	3199	3216	3239	3248	3253	3225	3163	3080	3024	2956	2915	2884	2850	2837	2807
2193.63	0	-6	2809	2772	2778	2771	2769	2743	2766	2767	2770	2778	2781	2796	2804	2819	2829	2835	2848
2177.24	0	-6	2857	2868	2874	2896	2898	2901	2912	2928	2941	2940	2943	2944	2973	2975	2985	3007	3010
2154.10	3	-6	3119	3226	3335	3457	3552	3658	3745	3850	3936	4011	4150	4359	4192	4030	3901	3793	3712
2022.96	3	-6	3610	3494	3390	3264	3151	3033	2896	2788	2685	2565	2457	2367	2294	2237	2145	2094	2051
1891.83	3	-6	2020	2005	2021	2037	2034	2056	2189	2271	2495	2348	2293	2357	2497				
1797.33	1	-6	2474	2515	2525	2553	2597	2623	2643	2688	2735	2770	2811	2853	2898	3034	2994	3150	3161
1764.55	1	-6	3227	3303	3380	3490	3643	3659	3755	4011	3989	4105	4226	4414	4525	4815	4903	5128	5334
1731.76	1	-5	554	582	600	626	654	683	713	754	782	822	865	912	962	1016	1074	1130	1213
1698.98	1	-5	1267	1348	1431	1516	1610	1712	1819	1933	2064	2185	2324	2465	2616	2774	2937	3109	3290
1666.19	1	-5	3470	3662	3856	4042	4237	4428	4630	4801	4964	5122	5253	5360	5445	5497	5506	5491	5434
1633.41	1	-5	5319	5169	4997	4800	4564	4325	4066	3810	3565	3320	3092	2879	2684	2507	2346	2201	2070
1600.63	1	-5	1952	1845	1752	1670	1595	1528	1470	1415	1368	1329	1293	1262	1238	1209	1191	1170	1169
1567.84	1	-5	1146	1136	1129	1127	1137	1132	1121	1139	1125	1131	1133	1134	1145	1143	1151	1172	1166
1535.06	1	-5	1175	1188	1195	1202	1226	1235	1235	1254	1264	1279	1280	1322	1314	1324	1342	1343	1360
1502.28	1	-5	1376	1391	1425	1433	1440	1465	1494	1514	1542	1574	1610	1650	1700	1735	1791	1862	1917
1469.49	1	-5	1995	2082	2176	2316	2407	2531	2679	2814	2970	3111	3245	3348	3424	3468	3476	3453	3416
1436.71	1	-5	3392	3329	3267	3228	3205	3196	3195	3200	3211	3199	3160	3105	3039	2972	2900	2818	2732
1403.92	1	-5	2648	2568	2492	2424	2367	2326	2286	2276	2294	2340	2442	2640	2997	3591	4381	4753	4123
1371.14	1	-5	3198	2550	2165	1928	1769	1639	1551	1480	1429	1385	1353	1327	1303	1282	1267	1249	1235
1338.36	1	-5	1217	1198	1179	1165	1152	1140	1131	1119	1112	1100	1089	1078	1065	1053	1044	1036	1025
1305.57	1	-5	1018	1011	1005	996	990	987	977	974	968	967	963	960	954	953			
1272.79	3	-5	946	932	930	934	931	935	933	935	934	948	939	950	970	987	999	1011	1026
1147.44	1	-5	1031	1037	1041	1044	1050	1055	1059	1065	1070	1076	1083	1088	1098	1109	1121	1130	1143
1114.65	1	-5	1155	1166	1179	1191	1206	1220	1234	1250	1261	1281	1298	1315	1330	1348	1366	1380	1400
1081.87	1	-5	1420	1440	1464	1493	1516	1546	1583	1614	1656	1706	1753	1811	1891	1972	2076	2214	2376
1049.09	1	-5	2582	2836	3125	3421	3562	3790	3747	3567	3293	3018	2756	2530	2346	2179	2049	1947	1861
1016.3	1	-5	1795	1739	1699	1665	1635	1613	1595	1576	1563	1554	1545	1535	1530	1526	1517	1519	1508
983.52	1	-5	1503	1503	1500	1503	1506	1511	1513	1518	1521	1522	1531	1539	1545	1557	1570	1584	
951.70	0	-5	1589	1599	1604	1611	1622	1628	1640	1650	1660	1668	1682	1693	1709	1722	1747	1761	1788
935.31	0	-5	1811	1843	1886	1927	1987	2056	2146	2260	2392	2569	2792	3074	3411	3801	4185	4424	4423
918.91	0	-5	4185	3795	3338	2930	2651	2468	2355	2282	2228	2190	2155	2129	2108	2094	2085	2082	2081
902.52	0	-5	2076	2080	2078	2083	2086	2091	2103	2116	2124	2140	2152	2164	2175	2192			
886.13	2	-5	2237	2286	2355	2432	2525	2607	2683	2764	2861	2964	3070	3169	3278	3398	3524	3642	3765
820.56	2	-5	3896	4032	4183	4330	4478	4631	4785	4957	5114	5292	5461	5652	5857	6101	6362	6698	7106
754.99	2	-5	7513	7715	7713	7601	7571												

Table 6.5. Imaginary refractive indices between 8000.25 and 700.0 cm⁻¹ of liquid water-acetonitrile with $x_{\text{CH}_3\text{CN}}=0.70$ at 25 °C.^{a,b}

cm ⁻¹	XE	YE	0	1	2	3	4	5	6	7	8	9	10	11	12	13	14	15	16
8000.25	7	0	0	0	0	0	0	0	0	0	0	0	0	0	0	0	0	0	0
6488.33	5	-7	0	3948	98	0	0	463	0	1549	1758	0	1383	0	0	1274	0	2856	1264
5963.78	5	-7	623	0	902	305	0	22	438	969	708	0	0	1231	417	17	0	314	0
5439.24	5	-7	0	2	0	0	63	416	1574	1293	861	495	509	300	385	563	0	787	521
4914.70	5	-7	454	305	220	359	38	395	459	30	46	292	147	227	250	1525	597	3257	2493
4390.15	5	-7	4780	6899	2597	286	310	316	0	0	84	223	693	1233	3382	2225	1800	1182	428
3865.61	5	-5	3	16	8	31	63	167	761	2008	2826	3229	3362	3266	3070	2917	2719	2394	1976
3356.50	4	-5	1771	1604	1472	1375	1314	1263	1214	1149	1058	958	881						
3200.29	1	-6	8654	8411	8153	7931	7723	7577	7436	7332	7217	7149	7119	7115	7157	7270	7465	7697	8002
3167.51	1	-6	8301	8481	8175	7499	6827	6366	6029	5792	5589	5440	5291	5197	5095	5031	4931	4925	4863
3134.72	1	-6	4802	4771	4691	4624	4593	4551	4538	4513	4458	4452	4411	4402	4362	4309	4269	4261	4221
3101.94	1	-6	4215	4184	4171	4174	4169	4147	4141	4109	4099	4100	4080	4052	4039	4059	4009	4027	4019
3069.15	1	-6	4021	4061	4013	4036	4033	4046	4039	4037	4093	4101	4163	4167	4196	4248	4294	4408	4399
3036.37	1	-6	4439	4518	4650	4732	4847	5009	5152	5364	5530	5800	6048	6384	6843	7041	7398	7729	7966
3003.59	1	-6	8127	8033	7862	7563	7197	6809	6404	6030	5702	5406	5122	4919	4720	4590	4439	4366	4284
2970.80	1	-6	4229	4189	4178	4161	4167	4184	4214	4360	4540	4810	5290	6131	7375	8769	9163	8089	6724
2938.02	1	-6	5735	5017	4512	4064	3744	3470	3268	3075	2920	2776	2682	2582	2521	2474	2395	2310	2297
2903.31	2	-6	2155	2061	1964	1888	1807	1713	1655	1585	1493	1444	1385	1319	1261	1210	1174	1121	1099
2837.74	2	-6	1051	994	924	850	789	731	691	659	630	555	532	522	486	469	444	418	414
2772.17	2	-7	3991	3730	3517	3378	3404	3244	3111	3224	3302	3423	3425	2957	2500	2171	2090	1881	1762
2706.60	2	-7	1438	1392	1480	1381	1344	1187	1287	1498	1594	1577	1282	944	1084	1045	1084	1384	
2646.82	1	-6	164	191	227	288	373	460	585	737	925	1070	1060	893	765	641	523	444	350
2614.04	1	-7	2768	2443	2013	1724	1414	1106	1092	1252	972	742	712	1095	886	1178	1075	759	1164
2581.25	1	-7	736	742	1221	645	778	847	927	982	1045								
2558.11	3	-7	1075	1260	1460	1579	1902	2290	2828	3569	4197	5128	5467	5603	5307	5684	6518	7859	9170
2426.98	3	-6	1061	1385	1753	1613	1195	908	769	722	733	793	923	1067					
2341.16	0	-6	1081	1082	1092	1084	1107	1097	1107	1119	1116	1140	1132	1170	1191	1209	1236	1270	1296
2324.77	0	-6	1342	1382	1425	1472	1514	1561	1619	1684	1737	1803	1879	1975	2061	2175	2296	2440	2624
2308.37	0	-5	282	306	336	373	416	472	541	626	732	856	1000	1151	1305	1429	1509	1528	1478
2291.98	0	-5	1380	1255	1121	999	891	803	732	671	621	582	546	522	500	488	479	477	478
2275.59	0	-5	480	488	495	507	523	542	567	602	654	729	827	963	1148	1404	1746	2194	2741
2259.20	0	-5	3348	3948	4498	5006	5479	5797	5692	5106	4333	3643	3076	2607	2204	1859	1570	1329	1126
2242.81	0	-6	9595	9217	7081	6156	5384	4750	4218	3780	3427	3136	2889	2695	2538	2416	2335	2260	2195
2226.41	0	-6	2124	2047	1994	1947	1912	1865	1828	1786	1756	1711	1692	1676	1644	1638	1645	1658	1699
2210.02	0	-6	1745	1788	1849	1901	1939	2006	2052	2045	1936	1820	1734	1645	1590	1541	1502	1456	1413
2193.63	0	-6	1391	1370	1356	1313	1307	1300	1290	1278	1266	1270	1274	1260	1265	1270	1262	1276	1279
2177.24	0	-6	1279	1275	1296	1281	1292	1295	1294	1292	1307	1295	1306	1293	1294	1305	1296	1308	1306
2154.10	3	-6	1359	1432	1491	1563	1628	1693	1792	1876	1989	2093	2265	2537	2393	2238	2174	2118	2079
2022.96	3	-6	2035	2017	1951	1896	1850	1772	1727	1658	1600	1537	1484	1421	1353	1313	1273	1248	1219
1891.83	3	-6	1178	1182	1236	1217	1207	1237	1323	1419	1633	1457	1346	1329	1366				
1797.33	1	-6	1365	1374	1382	1376	1409	1416	1433	1426	1442	1447	1459	1467	1476	1543	1513	1574	1579
1764.55	1	-6	1598	1624	1652	1690	1782	1776	1811	1932	1905	1958	1978	2074	2125	2255	2285	2371	2476
1731.76	1	-6	2580	2675	2716	2814	2933	3031	3160	3332	3440	3583	3770	3938	4132	4379	4612	4837	5204
1698.98	1	-5	542	579	616	655	697	743	795	850	913	975	1047	1123	1203	1290	1383	1483	1593
1666.19	1	-5	1706	1827	1953			7757	2505	2646	2783	2912	3039	3149	3245	3323	3372	3393	3388
1633.41	1	-5	3336	3261	3152			2712	2532	2355	2185	2021	1867	1723	1595	1477	1374	1282	1199
1600.63	1	-5	1128	1068	1011			886	854	826	805	785	769	760	747	738	734	730	736
1567.84	1	-6	7292	7324	7383	74		7642	7711	7960	7886	8030	8110	8223	8344	8434	8597	8780	8834
1535.06	1	-5	900	914	925	943	968	975	986	1006	1020	1038	1045	1104	1081	1098	1117	1125	1144
1502.28	1	-5	1158	1179	1219	1225	1241	1265	1297	1320	1353	1389	1437	1476	1544	1583	1648	1719	1791
1469.49	1	-5	1887	1987	2101	2279	2375	2523	2696	2861	3042	3210	3364	3476	3561	3608	3601	3570	3520
1436.71	1	-5	3461	3408	3314	3265	3229	3215	3213	3222	3239	3214	3180	3123	3052	2971	2887	2796	2688
1403.92	1	-5	2595	2502	2422	2338	2273	2236	2188	2185	2207	2272	2405	2647	3077	3769	4609	4685	4126
1371.14	1	-5	3123	2431	2007	1737	1551	1408	1304	1224	1164	1110	1070	1039	1011	985	962	941	921
1338.36	1	-6	8987	8765	8529	8315	8193	8015	7866	7725	7589	7414	7251	7103	6949	6831	6679	6545	6419
1305.57	1	-6	6336	6257	6148	6046	5944	5865	5766	5694	5635	5570	5513	5456	5400	5352			
1272.79	3	-6	5145	4985	4892	4842	4812	4792	4751	4778	4705	4851	4881	4960	5120	5270	5384	5487	5625
1147.44	1	-6	5671	5704	5744	5796	5818	5882	5928	5980	6046	6079	6180	6253	6329	6425	6531	6628	6746
1114.65	1	-6	6864	6990	7104	7237	7360	7521	7654	7818	7999	8151	8308	8509	8686	8869	9065	9223	9429
1081.87	1	-5	963	985	1009	1041	1067	1099	1140	1174	1219	1273	1325	1393	1484	1571	1686	1848	2036
1049.09	1	-5	2276	2575	2910	3254	3528	3660	3594	3361	3032	2718	2417	2153	1946	1747	1597	1479	1376
1016.3	1	-5	1298	1231	1178	1135	1101	1069	1048	1022	1005	987	972	961	948	936	924	917	906
983.52	1	-6	8953	8879	8797	8702	8663	8627	8600	8601	8568	8522	8487	8481	8453	8489	8514	8568	8616
951.70	0	-6	8664	8698	8733	8786	8797	8858	8900	8987	9023	9097	9162	9273	9347	9485	9586	9759	9909
935.31	0	-5	1010	1038	1070	1107	1158	1216	1297	1396	1521	1682	1882	2134	2440	2811	3228	3607	3840
918.91	0	-5	3821	3537	3001	2432	2008	1736	1558	1442	1364	1304	1255	1208	1169	1135	1115	1095	1083
902.52	0	-5	1072	1063	1049	1037	1028	1027	1024	1023	1021	1028	1026	1030	1034	1036			
886.13	2	-5	1041	1043	1053	1081	1113	1138	1156	1177	1203	1232	1268	1298	1331	1369	1407	1452	1498
820.56	2	-5	1539	1589	1638	1692	1748	1811	1873	1934	2005	2085	2162	2262	2375	2506	2689	2943	3300

Table 6.6. Imaginary refractive indices between 8000.25 and 700.0 cm⁻¹ of liquid acetonitrile at 25 °C.^{a,b}

cm ⁻¹	XE	YE	0	1	2	3	4	5	6	7	8	9	10	11	12	13	14	15	16
8000.25	7	0	0	0	0	0	0	0	0	0	0	0	0	0	0	0	0	0	0
6488.33	5	-7	0	3216	0	0	0	0	0	0	0	0	0	0	0	0	0	0	0
5963.78	5	0	0	0	0	0	0	0	0	0	0	0	0	0	0	0	0	0	0
5439.24	5	0	0	0	0	0	0	0	0	0	0	0	0	0	0	0	0	0	0
4914.70	5	-7	0	0	0	0	0	0	0	0	0	0	0	0	0	0	33	2978	1702
4390.15	5	-7	5334	5980	733	0	0	0	0	0	0	0	0	0	905	0	0	0	0
3865.61	5	-7	0	0	0	0	0	0	0	347	316	48	227	177	56	0	64	276	860
3356.50	4	-6	105	123	226	197	254	241	297	354	477	110	1487						
3200.29	1	-6	1500	1427	1302	1221	1176	1130	1129	1110	1079	1116	1156	1292	1362	1482	1700	2050	2646
3167.51	1	-6	3527	4467	4644	3870	2948	2347	1983	1737	1591	1505	1442	1382	1340	1314	1321	1336	1381
3134.72	1	-6	1419	1444	1463	1473	1479	1500	1541	1581	1606	1629	1665	1727	1763	1783	1773	1801	1822
3101.94	1	-6	1880	1863	1911	1921	1981	2003	2012	2065	2089	2153	2146	2173	2209	2266	2254	2313	2327
3069.15	1	-6	2392	2489	2462	2484	2542	2593	2621	2653	2688	2756	2868	2878	2927	3000	3068	3369	3199
3036.37	1	-6	3311	3411	3569	3685	3822	3968	4151	4396	4561	4817	5103	5415	6104	6142	6556	6895	7173
3003.59	1	-6	7421	7284	7109	6827	6510	6092	5692	5346	5033	4779	4506	4332	4190	4076	3976	3909	3853
2970.80	1	-6	3834	3827	3824	3781	3816	3842	3912	4029	4205	4452	4822	5438	6336	7282	7526	6783	5815
2938.02	1	-6	5082	4488	4078	3727	3458	3212	3003	2841	2718	2612	2513	2401	2371	2276	2233	2167	2116
2903.31	2	-6	2019	1898	1806	1738	1650	1612	1559	1478	1399	1387	1290	1231	1153	1086	1059	1035	1034
2837.74	2	-7	9934	9175	8184	7718	6925	6250	5909	5595	5345	4833	4433	4302	3999	3926	3478	3419	3169
2772.17	2	-7	3117	2910	2811	2597	2768	2566	2419	2510	2514	2546	2515	2532	2211	1721	1616	1378	1385
2706.60	2	-7	1124	1019	855	902	688	641	883	954	1176	1173	1099	1041	622	481	564	738	
2646.82	1	-6	101	96	114	154	174	245	393	603	974	1415	1561	1314	1091	898	759	623	476
2614.04	1	-7	3860	3130	2600	2068	1469	1180	1104	711	773	662	409	535	425	547	507	400	396
2581.25	1	-7	525	390	386	512	486	605	738	823	660								
2558.11	3	-7	620	696	1000	953	1291	1833	2477	3072	3814	4687	5127	4937	4650	4756	5653	7178	8304
2426.98	3	-6	991	1340	1713	1516	1024	701	542	471	460	478	589	733					
2341.16	0	-7	7675	7440	7748	7586	7747	7777	7760	7786	7697	7741	7817	8147	8132	8498	8824	8998	
2324.77	0	-6	926	952	999	1018	1085	1094	1146	1205	1245	1308	1357	1432	1484	1583	1676	1772	1918
2308.37	0	-5	208	229	251	281	311	349	400	460	534	625	734	859	997	1136	1262	1356	1390
2291.98	0	-5	1359	1274	1153	1021	901	800	714	644	588	537	495	462	433	413	396	385	378
2275.59	0	-5	373	374	376	381	386	393	398	407	425	448	480	517	571	646	759	925	1158
2259.20	0	-5	1501	1998	2733	3792	5153	6370	6683	6029	5086	4288	3659	3122	2638	2211	1854	1550	1227
2242.81	0	-5	1086	911	771	653	559	480	414	358	311	274	241	214	192	176	166	158	149
2226.41	0	-6	1436	1302	1225	1168	1140	1082	1054	1022	972	941	881	849	808	760	714	706	679
2210.02	0	-6	682	701	737	788	933	1115	1285	1303	1165	1022	895	900	744	677	611	550	501
2193.63	0	-7	4520	4393	3922	3656	3437	3175	3051	2737	2558	2434	2255	2101	2014	2138	1799	1951	1869
2177.24	0	-7	1921	1828	1846	1791	1669	1689	1613	1509	1597	1442	1341	1322	1217	1228	1068	1024	941
2154.10	3	-7	658	492	266	197	315	224	124	375	955	1513	3176	5455	3687	1766	908	566	298
2022.96	3	-7	191	279	236	245	157	145	442	497	570	460	555	705	816	1116	1185	1279	1516
1891.83	3	-7	1636	1915	3027	3175	3042	3564	4545	6234	7701	7267	5087	4574	4378				
1797.33	1	-7	4390	4452	4478	4533	4539	4515	4468	4469	4287	4104	4000	4025	3998	3954	3731	3901	3896
1764.55	1	-7	3903	3868	3880	4035	4065	4222	4135	4268	4389	4226	4391	4279	4606	4503	4834	4952	4990
1731.76	1	-7	4852	4552	4585	4097	4089	3762	3725	3677	3658	3676	3756	3679	3643	3676	3798	3784	3950
1698.98	1	-7	4038	4198	4538	4488	4869	4910	5267	5440	5820	5968	6155	6399	6724	6883	7083	7378	7587
1666.19	1	-6	764	792	809	838	868	851	911	904	932	930	943	1008	1050	1061	1121	1142	1181
1633.41	1	-6	1230	1264	1303	1334	1378	1412	1417	1434	1489	1541	1580	1627	1706	1775	1840	1941	2003
1600.63	1	-6	2117	2170	2292	2382	2495	2579	2721	2795	2929	3063	3180	3396	3438	3572	3721	3867	4052
1567.84	1	-6	4241	4417	4682	4843	5052	5266	5461	5909	5892	6152	6299	6511	6500	6886	7159	7283	7513
1535.06	1	-5	768	790	806	840	881	873	899	913	940	954	970	1028	1007	1032	1055	1068	1086
1502.28	1	-5	1108	1129	1185	1175	1187	1224	1250	1280	1319	1357	1422	1456	1555	1572	1654	1718	1805
1469.49	1	-5	1918	2031	2169	2433	2482	2641	2842	3046	3253	3443	3537	3753	3841	3899	3868	3620	3751
1436.71	1	-5	3655	3617	3461	3384	3331	3305	3305	3321	3372	3313	3299	3242	3172	3083	2993	2902	2769
1403.92	1	-5	2671	2567	2485	2390	2326	2272	2235	2233	2267	2349	2507	2796	3293	4058	4927	5073	4196
1371.14	1	-5	3141	2410	2611	2670	1464	1302	1188	1097	1024	959	912	879	834	806	780	751	722
1338.36	1	-6	6964	6729	6378	6131	5908	5715	5498	5318	5173	4889	4727	4497	4331	4110	3964	3812	3597
1305.57	1	-6	3469	3347	3210	3075	2925	2814	2690	2570	2486	2369	2311	2189	2146	2035	--	--	--
1272.79	3	-6	1756	1459	136	1137	1019	930	893	860	804	797	797	838	905	999	1084	1144	1193
1147.44	1	-6	1240	1236	1257	1277	1314	1353	1387	1419	1471	1541	1591	1622	1692	1778	1864	1959	2073
1114.65	1	-6	2182	2287	2386	2541	2673	2765	2912	3082	3231	3417	3559	3735	3903	4075	4281	4456	4664
1081.87	1	-5	487	507	531	572	592	625	669	700	743	810	859	926	1037	1119	1246	1424	1626
1049.09	1	-5	1894	2227	2614	3011	3319	3462	3359	3083	2718	2351	2003	1710	1492	1257	1090	961	841
1016.3	1	-6	7515	6751	6147	5651	5236	4855	4594	4272	4032	3795	3596	3416	3256	3084	2895	2778	2595
983.52	1	-6	2460	2321	2208	2091	1972	1860	1790	1721	1648	1561	1496	1416	1357	1310	1289	1314	1316
951.70	0	-6	1327	1349	1370	1368	1393	1408	1428	1450	1502	1526	1590	1661	1716	1773	1856	1956	2062
935.51	0	-5	221	238	259	287	324	371	430	505	597	716	867	1061	1290	1546	1822	2157	2633
918.91	0	-5	3182	3498	3145	2370	1698	1247	964	779	660	582	524	466	409	356	316	282	263
902.52	0	-6	2468	2361	2220	1999	1832	1687	1553	1475	1396	1373	1325	1282	1265	1222			
886.13	2	-6	1178	968	818	803	852	847	778	752	712	651	700	658	644	611	649	654	653
820.56	2	-6	699	694	734	702	717	795	860	903	988	1067	1219	1429	1726	2216	3033	4419	7059
754.99	2	-5	1158	1596	1564	1213	820	534	358	253	186	154	136	122	107	105	103		

Note: Footnotes follow Table 6.10

Table 6.7. Real refractive indices between 8000.25 and 700 cm^{-1} of liquid mixture water -acetonitrile with $x_{\text{CH}_3\text{CN}}=0.20$ at 25°C ^{a,b}

cm^{-1}	$\lambda/\mu\text{m}$	0	1	2	3	4	5	6	7	8	9	10	11	12	13	14	15	16
8000.25	7	13211	13209	13208	13206	13204	13203	13200	13198	13196	13193	13190	13187	13182				
6488.33	5	13180	13183	13181	13183	13178	13178	13173	13173	13179	13186	13181	13181	13176	13176	13176	13173	13170
5963.78	5	13171	13169	13167	13166	13165	13165	13162	13160	13159	13157	13156	13160	13158	13153	13152	13149	13147
5439.24	5	13145	13143	13141	13138	13136	13132	13131	13128	13128	13128	13126	13123	13121	13118	13115	13112	13109
4914.70	5	13104	13100	13096	13093	13090	13086	13087	13078	13074	13070	13066	13061	13058	13054	13047	13039	13031
4390.15	5	13023	13015	13007	12997	12988	12977	12966	12953	12940	12925	12908	12890	12872	12849			
3981.32	3	12843	12838	12832	12826	12819	12813	12805	12797	12790	12781	12774	12764	12755	12746	12736	12725	12714
3850.18	3	12702	12690	12678	12665	12650	12634	12619	12604	12585	12565	12545	12524	12501	12476	12447	12417	12382
3719.05	3	12345	12302	12253	12201	12145	12087	12036	11994	11966	11952	11950	11958	11970	11983	12000	12016	12037
3587.91	3	12059	12082	12111	12142	12176	12216	12257	12304	12350	12397	12446	12498	12550	12604	12659	12718	12780
3456.78	3	12844	12910	12981	13053	13129	13205	13279	13353	13420	13484	13543	13598	13643	13685	13720	13750	13776
3325.64	3	13800	13822	13841	13863	13884	13905	13929	13952	13978	14004	14032	14057	14081	14104	14122	14139	14152
3194.50	3	14159	14162	14161	14164	14163	14154	14143	14132	14119	14105	14091	14076	14061	14046	14030	14015	13999
3067.23	2	13991	13983	13975	13967	13959	13951	13943	13935	13927	13919	13911	13903	13896	13889	13885	13881	13879
3001.66	2	13877	13874	13869	13863	13856	13849	13841	13833	13825	13817	13809	13800	13790	13779	13766	13757	13802
2936.09	2	13794	13786	13778	13770	13763	13755	13748	13742	13736	13730	13724	13719	13713	13708	13704	13706	13693
2870.52	2	13688	13684	13679	13674	13669	13665	13660	13655	13650	13645	13642	13638	13634	13629	13625	13621	13617
2804.95	2	13613	13609	13605	13601	13597	13593	13590	13586	13582	13579	13576	13572	13569	13565	13562	13558	13555
2739.39	2	13551	13548	13545	13542	13539	13535	13532	13529	13526	13523	13520	13517	13514	13511	13508	13505	13502
2673.82	2	13500	13497	13494	13491	13488	13486	13482	13479	13476	13473	13470	13467	13464	13461	13458	13455	13452
2608.25	2	13457	13454	13451	13449	13446	13444	13441	13439	13437	13434	13431	13429					
2558.11	3	13425	13420	13415	13411	13406	13401	13397	13393	13388	13384	13380	13376	13372	13367	13362	13358	13354
2426.98	3	13350	13345	13343	13341	13338	13333	13328	13322	13317	13311	13305	13299					
2340.19	1	13297	13295	13294	13291	13289	13287	13284	13282	13279	13277	13274	13271	13267	13264	13260	13256	13250
2307.41	1	13244	13236	13228	13223	13224	13239	13267	13291	13309	13300	13294	13288	13279	13271	13263	13254	13245
2274.63	1	13234	13221	13204	13181	13154	13123	13103	13128	13141	13157	13169	13181	13192	13202	13210	13217	13224
2241.84	1	13419	13406	13394	13384	13376	13368	13363	13358	13353	13350	13346	13342	13339	13336	13333	13330	13328
2209.06	1	13327	13327	13326	13324	13323	13321	13320	13318	13317	13315	13314	13313	13312	13311	13310	13309	13308
2176.27	1	13307	13306	13306	13305	13304	13303	13303	13302	13301	13301							
2151.20	3	13299	13298	13297	13296	13295	13294	13294	13294	13293	13293	13292	13294	13294	13292	13291	13289	13287
2020.07	3	13285	13282	13279	13276	13272	13268	13263	13258	13253	13248	13242	13236	13230	13224	13216	13209	13202
1888.93	3	13194	13186	13177	13169	13160	13151	13141	13131	13120	13109	13096	13083	13068				
1794.44	1	13065	13061	13057	13053	13049	13045	13040	13036	13032	13027	13022	13017	13013	13008	13003	12997	12992
1761.65	1	12986	12981	12975	12969	12963	12957	12951	12944	12938	12931	12924	12917	12909	12902	12894	12887	12879
1728.87	1	12871	12863	12855	12847	12839	12830	12821	12813	12805	12796	12788	12780	12772	12764	12757	12750	12743
1696.09	1	12738	12733	12729	12725	12723	12722	12723	12724	12728	12733	12740	12748	12759	12771	12785	12802	12822
1663.30	1	12843	12868	12894	12924	12955	12990	13027	13067	13108	13152	13197	13243	13290	13335	13380	13424	13464
1630.52	1	13503	13537	13568	13594	13615	13632	13645	13653	13658	13660	13660	13656	13652	13646	13638	13630	13621
1597.73	1	13612	13602	13592	13582	13572	13563	13553	13544	13535	13525	13517	13508	13500	13492	13484	13477	13469
1564.95	1	13463	13455	13449	13443	13437	13431	13425	13420	13415	13409	13404	13399	13394	13389	13383	13378	13374
1532.17	1	13369	13366	13362	13358	13354	13349	13346	13342	13339	13335	13332	13328	13325	13321	13318	13314	13311
1499.38	1	13308	13304	13301	13297	13294	13290	13287	13284	13280	13276	13273	13268	13265	13262	13258	13254	13251
1466.60	1	13248	13245	13242	13241	13239	13239	13240	13242	13245	13250	13256	13263	13271	13278	13284	13290	13294
1433.81	1	13297	13300	13302	13304	13306	13308	13312	13316	13320	13324	13327	13330	13332	13334	13335	13334	13334
1401.03	1	13332	13331	13327	13324	13319	13314	13308	13300	13291	13280	13268	13256	13256	13251	13241	13231	13221
1368.25	1	13418	13405	13394	13383	13375	13367	13360	13354	13349	13344	13340	13336	13332	13329	13326	13324	13321
1335.46	1	13318	13315	13313	13310	13308	13305	13303	13300	13298	13296	13295	13293	13291	13289	13287	13285	13283
1302.68	1	13281	13280	13277	13276	13274	13272	13269	13268	13266	13264	13262	13261	13259				
1271.82	3	13252	13245	13239	13233	13226	13220	13214	13206	13200	13194	13186	13179	13170	13163	13155	13146	13138
1146.47	1	13136	13134	13132	13130	13128	13125	13123	13120	13118	13115	13113	13110	13107	13104	13101	13098	13096
1113.69	1	13093	13090	13087	13084	13081	13078	13075	13073	13069	13067	13064	13061	13058	13055	13052	13049	13045
1080.91	1	13042	13038	13034	13031	13026	13022	13018	13013	13008	13004	12999	12994	12989	12983	12978	12973	12969
1048.12	1	12966	12965	12970	12980	12997	13017	13037	13051	13060	13064	13063	13060	13054	13048	13042	13035	13028
1015.34	1	13021	13014	13008	13001	12995	12989	12983	12976	12971	12965	12959	12953	12947	12941	12934	12928	12922
982.55	1	12916	12910	12904	12898	12891	12885	12878	12872	12865	12858	12851	12844	12837	12829	12821	12814	12805
949.77	1	12798	12789	12781	12772	12763	12753	12742	12731	12718	12704	12688	12671	12657	12645	12632	12625	
916.99	1	12782	12761	12744	12729	12716	12704	12693	12683	12673	12665	12656	12647	12640	12632	12625		
886.13	2	12609	12595	12580	12569	12558	12550	12543	12533	12527	12522	12518	12514	12512	12512	12514	12518	12524
820.56	2	12528	12535	12545	12556	12566	12579	12592	12607	12627	12649	12666	12687	12712	12738	12764	12796	12829
754.99	2	12879	12935	12978	13021	13060	13099	13141	13182	13223	13262	13298	13341	13392	13450	13501		

Note: Footnotes follow Table 6.10.

Table 6.8. Real refractive indices between 8000.25 and 700.0 cm^{-1} of liquid water-acetonitrile with $x_{\text{CH}_3\text{CN}}=0.50$ at 25 $^{\circ}\text{C}$.^{a,b}

cm^{-1}	ΔE	0	1	2	3	4	5	6	7	8	9	10	11	12	13	14	15	16
8000.25	7	13234	13233	13232	13232	13231	13230	13229	13229	13228	13227	13226	13224	13223				
6488.33	5	13223	13222	13223	13222	13221	13221	13221	13221	13220	13220	13219	13219	13219	13218	13218	13218	13217
5963.78	5	13216	13216	13215	13215	13214	13214	13213	13212	13212	13211	13208	13213	13211	13210	13209	13208	13207
5439.24	5	13206	13205	13205	13204	13203	13202	13201	13199	13202	13199	13198	13197	13196	13195	13193	13192	13191
4914.70	5	13189	13188	13187	13185	13183	13182	13180	13178	13176	13174	13172	13170	13167	13167	13162	13158	13157
4390.15	5	13154	13155	13149	13145	13140	13136	13131	13125	13120	13113	13105	13097	13091	13081	13072	13059	13044
3865.61	5	13025	13005	12976	12940	12892	12815	12695	12657	12722	12813	12920	13031	13120	13205	13304	13404	13475
3356.50	4	13495	13504	13509	13510	13515	13521	13533	13547	13561	13569	13575						
3200.29	1	13576	13576	13576	13574	13573	13572	13571	13569	13568	13566	13564	13563	13561	13560	13560	13560	13562
3167.51	1	13564	13567	13571	13572	13571	13568	13566	13563	13561	13558	13556	13554	13551	13549	13547	13545	13543
3134.72	1	13542	13540	13538	13536	13534	13532	13530	13528	13527	13525	13523	13521	13520	13518	13516	13515	13513
3101.94	1	13511	13509	13507	13506	13504	13503	13501	13499	13498	13495	13494	13493	13491	13490	13488	13486	13485
3069.15	1	13483	13481	13480	13478	13476	13475	13473	13471	13470	13468	13466	13465	13463	13461	13459	13458	13456
3036.37	1	13454	13452	13450	13449	13447	13445	13444	13442	13441	13440	13439	13438	13438	13439	13441	13443	13446
3003.59	1	13450	13454	13458	13460	13462	13463	13463	13463	13462	13460	13459	13457	13455	13452	13450	13448	13446
2970.80	1	13444	13442	13439	13437	13435	13432	13429	13426	13422	13418	13414	13410	13411	13423	13445	13461	13465
2938.02	1	13464	13462	13459	13456	13453	13451	13448	13446	13444	13441	13439	13438	13436	13434	13432	13431	13429
2903.31	2	13427	13424	13422	13419	13417	13415	13413	13411	13408	13406	13405	13402	13401	13399	13397	13395	13393
2837.74	2	13392	13390	13388	13387	13385	13383	13381	13380	13378	13376	13374	13373	13371	13370	13368	13366	13365
2772.17	2	13363	13362	13360	13359	13357	13356	13355	13353	13352	13350	13349	13348	13347	13346	13344	13343	13342
2706.60	2	13340	13339	13337	13336	13335	13333	13332	13331	13330	13329	13327	13326	13325	13323	13322	13320	
2646.82	1	13319	13318	13317	13316	13316	13315	13315	13315	13316	13317	13318	13319	13319	13319	13318	13318	13317
2614.04	1	13316	13315	13314	13314	13313	13312	13311	13311	13310	13309	13309	13308	13307	13306	13306	13305	
2581.25	1	13304	13304	13303	13302	13302	13301	13301	13300	13299								
2558.11	3	13297	13295	13293	13290	13288	13286	13283	13281	13279	13277	13275	13273	13271	13268	13265	13263	13260
2426.98	3	13257	13255	13256	13258	13257	13254	13249	13244	13239	13234	13229	13223					
2341.16	0	13222	13222	13221	13220	13219	13218	13217	13216	13215	13214	13213	13212	13210	13209	13208	13206	13205
2324.77	0	13204	13202	13201	13199	13197	13196	13194	13192	13190	13188	13186	13184	13181	13178	13175	13172	13169
2308.37	0	13165	13161	13157	13152	13148	13143	13138	13134	13131	13131	13134	13141	13154	13170	13190	13209	13225
2291.98	0	13237	13243	13246	13246	13243	13240	13236	13231	13226	13221	13216	13210	13205	13199	13193	13187	13180
2275.59	0	13174	13167	13160	13152	13143	13133	13121	13108	13094	13077	13059	13040	13020	13001	12988	12985	13000
2259.20	0	13035	13088	13151	13214	13279	13352	13429	13490	13523	13534	13535	13530	13522	13511	13500	13488	13476
2242.81	0	13463	13452	13441	13431	13421	13412	13404	13396	13389	13382	13376	13371	13365	13361	13356	13352	13349
2226.41	0	13346	13343	13339	13337	13334	13332	13329	13327	13325	13322	13320	13318	13316	13314	13312	13311	13309
2210.02	0	13308	13307	13306	13305	13305	13304	13304	13304	13303	13303	13302	13301	13300	13299	13298	13297	13295
2193.63	0	13295	13294	13293	13292	13291	13290	13289	13288	13287	13286	13286	13285	13284	13283	13283	13282	13282
2177.24	0	13281	13280	13280	13279	13279	13278	13278	13277	13277	13276	13276	13275	13275	13274	13273	13273	13273
2154.10	3	13269	13266	13264	13262	13260	13259	13257	13256	13255	13254	13253	13254	13256	13256	13255	13253	13253
2022.96	3	13251	13250	13249	13247	13246	13244	13242	13240	13237	13235	13232	13225	13226	13223	13219	13216	13212
1891.83	3	13208	13204	13200	13197	13192	13187	13182	13177	13173	13170	13163	13157	13151				
1797.33	1	13148	13146	13144	13143	13141	13139	13137	13135	13133	13131	13129	13126	13124	13123	13120	13116	13114
1764.55	1	13112	13109	13107	13104	13101	13098	13095	13092	13089	13086	13082	13079	13075	13072	13068	13064	13061
1731.76	1	13057	13053	13049	13045	13040	13036	13031	13028	13022	13018	13013	13007	13002	12997	12991	12987	12980
1698.98	1	12977	12971	12967	12961	12956	12951	12947	12942	12939	12936	12934	12932	12931	12931	12931	12933	12937
1666.19	1	12941	12947	12956	12965	12976	12990	13005	13024	13044	13066	13093	13120	13149	13179	13211	13243	13275
1633.41	1	13306	13335	13361	13386	13406	13422	13436	13445	13451	13455	13455	13453	13449	13445	13438	13432	13425
1600.63	1	13418	13416	13403	13395	13388	13380	13373	13366	13358	13352	13345	13339	13332	13327	13321	13315	13309
1567.84	1	13304	13299	13294	13289	13284	13281	13277	13272	13269	13265	13262	13258	13255	13251	13248	13245	13242
1535.06	1	13239	13236	13233	13229	13229	13225	13222	13218	13218	13214	13212	13210	13209	13204	13203	13200	13197
1502.28	1	13194	13191	13190	13184	13183	13179	13176	13172	13169	13164	13159	13157	13151	13148	13144	13140	13136
1469.49	1	13131	13127	13123	13118	13121	13120	13122	13126	13132	13141	13152	13167	13183	13199	13216	13230	13242
1436.71	1	13252	13261	13267	13271	13275	13279	13284	13290	13297	13306	13315	13324	13331	13337	13342	13345	13349
1403.92	1	13349	13349	13347	13343	13338	13332	13324	13315	13304	13291	13276	13258	13243	13242	13288	13405	13514
1371.14	1	13545	13532	13512	13493	13476	13462	13450	13439	13429	13421	13413	13407	13401	13396	13391	13387	13384
1338.36	1	13380	13377	13373	13370	13367	13364	13361	13358	13356	13354	13351	13349	13347	13344	13342	13340	13337
1305.57	1	13335	13333	13331	13329	13327	13325	13323	13321	13319	13317	13315	13313	13311	13310			
1272.79	3	13303	13297	13290	13284	13279	13274	13268	13263	13258	13252	13246	13240	13234	13229	13224	13218	13212
1147.44	1	13211	13209	13207	13206	13204	13203	13201	13199	13197	13195	13193	13191	13189	13187	13185	13183	13181
1114.65	1	13179	13178	13175	13173	13171	13170	13167	13165	13163	13161	13159	13157	13155	13153	13151	13149	13146
1081.87	1	13143	13141	13138	13134	13132	13128	13124	13121	13117	13112	13108	13103	13098	13091	13085	13080	13075
1049.09	1	13072	13074	13082	13102	13135	13176	13220	13257	13283	13297	13303	13304	13300	13296	13289	13283	13275
1016.3	1	13268	13262	13255	13249	13244	13239	13234	13229	13225	13220	13216	13212	13208	13205	13201	13198	13194
983.52	1	13191	13187	13183	13179	13176	13172	13168	13165	13161	13157	13153	13149	13144	13140	13135	13131	13126
951.70	0	13124	13121	13118	13116	13113	13											

Table 6.9. Real refractive indices between 8000.25 and 700.0 cm^{-1} of liquid water-acetonitrile with $x_{\text{CH}_3\text{CN}}=0.70$ at 25 $^{\circ}\text{C}$.^{a,b}

cm^{-1}	χ_E	0	1	2	3	4	5	6	7	8	9	10	11	12	13	14	15	16
8000.25	7	13241	13241	13241	13240	13240	13239	13239	13239	13238	13237	13237	13236	13235				
6488.33	5	13236	13234	13237	13238	13235	13234	13234	13234	13235	13235	13234	13234	13233	13232	13233	13233	13232
5963.78	5	13231	13232	13233	13232	13231	13231	13232	13231	13230	13229	13226	13234	13231	13230	13229	13229	13228
5439.24	5	13228	13227	13227	13226	13225	13225	13225	13225	13225	13225	13223	13222	13222	13222	13221	13221	13220
4914.70	5	13219	13218	13217	13217	13216	13215	13214	13213	13212	13211	13210	13208	13208	13205	13203	13200	13203
4390.15	5	13202	13204	13201	13200	13197	13194	13191	13188	13185	13181	13177	13172	13171	13165	13162	13154	13147
3865.61	5	13136	13125	13110	13089	13061	13015	12941	12940	13003	13078	13149	13213	13255	13291	13329	13362	13380
3356.59	4	13381	13378	13374	13369	13366	13364	13365	13368	13371	13369	13370						
3200.29	1	13371	13371	13370	13370	13368	13367	13365	13364	13362	13360	13359	13357	13355	13354	13352	13352	13353
3167.51	1	13356	13362	13369	13373	13373	13371	13369	13367	13364	13362	13361	13359	13357	13356	13354	13353	13352
3134.72	1	13350	13349	13348	13347	13346	13345	13344	13343	13342	13341	13340	13339	13339	13337	13337	13336	13335
3101.94	1	13334	13333	13332	13331	13330	13330	13329	13328	13328	13327	13326	13325	13325	13324	13323	13322	13321
3069.15	1	13321	13319	13319	13318	13317	13317	13316	13315	13314	13313	13312	13311	13310	13309	13308	13308	13307
3036.37	1	13306	13304	13303	13303	13301	13300	13300	13298	13298	13298	13297	13297	13298	13300	13303	13306	13310
3003.59	1	13316	13321	13326	13331	13334	13337	13338	13338	13337	13336	13335	13333	13333	13332	13330	13329	13327
2970.80	1	13326	13324	13322	13321	13319	13317	13315	13313	13310	13307	13303	13301	13302	13313	13334	13351	13357
2938.02	1	13357	13356	13354	13352	13350	13348	13346	13344	13342	13341	13339	13338	13336	13335	13334	13333	13333
2903.31	2	13331	13329	13328	13327	13325	13324	13323	13322	13320	13319	13318	13317	13317	13315	13314	13313	13312
2837.74	2	13312	13311	13310	13309	13309	13307	13306	13305	13304	13303	13302	13301	13300	13299	13298	13297	13297
2772.17	2	13296	13295	13294	13293	13292	13292	13291	13290	13289	13289	13288	13288	13287	13286	13285	13285	13284
2706.60	2	13283	13282	13281	13281	13280	13279	13278	13277	13277	13276	13276	13275	13274	13273	13272	13272	13270
2646.82	1	13270	13269	13268	13267	13267	13266	13266	13266	13267	13269	13271	13273	13273	13274	13273	13273	13273
2614.04	1	13272	13271	13271	13270	13270	13269	13268	13268	13267	13267	13266	13266	13266	13265	13265	13264	13264
2581.25	1	13263	13263	13263	13262	13262	13261	13261	13261	13260								
2558.11	3	13259	13257	13256	13254	13252	13251	13249	13248	13246	13245	13244	13244	13242	13239	13237	13235	13234
2426.98	3	13232	13230	13232	13236	13236	13233	13229	13225	13220	13215	13210	13205					
2341.16	3	13205	13204	13203	13203	13202	13201	13200	13199	13198	13197	13196	13195	13194	13192	13191	13190	13189
2324.77	0	13187	13186	13184	13183	13181	13180	13178	13176	13174	13172	13170	13168	13166	13163	13160	13157	13153
2308.37	0	13150	13146	13142	13138	13133	13129	13124	13120	13116	13115	13115	13120	13130	13144	13162	13182	13201
2291.98	0	13217	13227	13232	13234	13233	13230	13227	13222	13218	13213	13208	13202	13197	13191	13185	13179	13173
2275.59	0	13166	13160	13153	13146	13137	13129	13118	13106	13093	13077	13061	13042	13022	13001	12982	12967	12962
2259.20	0	12972	12999	13038	13090	13159	13254	13368	13462	13513	13535	13541	13540	13535	13527	13515	13503	13490
2242.81	0	13477	13464	13452	13441	13430	13420	13411	13402	13394	13387	13380	13374	13368	13363	13358	13353	13349
2226.41	0	13346	13342	13339	13336	13333	13330	13328	13325	13323	13321	13319	13316	13314	13312	13310	13308	13306
2210.02	0	13305	13304	13302	13301	13301	13300	13300	13300	13300	13300	13299	13298	13297	13296	13295	13294	13293
2193.63	0	13292	13291	13290	13288	13288	13287	13286	13285	13284	13283	13282	13282	13281	13280	13279	13279	13278
2177.24	0	13277	13277	13276	13276	13275	13274	13274	13273	13273	13272	13272	13271	13271	13270	13270	13269	13268
2154.10	3	13265	13262	13259	13256	13254	13252	13250	13249	13247	13246	13245	13246	13248	13247	13246	13246	13245
2022.96	3	13244	13243	13242	13241	13240	13239	13238	13236	13235	13233	13232	13230	13228	13226	13224	13222	13220
1891.83	3	13217	13215	13212	13211	13208	13204	13201	13199	13197	13196	13193	13189	13185				
1797.33	1	13184	13182	13181	13180	13179	13178	13177	13176	13175	13174	13172	13171	13170	13169	13167	13165	13164
1764.55	1	13163	13161	13160	13158	13156	13155	13153	13152	13150	13148	13146	13144	13142	13140	13138	13136	13134
1731.76	1	13132	13130	13127	13125	13122	13120	13117	13115	13112	13109	13106	13102	13099	13096	13092	13089	13085
1698.98	1	13082	13078	13075	13071	13067	13063	13059	13055	13052	13048	13045	13041	13038	13036	13033	13031	13030
1666.19	1	13030	13030	13032	13034	13037	13042	13048	13057	13068	13079	13094	13110	13128	13148	13169	13192	13214
1633.41	1	13236	13258	13277	13296	13311	13323	13332	13339	13343	13345	13344	13343	13339	13335	13331	13325	13320
1600.63	1	13315	13309	13303	13298	13292	13287	13282	13277	13271	13266	13262	13257	13253	13249	13244	13240	13236
1567.84	1	13232	13228	13225	13221	13218	13215	13212	13209	13207	13204	13202	13199	13197	13194	13193	13190	13189
1535.06	1	13186	13184	13182	13179	13181	13177	13174	13172	13171	13169	13167	13166	13165	13162	13160	13158	13156
1502.28	1	13153	13150	13150	13144	13143	13139	13137	13133	13129	13125	13120	13117	13112	13110	13105	13101	13096
1469.49	1	13091	13087	13083	13077	13083	13082	13084	13090	13098	13110	13124	13145	13163	13183	13203	13220	13235
1436.71	1	13247	13258	13265	13270	13274	13278	13283	13289	13298	13309	13319	13330	13339	13346	13352	13357	13361
1403.92	1	13361	13361	13359	13355	13350	13343	13334	13323	13311	13297	13281	13262	13247	13252	13315	13448	13560
1371.14	1	13590	13576	13554	13533	13515	13500	13487	13475	13464	13455	13447	13440	13434	13428	13423	13419	13414
1338.36	1	13411	13408	13404	13400	13397	13394	13391	13388	13386	13383	13381	13378	13376	13373	13371	13369	13367
1305.57	1	13364	13362	13360	13358	13356	13353	13352	13349	13347	13345	13343	13341	13340	13338			
1272.79	3	13331	13324	13317	13311	13306	13301	13296	13291	13286	13280	13276	13270	13266	13261	13257	13252	13247
1147.44	1	13245	13244	13243	13242	13240	13239	13237	13235	13234	13232	13231	13229	13227	13225	13224	13222	13220
1114.65	1	13218	13217	13215	13213	13212	13210	13208	13206	13204	13203	13201	13199	13198	13196	13194	13192	13190
1081.87	1	13187	13185	13182	13179	13176	13173	13170	13166	13162	13158	13153	13147	13143	13136	13130	13124	13119
1049.09	1	13116	13120	13131	13156	13196	13246	13298	13341	13370	13385	13394	13395	13392	13387	13380	13374	13366
1016.3	1	13359	13353	13346	13340	13335	13330	13326	13321	13317	13314	13310	13307	13304	13301	13298	13295	13292
983.52	1	13289	13287	13284	13281	13278	13275	13272	13269	13267	13264	13261	13258	13255	13251	13247	13244	13240
951.70	0	13238	13235	13235	13233	13230	1322											

Table 6.10. Real refractive indices between 8000.25 and 700.0 cm^{-1} of liquid acetonitrile at 25 °C.^{a,b}

cm^{-1}	$\lambda, \mu\text{m}$	0	1	2	3	4	5	6	7	8	9	10	11	12	13	14	15	16
8000.25	7	13248	13248	13248	13248	13247	13247	13247	13247	13247	13247	13247	13247	13246				
6488.33	5	13247	13247	13247	13247	13247	13247	13247	13247	13247	13247	13247	13246	13246	13246	13246	13246	13246
5963.78	5	13246	13246	13246	13246	13246	13246	13246	13246	13245	13245	13245	13243	13247	13247	13246	13246	13246
5439.24	5	13246	13245	13245	13245	13245	13245	13245	13245	13245	13245	13245	13245	13245	13245	13244	13244	13244
4914.70	5	13244	13244	13244	13244	13244	13244	13243	13243	13243	13243	13243	13243	13242	13242	13242	13241	13241
4390.15	5	13242	13247	13245	13244	13243	13243	13243	13242	13242	13242	13241	13241	13242	13240	13241	13240	13240
3865.61	5	13240	13239	13239	13239	13238	13238	13237	13237	13236	13236	13235	13235	13234	13233	13232	13230	13229
3356.50	4	13228	13227	13227	13226	13226	13225	13223	13221	13219	13216	13215						
3200.29	1	13217	13219	13219	13219	13218	13218	13217	13216	13215	13214	13213	13211	13210	13208	13206	13204	13202
3167.51	1	13203	13211	13225	13236	13238	13237	13235	13233	13232	13230	13229	13228	13227	13226	13225	13224	13223
3134.72	1	13223	13223	13222	13222	13222	13221	13221	13221	13220	13220	13220	13219	13220	13219	13219	13219	13219
3101.94	1	13219	13219	13219	13218	13218	13218	13218	13218	13218	13218	13217	13217	13217	13217	13217	13217	13217
3069.15	1	13216	13216	13216	13216	13216	13215	13216	13215	13215	13214	13214	13214	13214	13213	13212	13214	13212
3036.37	1	13212	13211	13210	13211	13210	13209	13209	13208	13209	13209	13209	13209	13209	13210	13213	13216	13219
3003.59	1	13232	13237	13243	13247	13251	13254	13255	13256	13256	13255	13256	13254	13253	13252	13251	13251	13250
2970.80	1	13249	13248	13247	13247	13245	13244	13243	13242	13239	13239	13236	13235	13238	13247	13262	13274	13279
2938.02	1	13280	13280	13279	13278	13277	13276	13275	13274	13273	13272	13271	13270	13269	13269	13268	13268	13267
2903.31	2	13236	13266	13265	13264	13264	13263	13262	13262	13261	13261	13261	13261	13260	13259	13259	13258	13258
2837.74	2	13258	13258	13258	13258	13257	13256	13256	13255	13255	13254	13254	13253	13253	13252	13251	13251	13251
2772.17	2	13250	13250	13249	13249	13248	13248	13248	13247	13247	13247	13246	13246	13246	13246	13245	13245	13245
2706.60	2	13244	13244	13243	13243	13242	13242	13241	13241	13240	13240	13240	13239	13239	13238	13237	13237	13237
2646.82	1	13236	13236	13235	13234	13233	13232	13231	13230	13229	13232	13237	13241	13242	13243	13243	13243	13243
2614.04	1	13243	13242	13242	13241	13241	13240	13240	13239	13239	13238	13238	13238	13237	13237	13237	13236	13236
2581.25	1	13236	13236	13235	13235	13235	13234	13234	13234	13234								
2558.11	3	13233	13232	13231	13230	13229	13228	13227	13226	13225	13225	13225	13224	13224	13222	13220	13219	13218
2426.98	3	13216	13216	13219	13224	13225	13222	13219	13215	13212	13208	13204	13199					
2341.16	0	13199	13198	13198	13197	13197	13196	13195	13195	13194	13193	13192	13191	13190	13189	13188	13187	13186
2324.77	0	13185	13184	13182	13181	13180	13178	13177	13176	13174	13172	13171	13169	13167	13165	13162	13160	13157
2308.37	0	13154	13151	13147	13144	13140	13136	13132	13128	13124	13121	13119	13120	13123	13131	13142	13159	13178
2291.98	0	13197	13213	13224	13230	13232	13231	13229	13226	13222	13218	13214	13210	13205	13200	13195	13190	13185
2275.59	0	13179	13174	13168	13163	13157	13151	13143	13135	13126	13115	13105	13091	13076	13058	13036	13012	12983
2259.20	0	12952	12920	12891	12881	12923	13050	13234	13384	13463	13498	13516	13526	13529	13525	13517	13507	13495
2242.81	0	13482	13469	13456	13444	13433	13423	13413	13404	13396	13388	13381	13374	13367	13361	13356	13351	13347
2226.41	0	13344	13340	13337	13333	13330	13328	13325	13323	13321	13318	13316	13314	13313	13311	13309	13307	13305
2210.02	0	13303	13301	13299	13297	13295	13295	13295	13297	13298	13298	13297	13296	13295	13294	13293	13292	13291
2193.63	0	13290	13290	13289	13288	13287	13286	13285	13284	13284	13283	13282	13281	13280	13280	13279	13278	13278
2177.24	0	13277	13277	13276	13276	13275	13275	13274	13274	13273	13273	13272	13272	13271	13271	13271	13270	13270
2154.10	3	13266	13264	13261	13259	13257	13255	13253	13251	13249	13248	13246	13247	13249	13248	13246	13245	13244
2022.96	3	13242	13241	13240	13239	13238	13237	13236	13235	13234	13233	13232	13231	13230	13229	13228	13227	13226
1891.83	3	13225	13224	13223	13222	13221	13220	13218	13218	13218	13221	13220	13218	13216				
1797.33	1	13216	13216	13216	13215	13215	13215	13215	13214	13214	13214	13213	13213	13213	13212	13212	13211	13211
1764.55	1	13211	13210	13209	13209	13209	13209	13208	13208	13207	13207	13207	13206	13206	13205	13205	13205	13205
1731.76	1	13205	13204	13204	13203	13203	13202	13202	13201	13200	13200	13199	13198	13198	13197	13196	13196	13195
1698.98	1	13194	13194	13193	13192	13192	13191	13190	13190	13189	13188	13188	13187	13186	13186	13185	13184	13184
1666.19	1	13183	13182	13182	13181	13180	13180	13179	13178	13177	13176	13175	13174	13174	13173	13172	13171	13170
1633.41	1	13169	13168	13167	13166	13165	13164	13163	13162	13161	13159	13158	13157	13155	13154	13153	13151	13150
1600.63	1	13149	13147	13146	13145	13143	13142	13141	13139	13138	13137	13135	13134	13133	13131	13130	13128	13126
1567.84	1	13124	13124	13123	13122	13121	13119	13118	13117	13117	13117	13116	13115	13114	13113	13115	13112	13111
1535.06	1	13110	13110	13109	13107	13114	13108	13106	13107	13105	13105	13103	13104	13105	13103	13102	13100	13099
1502.28	1	13097	13095	13097	13091	13091	13088	13085	13081	13078	13073	13067	13067	13061	13061	13055	13051	13046
1469.49	1	13041	13037	13033	13021	13038	13035	13038	13044	13054	13069	13087	13116	13136	13160	13185	13206	13223
1436.71	1	13237	13251	13260	13264	13267	13270	13273	13278	13288	13302	13312	13325	13335	13344	13352	13357	13363
1403.92	1	13364	13363	13362	13358	13352	13345	13337	13325	13312	13297	13280	13262	13250	13261	13341	13486	13598
1371.14	1	13625	13610	13587	13565	13547	13531	13516	13503	13492	13483	13474	13467	13460	13454	13449	13445	13440
1338.36	1	13436	13434	13430	13426	13423	13420	13416	13413	13411	13408	13406	13403	13401	13399	13396	13393	13391
1305.57	1	13388	13386	13384	13382	13380	13378	13375	13374	13371	13369	13367	13365	13364	13362			
1272.79	3	13355	13348	13341	13335	13329	13324	13319	13314	13309	13304	13300	13295	13290	13286	13282	13278	13274
1147.44	1	13273	13271	13270	13269	13267	13266	13265	13263	13262	13260	13259	13257	13255	13254	13252	13250	13249
1114.65	1	13247	13246	13244	13242	13241	13239	13237	13235	13234	13232	13231	13229	13227	13225	13224	13222	13219
1081.87	1	13217	13215	13212	13209	13207	13203	13200	13196	13192	13188	13183	13177	13173	13165	13158	13152	13145
1049.09	1	13142	13147	13158	13187	13236	13293	13352	13400	13432	13449	13458	13459	13455	13450	13443	13437	13429
1016.3	1	13421	13414	13408	13401	13396	13391	13387	13382	13378	13375	13372	13368	13365	13363	13360	13357	13355
983.52	1	13352	13350	13347	13345	13342	13339	13337	13334	13332	13329	13326	13324	13321	13318	13314	13311	13308
951.70	0	13306	13304	13303	13301	13299	13297	13295	13293	13290								

Footnotes to Tables 6.3 to 6.10.

- ^a. The column headed cm^{-1} contains the wavenumber of the first ordinate value in the row. The columns headed XE and YE contain the X-exponent and the Y-exponent, respectively, for the row. The columns headed 0, 1, 2, ..., 16, contain the ordinate values, and the headings give the indices of the ordinate values in the row. In a row which starts with $\tilde{\nu}(0)$, the wavenumber corresponding to the ordinate indexed J is $\tilde{\nu}(J) = \tilde{\nu}(0) - \frac{15798.002}{16384} \cdot J \cdot 2^{XE}$. In Tables 6.3, 6.5, 6.7 and 6.9, the $k(\tilde{\nu})$ values in that row are the ordinate value shown times 10^{YE} . In Table 6.4, 6.6, 6.8, 6.10, the $n(\tilde{\nu})$ values are given directly with the decimal point implicitly after the first digit. Thus the entry indexed 16 in the fifth row of Table 6.3 shows that at $\tilde{\nu} = 4914.70 - \frac{15798.002}{16384} \times 16 \times 2^5 = 4421.01 \text{ cm}^{-1}$ the k value is $1659 \times 10^{-7} = 1.659 \times 10^{-4}$; The entry indexed 16 in the fifth row of Table 6.10 shows that at $\tilde{\nu} = 4914.70 - \frac{15798.002}{16384} \times 16 \times 2^5 = 4421.01 \text{ cm}^{-1}$ the ordinate value is $n = 1.3243$.
- ^b. The 4-point spline interpolation program TRECOVER³² interpolated the $k(\tilde{\nu})$ values in the table to the original wavenumber spacing, 0.482117 cm^{-1} , and yielded the original values accurate to 1%. The original $n(\tilde{\nu})$ values were similarly recovered accurate to 0.1%.

Second, the simple Classical Damped Harmonic Oscillator theory of dielectric properties indicates that the α''_m spectrum is simply the sum of the contributions from each vibration. Thus the α''_m spectrum of a mixture is simply the sum of the α''_m spectra of the components multiplied by the mole fraction of the component. This is not true for A_{10} , E_m and k spectra, in which the contributions from the different vibrations interact.

Third, under the CDHO model, the peak wavenumbers in the $\tilde{\nu}\alpha''_m$ spectrum, which almost equal those in the α''_m spectrum, are the wavenumbers of the mechanical oscillators. The wavenumber of a peak in the A_{10} , E_m and k spectra depends also on the intensity of the peak.

Fourth, the area C_j under an absorption band j in the $\tilde{\nu}\alpha''_m$ spectrum is related to the transition moment, $|\bar{R}_j|$, of the corresponding transition by ¹⁴

$$C_j = \int_{band\ j} \tilde{\nu} \alpha_m''(\tilde{\nu}) d\tilde{\nu} = \frac{N\pi}{3hc} g_j \tilde{\nu}_j |\bar{R}_j|^2 \quad (6.1)$$

Where N is Avogadro's number, N_A , for a pure liquid, and Avogadro's number times the mole fraction of the absorbing compound i , $N_A x_i$, for a mixture. g_j is the degeneracy of vibration j , and c is the velocity of light in vacuum.

Therefore, the interaction between the water and acetonitrile molecules in the mixtures was studied quantitatively by examining the $\tilde{\nu} \alpha_m''(\tilde{\nu})$ spectrum as a function of composition.

6.4. Results and Discussion

6.4.1. The band shapes and peak positions in the $\tilde{\nu} \alpha_m''$ spectra

The $\tilde{\nu} \alpha_m''$ spectra are presented in figure 6.3 for the five compositions shown in figs. 6.1 and 6.2. The bands due to the O-H stretching vibration near 3500 cm^{-1} , $\text{C}\equiv\text{N}$ stretching vibration near 2267 cm^{-1} and H-O-H bending vibration near 1600 cm^{-1} bands clearly change shape and peak wavenumber with concentration, while the bands due to the CH_3 vibrations, such as the CH_3 s and d-deformations near 1385 cm^{-1} and 1448 cm^{-1} , respectively, and the CH_3 rock near 1041 cm^{-1} , and the C-C stretching vibration band near 920 cm^{-1} may not be affected by the presence of the water. An increase in the acetonitrile concentration causes a high-wavenumber shift of the O-H stretching peak, a low-wavenumber shift of the $\text{C}\equiv\text{N}$ stretching peak and slight low-wavenumber shift of the H-O-H bending peak. This is consistent with the independent observations

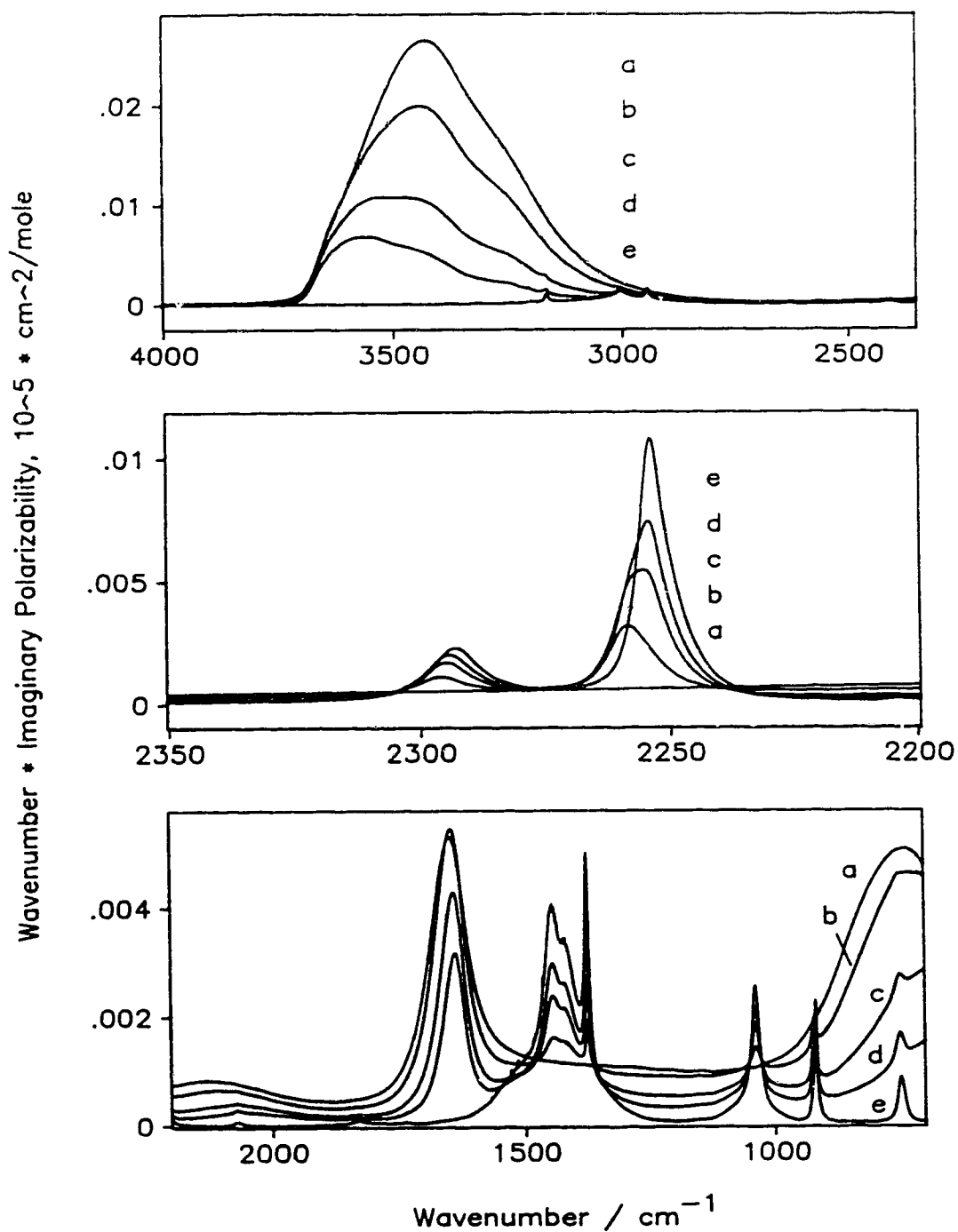


Figure 6.3. $\tilde{\nu}\alpha_m''(\tilde{\nu})$ spectra of five $\text{CH}_3\text{CN}+\text{H}_2\text{O}$ mixtures at 25 °C: a $x_{\text{CH}_3\text{CN}}=0.0$; b $x_{\text{CH}_3\text{CN}}=0.20$; c $x_{\text{CH}_3\text{CN}}=0.50$; d $x_{\text{CH}_3\text{CN}}=0.70$; e $x_{\text{CH}_3\text{CN}}=1.00$.

of the O-H stretching band by Narvor, Gentric and Saumagne¹⁶ and of the O-D and C \equiv N stretching bands by Jamroz, Stangret and Lindgren⁸.

6.4.2 Area C_j under bands in the $\tilde{\nu}\alpha_m''$ spectrum

The area C_j under the band due to vibration j in the $\tilde{\nu}\alpha_m''$ spectrum of a mixture is the intensity per mole of mixture. As noted above, the α_m'' spectrum of a mixture is simply the mole-fraction-weighted sum of the α_m'' spectra of the components, if the intensity and wavenumber of each vibration are not affected by the nature of the neighbouring molecules and the same as is true of the shape and width of the corresponding band. If this is the case, the area C_j under band j due to one of the components is linear in the mole fraction of the component. Thus, it is non-linearities in the plots of C_j versus mole fraction that must be interpreted to provide information about the intermolecular interactions.

To observe the effect of composition on the intensity of a particular band, the area under that band must be measured over the same wavenumber range for all compositions. Ideally these measurements are all relative to the same baseline, and this baseline is zero ordinate. Again ideally, each band is separated from its neighbors by curve fitting for each composition, and the area of each separated band is measured. Unfortunately, the spectra of the acetonitrile-water mixtures do not allow such an ideal treatment. The band shapes are unusual and to date have not allowed band separation to be achieved with any confidence in the significance of the results. Thus the areas under groups of bands have to be measured. Even this can not be done ideally, because

the relatively strong baseline absorption by water causes uncertainty in the significance of areas measured relative to zero ordinate, or even to the same baseline, in several regions.

To illustrate this point, note in Fig. 6.3 that the spectral baseline between 2350 and 2200 cm^{-1} is higher in the spectrum of pure water than in the spectra of mixtures and of pure acetonitrile. Changes with concentration in the areas measured relative to the same baseline contain offsetting effects of decrease in the absorption by acetonitrile and increase in the absorption by water, which makes their interpretation ambiguous. This is even more pronounced for the regions 1650 to 1200 cm^{-1} and 1200 to 900 or 800 cm^{-1} . To overcome these difficulties the areas were measured in non-ideal ways that are described in the following sub-sections together with the estimated significance of the resulting areas.

6.4.3 The Methyl Group Vibrations of Acetonitrile

The C-H stretching bands are too weak to be measurable in the water rich mixtures and are not discussed further. The CH_3 deformation bands near 1400 cm^{-1} and the CH_3 rocking band near 1040 cm^{-1} were measured relative to the baseline determined by the water absorption. In practical calculation, the baseline was taken as the straight line connecting the ordinate values at the integration limits. This seems useful because the bands are relatively sharp and their shapes and wavenumbers do not change with composition, which suggests that the water absorption is essentially independent of the acetonitrile absorption in these two cases. If that is the case, a linear plot of area versus mole fraction of acetonitrile is expected.

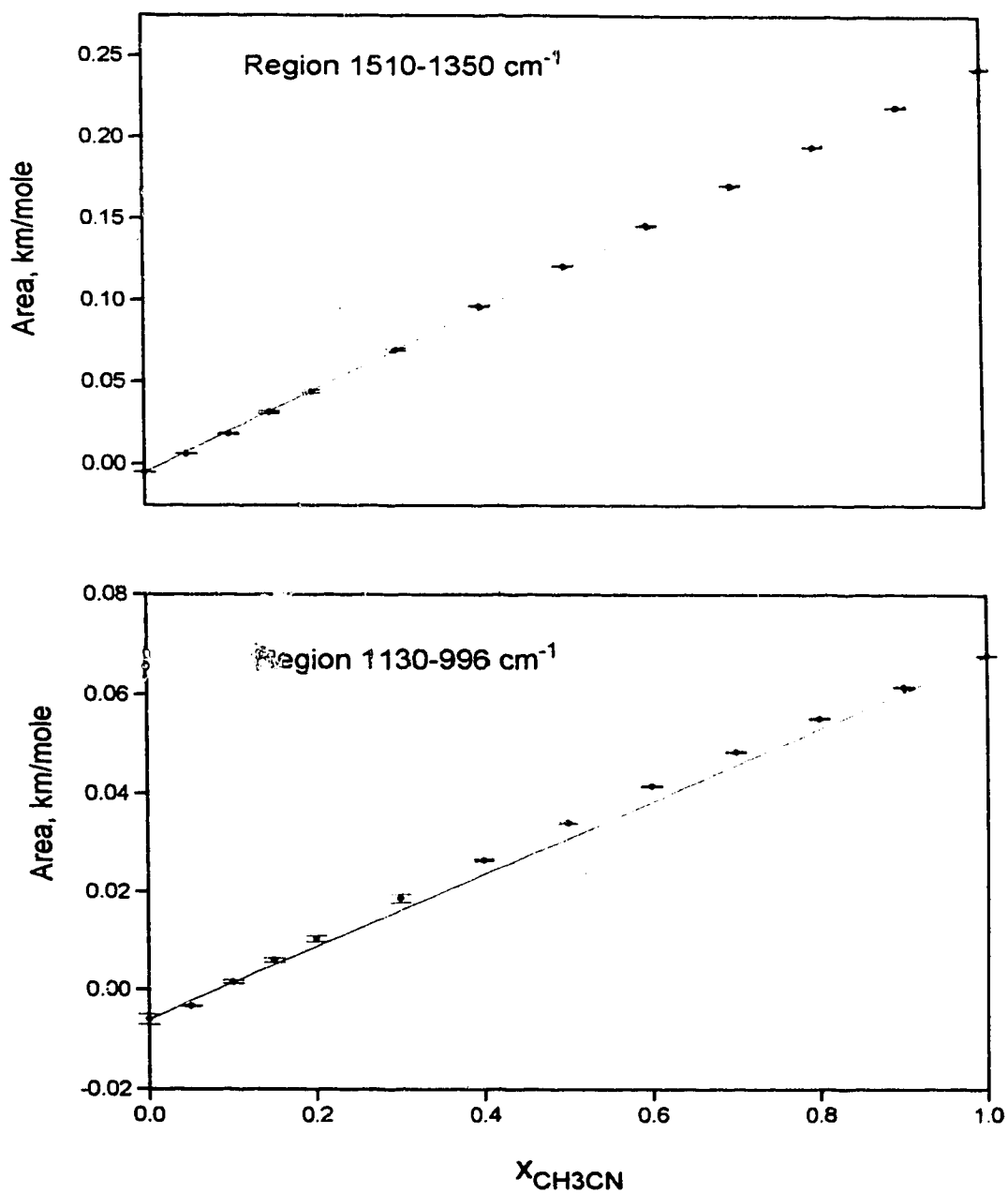


Figure 6.4. The areas under the $\tilde{\nu}\alpha''_m(\tilde{\nu})$ spectra in the CH_3 deformation (top box) and CH_3 rocking (bottom box) regions for thirteen $\text{CH}_3\text{CN}+\text{H}_2\text{O}$ mixtures at 25 °C. The baseline was a straight line through the curve at the integration limits. The integration limits are shown and the error bars show the maximum deviations. The straight lines show the behavior expected for an ideal solution.

For the deformation vibrations, the area was measured between 1510 and 1350 cm^{-1} , clearly omitting the high-wavenumber tail of the CH_3 deformation band. These wavenumbers were chosen to give ordinate values above or on all curves with more than 5 mole % of acetonitrile. The areas were measured above the linear baseline. The upper box of Fig 6.4 shows that the areas C_j so measured increase nearly linearly with the mole fraction of acetonitrile, confirming the near independence of the water vibrations and the CH_3 deformation vibrations.

For the CH_3 rocking vibrations, the area was measured between 1130 and 996 cm^{-1} above the linear baseline. The areas are not quite linear in mole fraction, and they increase more rapidly at low concentrations and less rapidly at high concentration of acetonitrile.

6.4.4 The Areas under the $\tilde{\nu}\alpha_m''$ Spectra in the O-H Stretching Region

In the O-H stretching region 4000-2660 cm^{-1} , the C-H stretching band can not be simply separated, especially for $x_{\text{CH}_3\text{CN}} < 0.8$. However, there are two facts which can be used to obtain the area resulting from the O-H stretching band with good accuracy. One is that the area of the C-H stretching band is much smaller than that of the O-H stretching band. Even for pure acetonitrile the area under $\tilde{\nu}\alpha_m''$ spectrum between 4000 and 2660 cm^{-1} is only 0.247 km/mole , about 2% of the area under the O-H stretching band for pure water. The other fact is that the presence of water probably does not affect the vibrations of the CH_3 group in water-acetonitrile mixtures. This has been demonstrated above for the CH_3 deformation and rocking modes, and also

observed for the C-H stretching vibration in $\text{H}_2\text{O}+\text{CH}_3\text{OH}$ system¹⁷. In these cases the area under the methyl band is linear in mole fraction of the methanol concentration. Therefore, the area of the OH band was calculated as

$$C_{\text{OH}} = (\text{Area between } 4000 \text{ and } 2660 \text{ cm}^{-1}) - x_{\text{CH}_3\text{CN}} (\text{Area for pure acetonitrile between } 4000 \text{ and } 2660 \text{ cm}^{-1}).$$

The resulting areas under the OH stretching band, C_{OH} , are presented as a function of $x_{\text{CH}_3\text{CN}}$ in figure 6.5, and their values are listed in Table 6.11. At low acetonitrile concentrations, $x_{\text{CH}_3\text{CN}} \leq 0.10$, the C_{OH} are on or very slightly above the straight line which corresponds to the ideal solution, i.e. to constant intensity per mole of water. As the acetonitrile concentration increases, the areas decrease and stay markedly below the straight line, clearly demonstrating non-ideal behavior due to the expected interaction between the CH_3CN and the OH groups of the water.

6.4.5 The areas under the $\tilde{\nu}\alpha''_m$ spectra in the $\text{C}\equiv\text{N}$ stretching region

The absorption between 2275 and 2210 cm^{-1} is mainly by the $\text{C}\equiv\text{N}$ stretching vibration⁸. The total area above zero ordinate is shown by the triangles in Fig. 6.6 plotted against mole fraction of acetonitrile. For the mixtures it is clearly well above the straight line between the end points (not drawn) that corresponds to constant intensity per mole.

Water also contributes to the area in this region. Two methods were used to obtain the intensity C_{CN} between 2275 and 2210 cm^{-1} due to the acetonitrile alone. The first method follows that used for the OH stretching band. The area under the

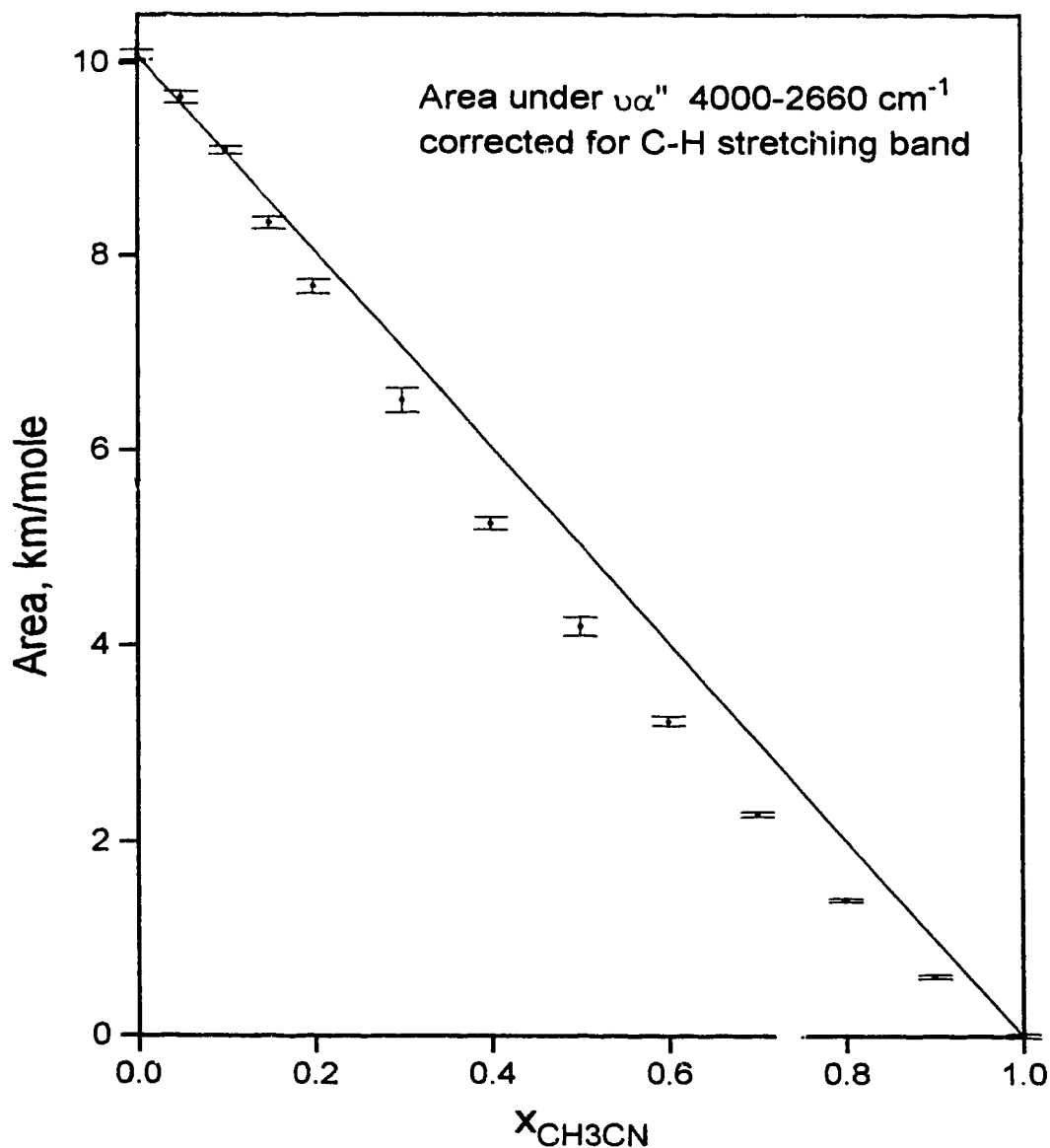


Figure 6.5. The areas under the $\tilde{\nu}_{OH}''(\tilde{\nu})$ spectra of thirteen $\text{CH}_3\text{CN}+\text{H}_2\text{O}$ mixtures at 25 °C in the O-H stretching region between 4000 and 2660 cm^{-1} . The C-H stretching contribution has been removed as described in the text. The error bars are the 95% confidence limits. The straight line shows the behavior expected for an ideal solution..

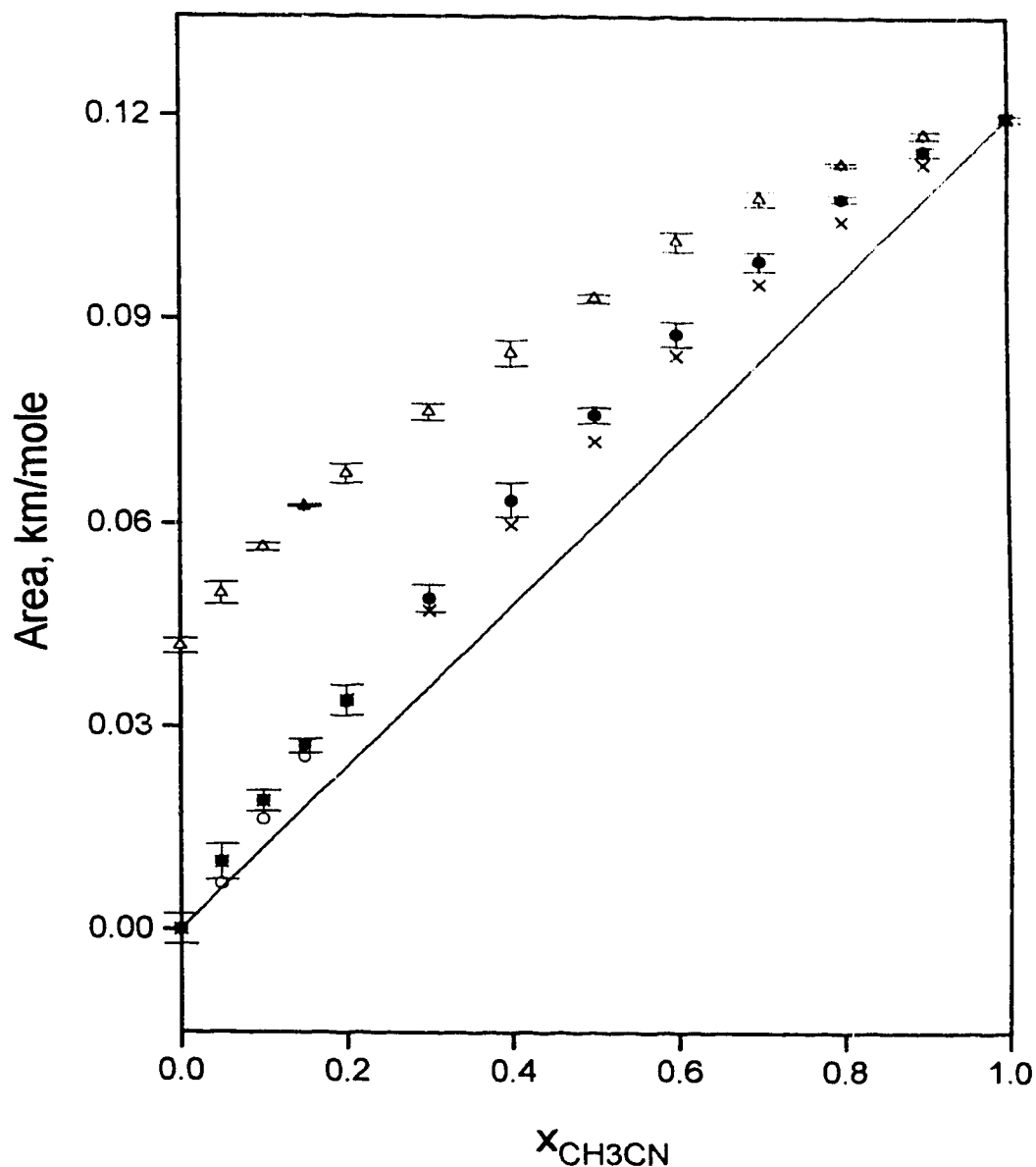


Figure 6.6. The areas under the $\tilde{\nu}\alpha''(\tilde{\nu})$ spectra of thirteen $\text{CH}_3\text{CN}+\text{H}_2\text{O}$ mixtures at 25 °C in the $\text{C}\equiv\text{N}$ stretching region $2275\text{--}2210\text{ cm}^{-1}$: (Δ) indicates the total area, (x) indicates the area corrected for the water contribution by the first method described in the text, (o) indicates the area corrected for the water contribution by the second method described in the text, (●) the final areas used. The error bars are the 95% confidence limits. The straight line shows the behavior expected for an ideal solution..

Table 6.11. The areas under the OH and CN stretching bands and the fractions of H-bonded CN groups and of O-H...O bonded and non bonded OH groups.

$x_{\text{CH}_3\text{CN}}$	C_{OH}^a km/mole	C_{CN}^b km/mole	x'_{CNH}^c	x'_{OHO}^d	x'_{OH}^d
0.00	10.08(5)	0.000(2)	1.000	0.855	0.145
0.05	9.64(6)	0.0099(26)	0.900	0.839	0.138
0.10	9.09(4)	0.0188(15)	0.799	0.814	0.142
0.15	8.34(6)	0.0270(21)	0.703	0.770	0.168
0.20	7.68(7)	0.0339(20)	0.578	0.741	0.187
0.30	6.50(12)	0.0489(25)	0.503	0.677	0.215
0.40	5.25(6)	0.0635(12)	0.454	0.585	0.264
0.50	4.20(9)	0.0760(18)	0.375	0.517	0.295
0.60	3.23(5)	0.0878(14)	0.309	0.445	0.323
0.70	2.28(3)	0.0986(5)	0.245	0.348	0.366
0.80	1.397(2)	0.1079(7)	0.176	0.228	0.421
0.90	0.612(2)	0.1149(5)	0.091	0.092	0.499
1.00	0.000(2)	0.1198(5)	0.000	0.000	0.55

^a. The area under the $\tilde{\nu}\alpha_m''$ spectrum between 4000 and 2660 cm^{-1} with the acetonitrile contribution removed as $C_{\text{OH}} = (\text{Area between 4000 and 2660 } \text{cm}^{-1}) - x_{\text{CH}_3\text{CN}} (0.247 \text{ m/mole})$ where 0.247 km/mole is the area between 4000 and 2660 cm^{-1} for pure acetonitrile.

The number in the brackets is the 95% confidence limit in the last digit.

^b. The intensity under the $\tilde{\nu}\alpha_m''$ spectrum between 2275 and 2210 cm^{-1} . At the concentrations $x_{\text{CH}_3\text{CN}} \leq 0.2$, the value shown is the area under the mixture minus the mole fraction of water times 0.04182 km/mole, which is the area under the spectrum of pure water. For $x_{\text{CH}_3\text{CN}} > 0.2$, the value shown is the area between 2275 and 2210 cm^{-1} measured above a straight line through the ordinate values at 2590.8 and 2150.2 cm^{-1} . The number in the brackets is the 95% confidence limit in the last digit.

^c. The fraction of H-bonded CN groups determined by Eqs. (6.2) with the intensity parameters $C'_{\text{CN}} = 0.1198 \text{ km/mole}$ and $C'_{\text{CNH}} = 0.206 \text{ km/mole}$.

^d. The fractions of water-bonded and free OH groups determined from Eqs. (6.3), x'_{CNH} , and $C'_{\text{OH}} = 0.41 \text{ km/mole}$, $C'_{\text{OHO}} = 5.82 \text{ km/mole}$ and $C'_{\text{OHN}} = 5.67 \text{ km/mole}$.

spectrum of pure water was multiplied by the mole fraction of water in the mixture and subtracted from the total area under the spectrum of the mixture. The intensities C_{CN} so obtained are shown for the mixtures in Fig. 6.6 by the crosses. The second method used a baseline drawn between the ordinate values at 2590.8 and 2150 cm^{-1} , and the area between 2275 and 2210 cm^{-1} was measured above this baseline. The intensities C_{CN} measured by the second method are shown for the mixtures in Fig. 6.6 by the open circles. They are about 3% larger than those from the first method for $x_{CH_3CN} > 0.2$ and are smaller for $x_{CH_3CN} < 0.2$.

For the higher concentrations of acetonitrile, $x_{CH_3CN} > 0.2$, the $\tilde{\nu}\alpha_m''$ spectrum of water multiplied by the mole fraction of water is slightly higher than the baseline of the spectrum of the mixture, so the first method clearly overestimates the water absorption. For $x_{CH_3CN} < 0.2$, the second method gives a distorted spectrum after the baseline is subtracted, clearly because it overestimates the water absorption at these high water concentrations.

Thus the final intensities C_{CN} are those from the first method for $x_{CH_3CN} \leq 0.2$ and those from the second method for the remaining solutions. They are shown in Fig. 6.6 by the filled circles. The error bars show the maximum observed deviation from the mean. The C_{CN} all lie on a curve well above the straight line. Their values are listed in Table 6.11.

6.4.6 The population of hydrogen bonded acetonitrile

The nonlinear curves in figures 6.5 and 6.6 indicate that the O-H and $C\equiv N$ groups are involved in the interaction between the water and acetonitrile molecules in

the mixtures. The interaction is undoubtedly hydrogen bonding between the lone pair electrons on the C≡N group and the proton of the O-H group. This is expressed as CH₃CN...H-O-H, or CNH for short. Thus, the CN group can be taken to be either bonded or not. The area under the C≡N stretching band in one mole of mixture at concentration $x_{\text{CH}_3\text{CN}}$ can be related to the extent of hydrogen bonding through

$$C_{\text{CN}} = x_{\text{CH}_3\text{CN}} (x'_{\text{CN}} C'_{\text{CN}} + x'_{\text{CNH}} C'_{\text{HCN}}) \quad (6.2)$$

with $x'_{\text{CN}} + x'_{\text{CNH}} = 1 \quad (6.2a)$

Here x'_j ($j=\text{CN}$ or CNH) is the fraction of free (CN) or hydrogen bonded (CNH) C≡N groups, and C'_j ($j=\text{CN}$ or CNH) is the area contributed by one mole of free (CN) or hydrogen bonded (HCN) C≡N groups.

In order to obtain the values of x'_{CNH} and x'_{CN} for the mixtures, the intensity parameters C'_{CN} and C'_{CNH} in equation (6.2) were assumed to be independent of composition. In pure acetonitrile, the C≡N group is not hydrogen bonded. Consequently, its area $C_{\text{CN}} = 0.1198 \text{ km/mole}$, was taken as the value for C'_{CN} .

Jamroz et al ⁸ found that the C≡N stretching band of free CD₃CN appeared only as a shoulder when the mole fraction of CD₃CN was less than 0.14. This indicated that nearly all of the CD₃CN is H-bonded to water at that low concentration. It was therefore assumed that at infinitely low concentration all of the acetonitrile in the water is hydrogen bonded. The intensity per mole of the hydrogen bonded CN stretching vibration is then given by the slope of the intensity versus mole fraction curve at the limit $x_{\text{CH}_3\text{CN}} \rightarrow 0$. This slope was found by fitting the intensities at $x_{\text{CH}_3\text{CN}}$

$\approx 0.05, 0.10, 0.15$ to the quadratic equation $C_{CN} = bx_{CH_3CN} + cx_{CH_3CN}^2$, from which the desired slope, which equals C'_{CNH} , is given by b. It was found that $C'_{CNH} = 0.206$ km/mole.

The fractions of acetonitrile molecules that are hydrogen-bonded, x'_{CNH} , were calculated for each mixture from Eqs. 6.2 and 6.2a and their values are listed in Table 6.11. They, and the fraction of free acetonitrile molecules, are plotted as percentages in Fig. 6.7 against mole fraction of acetonitrile. They are also plotted, in the lower box in Fig. 6.7, against the number of water molecules per 100 acetonitrile molecules. This inconvenient abscissa quantity is included to allow visual comparison with Fig. 6.3 of Jamroz et al's paper ⁸, which shows the same quantities calculated from fits of the absorbance spectra from their transmission study and from a close packed model. Their experimental values agree well with ours. Specifically, the two curves have the same general shape, the maximum percentage of hydrogen bonded CH_3CN molecules agrees at 79% and 78%, and the only significant differences are at $x_{CH_3CN} = 0.20$ and 0.30, 400 and 230 molecules of water per 100 CH_3CN , respectively, where our values are 56 % and 50 % compared with their 68 % and 59 %.

6.4.7 The Population of Water and Acetonitrile Bonded O-H Groups

In the O-H stretching region, the intensities of the mixtures result from free O-H groups and two types of hydrogen bonded O-H groups: OH groups bonded to CH_3CN , O-H...NCCH₃, abbreviated to OHN, and OH groups bonded to water, O-H...OH₂, abbreviated to OHO. Accordingly, the area C_{OH} is expressed as

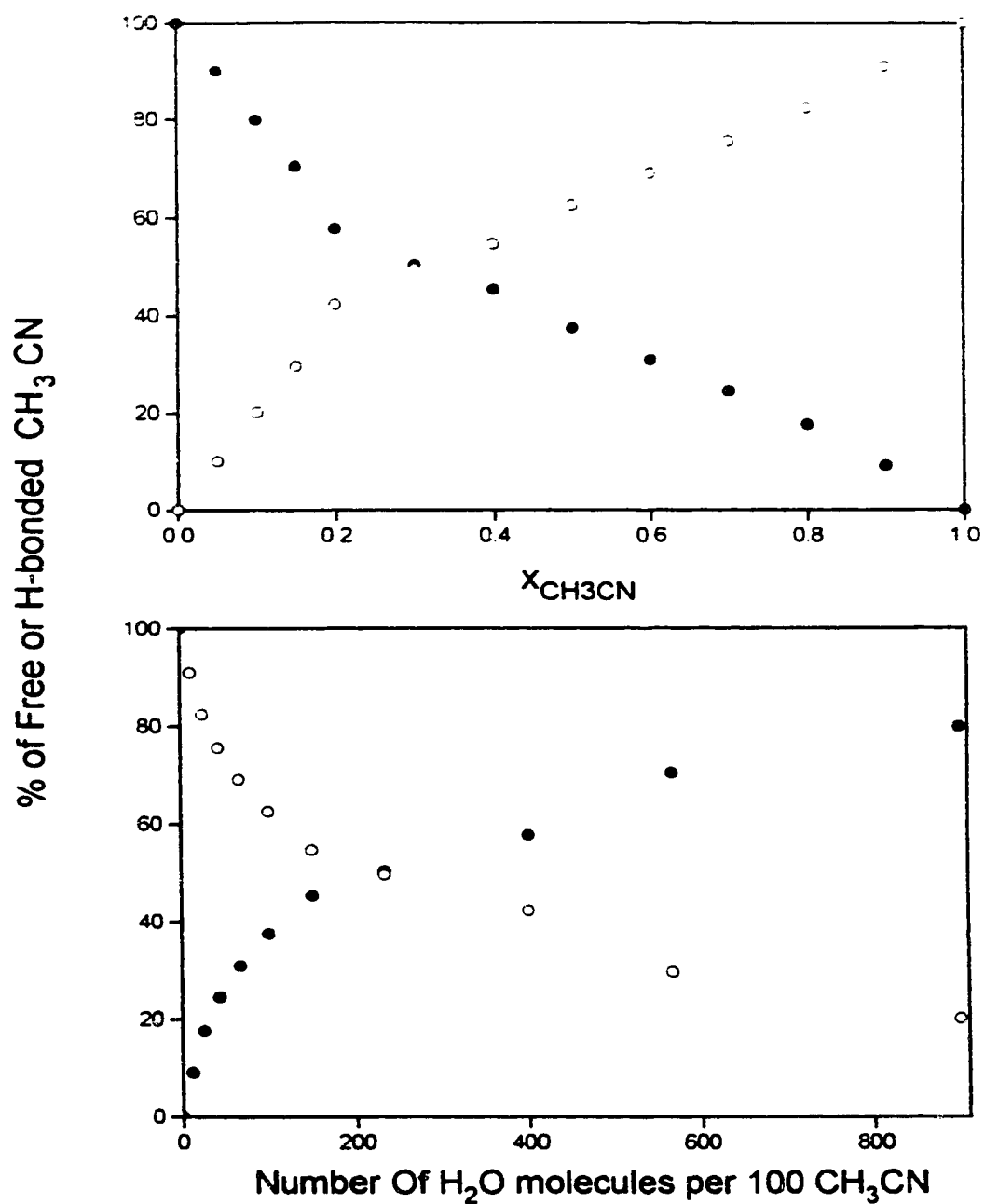


Figure 6.7. The percentages of acetonitrile molecules in water-acetonitrile mixtures that are free (o) and H-bonded (•).

$$C_{OH} = 2x_{H_2O} (x'_{OHN} C'_{OHN} + x'_{OHO} C'_{OHO} + x'_{OH} C'_{OH}) \quad (6.3)$$

where $x'_{OHN} + x'_{OHO} + x'_{OH} = 1 \quad (6.3a)$

Here x'_j ($j=OHN, OHO, OH$) is the fraction of OH groups that are of the type OHN or OHO, or free OH. C'_j ($j=OHN, OHO, OH$) is the area contributed by one mole of such OH groups.

The molar intensities C'_j ($j=OHN, OHO, OH$) were taken to be independent of composition. To find their values, information from the literature had to be used with the data from this work.

In pure liquid water at room temperature, not all of the O-H groups are hydrogen bonded (OHO). Luck et al ¹⁸ determined the concentration of OHO groups as 1.73 mole per mole water. Accordingly, the value of C'_{OHO} is calculated from the C_{OH} value for pure water as $10.08/1.73=5.82$ km/mole.

To find C'_{OH} it was noted that the integrated intensity of the O-H stretching vibrations in the gas phase is about 7% of that in the liquid ²¹. Therefore, the value of C'_{OH} was taken to be $0.07C'_{OHO} = 0.41$ km/mole.

C'_{OHN} was found in the following way from the OH stretching intensities at high CH_3CN concentrations. The slope of the graph of C_{OH} against x_{CH_3CN} (Fig. 6.5) as $x_{CH_3CN} \rightarrow 0$ was determined from a quadratic function fitted to the values at $x_{CH_3CN} = 0.70, 0.80$ and 0.90 , as described earlier for C_{CNH} . Its value is 5.55 ± 0.14 km/mole of water. To translate this into the intensity per mole of bonds, the fraction of the OH bonds in a water molecule that are hydrogen bonded to acetonitrile at infinite dilution is required. This was obtained from the previous determination of x'_{CNH} , the fraction of

the acetonitrile molecules that are hydrogen bonded. The number of H-bonded CH_3CN molecules per mole of mixture is given by $x_{\text{CH}_3\text{CN}} x'_{\text{CNH}}$. Thus, the number of H-bonded CH_3CN molecules per mole of water molecules is given by $x_{\text{CH}_3\text{CN}} x'_{\text{CNH}} \div x_{\text{H}_2\text{O}}$, which is the slope of the graph of $x_{\text{CH}_3\text{CN}} x'_{\text{CNH}}$ versus mole fraction of water. This is the same as the number of OHN hydrogen bonds per mole of water molecules, the number that is sought for infinite dilution. To find this quantity at infinite dilution the product quantity of $x_{\text{CH}_3\text{CN}}$ and $x'_{\text{CH}_3\text{CN}}$ was calculated for $x_{\text{CH}_3\text{CN}} = 0.70, 0.80$ and 0.90 , i.e. for $x_{\text{H}_2\text{O}} = 0.30, 0.20$ and 0.10 , and fitted to a quadratic function in $x_{\text{H}_2\text{O}}$ which passes through the origin, as described previously for C_{CNH} . The slope was 0.90 at $x_{\text{H}_2\text{O}} = 0.0$. Consideration of the difficulty of separating the H_2O and CH_3CN absorptions, and the fact that the fit includes data for water mole fractions as high as 0.30 , yielded an estimated error in this slope of ± 0.2 . Thus, the number of OHN bonds per mole of water molecules was found to be 0.90 ± 0.2 . Half of this value, 0.45 ± 0.1 is ideally the fraction of OH groups that are hydrogen bonded to acetonitrile at infinitely dilute water concentration.

It may seem anomalous that about half of the OH groups of dilute water in acetonitrile are not hydrogen bonded. This idea is not new, although the evidence that has been cited in the past is not convincing. Bonner and Choi²⁰ studied the water overtone band, $\nu_2 + \nu_3$ near 5250 cm^{-1} for various water-acetonitrile mixtures. The band they assigned to the free bonds provided 28% of the total area at 5 mole % of

water. However the detailed significance for this work of their results and conclusions is very much in doubt.

At very low water concentration, there is little doubt that all water molecules are isolated and no water-water hydrogen bonding occurs in the solution. Therefore, the derivative of the area C_{OH} at $x_{H_2O}=0.0$ was derived from Eq. 6.3 as

$$dC_{OH}/dx_{H_2O} = 2(x'_{OHN} C'_{OHN} + x'_{OHO} C'_{OHO} + x'_{OH} C'_{OH}) \quad (6.4)$$

with $dC_{OH}/dx_{H_2O}=5.55$ km/mole, $x'_{OHN}=0.45$, $x'_{OHO}=0.0$, $C'_{OHO}=5.82$ km/mole, $x'_{CH}=0.55$, and $C'_{OH}=0.41$ km/mole. Accordingly the value of C'_{OHN} is 5.67 km/mole. The possible error in the number of OH bond per mole of water molecule, 0.90 ± 0.2 , allows C'_{OHN} to be as large as 7.3 km/mole and as small as 4.63 km/mole.

Eqs. (6.3) were then used with these values of the parameters C'_{OH} , C'_{OHO} , C'_{OHN} to calculate the fractions of non-bonded and OHO bonded OH bonds at the different concentrations. The fractions of OHN bonds, x'_{OHN} , are needed for this and were calculated from the fractions of acetonitrile molecules that are hydrogen bonded which were calculated above from the CN stretching band. Specifically the number of hydrogen-bonded CH_3CN molecules per mole of solution is $x'_{CNH} x_{CH_3CN}$. This equals the number of OHN bonds per mole of solution, which is given by $2x'_{OHN} x_{H_2O}$. Hence,

$$x'_{OHN} = \frac{x'_{CNH} x_{CH_3CN}}{2x_{H_2O}} \quad (6.5)$$

In view of Eq. 6.3a, Eq. 6.3 now contains one unknown at each concentration and the values of the fraction of OHO, OHN and OH bonds were calculated. They are

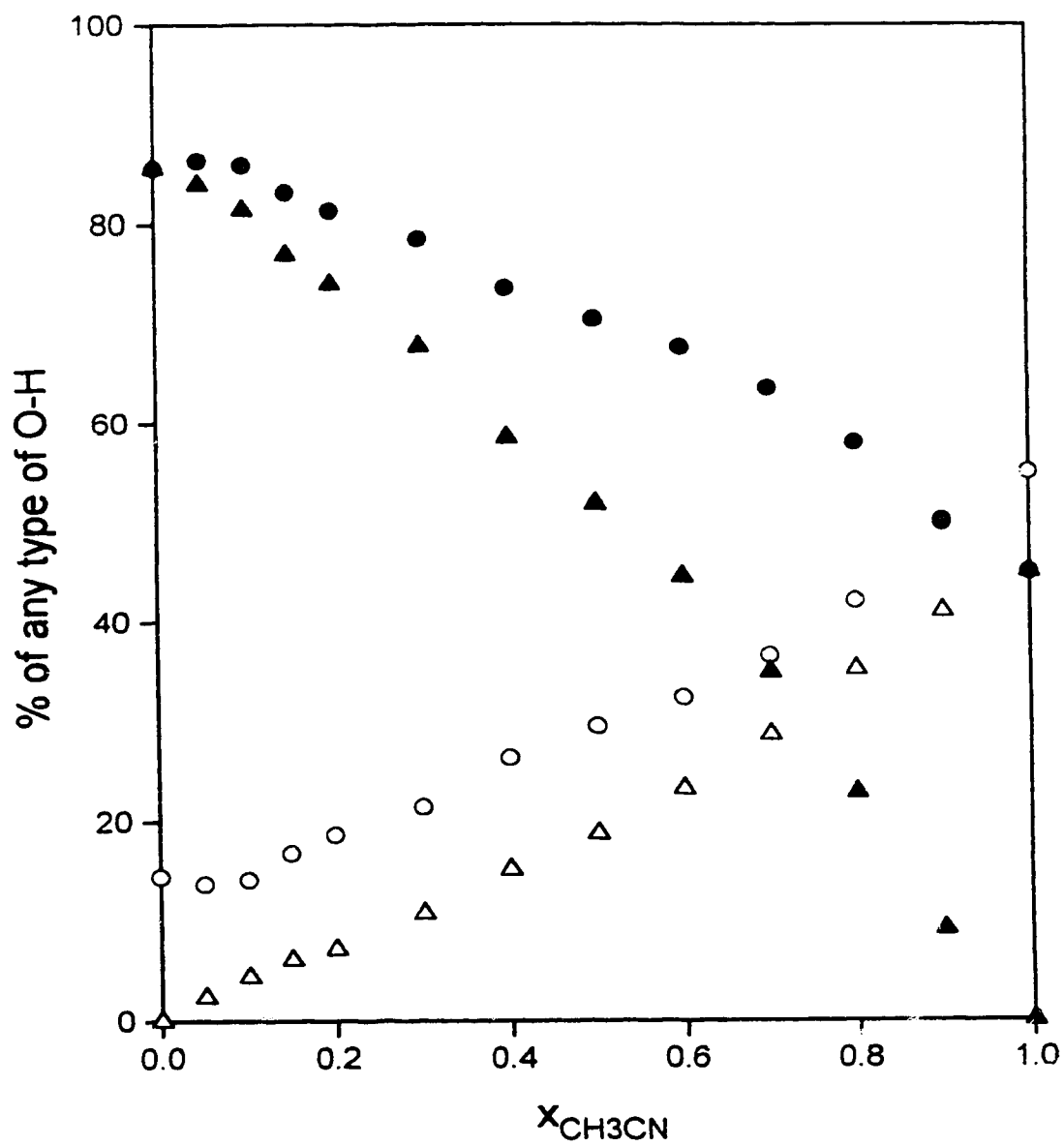


Figure 6.8. The percentage of free (o), water bonded (\blacktriangle), acetonitrile bonded (\triangle), and total hydrogen bonded O-H groups (\bullet) as functions of composition.

plotted against mole fraction of acetonitrile in Fig. 6.8 and the values of x'_{OH_2} and x'_{OH} are tabulated in Table 6.11 with the previously obtained values of x'_{CNH} .

6.4.8 Discussion

The numerical structural results of this work can be summarized as follows. At very low mole fraction of acetonitrile, where acetonitrile and water mix exothermically, the CH_3CN is all hydrogen bonded, The fraction that is bonded drops to 50% by $x_{\text{CH}_3\text{CN}} \sim 0.3$ and then drops more slowly but uniformly to zero in pure acetonitrile

The fraction of OH bonds that form OH--N bonds is zero in pure water and rises uniformly to 0.45 in slightly wet CH_3CN . At $x_{\text{CH}_3\text{CN}} = 0.3, 0.5$ and 0.7 this fraction is $\sim 0.10, 0.18$ and 0.30 .

The fraction of OH bonds that form OH--O bonds is ~ 0.86 in pure water and decreases monotonically to zero in pure CH_3CN . From $x_{\text{CH}_3\text{CN}} = 0.1$ it decreases roughly linearly in mole fraction to $x_{\text{CH}_3\text{CN}} \sim 0.6$ then decreases more rapidly to pure CH_3CN . At $x_{\text{CH}_3\text{CN}} = 0.3, 0.5$ and 0.7 this fraction is $\sim 0.68, 0.52$ and 0.35

The fraction of OH bonds that form hydrogen bonds of both types rises slightly or is constant from pure water to 10% CH_3CN then drops steadily to 0.45 in wet CH_3CN .

The fraction of OH bonds that are not hydrogen-bonded decreases slightly or remains constant at $\sim 13\%$ from pure water to $x_{\text{CH}_3\text{CN}} \sim 0.10$, then climbs steadily to 0.55 in wet CH_3CN . At $x_{\text{CH}_3\text{CN}} = 0.3, 0.5$ and 0.7 this fraction is $\sim 0.22, 0.30$ and 0.37

Thus, in the equimolar mixture, the fractions of OH that form OH--O bonds, form OH--N bonds, and are not bonded, are about 0.52, 0.18 and 0.30 .

These results must be compared with the large body of literature which reports studies of the CH₃CN - H₂O system by a variety of methods. Marcus and Migron ²¹ made a detailed experimental and theoretical study of this system and their 1990 paper makes a convenient starting point. They measured Kamlet and Taft's ²² π^* , α and β which reflect the polarity, hydrogen bond donor ability, and hydrogen-bond acceptor ability of mixtures of water and acetonitrile, and analyzed thermodynamic data from the literature by the inverse Kirkwood-Buff (IKBI) integrals ^{23,24} and the quasi-lattice quasi-chemical (QLQC) method ²⁵. From their results and an extensive survey of the previous literature they presented the following picture of the structure of these solutions.

At low CH₃CN concentrations the CH₃CN enters cavities in the water structure. Solvation by the water is generally agreed, but different methods disagree on the importance of water structure-making or structure-breaking to this process.

Beyond $x_{\text{CH}_3\text{CN}} \sim 0.15$ (0.10 to 0.33 by various methods) the CH₃CN can not be accommodated in the cavities. Beyond this limit microheterogeneity sets in, wherein the hydrogen-bonded structure in the water clusters is enhanced relative to that in neat water. More specifically, microheterogeneity means a preference for neighbors of the same kind that extends over several concentric shells around a given molecule. Thus the mole fraction of the water is greater near a water molecule than the bulk value, and the mole fraction of CH₃CN is greater near a CH₃CN molecule than the bulk value.

The weight of evidence is in favor of microheterogeneity existing in the middle range of compositions.

At $x_{\text{CH}_3\text{CN}} > 0.7$ the water clusters are so few and far apart that new kinds of interactions occur. Water- CH_3CN interactions that could be discounted in the middle range are now important. Marcus and Migron view this region as containing discrete water- CH_3CN complexes surrounded by a rather inert CH_3CN solvent. The complexes were taken to be $\text{CH}_3\text{CN} \cdots \text{HOH}$ and $\text{CH}_3\text{CN} \cdots \text{HOH} \cdots \text{NCCH}_3$.

At $x_{\text{CH}_3\text{CN}} = 0.95$ another change is indicated by some methods. The 1:1 H-bonded structure may still exist, but the CH_3CN "has a weakly manifested structure as in the neat liquid".

Three significant studies since Marcus and Migron's work should be noted.

D. Zhang et al.²⁶ studied CH_3CN in the gas-liquid surface of $\text{CH}_3\text{CN} - \text{H}_2\text{O}$ mixtures by Infrared-visible sum frequency generation, IVSFG. They found that at $x_{\text{CH}_3\text{CN}} < 0.07$ the CH_3CN molecules in the surface are hydrogen-bonded to the water and are inclined at 40° to the normal, but at $x_{\text{CH}_3\text{CN}} = 0.07$ a sharp transition occurs in the surface, and at $x_{\text{CH}_3\text{CN}} > 0.07$ the CH_3CN molecules are not hydrogen bonded and are inclined at 70° to the normal. The relation between these findings and the bulk properties is not clear.

Huang et al.⁷ studied $\text{CH}_3\text{CN} - \text{H}_2\text{O}$ mixtures by measuring the third harmonic susceptibility, which sensitively reflects the microstructure of the liquid. Their results clearly indicated the existence of microheterogeneity when the mole fraction of CH_3CN is > 0.3 .

Jamroz et al.⁸ have studied infrared spectra of $\text{CH}_3\text{CN} - \text{H}_2\text{O}$ mixtures as outlined in the introduction. Of relevance here are the following points. The fraction of hydrogen-bonded CH_3CN they found is in excellent agreement with that found in this work by a different method. Their comparison of these numbers with the much greater fractions they obtained from a random close-packing model led them to conclude that the arrangement in the mixture is remarkably non-random and strong preferential solvation of H_2O by H_2O and CH_3CN by CH_3CN occurs in the mixtures. Their study of dilute OD bonds in $\text{CH}_3\text{CN} - \text{H}_2\text{O}$ mixtures led them to conclude that two types of water and two types of acetonitrile exist over a wide composition range, $\text{H}_2\text{O}(\text{CH}_3\text{CN})$ in close contact with either $\text{H}_2\text{O}(\text{CH}_3\text{CN})$ or $\text{CH}_3\text{CN}(\text{H}_2\text{O})$. The CN stretching band and the bands assigned to OD--O bonds shifted steadily with mole fraction of CH_3CN , from which they concluded that the water molecules form dimers, trimers and other oligomers, because the formation of clusters would result in concentration-independent peak positions.

An important feature of the mixing of water and acetonitrile is that it is exothermic only below $x_{\text{CH}_3\text{CN}} = 0.04$ and is endothermic elsewhere. The present results (Fig. 6.8) show a slight increase in the total number of hydrogen bonded OH bonds roughly in this range, with the number returning to its value in pure water near $x_{\text{CH}_3\text{CN}} = 0.1$. The increase is achieved by forming OH--N bonds instead of OH--O bonds. Thus, the acceptance of CH_3CN into the lattice is not accompanied by enhancement of the water structure, the fraction of OH--O bonds decreasing steadily with increasing CH_3CN content. It can be noted that the ability of water to fully

surround an acetonitrile molecule must end at higher $x_{\text{CH}_3\text{CN}}$ than about 0.08, namely 1 CH_3CN to 12 waters.

The rapid decrease in the fraction of hydrogen-bonded CH_3CN molecules with increasing CH_3CN content ends at 50%, near $x_{\text{CH}_3\text{CN}} = 0.3$. This rapid decrease is consistent with the establishment of microheterogeneity, at least through formation of clusters of acetonitrile molecules, and the wide composition range reported for the onset may reflect the sensitivity of the different methods to the phenomenon. There is general agreement that microheterogeneity exists at $x_{\text{CH}_3\text{CN}} = 0.33$, which is where the fraction of hydrogen-bonded CH_3CN molecules is ~ 0.5 and starts to decrease more slowly. At this point, the fractions of OH bonds that form OH--N bonds, OH--O bonds, and are not bonded are about 0.1, 0.7 and 0.22. Thus, the present results do not support the proposal noted above that the water structure is enhanced by the microheterogeneity.

The fractions of OH bonds that are OH--O bonded show that the region of microheterogeneity can not extend much beyond $x_{\text{CH}_3\text{CN}} = 0.50$. This can be seen by considering the fraction of OH bonds that must be hydrogen bonded in various water clusters. In $\text{H}_2\text{O}(\text{H}_2\text{O})_4$, i.e. a water molecule solvated by four others, the fraction of bonded OH bonds is 0.40. It increases to 0.47 in $\text{H}_2\text{O}(\text{H}_2\text{O})_{14}$, 0.50 in H_2O chains and ice-like hexagonal rings, 0.67 in isolated dodecahedra, and 0.74 in a 39-molecule piece of ice Ih. Thus, the type of cluster that can form is severely limited when the fraction of the OH bonds that form OH--O bonds is 0.5 or less. This fraction is 0.5 in the equimolar mixture and is only 0.35 at $x_{\text{CH}_3\text{CN}} = 0.7$, where the fraction that form OH--N

bonds is nearly the same, 0.30, and about 35% of the OH bonds are not hydrogen bonded.

These considerations lead to broad agreement with Jamroz et al. with respect to the acetonitrile-rich mixtures, namely that the system changes from a microheterogeneous structure at $x_{\text{CH}_3\text{CN}} < \sim 0.5$ to one in which H_2O is bonded to CH_3CN and H_2O , probably with short water chains and rings as well as some isolated water molecules, to a structure at $x_{\text{CH}_3\text{CN}} > \sim 0.85$ in which there are enough CH_3CN molecules to surround each water molecule, which forms a single hydrogen bond to one of the CH_3CN molecules.

6.4.9 The bond moments

The dipole moment derivatives with respect to the normal coordinates were calculated through equation 6.1 for the O-H and $\text{C}\equiv\text{N}$ stretching vibrations in the mixtures. Specifically, under the approximation of electrical and mechanical harmonicity the equation

$$C_j = \frac{N_A \pi}{24 \pi c^2} g_j \left| \frac{\partial \mu}{\partial Q_j} \right|^2 \quad (6.1a)$$

was used from which $1.8686 C_j$ gives $\left| \frac{\partial \mu}{\partial Q_j} \right|^2$ in $(\text{D}\text{\AA}^{-1}\text{amu}^{-1/2})^2$ if C_j is in $\text{km/mole}^{14, 27}$.

The bond moments were then calculated from $\partial \mu / \partial Q_j$ values under the diatomic OH or CN oscillator model. In Table 6.12, the values determined are given. Note that the bond dipole moments for the OH bands are for the O-H...O or O-H...N bonds not for the free O-H. Both O-H...O and O-H...N have about the same bond dipole

Table 6.12. The integrated Intensities and Dipole Moment Derivatives of the O-H and C≡N Stretching Vibrations in CH₃CN+H₂O mixture at 25 °C

Stretching Vibration	C_j^a km/mole	$(\partial\mu/\partial Q)^2$ (Debye Å ⁻¹ amu ^{-1/2}) ²	$ \partial\mu/\partial R $ ^b Debye Å ⁻¹
O-H...O	5.82	10.88	3.21 ^c
O-H...N	5.67	10.60	3.17 ^d
C≡N	0.120	0.22	1.21
C≡N...H	0.206	0.38	1.58

^a. The areas under the spectrum $\tilde{\nu}\alpha_m''(\tilde{\nu})$, per mole of O-H or C≡N bonds.

^b. The magnitude of the bond dipole moment derivative evaluated from the diatomic OH or CN oscillation model.

^c. From the simple bond dipole moment model with the molecular structure used in the reference 28, the value is 3.20 Debye Å⁻¹.

^d. From the simple bond dipole moment model with the molecule structure used in reference 28, the value is 3.16 Debye Å⁻¹.

moment. For the O-H stretching vibration in pure liquid water, the same $(\partial\mu/\partial Q_j)^2$ was determined previously from the area under the molar conductivity spectrum without considering the existence of the 15 % of non H-bonded O-H groups. Consequently, the reported value²⁸, 3.04 D / Å, is smaller than 3.21 D / Å, the value obtained in this work. The previous intensities and these from this work give the same value of $|\partial\mu/\partial Q_j|$ if the same assumption is applied to both sets.

The bond dipole moment of the H-bonded CN bond is larger than that of the free bond by about 15%. No values that can be used for comparison with this results are known.

6.5. Conclusions

The results of this study are generally supportive of the current picture of the structure of acetonitrile - water mixtures, and provide the following specific details for the first time. The fraction of hydrogen - bonded OH groups increases slightly in the region below $x_{\text{CH}_3\text{CN}} \sim 0.05$, where the mixing process is exothermic. This largely arises from the formation of rather more OH--N bonds than the OH--O bonds that are destroyed. The fraction of hydrogen - bonded CH_3CN molecules decreases rapidly as $x_{\text{CH}_3\text{CN}}$ increases to 0.3, which supports the existence of microheterogeneity in mixtures with $x_{\text{CH}_3\text{CN}}$ near 0.3. The water structure is not, however, enhanced by the microheterogeneity since the fraction of OH bonds that are OH--O bonded decreases monotonically with increasing CH_3CN content. The microheterogeneity can not exist far into the region with $x_{\text{CH}_3\text{CN}} > 0.5$, because there are insufficient OH--O bonds to support larger units than short chains or small rings of water molecules. At very high acetonitrile mole fractions, 90% of the water molecules bond to one CH_3CN molecule and are presumably solvated by other CH_3CN molecules.

6.6 References:

1. H. Kovacs and A. Laaksonen, J. Am. Chem. Soc., **113**, 5596 (1991)
2. E. Goldammer, H. G. Herz, J. Phys. Chem., **74**, 3734 (1970)
3. G. Z. Kabish, Z. Phys. Chem., Leipzig, **263**, 48 (1982)
4. C. Moreau and G. Douheret, Thermochim. Acta, **13**, 385 (1975)
5. D. A. Armitage, M. J. Blandamer, M. J. Foster, N. J. Hidden, K. W. Morcom, M. C. R. Symons and M. J. Wootten, Trans. Faraday Soc., **64**, 1193 (1968)

6. B. Z. Gorbunov and Y. I. Naberukhin, *Zh. Strukt. Khim.*, **16**, 816 (1975)
7. J. Y. Huang and M. H. Wu, *Phys. Rev. E*, **50**, 3737 (1994)
8. D. Jamroz, J. Stangret and J. Lindgren, *J. Am. Chem. Soc.*, **115**, 6165 (1993)
9. J. E. Bertie, S. L. Zhang, *J. Chem. Phys.*, **100**, 8364 (1994)
10. J. E. Bertie, S. L. Zhang and R. Manji, *Appl. Spectrosc.*, **46**, 1660 (1992)
11. L. W. Tilton and J. K. Taylor, *J. Res. Natl. Bur. Std.*, **20**, 419 (1938)
12. J. Timmermans, *Physico-Chemical Constants of Pure Organic Compounds*, **2**, 529 (Elsevier, Amsterdam, 1965).
13. J. E. Bertie and Z. Lan, submitted to *Appl. Spectrosc.*
14. J. E. Bertie, S. L. Zhang and C. D. Keefe, *J. Mol. Struct.* **324**, 157 (1994)
15. J. Timmermans, *Physico-Chemical Constants of binary systems*, **4**, 65 (Interscience, New York, 1961).
16. A. L. Narvor, E. G. Gentric and P. Saumagne, *Can. J. Chem.*, **49**, 1933(1971)
17. J. E. Bertie and Z. Lan, to be published
18. W. A. P. Luck, H. Borgholte and T. Habermehl, *J. Mol. Struct.* **177**, 523 (1988)
19. L. E. Kretzer, M. Fritzsche and W. A. P. Luck, *J. Mol. Struct.* **175**, 277 (1988)
20. O. D. Bonner and Y. S. Choi, *J. Phys. Chem.*, **78**, 1723 (1974)
21. Marcus and Y. Migron. *J. Phys. Chem.* **95**, 400 to 406 (1991)
22. M.J. Kamlet, J.-L. M. Abboud, M.H. Abraham and R.W. Taft. *J. Org. Chem.* **48**, 2877 (1983)
23. E. Matteoli and L. Lepori. *J. Chem. Phys.* **80**, 2856 (1984)

24. M. J. Blandamer, N.J. Blundell, J. Burgess, H. J. Cowless and I.M. Horn. J. Chem. Soc. Farad. Trans. **86**, 277 (1990)
25. Y. Marcus. J. Chem. Soc. Farad. Trans. I **85**, 381 (1989)
26. D. Zhang, J. H. Gutow, K. B. Eisenthal and T. F. Heinz, J. C. P. **98**, 5099 (1993)
27. J. E. Bertie, S. L. Zhang, H. H. Eysel, S. Baluja, and M. K. Ahmed, Appl. Spectrosc., **47**, 1100 (1993)
28. J. E. Bertie, M. K. Ahmed and H. H. Eysel, J. Phys. Chem., **93**, 2210 (1989)

Chapter 7 Conclusion

The previous chapters present the work done to measure absolute intensities in the IR spectra of liquid samples by transmission and attenuated total reflection (ATR) methods, and to apply the intensities to investigate the hydrogen bonding interaction in water solutions. The accomplishments are summarized in this chapter.

The infrared optical constant, k and n , spectra are fundamental spectra for absolute intensities. In Chapter 2 the effect of the infrared imaginary refractive index spectrum on the visible real refractive index of colorless liquids is investigated through the Kramers-Kronig transform. For ten common liquids, the IR contributions to the visible refractive indices have been determined. Their values are <0.001 except for the four hydrogen-bonded liquids. From these results, a proper function can be selected for a fitting procedure to determine the electronic contribution to the real refractive index at visible and infrared wavenumbers from the reported values of the real refractive index in the visible region. The obtained electronic contribution is described by the function $n_{el}(\tilde{\nu}) = a_0 + a_2 \tilde{\nu}^2 + a_4 \tilde{\nu}^4$. For the liquids examined, the best equations to use to revise the reported values of the real refractive index in the IR region have been determined. The known errors indicate that this revision gives the n_{el} spectrum in the IR region with errors of 0.001 or less.

Liquid dichloromethane was measured by the transmission method. Its optical constant spectra, $k(\tilde{\nu})$ and $n(\tilde{\nu})$, and molar absorption coefficient spectrum, $E_m(\tilde{\nu})$, between 6500 and 800 cm^{-1} have been determined as described in Chapter 3. Their

accuracy was estimated from the agreement between intensities measured by five operators in four different laboratory. The peak heights of 36 measured bands of the imaginary refractive index and molar absorption coefficient spectra are believed to be accurate to $\pm 2.3\%$. The baseline k values are believed to be accurate to $\sim 8\%$ below 6000 cm^{-1} , $\sim 1\%$ below 4500 cm^{-1} and $\sim 25\%$ above 6500 cm^{-1} where the absorption is extremely weak. The integrated intensities over 25 measured band groups are believed to be accurate to $\pm 1.5\%$. Nine of the bands have been accepted as secondary infrared absorption intensity standards for liquids by the International Union of Pure and Applied Chemistry.

One approach to refine ATR spectra is to use the phase shift on reflection and the reflectance to calculate the optical constants in the IR region. In Chapter 4, this is explored. Two reasons that have made this approach less accurate than that used in our laboratory have been found to be the use of an inaccurate KK transform and failure to allow for the variation with wavenumber of the real refractive index of the incident medium. Accordingly, a new modified Kramers-Kronig (KK) transform with a non-constant correction to the phase shift has been developed to calculate the phase shift from the measured reflectance. The optical constants, $k(\tilde{\nu})$ and $n(\tilde{\nu})$, recovered from the simulated methanol ATR spectrum ($7800\text{--}2\text{ cm}^{-1}$) with silicon as the transparent phase are in error by less than 0.04% and 0.02% respectively. The results indicate that the new transform is more accurate than those previously used, and it makes this approach of comparable accuracy to the iterative procedure developed in

this laboratory previously, in much less calculation time and with no divergence problem.

Measurement of the OH stretching band of liquid water by the ATR method is examined in Chapter 5. The cause of the reported non-reproducibility of the ATR spectra has been found to be difficulty in filling the cell, and not inadequate temperature control. Several precise spectra have been obtained under superior experimental and computational conditions than previously available in this laboratory. The precision of the k spectrum is now 0.8% for the peak height and 0.3% for the area in the region 4000-2660 cm^{-1} , and 1.7% for the peak height and 0.9% for the area in the region 2660-1390 cm^{-1} . In addition, the available imaginary refractive index values between 15000 and 1 cm^{-1} for liquid water at 24.5 ± 1 °C have been compared, and recommended k and n spectra are presented with the probable limits to their accuracy.

As a second application of the ATR method, water and acetonitrile mixtures over the full composition range are investigated in Chapter 6. The real and imaginary refractive index and polarizability spectra between 6500-700 cm^{-1} were determined for the mixtures at 24.5 ± 1 °C. The areas under the $\tilde{\nu}\alpha''_m(\tilde{\nu})$ spectra in the OH and CN stretching vibration regions were calculated and examined as functions of composition to investigate the structure of the mixtures and the hydrogen bonding interaction between the water and acetonitrile molecules. The results of this study are generally supportive of the current picture of the structure of acetonitrile - water mixtures, and provide the following specific details for the first time. The fraction of hydrogen -

bonded OH groups increases slightly in the region below $x_{\text{CH}_3\text{CN}} \sim 0.05$, where the mixing process is exothermic. The fraction of hydrogen - bonded CH_3CN molecules decreases rapidly as $x_{\text{CH}_3\text{CN}}$ increases to 0.3, which supports the existence of microheterogeneity in mixtures with $x_{\text{CH}_3\text{CN}}$ near 0.3. The water structure is not, however, enhanced by the microheterogeneity since the fraction of OH bonds that are OH--O bonded decreases monotonically with increasing CH_3CN content. The microheterogeneity can not exist far into the region with $x_{\text{CH}_3\text{CN}} > 0.5$, because there are insufficient OH--O bonds to support larger units than short chains or small rings of water molecules. At very high acetonitrile mole fractions, 90% of the water molecules bond to one CH_3CN molecule and are presumably solvated by other CH_3CN molecules.

The methodologies developed in this work, especially the ATR method, are not limited to the samples which have been examined. The application of the ATR method to mixtures of water with other liquids such as acids, ketones, amides and peptides can be investigated. This will lead to a better understanding of the role water plays in nature.